

Global Warming Impacts on Hydrologic Extremes

by

Mesgana Seyoum Gizaw

A thesis submitted in partial fulfillment of the requirements for the degree of

Doctor of Philosophy

in

Water Resources Engineering

Department of Civil and Environmental Engineering
University of Alberta

©Mesgana Seyoum Gizaw, 2017

Abstract

Climate change could significantly alter precipitation and water availability in different parts of the world. Moreover, during the course of the 21st century, climate change impact can potentially enhance the severity and frequency of extreme precipitation and also increase prolonged drought periods. This research focuses on the potential impact of climate change on extreme precipitation, floods and droughts in some selected study areas in North America and Africa.

For the United States (US) and southern Canada, analysis of trends in Convective Available Potential Energy (CAPE) data and extreme precipitation indices for single or multiple storm events show an increasing trend over much of the eastern US and some parts of the Canadian prairies, e.g. southern Alberta, in the summer of 1979-2013. Statistically significant increasing trends in temperature and surface specific humidity is likely a major contributing factor to increasing trends in extreme precipitation events observed over these regions.

Next, changes in extreme precipitation events in Oldman, Bow and Red Deer River Basins of southern Alberta, Canada, were also assessed using six extreme climate indices for the rainy May-August (MJJA) season, using dynamically downscaled SRES A2 and A1B climate scenarios of four Coupled Model Intercomparison Project phase 3 (CMIP3) Global Climate Models (GCMs). The results suggest that in the 2050s (2041-2070) and 2080s (2071-2100), southern Alberta will be expected to experience more frequent and severe intensive storm events in the MJJA season that could potentially increase the risk of future flooding.

Regional Flood Frequency Analysis (RFFA) model based on the Support Vector Regression (SVR) was developed to estimate regional flood quantiles for two sites located in southeastern British Columbia (BC) and southern Ontario (ON), Canada. Based on historical predictors, SVR-RFFA satisfactorily estimated flood quantiles of 10, 25, 50 and 100 year return periods. Flood quantiles estimated by SVR-RFFA for 2041-2100 based on RCP4.5 and RCP8.5 climate scenarios project flood quantiles to increase by about 7% in southeastern BC and 29% in southern ON.

Next, the possible impact of climate change on droughts in sub-Saharan Africa (SSAF) was analyzed using the Palmer Drought Severity Index (PDSI) for 1971-2000 and RCP4.5 and RCP8.5 climate projections of the 2050s and 2080s. The results show that most areas in South Africa (SA) and West Africa (WA) will shift to a drier climate in the 2050s and 2080s while some areas in Greater Horn of Africa (GHA) could be relatively wetter in this period. In contrast, very little change is projected in the drought severity of Central Africa (CA). More frequent El Niño episodes in 21st century could also increase the drought prone regions of WA, SA and GHA while CA still remains virtually unaffected. These results suggest that SSAF will experience a drier climate in the 2050s and 2080s with an increase in drought prone areas in the four corners of the sub-continent.

The potential impact of climate change on water availability of parts of GHA was simulated by the Hydrologic Simulation Program-FORTRAN (HSPF) hydrologic model to predict changes in the streamflow of four major river basins in Ethiopia: Awash, Baro, Genale and Tekeze. The calibrated and validated HSPF model was forced with bias corrected daily climate data from 10

CMIP5 GCMs for the 1971-2000 control period and the RCP4.5 and RCP8.5 climate projections of 2050s and 2080s. The results suggest that the mean annual streamflow of Awash, Baro and Tekeze rivers is projected to increase by about 3% (6%) whereas for Genale river about 18% (33%) increase in streamflow is projected for the 2050s (2080s). Despite the increase in annual streamflow, the mean summer streamflow is projected to decrease for most river basins. However, such a decrease in summer streamflow was compensated with a significant increase in the autumn streamflow.

The results from this research suggest that climate change could significantly increase the frequency and intensity of hydrologic extremes such as severe precipitation and droughts which can also affect the streamflow of river basins in different parts of the world.

Preface

This thesis sheds some light on the possible impact of climate change on hydrologic extremes in parts of North America and Africa. It will familiarize the reader on the expected changes in intensity and frequency of extreme hydrologic events such as severe storms and scarcity in precipitation that can lead to prolonged droughts and reduction in water resources during the mid to late 21st century giving particular emphasis on one hydrologic extreme in a given study area. To date I have published the works in Chapters 3, 4 and 5 of this thesis on internationally peer-reviewed scientific journals. Chapter 3 of this thesis has been published as Gizaw, M. S., and Gan, T. Y., 2015, “Possible Impact of climate change on future extreme precipitation of the Oldman, Bow and Red Deer River Basins of Alberta”, *Int. Journal Climatology*, 36(1), 208-224. DOI:10.1002/joc.4338. Chapter 4 has been published as Gizaw, M. S., and Gan, T. Y., 2016, “Regional Flood Frequency Analysis using Support Vector Regression under historical and future climate”, *Journal of Hydrology*, 538, 387-398, [dx.doi.org/10.1016/j.jhydrol.2016.04.041](https://doi.org/10.1016/j.jhydrol.2016.04.041) while Chapter 5 is published as Gizaw, M. S., and Gan, T. Y., 2016, “Impact of Climate Change and El Niño Episodes on Droughts in sub-Saharan Africa”, *Climate Dynamics*, Springer, DOI: 10.1007/s00382-016-3366-2. For the work done in these Chapters, I was responsible for data collection and analysis as well as the manuscript composition. The work on Chapter 6 has been also submitted to journal of Climatic Change and is currently under review. This work was done principally in collaboration with Dr. Getu Biftu from Golder Associates. I was responsible for part of the climate and streamflow data collection from the Meteorological and Water Resources authorities of Ethiopia while additional data was provided by another co-author Dr. Semu Moges. In addition, I was also responsible for data preparation, model running, analysis of results and manuscript composition. I am also planning to submit the work done on Chapter 1 to

scientific journal. With the acceptance of Chapter1 and Chapter 6 for publication, the core work from my PhD study will lead to the publication of five papers on peer-reviewed scientific journals.

Mesgana Seyoum Gizaw

Edmonton, AB, December, 2016

Acknowledgements

I would like to express my gratitude to my supervisor Dr. Thian Yew Gan for his continuous guidance, support and encouragement during the course of this study. I would also like extend my gratitude to the members of the examination committee: Dr. Murugesu Sivapalan, Dr. Andrew Bush, Dr. Carlos Cruz-Noguez, Dr. Mark Lowen and Dr. Yuxiang Chen for their valuable comments and suggestions. I am grateful to the University of Alberta Doctoral Recruitment Scholarship and to the Natural Science and Engineering Research Council for financial assistance throughout the course of my research.

I am forever indebted to my mother Beshiwork Kidanewold, my father Seyoum Gizaw and also my brothers and sister, Yonathan, Daniel and Tsega for being a consistent source of strength and encouragement at difficult times that allowed me to finish my work. My sincere gratitude also goes to all my friends from Edmonton, especially Dere, Heni, Wende, Zelalem, Raie and Amarebhe, who made this city feel like a second home for me.

Above all, I give all the praise and credit to the almighty God for giving me this opportunity.

Table of Contents

Abstract.....	ii
Preface.....	v
Acknowledgements.....	vii
Table of Contents.....	viii
List of Tables	xii
List of Figures.....	xiv
List of Abbreviations	xxii
Chapter 1 Introduction.....	1
1.1. Background and Problem Statement.....	1
1.2. Research Objectives	4
1.3. Organization of Thesis	5
1.4. References	6
Chapter 2 Trends in Convective Available Potential Energy (CAPE) and extreme precipitation indices over the United States and southern Canada for summer 1979-2013 period.	
10	
2.1 Introduction	10
2.2 Study area, data and methodology	12
2.2.1 Study area.....	12
2.2.2 Data.....	13
2.2.3 Research Methodology	14
2.3 Discussions of Results.....	15
2.3.1 Spatial and seasonal CAPE variability	15

2.3.2	Trends in summer CAPE and extreme precipitation indices	16
2.3.3	Trends in summer temperature and surface specific humidity	18
2.4	Conclusions	21
2.5	References	23
Chapter 3 Possible Impact of climate change on future extreme precipitation of the Oldman, Bow and Red Deer River Basins of Alberta		
		32
3.1	Introduction	32
3.2	Research Methodology.....	36
3.2.1	Extreme Climate Indices.....	36
3.2.2	GCM data.....	37
3.2.3	Dynamic Downscaling of GCM data.....	37
3.2.4	Bias correction	40
3.3	Discussion of Results	42
3.3.1	R20mm Index.....	42
3.3.2	R95p and R99p Indices.....	44
3.3.3	P30yr.....	45
3.3.4	RX1day and RX5day	47
3.3.5	Changes in temperature and precipitable water	49
3.4	Summary and Conclusions.....	50
3.5	References	54
Chapter 4 Regional Flood Frequency Analysis using Support Vector Regression under historical and future climate.....		
		72
4.1	Introduction	72

4.2	Support Vector Regression.....	75
4.3	Data and Methodology.....	79
4.4	Discussions of Results.....	83
4.4.1	Predictor variables	83
4.4.2	Performance based on goodness-of-fit statistics.....	84
4.4.3	Comparing SVR based with ANN based RFFA models	86
4.4.4	Projected changes in future flood quantiles derived from SVR RFFA models.....	88
4.5	Summary and Conclusions.....	91
4.6	References	95
Chapter 5 Impact of Climate Change and El Niño Episodes on Droughts in sub-Saharan		
Africa	110	
5.1	Introduction	110
5.2	Study area, data and methods.....	114
5.2.1	Study area.....	114
5.2.2	Data	114
5.2.3	Research Methodology	115
5.3	Results and discussions	119
5.3.1	Changes in median PDSI values and drought prone regions	120
5.3.2	Changes in frequency and length of persistent droughts	121
5.3.3	Impact of El Niño and combined impact of El Niño and climate change on SSAF droughts.....	124
5.4	Summary, Conclusions and Recommendations	128
5.4.1	Adaptive Measures to Mitigate Impacts of Future Droughts.....	130

5.5	References	133
Chapter 6	Potential Impact of climate change on streamflow of major Ethiopian rivers	150
6.1	Introduction	150
6.2	Study Area, data and methodology	152
6.2.1	Study area.....	152
6.2.2	Data.....	154
6.2.3	Methodology.....	156
6.3	Results and discussion.....	157
6.3.1	Model calibration.....	157
6.3.2	Projected changes in streamflow	159
6.3.3	Comparing projections of precipitation of Ethiopia by GCMs with observations	161
6.4	Summary and Conclusions.....	163
6.5	References	165
Chapter 7	Summary, conclusions and recommendations	180
7.1	Summary and Conclusions.....	180
7.2	Recommendations	188
7.3	References	191
	Bibliography.....	193
	APPENDIX A.....	219
	APPENDIX B.....	225
	APPENDIX C.....	229

List of Tables

Table 3.1 Extreme climate indices adapted from Table 1 of Sillmann et al. (2013a)	62
Table 3.2 CMIP3 GCMs selected for investigating possible climate change impact to MJJA extreme precipitation of SSRB. More details about these GCMs can be found in http://www-pcmdi.llnl.gov/ipcc/model_documentation/ipcc_model_documentation.php	62
Table 3.3 Correlation between monthly precipitation data of gauging stations and data simulated by MM5 at a grid point closest to respective rain gauge stations.	63
Table 3.4 Statistics (% error, R2 and Root Mean Squared Error (RMSE)) of extreme climate indices of Table 1 derived from ERA-Interim reanalysis data and the base period data of four GCMs dynamically downscaled by MM5 for SSRB before and after bias correction, respectively. These statistics represent the difference between extreme climate indices estimated from these datasets and indices estimated from ANUSPLIN data.	63
Table 3.5 Medians of projected return periods of the P30yr index (daily precipitation intensities of 30-year return period of the control run) based on the A2 and A1B climate scenarios of four GCMs downscaled by MM5 for ORB, BRB, and RRB by 2050s and 2080s..	64
Table 4.1 List of predictors used in this study and their cross-correlations	101
Table 4.2 Thirteen combinations of predictors used in SVR-RFFA model	101
Table 4.3 Mean goodness-of-fit statistics of flood quantiles (Q10 to Q100) estimated by the SVR-RFFA model for the 13 sets of predictors considered for a group of 26 and 23 river basins in southeastern BC and southern ON, respectively.	102

Table 4.4 Comparing the mean goodness-of-fit statistics of flood quantiles estimated by ANN and SVR-RFFA models for thirteen sets of predictors considered for a group of 26 and 23 river basins in south eastern BC and southern ON, respectively.	102
Table 5.1 CMIP5 GCMs selected to investigate possible climate change impact to future drought events in SSAF.	140
Table 5.2 PDSI category table (Palmer, 1965)	140
Table 6.1 Calibration and validation results of HSPF in terms of Nash Sutcliffe coefficient (Ef), coefficient of determination (R ²), root mean squared error (RMSE) and percent bias (PBIAS) for the Awash, Baro, Genale and Tekeze river basins of Ethiopia	172
Table 6.2 Median changes in mean annual temperature, precipitation and streamflow in the 2050s and 2080s with respect to the control period (1971-2000) for the RCP4.5 and RCP8.5 climate scenarios of 10 CMIP5 GCMs selected for this study.	172

List of Figures

- Figure 2.1 Graphical representation of Convective Available Potential Energy (CAPE). 28
- Figure 2.2 (a) 30 arc second digital elevation model of the US and southern Canada, (b) prominent landscapes of US and southern Canada, (c) and (d) mean annual precipitation and temperature derived from GPCC and GHCN-CAMS gridded observational datasets, respectively, for 1971-2000 period. 28
- Figure 2.3 (a) Mean summer (June-August) CAPE for 1979-2013 period, (b) Mean annual CAPE values over US and southern Canada, the gray area shows the range of CAPE data while the dotted line shows the mean annual profile of CAPE over the region..... 29
- Figure 2.4 Trends in CAPE data for the summer of 1979-2013 period. (a) trends in CAPE in Joules/kg/year, (b) significance of trends at $p < 0.05$ 29
- Figure 2.5 Trends in extreme precipitation indices for 1979-2013 summer period for US and southern Canada. (a), (c) and (e) show decreasing trends at GHCN stations for RX1day, RX5day and R20mm, respectively while (b), (d) and (f) show increasing trends at GHCN stations for the same variables. Grey circles indicate trends that are statistically significant. 30
- Figure 2.6 Trends in average surface temperature and surface specific humidity for the 1979-2013 summer period of US and southern Canada (a) decreasing trends in average temperature at GHCN stations, (b) increasing trends in average surface temperature at GHCN stations, (c) trends in surface specific humidity, (d) spearman rank correlation between CAPE and surface specific humidity. Grey circles in (a) and (b) indicate trends that are statistically significant. 31

Figure 3.1 MM5 domain configurations (encompassed by thin red lines), with the outer domain (D1) at a 27-km resolution, the inner domain (D2) at a 9-km resolution encompassing ORB, BRB and RRB. 65

Figure 3.2 Comparison between 10-km resolution ANUSPLIN gridded precipitation data and 9-km resolution ERA-Interim precipitation downscaled by MM5 for 1979-2007, (a) and (b) average MJJA total precipitation for MM5 D2 and ANUSPLIN, respectively and (c) and (d) average total precipitation exceeding 10 mm/d for MM5 D2 and ANUSPLIN, respectively. 66

Figure 3.3 Quantile-quantile bias correction procedure for MM5's simulated precipitation from x to x' , such that the quantile of x' based on the cumulative distribution function (CDF) of the observed rainfall is the same as that of x based on the CDF of the simulated rainfall of MM5. 67

Figure 3.4 With respect to the base period (1971-2000), medians of the projected changes to the R20mm index of the ORB, BRB and RRB derived from climate projections of four CMIP3 GCMs under the SRES A2 and A1B scenarios downscaled by MM5. 67

Figure 3.5 Boxplots of R95p and R99p derived from ensemble projections of four GCMs and A2 and A1B climate scenarios downscaled by MM5 for ORB, BRB and RRB for the base period, 2050s and 2080s, respectively. The line and the circle within the box plots represent the ensemble median and ensemble mean, respectively. 68

Figure 3.6 Medians of daily rainfall intensities of different return periods derived from 1961-2010 MJJA ANUSPLIN daily gridded precipitation data for ORB, BRB and RRB. The rainfall intensities of 5 to 30-yr return periods for ORB are approximately 20% higher than that of BRB and RRB. 68

Figure 3.7 With respect to the base period (1971-2000), medians of the projected changes to the P30yr index of the ORB, BRB and RRB derived from climate projections of four CMIP3 GCMs under the SRES A2 and A1B scenarios downscaled by MM5..... 69

Figure 3.8 The average MJJA maximum precipitation and the corresponding average increase in air temperature of ORB, BRB, and RRB from the base period to 2041-2100, based on the A2 scenarios of four GCMs downscaled by MM5..... 69

Figure 3.9 With reference to the RX1day index of the base period (1971-2000), the figure shows medians of the projected changes to the RX1day index of the ORB, BRB and RRB derived from downscaled SRES A2 and A1B climate change scenarios of four CMIP3 GCMs downscaled by MM5. 70

Figure 3.10 With reference to the RX5day index of the base period (1971-2000), the figure shows medians of the projected changes to the RX5day index of the ORB, BRB and RRB derived from downscaled SRES A2 and A1B climate change scenarios of four CMIP3 GCMs..... 70

Figure 3.11 With reference to the base period of 1971-2000, both 2 m temperature and precipitable water for MJJA derived from SRES A2 and A1B climate scenarios of four GCMs downscaled by MM5 over the three southern Alberta river basins (ORB, BRB and RRB) are projected to consistently increase to the end of the 21st century. 71

Figure 4.1 A group of 26 and 23 streamflow stations located in southeastern BC and southern ON, Canada, respectively selected for this study. 103

Figure 4.2 Predictor combinations used in the SVR-RFFA model arranged in descending order of their overall performance with respect to goodness-of-fit statistics of estimated flood quantiles (Q10 to Q100) for a group of 26 and 23 river basins in southeastern BC and

	southern ON, respectively. Note: for ease of visual presentation the absolute values of BIAS and BIASr(%) are given in log scales.	104
Figure 4.3	Scatterplots of local versus regional estimates of flood quantiles of various return periods that were best predicted by the SVR model based on predictors of set #9 for a group of 26 catchments selected in southeastern BC.	105
Figure 4.4	Scatterplots of local versus regional estimates of flood quantiles of various return periods that were best predicted by the SVR model based on predictors of set #9 for a group of 23 catchments selected in southern ON.	105
Figure 4.5	Range of CV of flood quantiles, Q10, Q25, Q50 and Q100 predicted by the ANN and SVR-RFFA models using 13 sets of predictors for 26 selected stations of southeastern BC. The CV of the set of predictors (#9) that led to the best overall flood quantile estimates is shown in dotted and dashed lines for ANN and SVR-RFFA models, respectively.	106
Figure 4.6	Range of CV of flood quantiles, Q10, Q25, Q50 and Q100 predicted by the ANN and SVR-RFFA models using 13 sets of predictors for 23 selected stations of southern ON. The CV of the set of predictors (#9) that lead to the best overall flood quantile estimates is shown in dotted and dashed lines for ANN and SVR-RFFA models, respectively.	106
Figure 4.7	Boxplots of percent changes in T year return period precipitation between the base period (1971-2000) and 2050s and 2080s derived from RCP4.5 and RCP8.5 climate projections of five CMIP5 GCMs for the southeastern BC and southern ON study sites. The line and the circle in boxplots represent the median and the mean percent change, respectively.	107

Figure 4.8 Boxplots of percent changes in the mean annual precipitation between the base period and 2050s and 2080s derived from RCP4.5 and RCP8.5 climate projections of five CMIP5 GCMs for the southeastern BC and southern ON study sites. The line and circle in boxplots represent the median and the mean percent change, respectively. 108

Figure 4.9 Changes in Q10, Q25, Q50 and Q100 between the base period and 2050s and 2080s derived from five CMIP5 GCMs and RCP45 and RCP85 climate projections for the southeastern BC and south ON study sites..... 109

Figure 5.1 (a) Sub-regions of SSAF based on political boundaries, (b) Elevation map of Africa, (c) Mean annual precipitation for 1971-2000 derived from Global Precipitation Climatology Centre (GPCC) gridded monthly precipitation data, (d) Mean annual temperature for 1971-2000 derived from ERA40 reanalysis data. 141

Figure 5.2 Median PDSI values of the SSAF for the base period (1971-2000), and the 2050s and 2080s under RCP4.5 and RCP8.5 climate projections of five CMIP5 GCMs..... 142

Figure 5.3 Variability of PDSI in the East-West and North-South direction of SSAF for the base period, 2050s and 2080s RCP4.5 and RCP8.5 climate projections of five CMIP5 GCMs. The light grey band in the figure shows the near normal condition whereas the dashed vertical and horizontal lines respectively represent the 25° meridian and the equator partitioning SSAF into East-West and North-South parts, respectively. 143

Figure 5.4 With reference to the base period, changes in the frequency (5a and 5b) and average length (5c and 5d) of short (6 to 12 months) and long (more than 12 months) duration drought events in the 2050s and 2080s based on the ensemble mean projected PDSI values of five CMIP5 GCMs..... 144

Figure 5.5 Cumulative monthly precipitation volumes in the 2050s and 2080s for WA, CA, GHA and SA that are above (a-d) or below (e-h) the P95b threshold for RCP4.5 and RCP8.5 climate projections of five CMIP5 GCMs. 145

Figure 5.6 Scatterplots of 5-year return period rainfall intensity between the base period and the 2050s and 2080s under RCP4.5 and RCP8.5 climate projections of five CMIP5 GCMs. 146

Figure 5.7 Based on GPCP data, (a) areas in SSAF that receive most of their annual rainfall in one or two rainy seasons. Coloured patches represent areas where more than half of the annual precipitation occurs in one season, while hatched and dotted patches represent areas where 30% or more of the annual precipitation occurs in two or more seasons. The seasons in the Figure refer to MAM (March to May), JJA (June to August), SON (September to November) and DJF (December to February) (b) Boxplots showing composites of MAM, JJA, SON and DJF precipitation associated with El Niño for the four regions of SSAF. 147

Figure 5.8 MEI.ext over the 1871-2005 periods. The grey band in the background is derived from running a 15-year variance plotted at the midpoint of the 15 year period..... 147

Figure 5.9 Median PDSI values derived for two hypothetical climates, one dominated by the influence of active El Niño events (a) and (b) and another that is not influenced by either El Niño or La Niña events (c) and (d) for the base period (1971-2000) and the RCP4.5 and RCP8.5 climate projections of the 2050s and 2080s. 148

Figure 5.10 Percentage of area falling under the incipient wet to moderate drought PDSI categories for two hypothetical climates, one dominated by the influence of active El Niño events (a)-(d) and another that is totally not influenced by either El Niño or La

Niña events (e) and (h) for the base period (1971-2000) and the RCP4.5 and RCP8.5 climate projections of the 2050s and 2080s. 149

Figure 6.1 Topographic and climate variability of Ethiopia, (a) Digital Elevation Model (DEM) of Ethiopia derived from 30 arc second DEM from USGS (United States Geological Survey), (b) mean annual precipitation during 1961-1990 period derived from GPCC gridded monthly precipitation data, (c) mean annual temperature during 1961-1990 period derived from GHCN-CAMS gridded monthly average 2 m temperature data. 173

Figure 6.2 Major climatic regions (region A, B and C) in Ethiopia and the location of the four river basins analyzed in this study with respect to each climatic region. The light gray part of the river basins represents the overall drainage area within the country’s political boundary while the dark gray parts represent the portion of the river basin analyzed in this study. For each of the river basin analyzed in this study, the Figure also shows the location of the streamflow and climate stations..... 174

Figure 6.3 Comparison between observed and simulated daily flow for Awash, Baro, Genale and Tekeze river basins for daily flow (left) and monthly average flow (right) for calibration period..... 175

Figure 6.4 Flow duration curves of observed versus simulated streamflow of HSPF calibrated for the four selected river basins of Ethiopia for calibration period. 176

Figure 6.5 Projected changes in the mean annual air temperature versus changes in precipitation for RCP4.5 and RCP8.5 climate projections of 10 CMIP5 GCMs in the 2050s and 2080s for (a) Awash, (b) Baro, (c) Genale and (d) Tekeze River basins. 177

Figure 6.6 Projected changes in the mean annual air temperature versus changes in streamflow simulated (%) by HSPF forced with RCP4.5 and RCP8.5 climate projections of 10 CMIP5 GCMs in the 2050s and 2080s for (a) Awash, (b) Baro, (c) Genale and (d) Tekeze River basins..... 178

Figure 6.7 Projected changes in spring, summer, autumn and winter streamflows of (a) Awash, (b) Baro, (c) Genale and (d) Tekeze river basins, for the RCP4.5 and RCP8.5 climate projections of the mid- and late 21st century. The bottom pie charts show the seasonal streamflow contribution to mean annual runoff for the four river basins based on streamflow observations..... 179

List of Abbreviations

ANN	Artificial Neural Network
ANUSPLIN	Historical gridded precipitation dataset (Australian National University Spline)
BRB	Bow River Basin
CA	Central Africa
CAPE	Convective Available Potential Energy
CMIP3	Coupled Model Intercomparison Project phase 3
CMIP5	Coupled Model Intercomparison Project phase 5
CORDEX	Coordinated Regional Climate Downscaling Experiment
DJF	December-January-February
ECMWF	European Centre for Medium-Range Weather Forecast
ENSO	El Niño Southern Oscillation
GCM	Global Climate Model
GEV	Generalized Extreme Value distribution
GHA	Greater Horn of Africa
HSPF	Hydrologic Simulation Program-FORTRAN
IPCC	Intergovernmental Panel on Climate Change
JJA	June-July-August
MAM	March-April-May
MJJA	May-June-July-August
MM5	Regional climate model, the fifth-generation NCAR/Penn State mesoscale atmospheric model
RCM	Regional Climate Model

RFFA	Regional Flood Frequency Analysis
ORB	Oldman River Basin
PDSI	Palmer Drought Severity Index
PET	Potential Evapotranspiration
RCP	Representative Concentration Pathways
RRB	Red Deer River Basin
SA	South Africa
SON	September-October-November
SRES	Special Report on Emission Scenarios
SSAF	Sub-Saharan Africa
SSRB	South Saskatchewan River Basin
SVM	Support Vector Machines
SVR	Support Vector Regression
US	United States
USGS	United States Geological Survey
WA	West Africa

Chapter 1 Introduction

1.1. Background and Problem Statement

Historical temperature data since instrumental records began in the late 19th century show that the global mean surface temperature has been rising, with the recent past three decades being successively warmer than any of the previous decades (IPCC, 2013). Such a consistent increase in the Earth's global mean temperature, commonly known as climate change, has been mainly attributed to warming effects of increasing anthropogenic greenhouse gas emissions to the Earth's atmosphere. Climate change leads to changes in the hydrologic cycle and especially to changes in extreme hydrologic events such as floods, droughts, hurricanes, etc. There has been skepticisms about the impact of climate change on hydrologic extremes with some even arguing that the present changes in climate is merely a small part of the long term climate variability of the Earth and the ease of access to information in the global theatre, empowered by the advent of personal computers and the internet, could have artificially lead to the perception that hydrologic extremes have increased in recent decades. However, IPCC (Intergovernmental Panel on Climate Change) (IPCC, 2007; 2013) and some scientists (e.g., Tierney et al., 2015; Williams and Funk, 2011) suggest that the recent warming of the Earth's atmosphere is unusual in the context of the past two millennia and hydrologic extremes have indeed increased in frequency and severity in different parts of the world.

Citing different studies, the latest IPCC report (IPCC, 2013) suggests that there have been a likely increase in the frequency and intensity of extreme weather and climate events globally since the 1950s, with the observed changes in climate extremes in some parts of the world

considered to be very likely. Similarly, citing studies regarding changes in extreme precipitation events in the second half of the 20th century, the Working Group I (WGI) of IPCC (2007) suggested that increase in heavy and very heavy precipitation that are statistically significant had occurred despite of a decrease in the mean annual rainfall (Alpert et al., 2002; Groisman et al., 2004; Maheras et al., 2004 and others). Over North America, the WGI of IPCC (2013) noted that since the middle of the 20th century there is a high confidence of an overall increase in extreme precipitation events. Some studies also suggested that the frequency of precipitation for Canada had increased over the course of the 20th century although there is no identifiable trend in precipitation extremes (Akinremi et al., 1998; Zhang et al., 2001; Vincent and Mekis, 2006). However, recent extreme floods in some parts of Canada, such as the Alberta floods of 2005 and 2013 could be a harbinger for more frequent and extreme precipitation events in parts of North America over the course of the 21st century.

In contrast, Africa, a relatively dry and water scarce continent, has experienced more pronounced drought events during the late 20th century than flooding due to extreme precipitation events. Notable droughts that hit sub-Saharan Africa include, but are not limited to, severe droughts in West Africa during the 1970s and 1980s (Lamb, 1982), the 1983-85 drought event in Ethiopia (Africa Watch, 1991), the 2011 East African drought (Lyon, 2011) and the current 2015-16 severe drought in parts of eastern Ethiopia. In addition, precipitation and runoff trends had generally been negative for many large river basins in Africa leading to increased aridity in Africa (Dai, 2011a; Dai, 2011b). The observed drying trends in different parts of Africa are at times amplified by large scale climate anomalies such as El Niño Southern Oscillation (ENSO). Warm El Niño episodes and its cooler cousin La Niña are associated with a decrease (El Niño) or

an increase (La Niña) in precipitation over most of Africa (Lindesay and Vogel, 1990; Mason and Goddard, 2001; Lyon and Mason, 2007 and Ratnam et.al 2014). Historical records of ENSO activity extending back to 1871 show the dominance of La Niña events in pre-1920s while El Niño events were more prevalent in post-1960 (Wolter and Timlin, 2011). Since the last few decades of the 20th and early 21st century have been the warmest since instrumental records began (Stocker et.al, 2013), such a warming compounded by the higher frequency of recent El Niño events have exacerbated the frequency and severity of drought events in different parts of Africa.

In addition to increasing trends observed in the global mean temperature in 20th century, successive IPCC reports (IPCC, 2007; IPCC, 2013) have projected a significant increase in the global mean temperature if greenhouse gas emissions continue to increase unabated over the 21st century. As discussed above, climate change could lead to the occurrence of opposite hydrologic extremes in different parts of the world. While the increased water holding capacity of a warmer atmosphere could lead to higher frequency of extreme precipitation events (Trenberth, 1998; 1999) in some parts of the world such as North America, the increase in temperature could also lead to serious water scarcity and frequent and prolonged severe drought events in parts of Africa during the 21st century (Dai, 2011b). Climate change could therefore have profound socio-economic consequence globally and in particular for Africa, such adverse effects could be felt by millions during the 21st century.

1.2. Research Objectives

To more precisely analyze the impact of climate change on hydrologic extremes (floods and droughts) during the mid and late 21st century (2041-2100), the specific objectives of this research are

1. To analyze historical trends in Convective Available Potential Energy (CAPE) and extreme precipitation indices in the United States (US) and southern Canada.
2. To investigate the impact of climate change on extreme precipitation events in southern Alberta using dynamically downscaled projected climate data from Global Climate Models (GCMs) for the 2041-2070 (2050s) and 2071-2100 (2080s) period relative to the 1971-2000 base period.
3. To test the application of a relatively new machine learning algorithm for Regional Flood Frequency Analysis (RFFA) in eastern and western Canada for historical climate and for estimating possible changes to future flood quantiles in the 2050s and 2080s.
4. To investigate the potential impact of climate change on the frequency, persistency and average drought durations in sub-Saharan Africa during the mid and late 21st century.
5. To investigate the impact of historical ENSO events and the combined impact of ENSO and climate change on average drought severity in sub-Saharan Africa during the 2050s and 2080s.
6. To analyze the potential impact of climate change on water resources of four major river basins of Ethiopia in the mid and late 21st century as a case study for Africa.

1.3.Organization of Thesis

The Thesis is organized into seven chapters. Chapter 1 gives introduction, problem statement and the specific objectives of this research. Chapter 2 discusses trends in CAPE and extreme precipitation indices over the US and southern Canada for 1979-2013, while Chapter 3 presents possible impact of climate change on future extreme precipitation events of the Oldman, Bow and Red Deer River basins of Alberta. Chapter 4 provides a study on Regional Flood Frequency Analysis using Support Vector Regression under historical and future climate. Chapter 5 shows the impact of climate change and El Niño episodes on droughts in sub-Saharan Africa, and Chapter 6 gives the potential impact of climate change on water resources of four major rivers of Ethiopia. Finally the overall research summary, conclusions and recommendations are given in Chapter 7.

1.4. References

- Africa Watch, 1991: Evil days: 30 years of war and famine in Ethiopia. Africa Watch Rep., 381 pp. <https://www.hrw.org/sites/default/files/reports/Ethiopia919.pdf>
- Akinremi, O.O, McGinn, M.S., Cutforth, H.W. 1998. Precipitation trends in Canadian prairies. *J Climate*, 12: 2996-3003
- Alexander, L. V. and co-authors, 2006. Global observed changes in daily climate extremes of temperature and precipitation. *J Geophys. Res.*, 111: D05109, doi:10.1029/2005JD006290.
- Alpert, P., Ben-Gai, T., Baharad, A., Benjamini Y., Yekutieli, D., Colancio, M. Diodato, L., Ramis, C., Homar, V., Romero, R., Michaelides, S., Manes, A. 2002. The paradoxical increase of Mediterranean extreme daily rainfall in spite of decrease in total values. *J Geophys. Res – Letter*, 29: 31-1 to 31-4, doi: 10.1029/2001GL013554.
- Dai, A., 2011a, Characteristics and trends in various forms of the Palmer Drought Severity Index during 1900-2008. *J of Geophys. Res.*, 116: D12115, doi:10.1029/2010JD015541.
- Dai, A., 2011b, Drought under global warming: a review, *WIREs Clim Change*, 2:45-65, John Wiley and Son, DOI: 10.1002/wcc.81
- Groisman, P. Ya., Knight, R.W, Karl, T.R, Easterling, D.R, Sun, B. and Lawrimore, J.H. 2004. Contemporary Changes of the Hydrological Cycle over the Contiguous United States: Trends Derived from In Situ Observations. *J Hydrometeorology*, 5: 64-85.
- Lamb, P. 1982. Persistence of Subsaharan drought. *Nature*, 299: 46-47.
- Lindesay, J. A. and Vogel, C. H. 1990. Historical evidence for southern oscillation-southern Africa rainfall relationships. *Int. J of Climatology*, 10: 679-689.
- Lyon, B. 2014. Seasonal drought in Greater Horn of Africa and its increase during the March-May long rains. *J of Climate*, 27: 7953-7975. doi: 10.1175/JCLI-D-13-00459.1

- Lyon, B. and Mason, S. 2006. The 1997-98 summer rainfall season in southern Africa. Part I: Observations. *J of Climate*, 20: 5134-5148. doi: 10.1175/JCLI4225.1
- Maheras, P., Tolika, K., Anagnostopoulou, C., Vafiadis, M. Patrikas, I. and Flocas, H. 2004. On the relationship between circulation types and changes in rainfall variability in Greece. *Int J Climatology*, 24: 1695-1712, doi: 10.1002/joc.1088.
- Mason, S. J. and Goddard, L. 2001. Probabilistic precipitation anomalies associated with ENSO. *AMS, BAMS*, 82, no 4, 619-638.
- IPCC, 2013: Summary for Policymakers. In: *Climate Change 2013: The Physical Science Basis. Contribution of Working Group I to the Fifth Assessment Report of the Intergovernmental Panel on Climate Change* [Stocker, T.F., D. Qin, G.-K. Plattner, M. Tignor, S.K. Allen, J. Boschung, A. Nauels, Y. Xia, V. Bex and P.M. Midgley (eds.)]. Cambridge University Press, Cambridge, United Kingdom and New York, NY, USA.
- IPCC, 2007: *Climate Change 2007: The Physical Science Basis. Contribution of Working Group I to the Fourth Assessment Report of the Intergovernmental Panel on Climate Change* [Solomon, S., D. Qin, M. Manning, Z. Chen, M. Marquis, K.B. Averyt, M. Tignor and H.L. Miller (eds.)]. Cambridge University Press, Cambridge, United Kingdom and New York, NY, USA, 996 pp.
- Ratnam, J. V., Behera S.K., Masumoto and Yamagata, T. 2014. Remote effects of El Niño and Modoki events on the austral summer precipitation of southern Africa. *AMS, J of Climate*, 27: 3802-3815. doi: 10.1175/JCLI-D-13-00431.1
- Stocker, T.F., D. Qin, G.-K. Plattner, L.V. Alexander, S.K. Allen, N.L. Bindoff, F.-M. Bréon, J.A. Church, U. Cubasch, S. Emori, P. Forster, P. Friedlingstein, N. Gillett, J.M. Gregory, D.L. Hartmann, E. Jansen, B. Kirtman, R. Knutti, K. Krishna Kumar, P. Lemke, J.

- Marotzke, V. Masson-Delmotte, G.A. Meehl, I.I. Mokhov, S. Piao, V. Ramaswamy, D. Randall, M. Rhein, M. Rojas, C. Sabine, D. Shindell, L.D. Talley, D.G. Vaughan and S.-P. Xie, 2013: Technical Summary. In: *Climate Change 2013: The Physical Science Basis. Contribution of Working Group I to the Fifth Assessment Report of the Intergovernmental Panel on Climate Change* [Stocker, T.F., D. Qin, G.-K. Plattner, M. Tignor, S.K. Allen, J. Boschung, A. Nauels, Y. Xia, V. Bex and P.M. Midgley (eds.)]. Cambridge University Press, Cambridge, United Kingdom and New York, NY, USA.
- Tierney, J.E., Ummenhofer, C.C., and deMenocal, P.B. 2015. Past and future rainfall in Horn of Africa. *Sci. Adv.* 1. doi: 10.1126/sciadv.1500682
- Williams, A.P., and Funk, C. 2011. A westward extension of the warm pool leads to a westward extension of the Walker circulation, drying east Africa. *J of Clim Dyn.* 37: 2417–2435. doi: 10.1007/s00382-010-0984-y
- Trenberth, K. E. 1998. Atmospheric moisture residence time and cycling: Implication for rainfall rates and climate change. *J of Climatic Change*, 39: 668-694
- Trenberth, K. E. 1999. Conceptual framework for changes of extremes of the hydrological cycle with climate change. *Climatic Change*, 42: 327-339
- Vincent, L.A. and Éva Mekis. 2006. Changes in Daily and Extreme Temperature and Precipitation Indices for Canada over the Twentieth Century, *Atmosphere-Ocean*, 44:2, 177-193, doi: 10.3137/ao.440205.
- Wolter, K. and Timlin M.S. 2011. El Niño/Southern Oscillation behaviour since 1871 as diagnosed in an extended multivariate ENSO index (MEI.ext). *Int. J. Climatol.* 31: 1074–1087, DOI: 10.1002/joc.2336

Zhang, X., Hogg, W.D. and Mekis, E., 2001. Spatial and temporal characteristics of heavy precipitation events over Canada. American Meteorological Society, J Climate, vol 14, pp 1923-1936.

Chapter 2 Trends in Convective Available Potential Energy (CAPE) and extreme precipitation indices over the United States and southern Canada for summer 1979-2013 period.

2.1 Introduction

Convective Available Potential Energy (CAPE) is one of the widely used indicators on meteorological conditions favorable for the occurrence of intense precipitation events (Seeley and Romps, 2015). CAPE, (Equation 2.1, and Figure 2.1) is the vertical integral of parcel buoyancy between the level of free convection and the level of neutral buoyancy (Ye et.al 1997), has been widely used to measure the onset of convection such that higher values of CAPE in Joules/kg indicate favorable conditions for severe convective storms and tornado events (Rasmussen and Blanchard, 1998; Brooks et al, 2003; Doswell and Evans, 2003; Brooks et al, 2007). CAPE and its opponent parameter, Convective Inhibition (CI) are used to analyze convective precipitation variability, and trends in CAPE data of a region could be used to identify changes in convective systems of that region (Murugavel et al, 2012; Riemann-Campe et al, 2008).

$$CAPE = \int_{LFC}^{LNB} R_d (T_{vp} - T_{ve}) d \ln(P)$$

where:

T_{vp} = virtual temperature of air parcel

T_{ve} = virtual temperature of environment of the air parcel (2.1)

LFC = Level of Free Convection

LNB = Level of Neutral Buoyancy

R_d = Gas constant of dry air

P = Pressure

Studies by the Intergovernmental Panel on Climate Change (IPCC) suggest that the global mean surface temperature has been increasing since instrumental records began in late 19th century and the past three decades have been the warmest of any of the previous decades (IPCC, 2013). This increase in global mean temperature has mainly been attributed to an increase in anthropogenic greenhouse gas emissions and it is likely to lead to more frequent and severe extreme hydrologic events occurring across the world, which has already been observed in recent decades (IPCC, 2013). In addition, previous studies have also detected statistically significant increase in the frequency of heavy and very heavy precipitation events in different parts of the world (Alpert et al., 2002; Groisman et al., 2004; Maheras et al., 2004). Since CAPE is a proxy for amenable conditions leading to the occurrence of extreme weather events (Rasmussen and Blanchard, 1998; Brooks et al, 2003; Doswell and Evans, 2003; Brooks et al, 2007) recent changes in the global climate could also manifest itself with increasing or decreasing trends of CAPE in different parts of the world.

Previous studies analyzing CAPE data derived from radiosonde records have detected statistically significant trends in different parts of the world during late 20th and early 21st century. For instance, Meukaleuni et al (2016) detected significant trends in CAPE data in parts of West Africa for 1979-2014 with the largest increase in CAPE occurring in the Congo basin during the January to March season. Similarly, Murugavel et al. (2012) detected an increase in the monsoon rainfall and CAPE over the Indian region in 1984-2008 and suggested that a large increase in CAPE over this region could increase the frequency of its extreme rainfall events. Based on six hourly ERA-40 reanalysis data of the European Centre for Medium-Range Weather Forecast (ECMWF), Riemann-Campe et al (2009) found a high variability of CAPE in the

Tropics and a general increasing trend over 1958-2001. Their results agree with that of DeMott and Randall (2004) who analyzed CAPE data derived from tropical radiosonde stations and found a slightly higher number of stations with increasing trends in CAPE with the greatest concentrations of positive trends occurring in the western Pacific and Caribbean. Recent studies suggested an increase in CAPE correspond to rising Sea Surface Temperatures (SST) (Seeley and Romps, 2015) and a strong dependency of CAPE on the specific humidity (Riemann-Campe et al, 2009). The projected global warming of the 21st century will likely lead to an increase in SST and specific humidity globally, and given the positive relationship between CAPE and SST, this could lead to higher values of CAPE, and extreme weather events are expected to occur more frequently in the future.

The objective of this study is to identify trends in CAPE values over United States and southern Canada for the summer of 1979-2013, and if they correspond to trends in single or multiple event extreme precipitation, average surface temperature and surface specific humidity over this period. With this introduction, study area, data and methodology are given in Section 2.2, results and discussions in Section 2.3 and conclusions in Section 2.4.

2.2 Study area, data and methodology

2.2.1 Study area

North America is the third largest continent in the world, with the United States and Canada covering more than 80% of its landmass. With its landmass extending from around 10° north of the Equator to the North Pole, the climate of North America ranges from equatorial and humid subtropical in parts Mexico and southeastern United States (US) to bitter cold in the Canadian

Arctic. In addition, its climatic variability is also influenced by elevation ranging from the high mountain peaks of the Rockies to the vast expanses of the Great Plains in central US and Canada and the coastal lowlands of southern and eastern US (Figure 2.2). The characteristic of precipitation climatology varies significantly across the US and southern Canada, which are the focus of this study. The western parts of Oregon and Washington states in the US and the province of British Columbia in Canada receive significant amount of orographic precipitation between October and May while convective and cyclonic (frontal) precipitations dominate the May to September season of the Great Plains, the Atlantic and Gulf coast regions, respectively. Temperature is dependent on latitude and elevation with southern parts of the US having warmer temperature compared to the Rockies and southern Canada. Overall, with the exception of some areas, US and southern Canada are progressively drier moving west from the Atlantic to the Pacific coast, and considerably warmer moving from southern Canada to southern US (Figure 2.2).

2.2.2 Data

The monthly CAPE data used in this study was derived from the North American Land Data Assimilation System-phase 2 (NLDAS-2), a collaborative project among several research institutes in the United States including NCEP's (National Center for Environmental Prediction), Environmental Modeling Center (EMC), Princeton University and others (Mitchell et al, 2004; Xia et al, 2012). NLDAS-2 assimilates a large quantity of observation and model reanalysis data. NLDAS-2 data has been validated against observations and the final product is available at 0.125° spatial resolution over central North America. CAPE data in NLDAS-2 is interpolated from the NCEP's North America Regional Reanalysis (NARR) data. NARR data is generated

using, among others, lateral boundary conditions from NCEP-DOE R-2 reanalysis data (Kanamitsu et al, 2002), NCEP's operational version of Eta regional climate model (Mesinger, 2000) and some observed climate data assimilation systems. Because it assimilates observed data from climate stations, NARR can be considered as a pseudo-observation dataset. Similarly, monthly specific humidity data at various pressure levels is also derived from the NARR dataset. In addition, observed daily precipitation and temperature data for stations across continental US and southern Canada were collected from the Global Historical Climatology Network (GHCN)-Daily, which is a processing system for the official archive of US daily data. GHCN also incorporates quality assured data from over 80,000 stations in over 180 countries (Menne et al, 2012). Monthly and seasonal precipitation and temperature data over the US and southern Canada are computed from daily data of GHCN stations.

2.2.3 Research Methodology

Changes in CAPE and extreme precipitation over North America were mainly analyzed for the June-August (summer) season because primarily this is a period of high CAPE values and frequent convective storms occurring over much of US and southern Canada. The increasing or decreasing trend magnitudes in CAPE, extreme precipitation, surface temperature and specific humidity were estimated using the nonparametric Theil-Sen (Theil, 1950; Sen, 1968) regression estimator, a robust technique to determine trends of time series (Wilcox, 1998a; 1998b). Statistical significance of seasonal trends at $p < 0.05$ were tested using the nonparametric Mann-Kendall test (Mann, 1945; Kendall, 1975), which is a robust trend analysis tool because it is capable of handling seasonality, missing values and nonnormality in a time series (Hirsch et al, 1982; Gan et al, 2013). Only those GHCN stations with less than 0.5% of missing precipitation

or temperature data for the summer of 1979-2013 were selected for trend analysis in the US region. However, to have more stations for analysis, this selection criterion is slightly more lenient for southern Canada, and GHCN stations with less than 1% of the recorded data missing were selected for analysis. Changes in extreme precipitation at these GHCN stations were analyzed using extreme precipitation indices of the Expert Team on Climate Change Detection and Indices (ETCCDI) (Klein Tank, 2009). The indices selected in this study represent single or multiple event extreme precipitation events, such as the RX1day (the highest precipitation amount in one-day), RX5day (the highest precipitation amount in five-day period) and R20mm (the number of days where daily precipitation exceeded 20 mm). Each of these indices was computed for the summer season of a given year to analyze trends in extreme events for 1979-2013 over US and southern Canada. Besides changes in CAPE and extreme precipitation, trends in the average surface temperature at GHCN stations and surface specific humidity derived from NARR data were also computed.

2.3 Discussions of Results

2.3.1 Spatial and seasonal CAPE variability

The long-term mean of summer CAPE data for 1979-2013 has significant spatial variability across US and southern Canada, with the maximum summer CAPE values located along the Atlantic and Gulf coast and gradually decrease as we move inland to the Great Plains (Figure 2.3). Compared to coastal areas, e.g. Florida, CAPE values are significantly lower in mountainous regions such as the Rockies and surrounding foothills where orographic precipitation dominates (Figure 2.2). Similarly, with its cooler climate, southern Canada has also

lower CAPE compared to the warm, subtropical coastal plains of southeastern US. Annually, CAPE reaches the maximum in the warm summer of June-July-August which is also a period of intense convective storms over much of the US and southern Canada (Figure 2.3).

2.3.2 Trends in summer CAPE and extreme precipitation indices

For the summer season of 1979-2013, large statistically significant increasing trends in CAPE were detected in the low laying areas near the Gulf and Atlantic coasts, particularly in southern Florida and southern Texas (Figure 2.4). However, within the same region, significant decreasing trends were also detected for parts of northern Texas, Louisiana, Oklahoma and Arkansas. In addition, for much of the Great Plains of the US, there was a statistically significant decreasing trend in CAPE reaching up to 15 Joules/kg/year in southern parts of the Great Plains. Other than the Atlantic, Gulf coastal plains and the Great Plains, a slight decreasing trend in CAPE was detected for almost all of central and western US and parts of southern Canada. In contrast, statistically significant increasing trends in CAPE were detected for much the north Atlantic coast of the US, the Great Lakes region and parts of southern Ontario and Québec. Similarly, moderate increasing trends in CAPE were also detected in some parts of southern Alberta and parts of southern Saskatchewan and Manitoba.

Trends in extreme precipitation indices, namely, RX1day, RX5day and R20mm for 1979-2013 are shown in Figure 2.5. The spatial distribution of GHCN stations for which an increasing or decreasing trend in extreme precipitation indices was detected is similar to the spatial distribution of detected trends in CAPE data (Figure 2.4 and Figure 2.5). Generally, increasing precipitation indices dominate the eastern Atlantic coast of the US for all extreme precipitation

indices analyzed in this study. In addition, increasing trends in RX1day, RX5day and R20mm were also detected in southeastern Atlantic and Gulf coastal plains of the US, namely Florida, Georgia, Alabama, northern Texas etc., parts of the US mid-west and Great Lakes region and even areas in southern Alberta. In most of these areas, increasing trends were also detected in CAPE values as shown in Figure 2.4. On the other hand, decreasing trends were mainly detected for the Great Plains region, parts of southern Texas and the US mid-west and most parts of western US which is also in agreement with the detected decreasing trends in CAPE within these regions. For the mountainous region of western US where summer CAPE values are small (Figure 2.2 and Figure 2.3), either very small or no increasing or decreasing trends were detected in extreme precipitation indices.

The detected trends in extreme precipitation in terms of R20mm for the summer 1979-2013 across the study area show obvious spatial variability. Increasing trends in the summer R20mm were detected for eastern US, particularly the Atlantic coast and Gulf of Mexico region. In addition some parts of the Canadian prairies, such as southern Alberta, also show marginal increasing trends in R20mm. On the other hand, decreasing trends were limited to some parts of south and mid-west regions of US, while much of western US, where convection plays little role in its summer precipitation climatology, had no trend detected for R20mm. The spatial variations of trends in RX1day and RX5day are also very similar to that of R20mm. For areas east of the Great Plains where convective and cyclonic precipitation dominate the summer rainfall, increasing trends up to 14 mm/decade for single storm events (RX1day) and up to 24 mm/decade for multiple extreme storm events (RX5day) were detected. Similar to R20mm, most of the decreasing trends in RX1day and RX5day were in the Great Plains region and central US whereas only marginal decreasing or increasing trends were detected for GHCN stations west of

the Rockies where orographic precipitation dominates. On a whole, statistically significant trends were only detected for about 5.2% (RX1day), 6.7% (RX5day) and 2.7% (R20mm) of GHCN stations in US and southern Canada analyzed in this study.

In summary, results from the trend analysis of CAPE and extreme precipitation indices suggest that there has been an increasing trend in CAPE and extreme precipitation particularly in eastern US. In addition, an increasing trend was also detected in CAPE and extreme precipitation indices in Canadian prairies, such as parts of southern Alberta which recently has suffered some of the worst floods ever recorded. Areas within and around the Great Plains of US, and some parts of southern US were mainly dominated by decreasing trends in CAPE and extreme precipitation indices.

2.3.3 Trends in summer temperature and surface specific humidity

Because the rate of depletion of moisture from the atmosphere, via rainfall, far exceeds its rate of replenishment, via local surface evaporation and atmospheric moisture transported from elsewhere, the increased water-holding capacity of a warmer atmosphere will likely favor a general increase in the occurrence of extreme precipitation events (Trenberth, 1999). Given the increasing trends in CAPE and extreme precipitation indices over the summer of 1979-2013, trends in the average surface temperature and surface specific humidity which influence the evolution of convective precipitation have also been analyzed. In almost all parts of the US and southern Canada, increasing trends of up to 1.35 °C/decade were detected in the average summer temperature with about 35% of the detected increasing trends at the GHCN stations being statistically significant at $p < 0.05$. However, decreasing trends were also detected for a few

stations around the US Great Plains and the Pacific coast of California although only 5% of the detected decreasing trends were statistically significant (Figure 2.6). Similarly, increasing trends in the surface specific humidity were also detected for almost all parts of southern Canada and most parts of eastern US, but the Rockies in southern US and the Great Basin region bordering Sierra Nevada mountain ranges of California (Figure 2.2) showed decreasing trends in surface specific humidity (Figure 2.6).

Based on the Clausius-Clapeyron relationship, changes in saturation vapor pressure of the atmosphere with respect to changes in temperature can be represented as:

$$\frac{\Delta e_s}{e_s} \approx \gamma \Delta T, \quad \gamma = \frac{L}{R_v T^2}$$

where:

e_s = Saturation vapor pressure

L = Latent heat of vaporization
 $(\approx 2.47 \times 10^6 \text{ J} \cdot \text{kg}^{-1}$ for water vapor) (2.2)

R_v = Gas constant
 $(\approx 461.5 \text{ J} \cdot \text{K}^{-1} \cdot \text{kg}^{-1}$ for water vapor)

T = Temperature in K

For a $\frac{\Delta T}{T} \ll 1$, $\gamma \approx 0.05 - 0.07 \text{ K}^{-1}$ which is approximately 7% increase in vapour pressure per degree Kelvin rise in temperature, termed as the Clausius-Clapeyron (C-C) rate. Recent studies have used the C-C rate to analyze the impact of higher surface temperatures on the intensification of extreme precipitation events. For instance, Lenderink and van Meijgaard (2008) analyzed 99 years of quality controlled 1-hour precipitation observations at De Bilt, the Netherlands, and found that hourly extreme rainfall intensities increase twice as fast with rising temperatures as expected from the C-C rate particularly during the summer season when daily

mean temperatures average more than 12 °C. On the other hand, daily extreme rainfall intensities were found to increase at a slower rate with temperature although there appears to be a steep increase in daily rainfall intensities for temperatures above 22 °C. For Germany, Berg et al (2013) found that the increase in higher percentiles of convective precipitation intensities substantially exceeded the C-C rate for an increase in daily mean temperatures above 10 °C while stratiform precipitation intensities generally increased at about the C-C rate. Similarly, for parts of Eastern US, Utsumi et al (2011) found that extreme daily precipitation intensities increased with temperature up to a peak-point temperature threshold (T_a) and then decreased with further increase in T_a . From our analysis in Sections 2.3.2 and 2.3.3, the detected increasing trends in temperature and specific humidity for most parts of eastern US and southern Canada complement the increasing trends in CAPE and extreme precipitation indices in these regions. Given that surface temperatures influence the latent heat release which drives the upward motion of moist air in convective precipitation (Lenderink and van Meijgaard, 2008) and also the strong dependency of CAPE on the surface specific humidity (Riemann-Campe et al, 2009) as depicted in the very high spearman correlation between the two variables in almost all parts of the US and southern Canada (Figure 2.5(d)), increasing trends in surface temperature and specific humidity could be responsible for much of the detected increase in extreme precipitation indices and CAPE over eastern US and parts of southern Canada where summer precipitation is mainly convective. Although increasing trends in surface temperatures are also detected in the mainly mountainous western US, such increasing trends in temperature were not mirrored with an increase in precipitation extremes since the precipitation in this region is mainly orographic rather than convective. These results also suggest that for the remaining course of the 21st century, the increase in temperature which contemporary GCMs (Global Climate Models)

overwhelmingly project would likely mean that we will witness more extreme precipitation events in eastern US and parts of southern Canada.

2.4 Conclusions and Recommendations

Analysis of the 1979-2013 North American summer CAPE data show an increasing trend in areas along the Atlantic and Gulf coastal plains, eastern and northern Atlantic coast of the US, the Great Lakes region, parts of southern Ontario and Québec and also some parts of southern Alberta, Saskatchewan and Manitoba. Similarly, for the same period, increasing trends were also detected in single or multiple event extreme precipitation indices (RX1day, RX5day and R20mm) over much of eastern US and south-eastern Canada, parts of the Atlantic and Gulf coastal plains and some parts of southern Alberta and Saskatchewan. In contrast, most parts of the US Great plains and areas west of the Rockies had decreasing trends in both CAPE and extreme precipitation indices. Trends in average temperature show that there has been an increasing trend in the summer temperature over most of the US and southern Canada with some stations having an increasing trend as high as 1.35 °C per decade. Similarly, increasing trends in the summer surface specific humidity were also found for almost all parts of southern Canada, eastern US and the Atlantic and Gulf coast regions. Given that an increase in surface temperature could lead to the intensification of extreme precipitation events (Lenderink and van Meijgaard, 2008; Berg et al, 2013; Utsumi et al, 2011), the observed increase in surface temperatures coupled with the increase in surface specific humidity could be the major cause for increasing trends observed in extreme precipitation indices and CAPE over much of eastern US and some parts of southern Canada for the summer of 1979-2013. If the observed increasing trends in temperature and specific humidity in these regions also extend through the course of the 21st

century, areas in eastern US and parts of southern Canada could experience even more intensive extreme precipitation events.

Future works could use CAPE computed from homogenized dew point depression (DPD) data from various radiosonds across the globe (Dai et al., 2011) and bias corrected temperature from ERA-Interim reanalysis. Unlike NLDAS-2 data which can be affected by noise due to inhomogeneities in radiosonde measurements, homogenized DPD (Dai et al., 2011) and bias corrected temperature from ERA-Interim reanalysis could give more accurate CAPE values over the US and southern Canada. In addition, NLDAS-2 CAPE and specific humidity data could be screened for noise using, say, the Savitzky–Golay filter, which has been used to adjust erroneous NDVI observations during cloudy days or in poor atmospheric conditions (Chen et al. 2004) or other filters.

Acknowledgements

This project was funded by the Natural Science and Engineering Research Council of Canada, and the first author was partly funded by the University of Alberta.

2.5 References

- Alpert, P., Ben-Gai, T., Baharad, A., Benjamini Y., Yekutieli, D., Colancio, M. Diodato, L., Ramis, C., Homar, V., Romero, R., Michaelides, S., Manes, A. 2002. The paradoxical increase of Mediterranean extreme daily rainfall in spite of decrease in total values. *J Geophys. Res – Letter*, 29: 31-1 to 31-4, doi: 10.1029/2001GL013554.
- Berg, P., Moseley, C., and Haerter, J. O. 2013. Strong increase in convective precipitation in response to higher temperatures. *Nature Geoscience, Letters*, 6, 181-185. doi: 10.1038/NGEO1731
- Brooks, H. E., Lee, J. W. and Craven, J. P. 2003. The spatial distribution of severe thunderstorm and tornado environments from global reanalysis data. *Atmos. Res.* 67-68, 73-94, doi:10.1016/S0169-8095(03)00045-0.
- Brooks, H. E., Anderson, A. R., Riemann, K., Ebberts, I., and Flachs, H. 2007. Climatological aspects of convective parameters from the NCAR/NCEP reanalysis. *Atmos. Res.* 83, 294-305, doi:10.1016/j.atmosres.2005.08.005
- Chen, J., Jönsson, P., Tamura, M., Gu, Z., Matsushita, B., Eklundh, L. 2004. A simple method for reconstructing a high-quality NDVI time-series data set based on the Savitzky–Golay filter, *Rem. Sens. Env.*, Vol. 91 (3–4), 332-344, doi.org/10.1016/j.rse.2004.03.014
- Dai, A., Wang, J., Thorne, P., Parker, D., Haimberger, L., and Wang, X., 2011, A New Approach to Homogenize Daily Radiosonde Humidity Data, *J Climate*, 965-991, DOI: 10.1175/2010JCLI3816.1
- DeMott, C. A. and Randall, D. A. 2004. Observed variations of tropical convective available potential energy. *J Geophys. Res.*, 109, D02102, doi:10.1029/2003JD003784.

- Doswell III, C. A., and Evans, J. S. 2003. Proximity sounding analysis for derechos and supercells: and assessment of similarities and differences. *Atmos. Res* 67-68, 117-113, doi:10.1016/S0169-8095(03)00047-4
- Gan, T. Y., Barry, R. B., Gizaw, M., Gobena, A., Balaji, R. 2013. Changes in North American snowpacks for 1979–2007 detected from the snow water equivalent data of SMMR and SSM/I passive microwave and related climatic factors. *J Geophys. Res, Atm.* 118, 7682–7697, doi:10.1002/jgrd.50507.
- Groisman, P. Ya., Knight, R.W, Karl, T.R, Easterling, D.R, Sun, B. and Lawrimore, J.H. 2004. Contemporary Changes of the Hydrological Cycle over the Contiguous United States: Trends Derived from In Situ Observations. *J Hydrometeorology*, 5: 64-85.
- Hirsch, R. M., Slack, J. R., and Smith, R. A. 1982. Techniques of trend analysis for monthly water quality data, *Water Resour. Res.*, 18(1), 107–121.
- IPCC, 2013: Chapter 2. Hartmann, D.L., A.M.G. Klein Tank, M. Rusticucci, L.V. Alexander, S. Bronnimann, Y. Charabi, F.J. Dentener, E.J. Dlugokencky, D.R. Easterling, A. Kaplan, B.J. Soden, P.W. Thorne, M. Wild and P.M. Zhai, 2013: Observations: Atmosphere and Surface. In: *Climate Change 2013: The Physical Science Basis. Contribution of Working Group I to the Fifth Assessment Report of the Intergovernmental Panel on Climate Change* (Stocker, T.F., D. Qin, G.-K.Plattner, M. Tignor, S.K. Allen, J. Boschung, A. Nauels, Y. Xia, V. Bex and P.M. Midgley (eds.)). Cambridge University Press, Cambridge, United Kingdom and New York, NY, USA.
- Kanamitsu, M., Ebisuzaki W., Woollen, J., Yang, S., Hnilo, J. J., Fiorino, M., and Potter, G. L. 2002. NCEP-DOE AMIP-II REANALYSIS (R-2). *AMS, BAMS*, 1631-1643, doi: 10.1175/BAMS-83-11-1631

- Kendall, M. G. (1975), Rank Correlation Methods, pp. 272, Charles Griffin, London.
- Lenderink, G. and van Meijgaard, E. 2008. Increase in hourly precipitation extremes beyond expectations from temperature changes. *Nature Geoscience, Letters*, 1, 511-514, doi:10.1038/ngeo262
- Mann, H. B. 1945. Nonparametric tests against trend, *Econometrica*, 13, 245–259.
- Maheras, P., Tolika, K., Anagnostopoulou, C., Vafiadis, M. Patrikas, I. and Flocas, H. 2004. On the relationship between circulation types and changes in rainfall variability in Greece. *Int J Climatology*, 24: 1695-1712, doi: 10.1002/joc.1088.
- Menne, M. J., Durre, I., Vose, R. S., Gleason, B. E., and Houston, T. G. 2012: An overview of the Global Historical Climatology Network-Daily Database. *Journal of Atmospheric and Oceanic Technology*, 29, 897-910, doi:10.1175/JTECH-D-11-00103.1
- Mesinger, F. et al 2006. North American Regional Reanalysis. *AMS, BAMS*, 340-360. DOI:10.1175/BAMS-87-3-343
- Meukaleuni, C., Lenouo, A., and Monkam, D. 2016. Climatology of convective available potential energy (CAPE) in ERA-Interim reanalysis over West Africa. *Atmos. Sci. Let.* 17: 65–70, DOI: 10.1002/asl.601
- Mitchell, K. E., et al. 2004. The multi-institution North American Land Data Assimilation System (NLDAS): Utilizing multiple GCIP products and partners in a continental distributed hydrological modeling system, *J. Geophys. Res.*, 109, D07S90, doi:10.1029/2003JD003823.
- Murugavel, P., Pawar, S. D., and Gopalakrishnan V. 2012. Trends of Convective Available Potential Energy over the Indian region and its effect on rainfall. *RMS, Int. J. Climatol.* 32: 1362–1372. DOI: 10.1002/joc.2359

- Rasmussen, E. N. and Blanchard, D. O. 1998. A Baseline Climatology of Sounding-Derived Supercell and Tornado Forecast Parameters. *AMS, Weather and Forecasting*, 13, 1148-1164.
- Riemann-Campe, K., Fraedrich, K., and Lunkeit, F. 2009. Global climatology of Convective Available Potential Energy (CAPE) and Convective Inhibition (CIN) in ERA-40 reanalysis. *Atmos. Res* 93, 534-545, doi:10.1016/j.atmosres.2008.09.037
- Seeley, J. T., and Romps, D. M. 2015. Why does tropical convective available potential energy (CAPE) increase with warming? *Geophys. Res. Lett.*, 42, 10,429–10,437, doi:10.1002/2015GL066199.
- Sen, P. K. 1968. Estimate of the regression coefficient based on Kendall's tau. *Journal of the American Statistical Association* 63, 1379-1389.
- Theil, H. 1950. A rank-invariant method of linear and polynomial regression analysis. *Indagationes Mathematicae* 12, 85-91.
- Trenberth, K.E. 1999. Conceptual framework for changes of extremes of the hydrological cycle with climate change. *Climatic Change*, 42: 327-339
- Utsumi, N., Seto, S., Kanae, S., Maeda, E. E., and Oki, T. 2011. Does higher surface temperature intensify extreme precipitation? *Geophys. Res. Lett.*, 38, L16708, doi:10.1029/2011GL048426
- Wilcox, R. R. 1998a. A Note on the Theil-Sen regression estimator when the regressor is random and the error term is heteroscedastic. *Biometrical Journal* 40, 3, 261-268
- Wilcox, R. R. 1998b. Simulations on the Theil-Sen regression estimator with right-censored data. *Statistics & Probability Letters* 39, 43-47

- Xia, Y., et al. 2012. Continental-scale water and energy flux analysis and validation for the North American Land Data Assimilation System project phase 2 (NLDAS-2): 1. Intercomparison and application of model products, *J. Geophys. Res.*, 117, D03109, doi:10.1029/2011JD016048.
- Ye, B., Geno, A, Lo, K., 1998. CAPE variation in the current climate and in a climate change. *J of Climate*, Vol 11, pp 1997-2015.

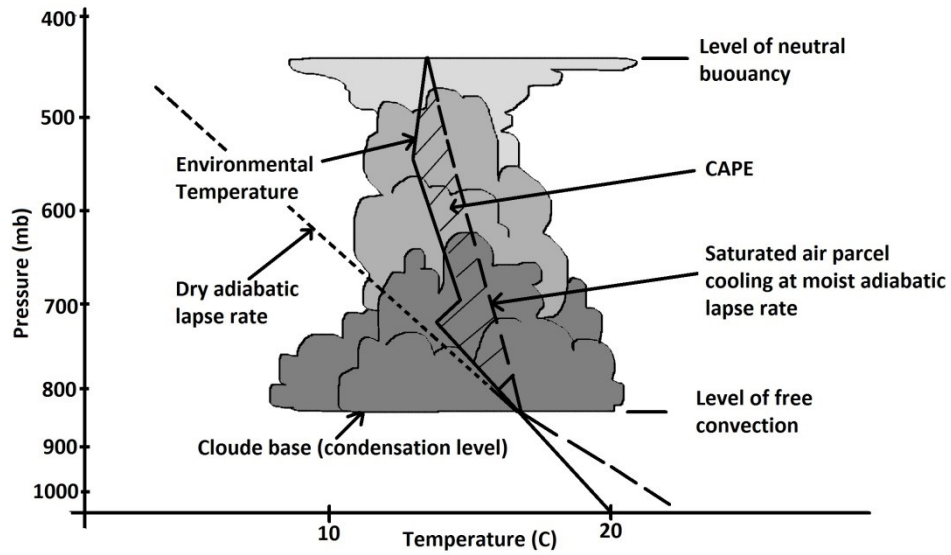


Figure 2.1 Graphical representation of Convective Available Potential Energy (CAPE) (adapted from <https://bmtc.moodle.com.au/mod/book/tool/print/index.php?id=3765>).

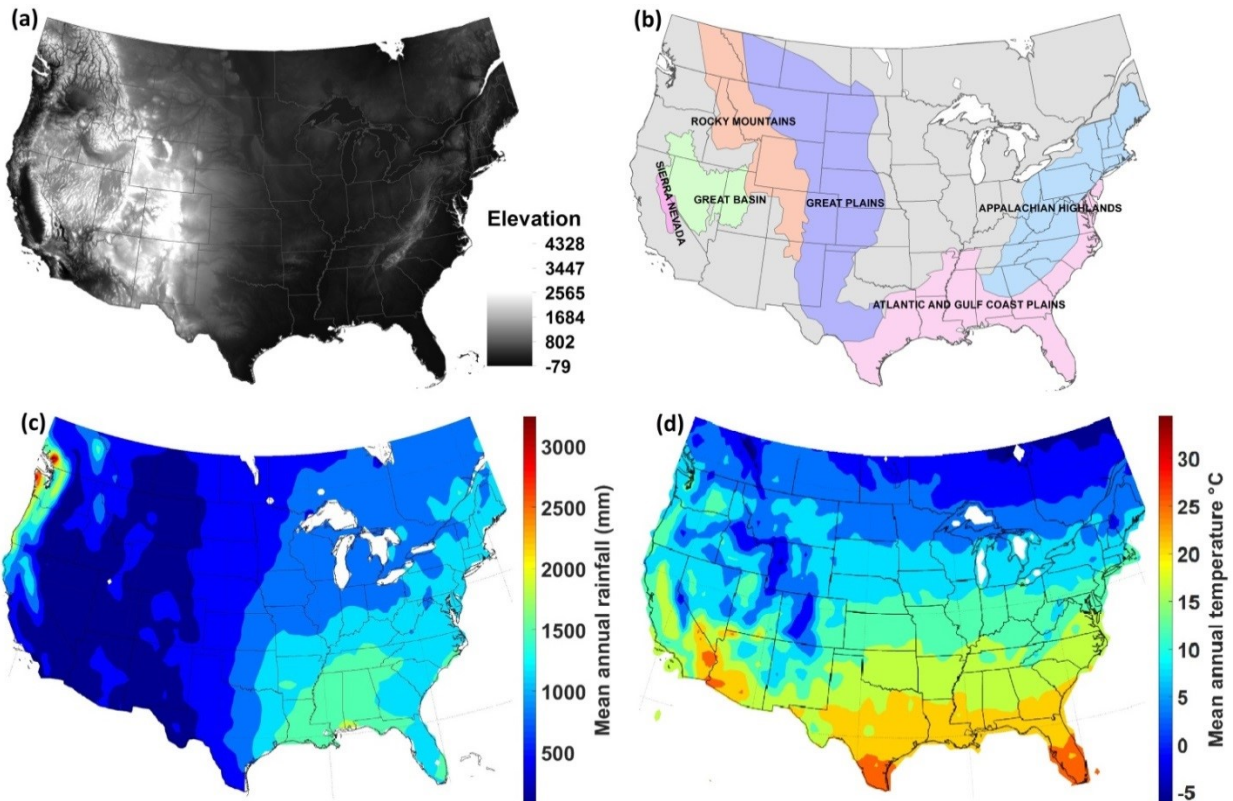


Figure 2.2 (a) 30 arc second digital elevation model of the US and southern Canada, (b) prominent landscapes of US and southern Canada, (c) and (d) mean annual precipitation and temperature derived from GPCP and GHCN-CAMS gridded observational datasets, respectively, for 1971-2000 period.

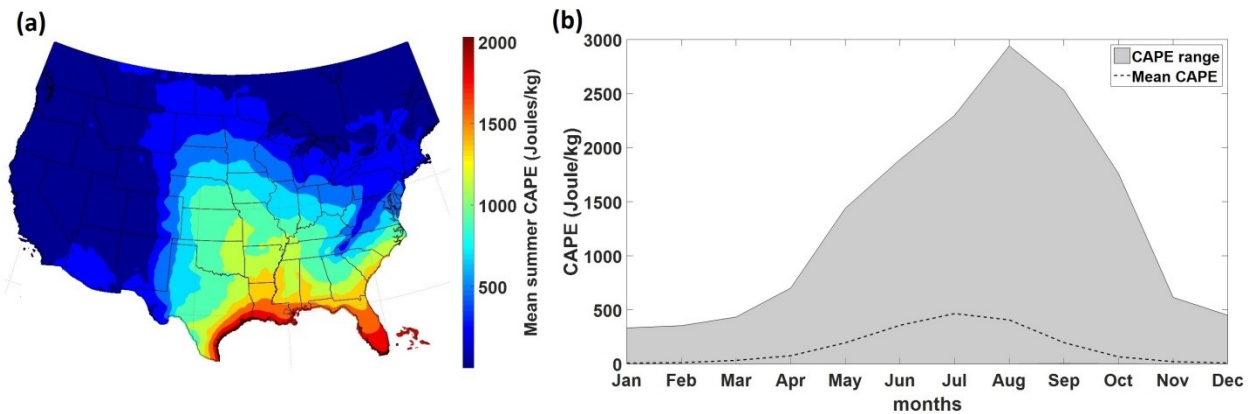


Figure 2.3 (a) Mean summer (June-August) CAPE for 1979-2013 period, (b) Mean annual CAPE values over US and southern Canada, the gray area shows the range of CAPE data while the dotted line shows the mean annual profile of CAPE over the region.

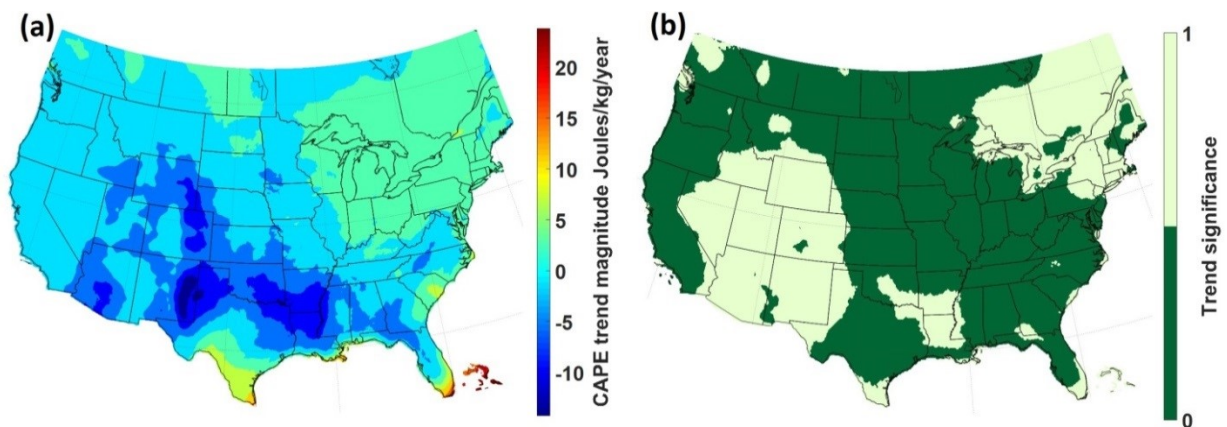


Figure 2.4 Trends in CAPE data for the summer of 1979-2013 period. (a) trends in CAPE in Joules/kg/year, (b) significance of trends at $p < 0.05$.

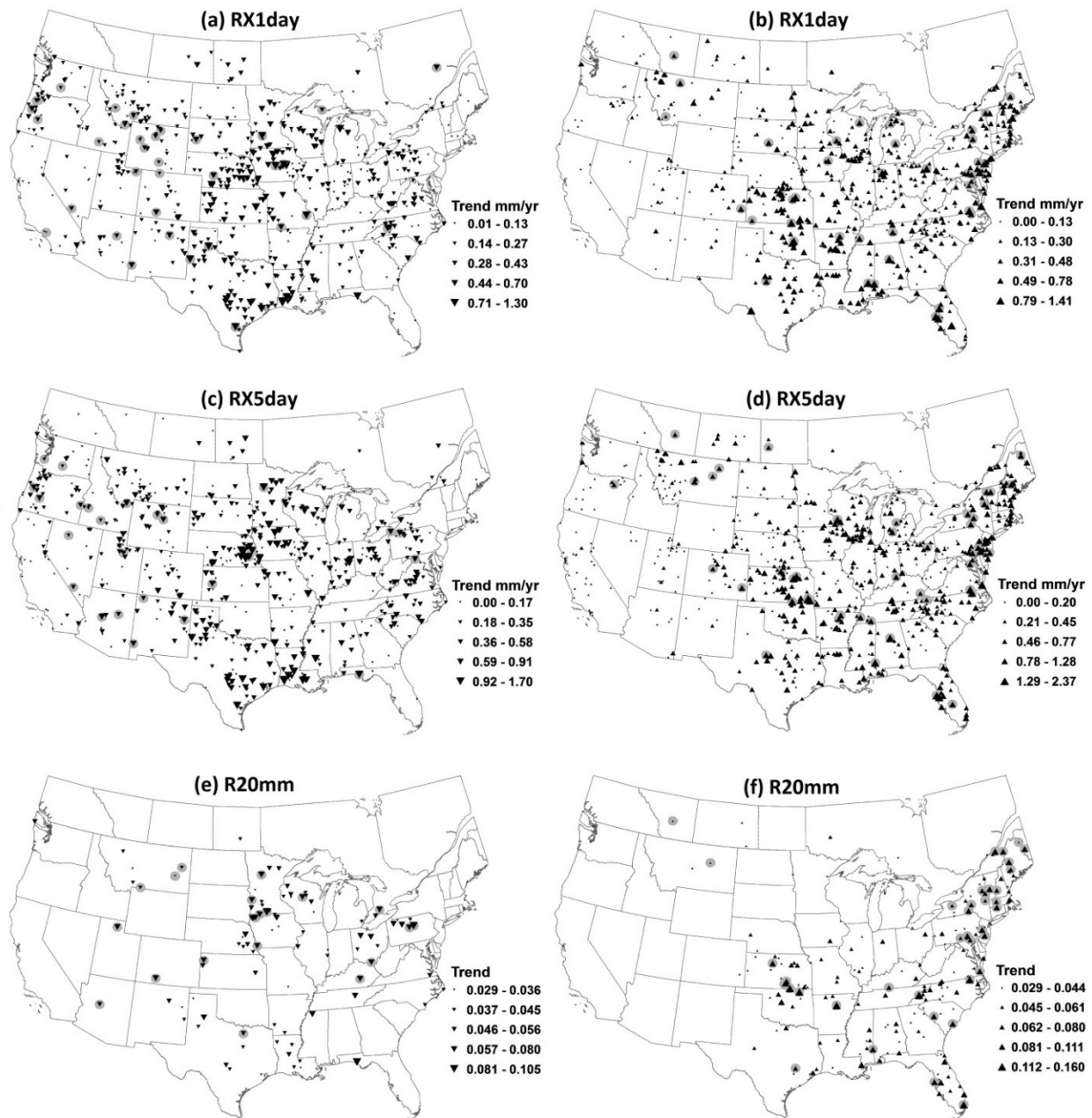


Figure 2.5 Trends in extreme precipitation indices for 1979-2013 summer period for US and southern Canada. (a), (c) and (e) show decreasing trends at GHCN stations for RX1day, RX5day and R20mm, respectively while (b), (d) and (f) show increasing trends at GHCN stations for the same variables. Grey circles indicate trends that are statistically significant.

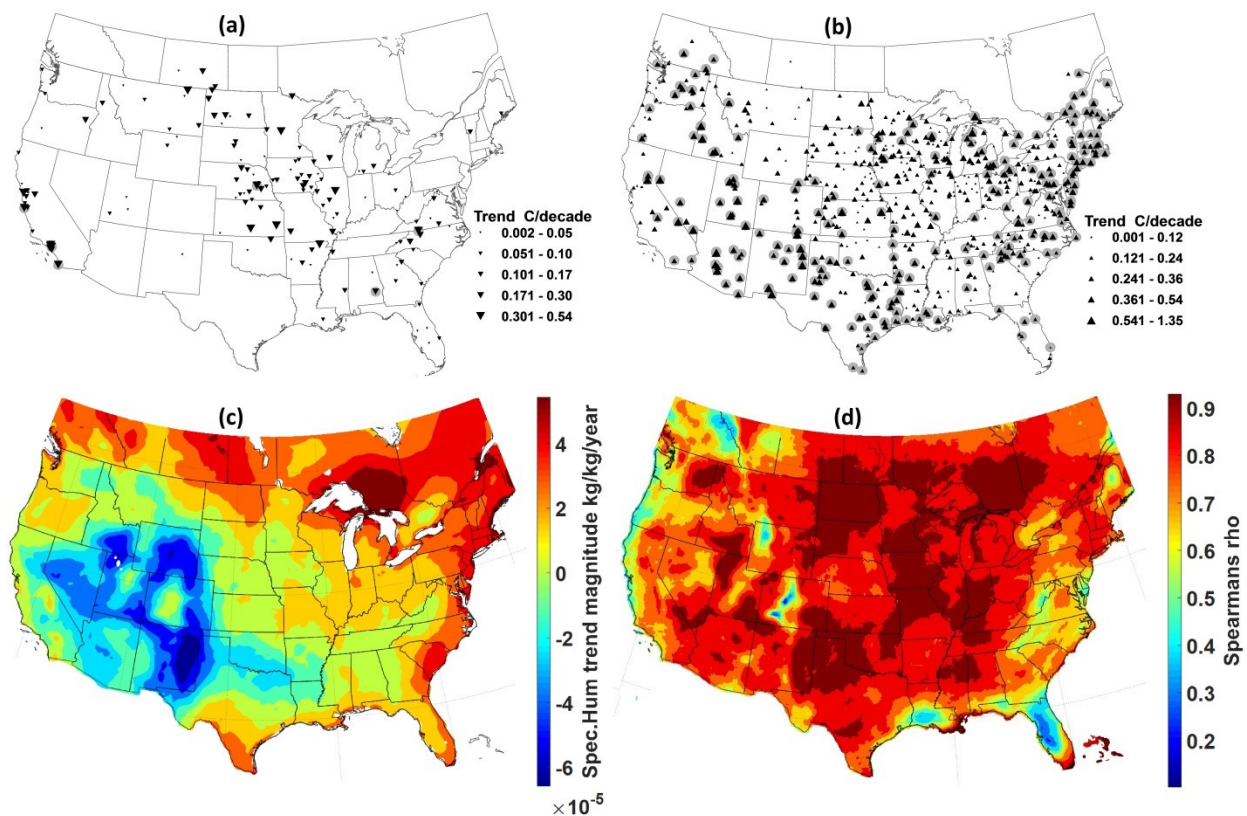


Figure 2.6 Trends in average surface temperature and surface specific humidity for the 1979-2013 summer period of US and southern Canada (a) decreasing trends in average temperature at GHCN stations, (b) increasing trends in average surface temperature at GHCN stations, (c) trends in surface specific humidity, (d) spearman rank correlation between CAPE and surface specific humidity. Grey circles in (a) and (b) indicate trends that are statistically significant.

Chapter 3 Possible Impact of climate change on future extreme precipitation of the Oldman, Bow and Red Deer River Basins of Alberta

3.1 Introduction

The South Saskatchewan River Basin (SSRB) in Alberta comprises of the Red Deer River Basin (RRB), Bow River Basin (BRB), Oldman River Basin (ORB) and South Saskatchewan River Basin with a total watershed area of 121,095 km² (Alberta Environment and Sustainable Resource Development AESRD). In terms of area, ORB occupies 22%, BRB occupies for 21% and RRB occupies 41% of the area of SSRB. Since most of the agriculture of Alberta is located in SSRB, water withdrawal in these three river basins, i.e. ORB, BRB and RRB, is mainly used for agriculture. For instance, in 2009, 73% of 2.74 billion m³ of water allocated by Alberta Environment from BRB was used for irrigation (Government of Alberta, 2010). Given that agriculture is one of the dominant economies of western Canada, there have been studies conducted on the impact of climate change to the water resources of SSRB, where past studies show that climate change impact could potentially result in decreased future streamflow for SSRB (Leung and Ghan, 1999; Lemmen et al., 2007; Pietroniro et al., 2006; Shoma and Gan, 2012) or other river basins of western Canada (Kerkhoven and Gan, 2011). However, even though the overall streamflow of SSRB could decrease, the occurrence of intensive storms that could cause flooding could still increase in the future. Given that the water holding capacity of the atmosphere will increase at about 7% per K^o rise in temperature (Clausius-Clapeyron equation), Trenberth et al. (2003) argued that the possible occurrence of fewer but more intensive storms will likely increase with a rise in air temperature. According to Allen and Ingram (2002),

even if the global mean precipitation is primarily constrained by the energy budget, most intensive storms are likely to occur when the moisture in a volume of air is mostly precipitated out, which suggests that the intensity of extreme events will increase with the availability of moisture and moisture is expected to increase as the atmosphere warms up.

The Working Group I (WGI) of IPCC (2007) cited studies regarding changes in extreme precipitation events in the second half of the 20th century, that increase in heavy and very heavy precipitation that are statistically significant had occurred despite of a decrease in the mean annual rainfall (Alpert et al., 2002; Groisman et al., 2004; Maheras et al., 2004 and others). Alexander et al. (2006) found that the percent contribution of very wet days to the total annual global precipitation had been greater in recent decades than before. Similarly, over North America, the WGI of IPCC (2013) also noted that since the middle of the 20th century there is a high confidence of likely overall increase of extreme precipitation events based on extreme climate indices of RX1day, R95p and R99p (defined in Table 3.1) although some spatial variations suggest a slightly decreasing trend around the Canadian Prairies (Table 2.13 and Figure 2.33 of the WGI report of IPCC, 2013). According to Zhang et al. (2001) and Vincent and Mekis (2006), the frequency of precipitation events for Canada had increased significantly over the 20th century even though there has been no identifiable trend in precipitation extremes.

From analyzing 75 years (1921-1995) of precipitation data for the three Prairies Provinces of Canada, Manitoba, Saskatchewan, and Alberta where SSRB is located, Akinremi et al. (1998) found a significant increase in the number of precipitation events at several climate stations but mainly due to the increase in low intensity precipitation events. However, recent severe flooding

events of 2005 and 2013 in the southern Alberta possibly indicate that there could be an increase in the number of intensive storm events occurring over SSRB in recent years. In the June 2005 flood, the total rainfall recorded in Calgary for June, which is normally the wettest month of the year, was 247.6 mm when compared to an average of 79.8 mm (Environment Canada). In that flood Oldman, Bow and Red Deer rivers were flowing at 10 to 30 times their normal runoff volume and the return period was estimated at about 1-in-200 year occurrence. However, the recent June 2013 flood was even worse, which affected about 55,000 km² in area, flooded 10,000 homes, and 100,000 people were evacuated. Although the return period of the 2013 flood event is still not available, based on the extent of the damage recorded, it should be of a return period higher than the 2005 flood, especially it resulted in an unprecedented, first ever, State of Provincial Emergency declared in Alberta.

Traditionally, most engineering design practices assume climate as a stationary process which means that return periods of design storms will not change over time (Gilroy and McCuen, 2012). However, this assumption has become questionable in recent years and climate is now widely accepted as non-stationary as climatic extremes have been occurring more frequently and in greater severity worldwide in recent years. Many scientists attribute these phenomena to climate change impact that resulted from significant increases in anthropogenic greenhouse gases (Milly et al., 2008). The recent extreme precipitation events of SSRB could also be related to climate change impact, and the city of Calgary and other major metropolitan centers of SSRB could experience more frequent and intense extreme precipitation events in the future. For example, Mailhot et al. (2012) found that Canadian Prairies will experience the largest increases in annual maxima precipitation in the 2041-2070 periods.

In this study, we analyzed the impact of climate change on extreme precipitation events in the ORB, BRB and RRB of southern Alberta. The key objective is to investigate possible changes to the intensity and frequency of future extreme precipitation of these three river basins in the 21st Century. We used MM5 to dynamically downscale the SRES (Special Report on Emission Scenarios) climate change scenarios (A1B, A2) of the Coupled Model Intercomparison Project Phase 3 (CMIP3) of IPCC (2007) to the three study sites at 9 km resolution.

To our knowledge, there has been no other study conducted on the potential impact of climate change to future extreme precipitation events of southern Alberta using climate data dynamically downscaled by a regional climate model, where intensive agricultural activities and major metropolitan and financial centers such as the City of Calgary are located. Results of this study demonstrate expected changes to the frequency and intensity of future extreme precipitation events in southern Alberta, where major floods estimated to be of 100-year or higher return periods have already occurred several times in recent years. The results of this study will be useful for the planning and the future development of municipal infrastructure in this region to minimize the potential impacts of future extreme precipitation events, which are expected to occur more frequently and in greater severity than the past. With the above introduction, research methodology is given in Section 3.2, discussion of results in Section 3.3, and summary and conclusions in Section 3.4.

3.2 Research Methodology

Flooding generally results directly from the occurrence of extreme precipitation events especially over river basins of wet antecedent moisture condition. A convenient approach to classify and to quantify properties of precipitation events is by precipitation indices (Klein Tank et al., 2009). Using the RCP (Representative Concentration Pathways) climate change projections of various Global Climate Models (GCMs) of IPCC's CMIP5, Sillmann et al. (2013a, 2013b) analyzed regional extreme annual climate indices for all the continents. In this study, various extreme climate indices were computed for ORB, BRB and RRB during MJJA (May, June, July and August) which not only is the rainy season but also the period where extreme floods usually occur. To use climate change scenarios of adequate resolutions for the three study sites, the SRES climate change scenarios of CMIP3, IPCC (2007) were first dynamically downscaled using a regional climate model, the fifth-generation NCAR/Penn State mesoscale atmospheric model, MM5 (Dudhia et al., 2005) to a spatial resolution of 9-km, which is of much higher resolution than that of GCM data which are typically of the order of 150-400 km in resolution (Table 3.2).

3.2.1 Extreme Climate Indices

To investigate the impact of climate change on future extreme precipitation events, based on a list of 27 extreme climate indices given in Klein Tank et al. (2009), the following indices are selected for this study (Table 3.1). The indices listed in Table 3.1 were selected because these indices are adequate to represent the frequency or volume of very to extremely intensive precipitation events over a given period (e.g. 30 years).

3.2.2 GCM data

The sub-daily atmospheric data of four GCMs of CMIP3 were selected and analyzed in this study. These are CGCM3 of Canada, CCSM3 of USA, ECHAM5 of Germany and MIROC3.2 of Japan (Table 3.2). For this study, the A2 and A1B climate change scenarios of CMIP3 were chosen because they represent more adverse future climate change projections of IPCC (2007).

To partly account for uncertainties associated with long-term climate change projections, which mainly arise from model uncertainties and also uncertainties in future emission scenarios (Hawkins and Sutton, 2009; Tebaldi and Knutti, 2007), two climate change scenarios and four GCMs were selected in this study. This study therefore adopts a technique referred to as “*poor man’s ensemble*” (Cloke and Pappenberger, 2009) in which ensemble runs were produced by using climate projections of A2 and A1B scenario from different climate research centers.

3.2.3 Dynamic Downscaling of GCM data

Coarse resolution data of GCMs cannot quite resolve regional scale atmospheric processes such as orographic or convective precipitation which require fine resolution of surface features that are not available from GCMs which are generally of 150 to 400 km resolutions (Bader et al., 2008). For instance, over Great Britain, Jones et al. (1995) found that Regional Climate Models’ (RCM) simulations, owing to their finer resolutions, had higher spatial correlation with the observed climatology than that of GCM simulations. Similarly, with regards to extreme events, although RCMs may still miss the most intensive precipitation, they generally simulate more realistic intensive storms that would otherwise be smoothed out by GCMs (Bader et al., 2008; Gutowski et al., 2003; Roeckner et al., 2006; Solman et al. 2003). In order to adequately

investigate the possible impact of climate change to future extreme storms of SSRB in this study, the climate change scenarios of GCMs have to be statistically or dynamically downscaled. In this study, we chose a RCM called MM5 (Dudhia et al., 2005) to dynamically downscale the climate projections of the four CMIP3 GCMs for the wet, MJJA season of SSRB, Alberta.

In this study, MM5 was set up using a one way nesting over a two-domain configuration (see Figure 3.1). The outer domain (D1) has a 27 km resolution while the inner domain (D2) has a 9 km resolution. Because the 27-km spatial resolution of D1 is not sufficient to resolve the small-scale convective precipitation events, the Kain-Fritsch 2 (Kain, 2004) cumulus parameterization (CP) scheme was applied in this outer domain. Using the Global Environmental Multiscale (GEM) data as input, Erfani et.al (2003) showed that a climate model set up at 4-km resolution could accurately simulate the precipitation systems at the rugged, Rocky Mountain foothills. On the basis of their regional climate modeling research conducted over Alberta, Hanrahan et.al (2014) and Kuo et.al (2014) show that 9 km resolution, domain D2 is sufficient to resolve most small scale summer convective rainfall events of Alberta and so no cumulus parameterization was necessary. After an extensive fine tuning of MM5, configurations of MM5 selected for this study consists of the high-resolution Blackadar planetary boundary layer (PBL) scheme, the mixed-phase (Reisner 1; Reisner et al., 1998) explicit moisture scheme, the Five Layer Soil model surface scheme (Dudhia et.al, 2005) and the rapid and accurate radiative transfer model longwave radiation scheme (RRTM; Mlawer et al., 1997).

The D1 domain chosen for MM5 extends in the East-West direction from Manitoba (97° W) to the Pacific Ocean off the coast of British Columbia (139° W). In the North-South direction D1

extends from just north of the border between Alberta and Northwest Territories in Canada (61° N) to the border between Idaho and Utah (41° N) in the United States (Figure 3.1). The inner domain D2 is centered on the SSRB. Based on the above MM5 configurations and the two-domain setup, the precipitation of ERA-Interim reanalysis data (1.5° x 1.5°) of the European Centre for Medium-Range Weather Forecast (ECMWF) downscaled by MM5 over SSRB was validated against observed precipitation data of selected gauging stations located across the SSRB and the ANUSPLIN (Australian National University Spline) dataset of Natural Resources Canada. ANUSPLIN is a 10-km resolution, daily gridded precipitation data derived from Environment Canada's daily precipitation data recorded at principal (observation taken on hourly to 6 hourly basis) and ordinary (observations taken once or twice a day) climate stations of Canada (Hopkinson et al., 2011; Hutchinson et al., 2009). Compared to observed data of some selected rain gauges and ANUSPLIN gridded precipitation, we found that MM5 has simulated representative areal pattern of MJJA precipitation of the three river basins of southern Alberta (Table 3.3 and Figure 3.2). However, compared to ANUSPLIN, the average MJJA precipitation simulated by MM5 over SSRB has a positive bias of about 40 mm (Figure 3.2 a-b). Most of this bias resulted from MM5 over simulated heavy precipitation events (precipitation exceeding 10 mm/d), with a positive bias of about 86 mm for the MJJA period (Figure 3.2 c-d) but precipitation less than 10 mm/d that MM5 simulated for D2 was underestimated by a lesser amount of about 32 mm when compared to the ANUSPLIN data (figure not shown). Given that extreme precipitation events are the focus of this study, a bias correction procedure was selected to correct the positive bias of heavy precipitation events simulated by MM5.

3.2.4 Bias correction

Using a similar MM5 model configuration for central Alberta, Kuo et al. (2014) found that MM5's simulated diurnal temperature range (DTR) has an overall negative bias of $-1.42\text{ }^{\circ}\text{C}$ when compared to the ERA-Interim reanalysis data. Because DTR and cloud cover are negatively correlated (Dai et al., 1997; Dai and Trenberth 1999), Kuo et al. (2014) found that MM5 over simulated cloud covers over its domains, resulting in over-simulated precipitation. On the basis of the findings of Kuo et al. (2014) with regard to over-simulation of storms of central Alberta by MM5, it seems that the under simulation of DTR by MM5 for southern Alberta (an overall negative bias of $-2.05\text{ }^{\circ}\text{C}$ compared to the ERA-Interim reanalysis data) should also be the cause for MM5's over simulation of heavy precipitation events in this region.

After comparing different bias correction methods, Lafon et al. (2013) found that the quantile based bias correction method provides the most reasonable results for bias correcting daily precipitation simulated by RCMs. This quantile based bias correction technique involves matching the cumulative distribution function (cdf) of the RCM's simulations to the cdf of the observed rainfall whereby simulated and observed data are ranked using an unbiased quantile estimator (Figure 3.3). The γ -distribution bias correction technique described by Lafon et al. (2013) assumes that the cumulative distributions of both observed and RCM precipitation data can be approximated by the gamma (γ) distribution. A similar bias correction procedure was adopted in this study where the cumulative distribution of precipitation data exceeding 10 mm/day for the observed (ANUSPLIN) and simulated (MM5) data is approximately described by a generalized extreme value (GEV) cumulative distribution function (Equation 3.1).

$$F(x) = \exp \left\{ - \left[1 - k \left(\frac{x - \mu}{\alpha} \right) \right]^{\frac{1}{k}} \right\} \quad (3.1)$$

k = shape, α = scale, μ = location parameters

To do the bias correction, two sets of shape (k), scale (α) and location (μ) parameters are first derived using MM5 and ANUSPLIN precipitation time series, respectively. Then the cumulative probability (F) for a discrete MM5 precipitation quantile (x) is calculated using Eq. 1 where, k , α and μ are derived from MM5 precipitation data. For this F value, the corresponding bias corrected precipitation (x') is then calculated from Eq. 2, but now, using k' , α' and μ' derived from ANUSPLIN precipitation data.

$$x' = \mu' + \frac{\alpha'}{k'} \left[1 - (-\log(F))^{k'} \right] \quad (3.2)$$

The parameters (k , α and μ) of the GEV distribution were derived using the method of moments (Rao and Hamed, 2000) for each of the months in the MJJA period. Using the above procedure, the precipitation that MM5 simulated for each MM5 D2 grid point that lies within ORB, BRB and RRB was bias corrected with respect to the ANUSPLIN gridded precipitation data at a grid point located closest to the MM5 grid point. The bias correction was done for the daily precipitation of each month within the MJJA period. This procedure has effectively reduced the over-simulation problem of MM5. As shown in Table 3.4, statistics (error, RMSE, R^2) of extreme precipitation indices computed for the MJJA seasonal precipitation of MM5 has significantly improved after bias correction. Therefore, this bias correction procedure is applied to both the base period and future SRES A2 and A1B climate scenarios of four CMIP3 GCMs dynamically downscaled by MM5.

3.3 Discussion of Results

The MJJA extreme climate indices (referred to as index or indices from now on) of ORB, BRB and RRB computed for the control runs and future climate change scenarios are herein discussed. The future MJJA indices were estimated using MM5's simulations at D2 (9 km resolution) driven by climate change scenarios of four CMIP3 GCMs listed in Table 3.2. The indices for the MJJA analysis were calculated for three 30-year periods using SRES A2 and A1B climate projections of the four GCMs. The first 30 year period is the base period or the control run of 1971-2000 for CGCM3, ECHAM5, MIROC3.2 and of 1970-1999 for CCSM3. The climate change impacts to extreme events were projected to 2041-2070 and 2071-2100 for the first three GCMs and to 2040-2069 and 2070-2099 for CCSM3 but both are referred to as 2050s and 2080s, respectively. Since Oldman (ORB), Bow (BRB) and Red Deer (RRB) rivers are all east flowing rivers, the upstream areas or the headwaters are located across the Canadian Rockies on the western sides of the ORB, BRB and RRB. Between indices computed from the four GCMs, indices derived from MIROC3.2 A2 projections were found to be significantly different from the rest, and we suspect this discrepancy could be partly due to the resolution of the raw MIROC3.2 A2 data, which is relatively coarse compared to the resolution of the raw data for the base period and A1B projections. Therefore, for MIROC3.2 GCM, only results for the base period and the A1B projection are discussed further.

3.3.1 R20mm Index

The R20mm index, also referred to as very heavy precipitation days (Klein Tank, 2009), is the number of days in a given period that the daily precipitation exceeded 20 mm. Figure A1 (APPENDIX A) shows the R20mm index computed for the three SSRB sub-basins using SRES

climate change scenarios of A2 and A1B dynamically downscaled by MM5. Overall, in comparison to other parts of ORB, higher R20mm are projected for the upstream and central parts of the basin, for most GCMs and A2 and A1B scenarios. Similarly, higher values of R20mm are projected for the upstream and central parts of the BRB and RRB for most GCMs and A2 and A1B scenarios when compared to downstream parts of these basins. Based on these projected spatial distributions of R20mm, it seems that upstream areas located along the Canadian Rockies and also central regions of the three river basins are expected to experience more frequent and possibly more severe extreme precipitation events when compared to downstream parts of these basins.

With respect to the base period, for A2 and A1B scenarios of all GCMs analyzed, the MJJA R20mm is projected to increase by about 2% and 5% for the ORB, 4% and 6% for the BRB, and 9% and 13% for the RRB in the 2050s and 2080s, respectively. However, as shown in Figure 3.4, between the four GCMs selected for this study, the change in R20mm index from the 2050s to the 2080s computed for the A2 and A1B scenarios vary substantially. Surprisingly, under the A2 scenario, the R20mm computed for CGCM3 in the 2050s turns out to be larger than that computed in the 2080s for all three basins. Similarly, with the exception of RRB where equal R20mm is projected in the 2080s, higher values of R20mm were computed for ECHAM5 in the 2050s when compared to the 2080s. On the contrary, for the A1B scenario, the R20mm index computed increases from the 2050s to the 2080s for all three basins with the exception of CCSM3 projections, for which higher R20mm is projected in the 2050s when compared to the 2080s. In addition, the projected increase in R20mm from the base period seems to progressively increase as we move northwards from the ORB for the A2 and A1B scenarios (Figure 3.4). This

suggests that RRB followed by BRB and ORB are expected to experience further very heavy precipitation days in the mid-late 21st century.

3.3.2 R95p and R99p Indices

R95p and R99p are indices that represent the total amount of precipitation in a given period for days when the daily precipitation is greater than the 95th (very wet days) and the 99th percentile (extremely wet days) precipitation of the base period, respectively. Compared to the base period, the projected increase in R95p for the three basins is around 4% and 10% for the 2050s and 2080s, respectively. On the other hand, R99p of the three southern Alberta basins is projected to increase by 39% and 42% during the 2050s and 2080s, respectively suggesting a relatively higher increase in extremely wet days over the region. Among the three southern Alberta river basins, ORB receives higher volume of precipitation than BRB and RRB in very wet and extremely wet days for both the base period and future climate scenarios (Figure 3.5).

Somewhat similar to the R20mm index, for most of the GCMs analyzed, the central and upstream areas of the ORB, BRB and RRB also have higher R95p and R99p indices for both the A2 and A1B scenarios (Figure A2 and A3). On the contrary, relatively low values have been projected for the downstream side of all the three basins. On a whole, with reference to the base period, the higher R95p and R99p indices of the ORB, BRB and RRB suggest an increase in the amount of precipitation that will occur in very wet and extremely wet days. This means that more frequent or more intensive extreme precipitation events are projected in the 2050s and 2080s.

3.3.3 P30yr

The P30yr index, similar to that explained in Chen and Knutson (2008), is proposed to estimate the daily rainfall intensity of 30-year return period for the control run, 2050s and 2080s. The GEV distribution was used to calculate the P30yr index with GEV parameters derived separately for the control run (base period) and the two future runs, 2050s and 2080s. Changes to this index between the base period and that of the two future runs for ORB, BRB and RRB represent how future daily storms intensities are projected to change in these three river basins.

Similar to R20mm, R95p and R99p indices, most GCMs projected higher daily rainfall intensities for storm events of 30 year return period over the central and upstream regions of ORB, BRB and RRB (Figure A4). Between the three river basins, daily rainfall intensities of 30-year return period estimated from 61 years of record (1951-2010) of ANUSPLIN daily gridded precipitation shows that the 30-year return period daily rainfall intensity of ORB is approximately 20% higher than that of BRB and RRB (Figure 3.6). Similarly, with respect to the base period, Figure 3.7 shows that the projected increase in the P30yr index of ORB based on all climate scenarios of GCMs downscaled by MM5 is relatively higher than BRB and RRB. For the four GCMs and A2 and A1B scenarios analyzed in this study, the P30yr index increased by 28% (2050s) and 35% (2080s) for the ORB, 17% (2050s) and 16% (2080s) for the BRB and 20% (2050s) and 21% (2080s) for the RRB. These results suggest that even though the future 30-year return period rainfall intensities are likely to increase for all three southern Alberta river basins, ORB, which has already experienced more severe precipitation events under current conditions, is projected to experience the highest increase in rainfall intensities in future.

The difference in the projected increase of future rainfall intensities between the three river basins could be partly caused by marginally higher increase in temperature that is projected for the ORB when compared to temperature projected for the more northern, BRB and RRB. For instance, for the A2 scenario, Figure 3.8 shows that the ORB is projected to have a relatively higher average maximum MJJA precipitation in conjunction with higher projected changes in temperature during the 2041-2100 periods when compared to the BRB and RRB. As explained earlier, according to the Clausius-Clapeyron equation, higher air temperature means larger water holding capacity of the atmosphere and vice versa, and that is why the projected increase in P30yr is relatively higher in the ORB because of its higher projected increase in temperature than that of the two northern basins, BRB and RRB.

Given that climate is non-stationary, return periods of future storms of ORB, BRB and RRB are expected to change. In parallel to higher values of P30yr estimated for the 2050s and 2080s, Table 3.5 shows that the return periods of the P30yr rainfall intensity for the ORB, BRB and RRB estimated for the base period is projected to decrease significantly by the mid or late 21st century. For the four GCMs and the two SRES climate scenarios considered, by the second half of the 21st century, the median of the projected return period corresponding to the 30-year return period of the control run dropped to about 12 years for ORB, 16 years for the BRB and 15 years RRB (Table 3.5). The consistently lower return periods estimated for the future (2050s and 2080s) probably implies that extreme precipitation events for ORB, BRB and RRB are expected to occur more frequently or more severely, or both, as we progress towards the mid and the late 21st century.

For the projected return periods (T), the associated risk or probability of at least one or more exceedances during a design life of n years can be estimated using Equation 3.3.

$$P = \left(1 - \frac{1}{T}\right)^n \quad (3.3)$$

Where

n = design life,

T = return period of storm, and

P = probability of no flooding

For instance, if both n and T are 30 years, the probability (P) of no flooding in 30 years is 0.362. Conversely, the risk of one or more exceedance in 30 years will be $1 - 0.362 = 0.638$. However, given that the median return periods of the P30yr index of the control run are projected to decrease to about 12, 16 and 15 years for ORB, BRB and RRB, respectively, during the mid and late 21st century the risk of one or more flooding ($1 - P$) within the design life of 30 years of a structure is expected to increase to about 0.926, 0.886 and 0.874 respectively. Thus, compared to the base period, by the mid and late 21st century, under the possible impact of climate change, the risk of one or more flooding occurring over the 30-year design life of a structure is projected to increase by about 45%, 34% and 37%, for ORB, BRB and RRB, respectively.

3.3.4 RX1day and RX5day

The RX1day index represents the maximum daily precipitation within a given period. With reference to the base period, Figure 3.9 shows that for A2 and A1B climate change scenarios of the four GCMs selected, there is a general increase in the MJJA RX1day index by about 30% and 36% for the ORB, 13% and 16% for the BRB and 18% and 15% for the RRB in the 2050s and 2080s, respectively. For some of the downscaled climate change scenarios of the four GCMs, this increase in the RX1day index is also accompanied by a projected increase in the

areal coverage of maximum daily precipitation events (Figure A5, base period plots not shown). This possibly implies that some areas in the three study sites that have yet not experienced intensive storms of certain magnitude may be hit by storms of unprecedented magnitude in the future.

Similar to results for the P30yr index, Figure 3.9 also shows that the 2050s and 2080s projected change in RX1day for the ORB based on all climate scenarios of GCMs' downscaled by MM5 is relatively higher than BRB and RRB. This implies that the projected impact of climate change on maximum daily precipitation events is most pronounced in the southern most portion of Alberta. Overall, results of RX1day (Figure 3.9) shows that with reference to the base period, more intensive extreme precipitation events are projected over southern Alberta in the 2050s and 2080s, especially in the ORB.

The RX5day index is similar to RX1day but it represents the largest amount of precipitation observed in five consecutive days over a given period, which should be another precipitation index suitable to identify flood causing storm events. With reference to the base period, Figure 3.10 shows that based on the downscaled A2 and A1B climate scenarios of the four GCMs, the MJJA RX5day is projected to increase by about 21% and 28% for ORB, 13% and 9% for BRB and 18% and 7% for RRB in the 2050s and 2080s, respectively. Similar to the P30yr and RX1day indices, Figure 3.10 shows that the 2050s and 2080s projected change in RX5day based on all climate scenarios of GCMs' downscaled by MM5 tends to decrease moving northwards from ORB to the two northern basins (BRB and RRB). The overall projected increase in RX5day likely implies a higher probability in the occurrence of flood causing storm events across the

three southern Alberta river basins by the mid and late 21st century (Figure A6). Similar to other indices, the RX5day results also suggest that the ORB will experience a higher risk of flooding whereas BRB and RRB will likely experience similar increase in the risk of flooding.

3.3.5 Changes in temperature and precipitable water

Precipitable water, a popular indicator to estimate the amount of atmospheric water vapor, represents the depth of water vapor integrated over the entire column of the atmosphere (Trenberth et al. 2005). Figure 3.11 shows the change in 2 m temperature and precipitable water for the three southern Alberta river basins from the base period, 1971-2000, to 2041-2100 based on the SRES A2 and A1B climate scenarios dynamically downscaled by MM5. As shown in Figure 3.11, the 2 m temperature and precipitable across the ORB, BRB and RRB show monotonous increase over 2041-2100. Within this period, these areas are projected to experience an increase of about 3 °C in temperature. Correspondingly, given that the water holding capacity of the atmosphere will increase at about 7% per K° rise in temperature (Clausius-Clapeyron equation), during the mid and late 21st century, the amount of precipitable water is also projected to increase by about 0.36 cm, a 23.7% increase from the average base period value of 1.52 cm. This expected increase in the atmospheric precipitable water partly explains the projected increase in extreme precipitation events over the study sites.

Other than precipitable water, the possible increase in the occurrence of extreme precipitation events can be explained in terms of the convective available potential energy (CAPE). CAPE measures the maximum kinetic energy per unit air mass achieved by an updraft movement of moist air (Ye et.al. 1998). Among others, the presence of moist air is one of the key ingredients

explained by CAPE for the creation of extreme precipitation events. Based on detailed analysis, Brooks (2013) suggested that climate models simulate an increase in CAPE in the future partly because of the increase in surface temperature and boundary layer moisture. Although in this study we did not simulate changes in CAPE between the current and future climate, the increase in 2 m temperature and precipitable water over the three southern Alberta river basins (Figure 3.11) suggest that these study sites are expected to experience an increase in CAPE in future. This expected increase in CAPE could also explain why extreme precipitation events are projected to increase in ORB, BRB and RRB.

3.4 Summary and Conclusions

The potential impact of climate change on extreme precipitation events of the three of southern Alberta river basins, i.e. Oldman, Bow and Red Deer river basins (ORB, BRB and RRB), was investigated. The analysis was done for the rainy season of May, June, July and August (MJJA) of the base period, 2050s and 2080s using six extreme precipitation indices, namely, R20mm, R95p, R99p, P30yr, RX1day and RX5day, and climate projections based on four CMIP3 GCMs' SRES climate scenarios dynamically downscaled by MM5 (Dudhia et al., 2005) to 9 km resolution.

For the MJJA season, with respect to the base period (1971-200), R20mm, R95p and R99p indices estimated from 2050s to 2080s are projected to increase for the upstream and central regions of ORB, BRB and RRB. In contrast, even though R20mm, R95p and R99p indices are generally projected to increase by the 2050s and 2080s, more marginal changes to these indices are projected for the downstream parts of these three basins. Concurrent with the increase in

R20mm, R95p and R99p indices with respect to the base period, the P30yr index for ORB, BRB and RRB is also projected to increase by 2050s and 2080s. This projected increase in future P30yr implies that if the same amount of precipitation as the control run were to fall in the 2050s and 2080s, the return period of this P30yr precipitation is expected to decrease from 30-year to about 12 years for the ORB, 16 years for BRB and 15 years for RRB, respectively. In other words, future extreme precipitation is expected to occur more frequently, which means that the risk of flooding in these river basins is expected to increase in the future. Similarly, the RX1day and RX5day indices are mostly projected to increase by 2050s and 2080s, which again implies a projected increase in flood causing precipitation events occurring over ORB, BRB and RRB during the rainy MJJA season by the mid- and late 21st century.

In addition, between the three southern Alberta river basins considered in this study, ORB is projected to experience the largest increase in precipitation indices representing the intensity of extremely heavy rainfall events (P30yr, RX1day and RX5day). Under current conditions, this river basin has already experienced relatively higher volumes of precipitation received in very to extremely wet days (R95p and R99p) and higher daily rainfall intensities of a given return period when compared to BRB and RRB. The projected change in P30yr, RX1day and RX5day between BRB and RRB are similar to each other, except that marginally higher changes in P30yr are projected for RRB than for BRB.

Compared with other climate change impact studies that include results in southern Alberta, we found general agreements between our study and previous studies regarding future extreme precipitation events (Tebaldi et.al 2006; Mailhot et.al 2012 and Sillmann et.al 2013). However,

we cannot do a direct comparison with the above studies that examined extreme climate indices that do not completely overlap with indices examined in our study. Tebaldi et.al (2006) used SRES A2 and A1B scenarios from 9 GCMs of CMIP3 to do a global analysis of changes in various extreme climate indices between 1980-1999 (base period) and 2080-2099. For the A1B scenario, they found approximately a 20% or higher increase in the mean RX5day and R95p indices of multiple GCMs for southern Alberta, which generally agrees with the 7% to 28% increase in these indices found for the 2080s in our study. Similar to the P30yr index of our study, Mailhot et.al (2012) also analyzed changes in the return periods of annual maximum precipitation using the A2 scenario and 15 simulations of the North American Regional Climate Change Assessment Program (NARCCAP) for the 1968-2000 and 2041-2070 periods. Their results shows that in 2041-2070, a 5-15% increase in the daily rainfall intensity of 2 year, 10 year and 20 year return periods are projected for southern Alberta. Our results also show that for southern Alberta, the MJJA rainfall of 30-year return period is projected to increase by 17% - 28% in 2041-2070. The increase in RX5day in 2050s and 2080s reported in our study also agrees with the expected global increase in this index by Sillimann et.al (2013b).

On a whole, the overall projected increase in extreme precipitation indices of ORB, BRB and RRB for the mid and the late 21st century is attributed to the monotonic increase in projected air temperature, which means a consistent increase in precipitable water expected over the three sub-basins of SSRB. Further, the relatively higher increase in temperature projected for ORB than BRB and RRB also means that higher changes to precipitation indices for this basin are projected for the future, particularly P30yr, RX1day, and RX5day.

Future extensions of this study will investigate the impact of climate change on CAPE (Convective Available Potential Energy) because it is an indicator of climatic conditions amenable for the occurrence of extreme rainfall events. The possible impact of climate change on extreme precipitation indices of SSRB will be repeated using the newly released, RCP (Representative Concentration Pathways) climate projections of IPCC (2013). Sillmann et al. (2013b) used coarse resolution GCMs' projections to estimate projected changes to various climate indices at sub-continental scales, e.g., western North America and others. They found that RCP8.5 of IPCC (2013) projects a larger increase in extreme precipitation events for western Canada than projections based on SRES climate change scenarios of IPCC (2007). We will expect future investigation of changes in extreme precipitation of SSRB using RCP climate projections of IPCC (2013) dynamically downscaled by a RCM such as MM5 is expected to project even higher increase in intensive precipitation events in southern Alberta.

Acknowledgments

Raw GCM data for CGCM3 were downloaded from Environment Canada's Climate Research Activities website <http://www.cccma.ec.gc.ca/data/cgcm3/cgcm3.shtml>. Raw GCM data for ECHAM5 and CCSM3 respectively downloaded from Deutsches KlimaRechenZentrum website <http://cera-www.dkrz.de/WDCC/ui/BrowseExperiments.jsp> and Earth Grid System website <https://www.earthsystemgrid.org/dataset/ucar.cgd.cesm.output.html>. The authors appreciate the kind cooperation of the staff from the National Institute for Environmental Studies and Frontier Research Center for Global Change, Japan, for providing SRES climate change scenarios of the MIROC3.2 GCM which was not available online. The authors would like to thank Daniel McKenny and Pia Papadopol from Natural Resources Canada for providing ANUSPLIN daily gridded precipitation data and supporting materials. The authors thank Westgrid for providing us access to high performance computers which was an essential resource for conducting MM5 simulations. The authors thank Chun Chao Kuo for his valuable advice and support throughout this study.

3.5 References

- Akinremi, O.O, McGinn, M.S., Cutforth, H.W. 1998. Precipitation trends in Canadian prairies. *J Climate*, 12: 2996-3003.
- Allen, M.R. and Ingram, W.J. 2002. Constraints on future changes in climate and the hydrologic cycle. *Nature* vol. 419, Nature publishing group.
- Alexander, L. V. and co-authors, 2006. Global observed changes in daily climate extremes of temperature and precipitation. *J Geophys. Res.*, 111, D05109, doi:10.1029/2005JD006290.
- Alpert, P., Ben-Gai, T., Baharad, A., Benjamini Y., Yekutieli, D., Colancio, M. Diodato, L., Ramis, C., Homar, V., Romero, R., Michaelides, S., Manes, A. 2002. The paradoxical increase of Mediterranean extreme daily rainfall in spite of decrease in total values. *J Geophys. Res – Letter*, 29: 31-1 to 31-4, doi: 10.1029/2001GL013554.
- Bader, D.C., C. Covey, W.J. Gutowski Jr., I.M. Held, K.E. Kunkel, R.L. Miller, R.T. Tokmakian and M.H. Zhang, 2008, CCSP: Climate Models: An Assessment of Strengths and Limitations. A Report by the U.S. Climate Change Science Program and the Subcommittee on Global Change Research. Department of Energy, Office of Biological and Environmental Research, Washington, D.C., USA, 124 pp.
- Brooks, H.E., 2013. Severe thunderstorms and climate change. *J of Atmospheric Research*, 123: 123-138, doi:10.1016/j.atmosres.2012.04.002.
- Chen, C.T., Knutson, T. 2008. On the verification and comparison of extreme rainfall indices from climate models. *Notes and Correspondence, AMS*, doi: 10.1175/2007JCLI1494.1.
- Cloke, H.L., and Pappenberger, F., 2009. Ensemble flood forecasting: a review. *J Hydrology*, 375: 613-626, doi:10.1016/j.jhydrol.2009.06.005.

- Dai, A., Del Genio, A.D., Fung, I.Y., 1997. Clouds, precipitation and temperature range. Scientific correspondence, *Nature* 386: 665-666.
- Dai, A., Trenberth, K.E., 1999. Effects of Clouds, Soil Moisture, Precipitation, and Water Vapor on Diurnal Temperature Range. *J Climate*, 12: 2451-2473.
- Dudhia, J., Gill, D., Manning, K., Wang, W., Bruyere, C., Kelly, S., Lackey, K. 2005. PSU/NCAR Mesoscale Modeling System, Tutorial Class Notes and User's Guide: MM5 Modeling System Version 3.
- Environment Canada. Alberta's Flood of Floods, Archived content last accessed January/25/2015:<http://www.ec.gc.ca/meteoweather/default.asp?lang=En&n=A4DD5AB1>
- Erfani A., Methot A., Goodson R., Belair S., Yeh K., Cote J., and Moffet R. 2003 Synoptic and Mesoscale Study of a Severe Convective Outbreak with the Nonhydrostatic Global Environmental Multiscale (GEM) model, *Meteorology and Atmospheric Physics*, 82: 31-53 doi: 10.1007/s00703-001-0585-8.
- Gilroy K.L., and McCuen R.H. 2012. A nonstationary flood frequency analysis method to adjust for future climate change and urbanization. *J Hydrology*, 414-415: 40-48, doi:10.1016/j.jhydrol.2011.10.009.
- Government of Alberta, 2010. Facts about water in Alberta: ISBN 978-0-7785-8970-9 last accessed January/25/2015. <http://environment.gov.ab.ca/info/library/6364.pdf>
- Groisman, P. Ya., Knight, R.W, Karl, T.R, Easterling, D.R, Sun, B. and Lawrimore, J.H. 2004. Contemporary Changes of the Hydrological Cycle over the Contiguous United States: Trends Derived from In Situ Observations. *J Hydrometeorology*, 5: 64-85.

- Gutowski Jr W.J., Kozak K.A., Arritt R.W., Christensen J.H., Patton J.C. and Takle E.S. 2007. A Possible Constraint on Regional Precipitation Intensity Changes under Global Warming. *J Hydrometeorology*, 8: 1382-1396, doi: 10.1175/2007JHM817.1.
- Hanrahan, J., Kuo, C.C., Gan, T.Y. 2014. Configuration and validation of a mesoscale atmospheric model for simulating summertime rainfall in central Alberta. *RMS, Int J Climatology*, doi: 10.1002/joc.4011.
- Hawkins, Ed., and Sutton, R. 2009. The potential to narrow uncertainty in regional climate predictions. *American meteorological society, BAMS*, 1095-1107.
- Hopkinson, R.F., McKenny D.W., Milewska E.J., Hutchinson, M.F., Papadopol P., Vincent, L.A., 2011. Impact of Aligning Climatological Day on Gridding Daily Maximum–Minimum Temperature and Precipitation over Canada. *J Applied Meteorology and Climatology, AMS*. doi: 10.1175/2011JAMC2684.1.
- Hutchinson, M.F., McKenny D.W., Lawrence, K., Pedlar, J.H., Hopkinson, R.F., Milewska E., Papadopol P. 2009. Development and Testing of Canada-Wide Interpolated Spatial Models of Daily Minimum–Maximum Temperature and Precipitation for 1961–2003. *J Applied Meteorology and Climatology, AMS*. 48: 725-741, doi: 10.1175/2008JAMC1979.1.
- IPCC, 2013: Chapter 2. Hartmann, D.L., A.M.G. Klein Tank, M. Rusticucci, L.V. Alexander, S. Bronnimann, Y. Charabi, F.J. Dentener, E.J. Dlugokencky, D.R. Easterling, A. Kaplan, B.J. Soden, P.W. Thorne, M. Wild and P.M. Zhai, 2013: Observations: Atmosphere and Surface. In: *Climate Change 2013: The Physical Science Basis. Contribution of Working Group I to the Fifth Assessment Report of the Intergovernmental Panel on Climate Change* (Stocker, T.F., D. Qin, G.-K. Plattner, M. Tignor, S.K. Allen, J. Boschung, A. Nauels, Y.

Xia, V. Bex and P.M. Midgley (eds.)). Cambridge University Press, Cambridge, United Kingdom and New York, NY, USA.

IPCC, 2007: Climate Change 2007: The Physical Science Basis. Contribution of Working Group I to the Fourth Assessment Report of the Intergovernmental Panel on Climate Change (Solomon, S., D. Qin, M. Manning, Z. Chen, M. Marquis, K.B. Averyt, M. Tignor and H.L. Miller (eds.)). Cambridge University Press, Cambridge, United Kingdom and New York, NY, USA, 996 pp.

Jones, R.G. Murphy, J.M. and Noguer, M. 1995. Simulation of climate change over Europe using a nested regional climate model. I: Assessment of control climate, including sensitivity to location of lateral boundaries. Q.J.R Meteorol. Soc, 121: 1413-1449.

Kain J.S., 2004. The Kain–Fritsch Convective Parameterization: An Update. J Applied Meteorology, 43(2004): 170-181.

Kerkhoven E.,and Gan T.Y. 2011. Differences and sensitivities in potential hydrologic impact of climate change to regional-scale Athabasca and Fraser River Basins of the leeward and windward sides of the Canadian Rocky Mountains respectively. J. Clim. Change 106: 583–607, doi:10.1007/s10584-010-9958-7.

Klein Tank, A.M.G, Zwiers F.W, Zhang X. 2009. Guidelines on Analysis of extremes in changing climate in support of informed decision for adaption. World Meteorological Organization, Climate Data and Monitoring, WCDMP-No. 72.

Kuo, C.C., Gan, T.Y., Hanrahan, J.L. 2014. Precipitation frequency analysis based on regional climate simulations in Central Alberta. J Hydrology, 510(2014): 436-446, doi: 10.1016/j.jhydrol.2013.12.051.

- Lafon, T., Dadson, S., Buys, G., and Prudhomme, C. 2013. Bias correction of daily precipitation simulated by a regional climate model: a comparison of methods. Royal Meteorological Society, Int. J Climatology, 33: 1367-1381,doi: 10.1002/joc.3518.
- Lemmen, D.S., Warren, F.J, Lacroix, J., and Bush, E., editors 2008: From impacts to Adaptation: Canada in a Changing Climate 2007; Government of Canada, Ottawa, ON, 448 p.
- Leung, L.R and Ghan, S.J 1999. Pacific Northwest climate sensitivity simulated by a regional climate model driven by a GCM. Part II: 2xCO₂ simulations; AMS, J Climate, 12, no. 7: 2031-2053.
- Maheras, P., Tolika, K., Anagnostopoulou, C., Vafiadis, M. Patrikas, I. and Flocas, H. 2004. On the relationship between circulation types and changes in rainfall variability in Greece. Int J Climatology, 24: 1695-1712, doi: 10.1002/joc.1088.
- Mailhot A, Beaugregard I, Talbot G, Caya D, Biner S. 2012. Future changes in intense precipitation over Canada assessed from multi-model NARCCAP ensemble simulations. Int. J. Climatol. 32(8): 1151–1163, doi: 10.1002/joc.2343.
- Mlawer E.J., Taubman S.J., Brown P.D., Iacono M.J., and Clough S.A. 1997. Radiative Transfer for Inhomogeneous Atmospheres: RRTM, a Validated Correlated-k Model for the Longwave, Journal of Geophysical Research, 102: 16663-16682.
- Milly, P.C.D, Betancourt, J., Falkenmark, M., Hirsch, R.H., Kundzewicz, Z.W., Lattenmaier, D.P., and Stouffer, R.J. 2008. Stationarity is Dead: Whither Water Management? Science, 319: 573-574.
- Pietroniro, A., Toth, B., and Toyra, J. 2006: Water availability in the South Saskatchewan River basin under climate change; presentation at Climate Change and Water in the Prairies Conference, Saskatoon, Saskatchewan, June 22, 2006.

- Rao, A.R, Hamed, K.H. 2000. Flood Frequency Analysis. CRC Press, New York.
- Reisner J., Rasmussen R.M., and Brintjes R.T. 1998. Explicit Forecasting of Supercooled Liquid Water in Winter Storms using the MM5 Mesoscale Model, Quarterly Journal of the Royal Meteorological Society, 124: 1071-1107 doi: 10.1002/qj.49712454804.
- Roeckner, E., Bäuml, G. Bonaventura , L., Brokopf , R., Esch, M., Giorgetta, M., Hagemann, S., Kirchner, I., Kornblueh, L., Manzini, E., Rhodin, A., Schlese, U., Schulzweida, U., Tompkins, A. 2003. The atmospheric general circulation model ECHAM5, Part I. Model description. Max Planck Institute for Meteorology. Report No 349. Last accessed January 23, 2015.http://www.mpimet.mpg.de/fileadmin/publikationen/Reports/max_scirep_349.pdf
- Roeckner, E., Brokopf R., Esch M. Giorgetta S., Hagemann and Kornblueh L. 2006. Sensitivity of Simulated Climate to Horizontal and Vertical Resolution in the ECHAM5 Atmosphere Model. American Meteorological Society, J Climate – Special Section, vol 19 pp. 3771-3791.
- Shoma, T and Gan, T.Y 2012. Potential impact of climate change on the water availability of South Saskatchewan River Basin. J Climatic Change, 112, no 2, doi: 10.1007/s10584-011-0221-7.
- Sillmann, J., V. V. Kharin, X. Zhang, F. W. Zwiers, and D. Bronaugh (2013a), Climate extremes indices in the CMIP5 multimodel ensemble: Part 1. Model evaluation in the present climate, J. Geophys. Res. Atmos., 118, doi:10.1002/jgrd.50203.
- Sillmann, J., V. V. Kharin, F. W. Zwiers, X. Zhang, and D. Bronaugh (2013b), Climate extremes indices in the CMIP5 multimodel ensemble: Part 2. Future climate projections, J. Geophys. Res. Atmos., 118, doi:10.1002/jgrd.50188.

- Solman, S.A, Nuñez, M.N., Rowntree, P.R. 2003. On the evolution of the representation of mid-latitude transient in the Southern Hemisphere by HadAM2B GCM and the impact of horizontal resolution. *Atmósfera* 257-283.
- Tebaldi, C., Hayhoe, K., Arblaster, J.M., Meehl, G.A. 2006. Going to the extremes. An intercomparison of model-simulated historical and future changes in extreme events. *J of Climate Change*, 79: 185-211, doi: 10.1007/s10584-006-9051-4.
- Tebaldi, C. and Knutti, R. 2007. The use of the multi-model ensemble in probabilistic climate projections, *Review. J Phyl. Trans.,R.Soc. A*, 365: 2053-2075, doi:10.1098/rsta.2007.2076.
- Trenberth, K.E, Dai, A., Rasmussen, R.M. and Parsons, D.B. 2003. The Changing Character of Precipitation. *American Meteorological Society Forum*, doi: 10.1175/BAMS-84-9-1205.
- Trenberth, K.E., Fasullo J., Smith, L. 2005. Trends and variability in column-integrated atmospheric water vapor. *J of Climate Dynamics* 24: 741-758, doi: 10.1007/s00382-005-0017-4.
- Vertenstein, M., Craig, T., Henderson, T., Murphy, S., Carr, G.R.Jr and Norton, N. 2004. *CCSM 3.0 User's Guide*. Community Climate System Model National Center for Atmospheric Research, Boulder, CO. Last accessed January 23, 2015. <http://www.cesm.ucar.edu/models/ccsm3.0/ccsm/doc/UsersGuide/UsersGuide.pdf>
- Vincent, L.A., & Éva Mekis. 2006. Changes in Daily and Extreme Temperature and Precipitation Indices for Canada over the Twentieth Century, *Atmosphere-Ocean*, 44:2, 177-193, doi: 10.3137/ao.440205.
- Ye, B., Geno, A.D., Lo, K.K. 1998. CAPE variations in the current climate and in a climate change. *J of Climate* 11: 1997-2015.

Zhang, X., Hogg, W.D. and Mekis, E., 2001. Spatial and temporal characteristics of heavy precipitation events over Canada. American Meteorological Society, J Climate, 14: 1923-1936.

Table 3.1 Extreme climate indices adapted from Table 1 of Sillmann et al. (2013a)

Label	Index name	Index definition	unit
R20mm	Very heavy precipitation days	Number of days where $PR_{ij}^1 > 20\text{mm}$ of a given period	days
P30yr	The 30 year return period rainfall	The rainfall intensity (mm/d) of a 30 year return period	mm/d
R95p	Very wet days	$R95pj = \sum_{w=1}^W PR_{wj}$, where $PR_{wj} > PR_{wn95}$; PR_{wn95} = The 95th percentile of precipitation on wet days in the 1971–2000 period. W = the number of wet days in the period.	mm
R99p	Extremely wet days	$R99pj = \sum_{w=1}^W PR_{wj}$, where $PR_{wj} > PR_{wn99}$; and PR_{wn99} = The 99th percentile of precipitation on wet days in the 1971–2000 period. W = the number of wet days in the period.	mm
RX1day	Max 1 day precipitation	$RX1day_j = \max (PR_{ij})$, the maximum 1 day precipitation for period j .	mm
RX5day	Max 5 day precipitation	$RX5day_j = \max (PR_{kj})$, the maximum 5 day precipitation for period j .	mm

1: PR_{ij} (PR_{wj}) = Daily precipitation amount in mm on day i (wet day w with $PR \geq 1$ mm), in period j .

Table 3.2 CMIP3 GCMs selected for investigating possible climate change impact to MJJA extreme precipitation of SSRB. More details about these GCMs can be found in http://www-pcmdi.llnl.gov/ipcc/model_documentation/ipcc_model_documentation.php

CMIP3 models		
Model	Institution	Resolution Lon × Lat (degrees)
CGCM3	Canadian Center for Climate Modeling and Analysis, Canada, model description: http://ec.gc.ca/ccmac-cccma/default.asp?lang=En&n=1299529F-1	3.75×3.71 (≈ 400 km)
CCSM3	National Center for Atmospheric Research, USA, (Vertenstein et.al, 2004)	1.406×1.401
ECHAM5	Max Plank Institute of Meteorology, Germany, (Roeckner et.al, 2003)	1.875×1.865 (≈ 200 km)
MIROC3.2	National Institute for Environmental Studies and Frontier Research Center for Global Change, Center for Climate System Research (University of Tokyo), Japan	1.125×1.125 (hires) 2.81×2.79 (medres)

Table 3.3 Correlation between monthly precipitation data of gauging stations and data simulated by MM5 at a grid point closest to respective rain gauge stations.

Correlation MM5 D2	Observation station						
	Lethbridge	Taber	Five Mile Creek	Calgary Airport	Elbow RS	Drumheller Andrew	Sundre Garrington
	0.72	0.71	0.7	0.79	0.75	0.66	0.68

Table 3.4 Statistics (% error, R^2 and Root Mean Squared Error (RMSE)) of extreme climate indices of Table 1 derived from ERA-Interim reanalysis data and the base period data of four GCMs dynamically downscaled by MM5 for SSRB before and after bias correction, respectively. These statistics represent the difference between extreme climate indices estimated from these datasets and indices estimated from ANUSPLIN data.

		ERA-Interim		CGCM3		ECHAM5		MIROC3.2		CCSM3	
		MM5	MM5b	MM5	MM5b	MM5	MM5b	MM5	MM5b	MM5	MM5b
R20mm	RMSE	49.4	16.9	42.0	22.5	55.3	25.1	62.8	23.6	19.0	14.6
	% Error	100.0	33.3	72.0	31.6	109.8	45.5	125.2	37.9	20.8	19.7
	R^2	0.32	0.77	0.16	0.51	0.21	0.54	0.31	0.55	0.19	0.52
R95p	RMSE	471.4	258.5	464.5	296.7	628.5	278.8	654.7	387.7	535.8	443.4
	% Error	26.1	10.5	20.9	9.0	33.4	7.2	34.7	17.0	30.2	19.4
	R^2	0.43	0.75	0.21	0.52	0.23	0.51	0.29	0.45	0.34	0.56
R99p	RMSE	157.0	97.6	160.4	90.9	216.4	87.7	222.6	137.2	171.2	138.9
	% Error	26.6	15.4	22.2	10.2	35.7	9.0	33.0	21.1	32.0	17.4
	R^2	0.41	0.80	0.14	0.58	0.14	0.57	0.20	0.46	0.24	0.61
RX1day	RMSE	45.1	8.9	56.0	11.7	62.9	10.2	57.5	10.6	38.2	10.4
	% Error	59.9	8.1	46.3	13.0	66.6	11.1	71.4	11.4	30.4	10.9
	R^2	0.09	0.80	0.03	0.57	0.00	0.68	0.02	0.65	0.00	0.60
RX5day	RMSE	49.7	22.0	63.2	25.3	74.1	24.4	72.6	22.3	35.3	25.3
	% Error	33.9	12.7	32.1	14.4	54.3	12.5	54.9	13.8	17.3	17.0
	R^2	0.38	0.69	0.00	0.13	0.02	0.36	0.06	0.26	0.08	0.46
P30yr	RMSE	35.4	4.0	28.3	4.7	39.6	4.6	46.4	4.9	22.8	5.0
	% Error	59.1	5.8	41.0	6.3	61.5	6.4	76.4	6.8	28.3	5.0
	R^2	0.33	0.93	0.01	0.87	0.04	0.89	0.09	0.85	0.02	0.79

Table 3.5 Medians of projected return periods of the P30yr index (daily precipitation intensities of 30-year return period of the control run) based on the A2 and A1B climate scenarios of four GCMs downscaled by MM5 for ORB, BRB, and RRB by 2050s and 2080s.

Model	Median of new return period					
	ORB		BRB		RRB	
	2050s	2080s	2050s	2080s	2050s	2080s
CGCM3 A2	14	11	15	16	11	14
ECHAM5 A2	5	10	6	8	10	10
CCSM3 A2	16	11	17	23	18	17
CGCM3 A1B	19	14	27	16	16	12
ECHAM5 A1B	14	8	9	9	12	12
CCSM3 A1B	11	15	15	23	13	20
MIROC3.2 A1B	13	9	21	17	32	14
Overall Average	13	11	16	16	16	14

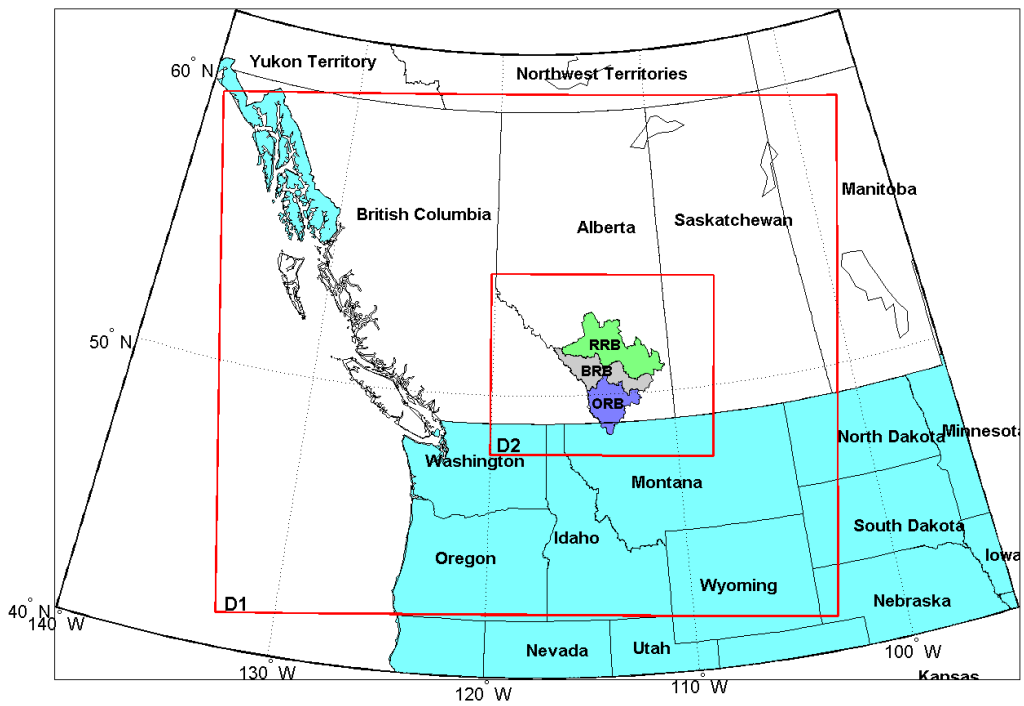


Figure 3.1 MM5 domain configurations (encompassed by thin red lines), with the outer domain (D1) at a 27-km resolution, the inner domain (D2) at a 9-km resolution encompassing ORB, BRB and RRB.

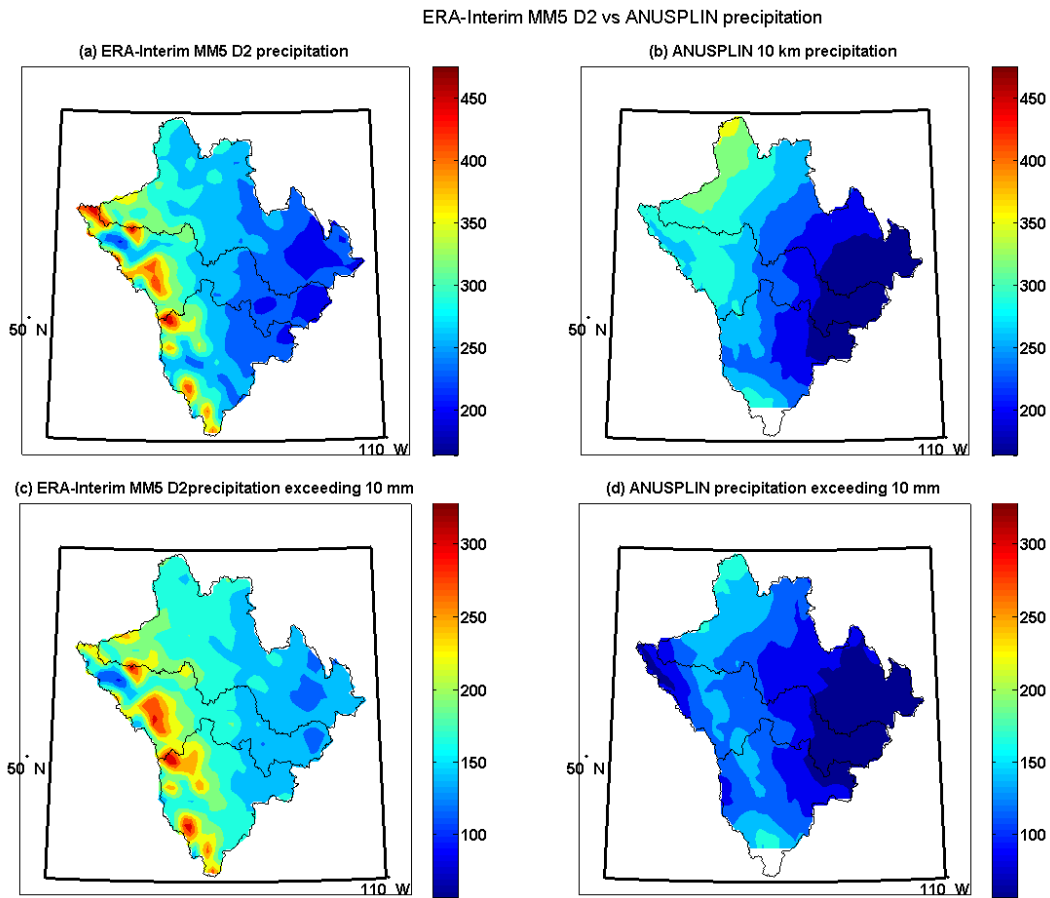


Figure 3.2 Comparison between 10-km resolution ANUSPLIN gridded precipitation data and 9-km resolution ERA-Interim precipitation downscaled by MM5 for 1979-2007, (a) and (b) average MJJA total precipitation for MM5 D2 and ANUSPLIN, respectively and (c) and (d) average total precipitation exceeding 10 mm/d for MM5 D2 and ANUSPLIN, respectively.

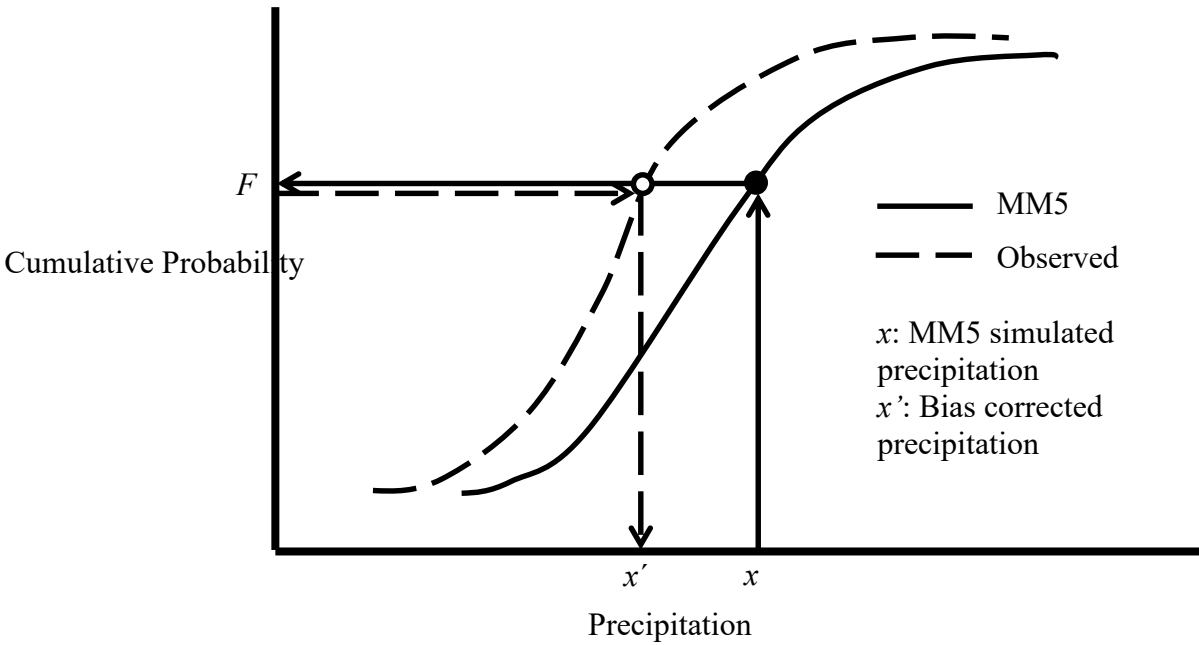


Figure 3.3 Quantile-quantile bias correction procedure for MM5's simulated precipitation from x to x' , such that the quantile of x' based on the cumulative distribution function (CDF) of the observed rainfall is the same as that of x based on the CDF of the simulated rainfall of MM5.

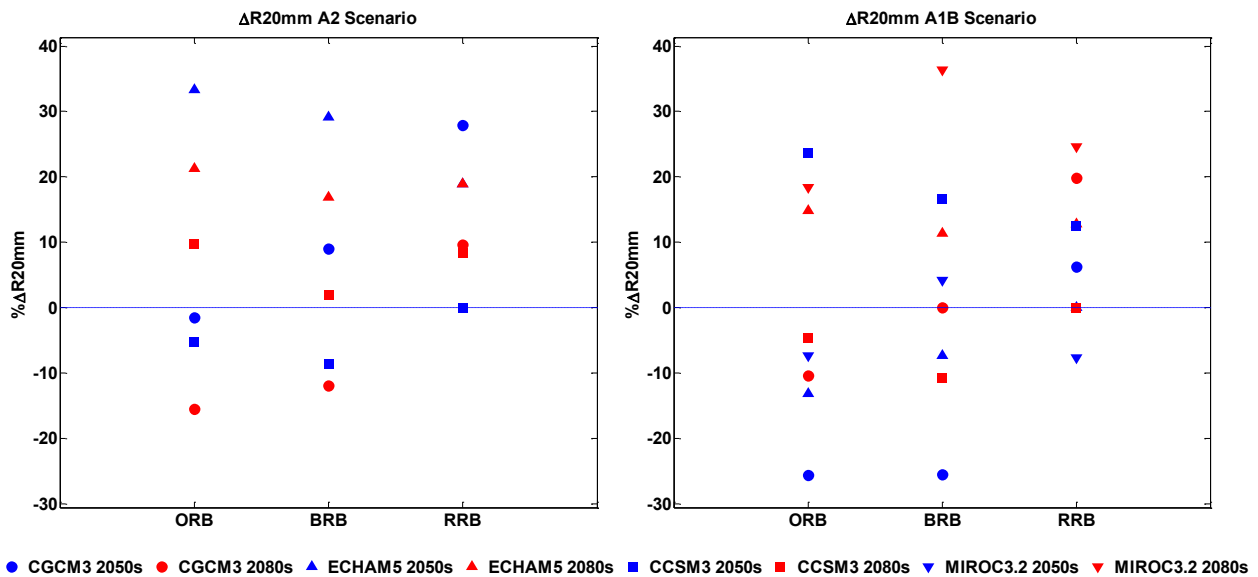


Figure 3.4 With respect to the base period (1971-2000), medians of the projected changes to the R20mm index of the ORB, BRB and RRB derived from climate projections of four CMIP3 GCMs under the SRES A2 and A1B scenarios downscaled by MM5.

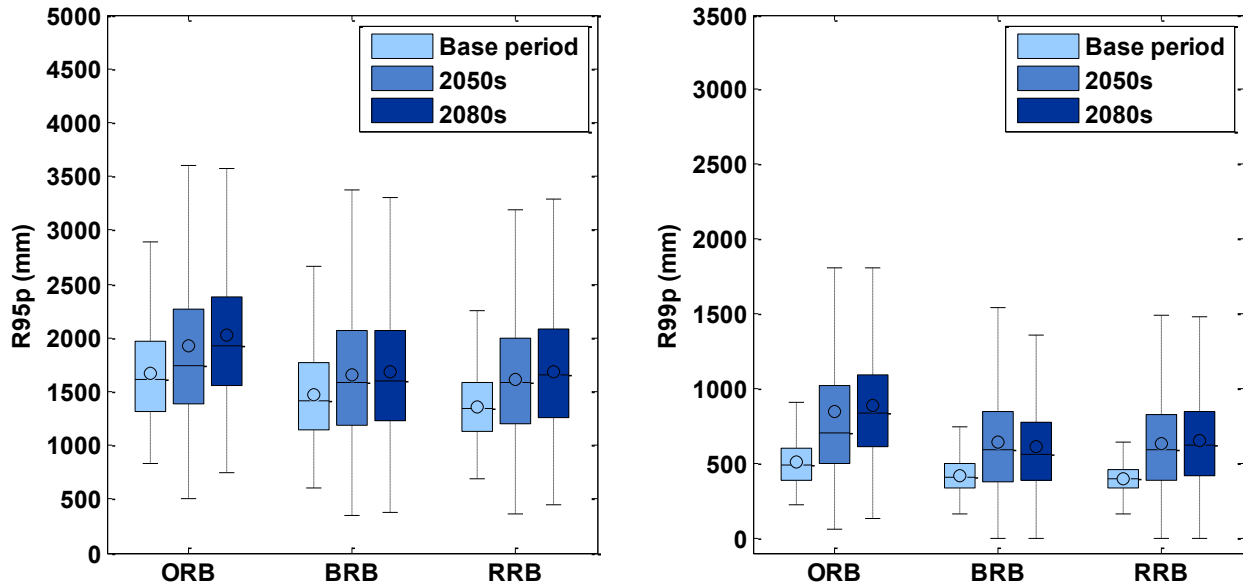


Figure 3.5 Boxplots of R95p and R99p derived from ensemble projections of four GCMs and A2 and A1B climate scenarios downscaled by MM5 for ORB, BRB and RRB for the base period, 2050s and 2080s, respectively. The line and the circle within the box plots represent the ensemble median and ensemble mean, respectively.

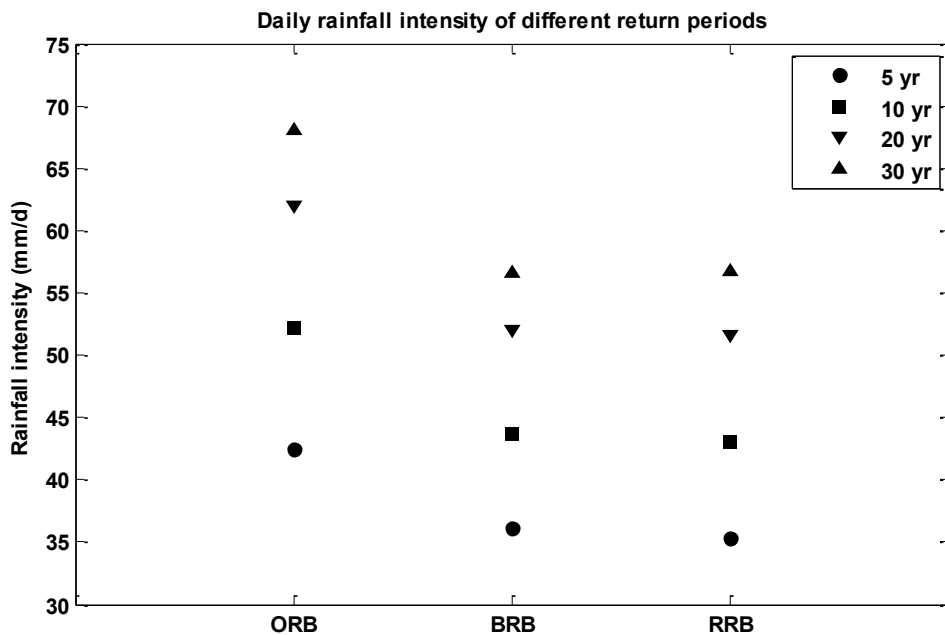


Figure 3.6 Medians of daily rainfall intensities of different return periods derived from 1961-2010 MJJA ANUSPLIN daily gridded precipitation data for ORB, BRB and RRB. The rainfall intensities of 5 to 30-yr return periods for ORB are approximately 20% higher than that of BRB and RRB.

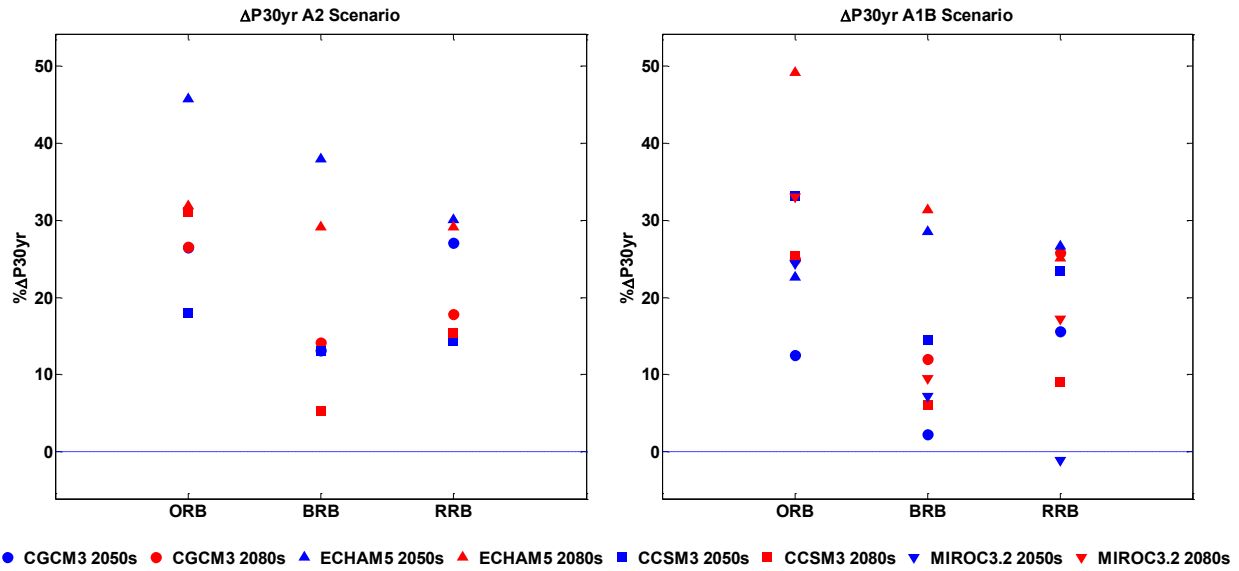


Figure 3.7 With respect to the base period (1971-2000), medians of the projected changes to the P30yr index of the ORB, BRB and RRB derived from climate projections of four CMIP3 GCMs under the SRES A2 and A1B scenarios downscaled by MM5.

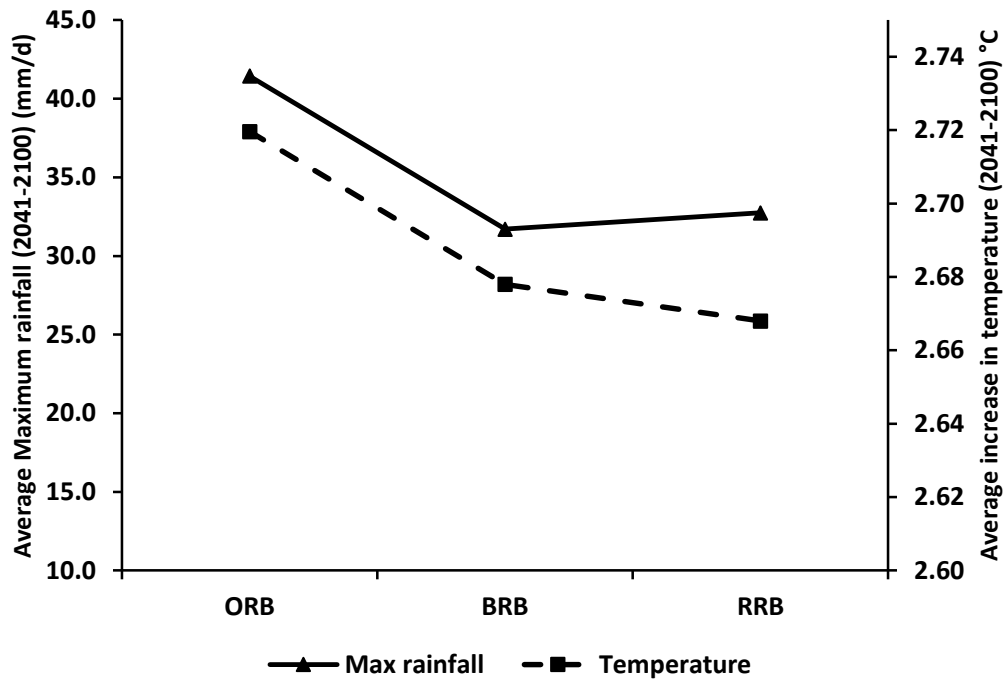


Figure 3.8 The average MJJA maximum precipitation and the corresponding average increase in air temperature of ORB, BRB, and RRB from the base period to 2041-2100, based on the A2 scenarios of four GCMs downscaled by MM5.

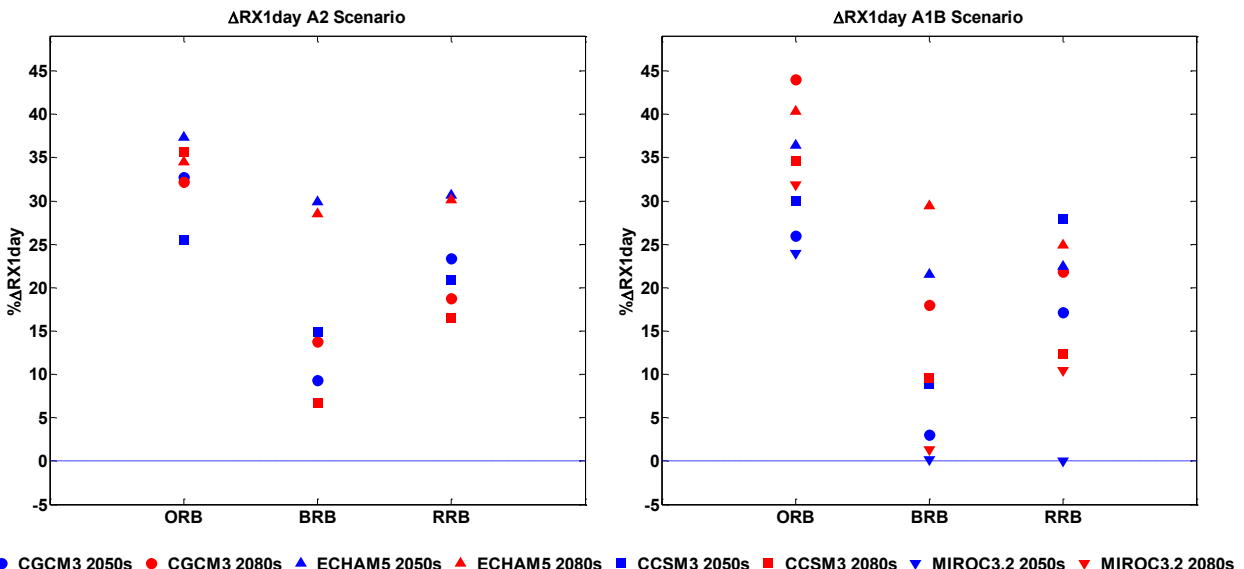


Figure 3.9 With reference to the RX1day index of the base period (1971-2000), the figure shows medians of the projected changes to the RX1day index of the ORB, BRB and RRB derived from downscaled SRES A2 and A1B climate change scenarios of four CMIP3 GCMs downscaled by MM5.

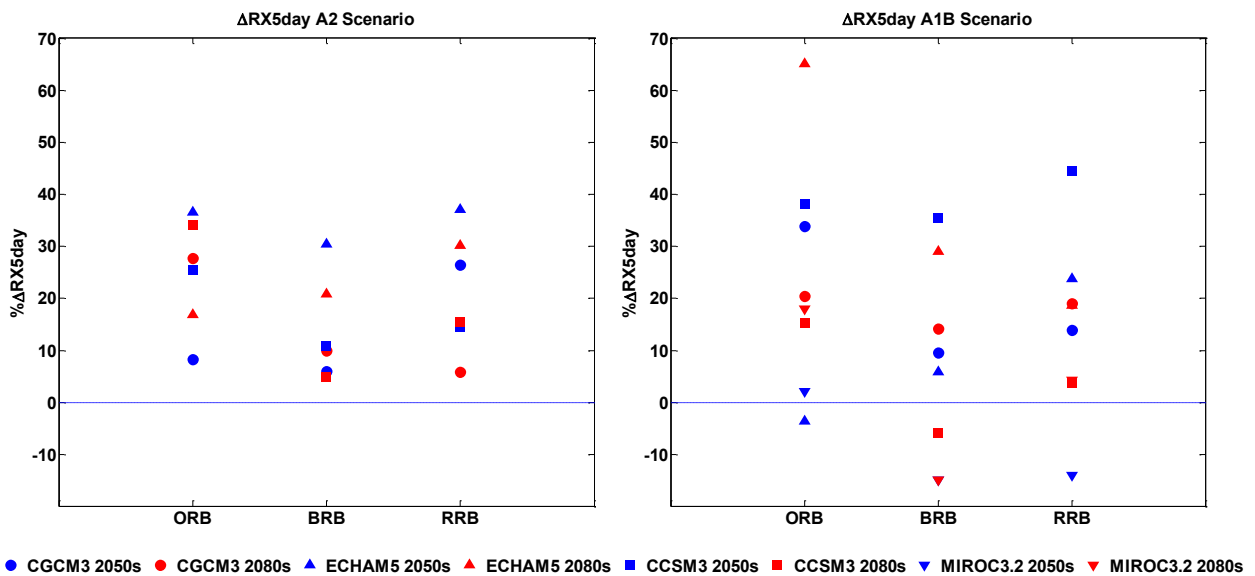


Figure 3.10 With reference to the RX5day index of the base period (1971-2000), the figure shows medians of the projected changes to the RX5day index of the ORB, BRB and RRB derived from downscaled SRES A2 and A1B climate change scenarios of four CMIP3 GCMs.

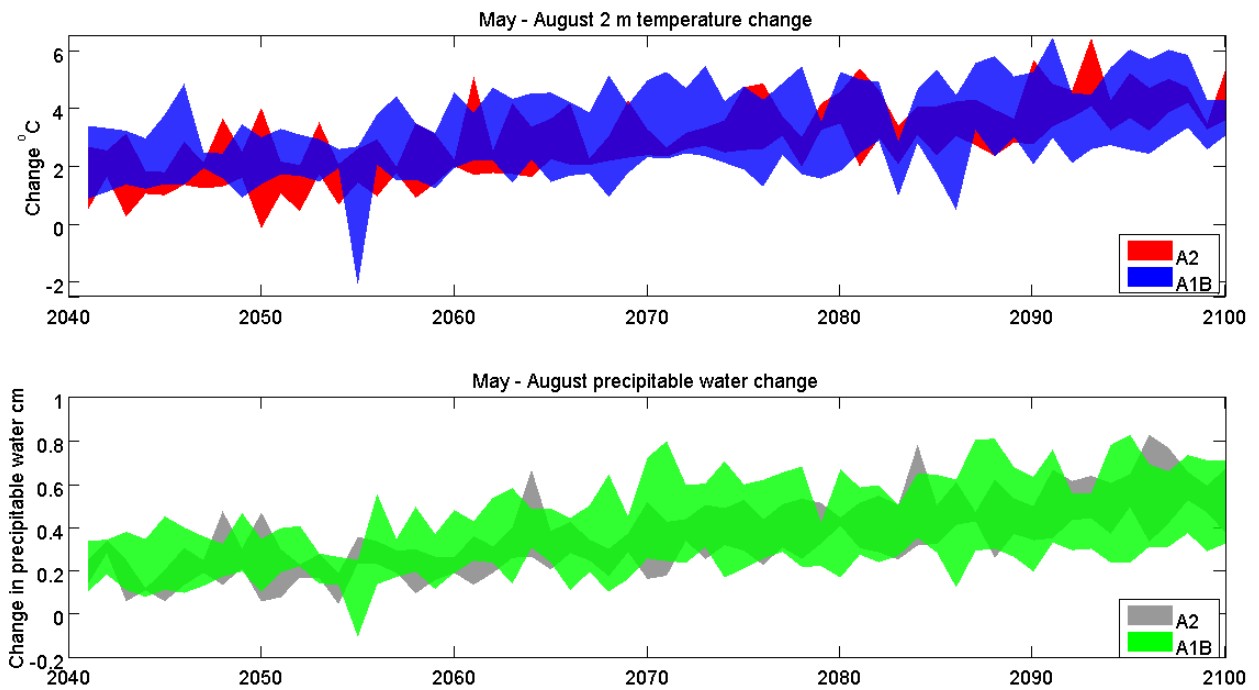


Figure 3.11 With reference to the base period of 1971-2000, both 2 m temperature and precipitable water for MJJA derived from SRES A2 and A1B climate scenarios of four GCMs downscaled by MM5 over the three southern Alberta river basins (ORB, BRB and RRB) are projected to consistently increase to the end of the 21st century.

Chapter 4 Regional Flood Frequency Analysis using Support Vector

Regression under historical and future climate

4.1 Introduction

Flood frequency analysis has been the classic approach to estimate the magnitude of flood events of various return periods. Assuming floods as stochastic processes, the magnitude and frequency of floods are predicted using certain probability distributions usually characterized by one to three parameters (Chow et al., 1988; Rao and Hamid, 2000) estimated from historical streamflow collected over an extended period. The Bulletin 17B (1982) of the United States Geological Survey (USGS) suggests at least ten years of stream gauging records should be analyzed to warrant statistical analysis as a meaningful basis for estimating future flood events, especially events of high return periods. However, if measured streamflow data is not available, flood frequency analysis can be done using flows simulated by hydrologic model, lumped conceptual models such as the Sacramento model (Burnash et al., 1973) or distributed, physically-based models such as MISBA (Kerkhoven and Gan, 2006) forced with observed climate data, or statistical methods that relate flood quantiles with catchment characteristics.

Regional flood frequency analyses (RFFA) are statistical methods that have been widely used to estimate flood quantiles in catchments where streamflow measurements are either limited or unavailable (Griffis and Stedinger 2007; Ouarda et.al. 2007; Shu and Ourada, 2007; Haddad and Rahman, 2011, Aziz et.al 2013). In the RFFA based on Quantile Regression Techniques (QRT), a large number of gauged basins are selected from a given geographical region and their flood quantiles, which are estimated from observed streamflow records, are then regressed against selected basin characteristics such as catchment area, main channel slope, design rainfall

intensity, etc. (Thomas and Benson, 1970; Haddad and Rahman 2011). The statistical relationship established by RFFA can then be used to estimate flood quantiles of river basins that have limited streamflow records but are located within the same geographic and climatic region of surrounding river basins with sufficient data for regional flood quantile estimation. As empirical methods with regional applications, RFFA are attractive and practical when compared to more physically-based methods that could be computationally intensive with massive input data requirements.

The commonly used RFFA include the rational method, index flood method and QRT (Aziz et.al., 2013). In QRT, regional flood prediction equations are developed by regressing flood quantiles (predictands) estimated from a large number of gauged catchments in a given geographic region based on the catchments' physiographic and climatic variables (predictors) (Thomas and Benson, 1970; Haddad and Rahman 2011). Early RFFA studies that utilized QRT methods based on ordinary least square (OLS) regression related flood quantiles with hydrologic characteristics of catchments (Thomas and Benson, 1970). However, many studies have shown that QRT based on generalized least square (GLS) regressions is more efficient than OLS. GLS based regressions generally provide more precise estimates because they account for differences between the variance of streamflow from various sites that mainly arise from differences in record length and cross correlation among concurrent streamflows (Stedinger and Tasker 1985; Griffis and Stedinger 2007; Haddad and Rahman 2011). On the other hand, there have been RFFA studies based on artificial neural networks (ANN). ANNs are machine learning algorithms which are information processing systems that partly function like the human brain (Shu and Ouarda, 2007). With certain built-in search algorithms, and only input and output data,

ANNs are capable of finding optimal nonlinear relationships of basin-scale hydrologic processes without requiring detailed physical information or data related to these processes (Nor et.al., 2007). Recent RFFA studies based on ANNs have been shown to be better than regression models in modeling complex relationships between flood quantiles and climatic/physiographic properties of a catchment. For example, Aziz et.al (2013) developed an ANN-based RFFA model for estimating flood quantiles in eastern Australia which gave a better performance than RFFA models based on QRT. Similarly, from testing different ANN based RFFA models in Québec, Canada, Shu and Ouarda (2007) showed that ANN based models are easier to apply and tend to be more accurate than regression based RFFA models.

Another machine learning approach that can also potentially be used for RFFA is Support Vector Regression techniques developed from a kernel-based classification algorithm called the Support Vector Machines (SVM). Over the years SVM has been extended as a regression tool referred to as Support Vector Regression Machine (SVR) (Drucker et al., 1997; Smola and Scholkopf, 1998). Even as relatively new techniques, SVM and SVR have been applied in various hydrologic studies, and in particular for streamflow prediction. Liong and Sivapragasam (2002) used SVM to predict the flood stage of the Brahmaputra, Ganges and Meghna Rivers which merge at the city of Dhaka, Bangladesh and they concluded that SVM is at least as good if not better than ANNs and has better generalization ability when the training dataset available is limited. Dibike et.al (2001) used SVM in the classification of remotely sensed data and rainfall-runoff modelling and found the generalization and performance of SVM to be better than other classification methods and traditional conceptual rainfall runoff models. Yu et.al (2006) used SVR to develop a real-time flood stage forecasting model that could effectively forecast flood

stages up to six hours of lead time. Wu et.al (2008) also used SVR for river stage prediction and concluded that their model could predict river stages more accurately than other machine learning algorithms such as ANN. Samui (2011) showed that a Least Square Support Vector Machine (LS-SVM) model could predict evaporation loss from reservoirs more accurately than an ANN model. Zakaria and Shabri (2012) found SVM to be better than multiple linear regressions (MLR) in predicting the streamflow of ungauged sites. SVM has also been used in predicting groundwater levels in coastal aquifers where it showed to have more superior generalization ability than ANN models (Yoon et.al, 2011).

As mentioned in the previous paragraph, the comparatively better generalization ability of SVR makes it an attractive alternative approach to perform RFFA with limited number of gauged surrounding river basins for estimating flood quantiles of an ungauged basin. In this study, our objective is to investigate the performance of a machine learning technique (SVR) in a RFFA and to compare its performance with ANN based RFFA models for two groups of river basins located in British Columbia (BC) and Ontario (ON) of western and eastern Canada, respectively. We will also extend the application of SVR-RFFA model to predict changes in projected flood quantiles over the two study areas under the impact of climate change. With this introduction, a brief description of SVR is given in Section 4.2, data and methodology in Section 4.3, discussion and results in Section 4.4, and summary and conclusions in Section 4.5.

4.2 Support Vector Regression

The Support Vector (SV) algorithm is a class of nonlinear search algorithm based on a statistical learning theory developed by Vapnik and Chervonenkis (Vapnik and Chervonenkis, 1964; Smola

and Schölkopf, 1998). Over the years, the SV algorithm has been successively developed as a classification tool such as the Support Vector Machines (SVM), and later combined with a regression technique to become the Support Vector Regression (SVR) (Drucker et al., 1997; Smola and Scholkopf, 1998). For a given $\{(x_1, y_1), \dots, (x_n, y_n)\} \subset X \times \mathfrak{R}$, the SVR technique aims to find a function $f(x)$ that has an ε deviation from the observed targets y_i for all training data x_i . $f(x)$ can be written for linear SVR as

$$f(x) = \langle \omega, x \rangle + b \text{ with } \omega \in X, b \in \mathfrak{R} \quad (4.1)$$

where $\langle \omega, x \rangle$ represents the dot product. In order to get a suitable fitting function f one will search for a small ω (weighting factor) and a constant C which will optimize an objective function given as

$$\begin{aligned} \text{minimize} \quad & \frac{1}{2} \|\omega\|^2 + C \sum_{i=1}^n (\xi_i + \xi_i^*) \\ \text{Subject to} \quad & \begin{cases} y_i - \langle \omega, x_i \rangle - b \leq \varepsilon + \xi_i \\ \langle \omega, x_i \rangle + b - y_i \leq \varepsilon + \xi_i^* \\ \xi_i, \xi_i^* \geq 0 \end{cases} \end{aligned} \quad (4.2)$$

where slack variables ξ_i, ξ_i^* are introduced so that the function f that approximates all pairs of (x_i, y_i) are given rooms for errors that are beyond the targeted deviation ε . The constant $C > 0$ determines the amount of slack that can be tolerated beyond the deviation target ε to achieve an optimal search for the fitting function f . The solution of (4.2) can be found by introducing a Lagrangian function with a dual set of variables given as

$$\begin{aligned}
L = & \frac{1}{2} \|\omega\|^2 + C \sum_{i=1}^n (\xi_i + \xi_i^*) - \sum_{i=1}^n (\eta_i \xi_i + \eta_i^* \xi_i^*) - \sum_{i=1}^n \alpha_i (\varepsilon + \xi_i - y_i + \langle \omega, x_i \rangle + b) \\
& - \sum_{i=1}^n \alpha_i^* (\varepsilon + \xi_i + y_i - \langle \omega, x_i \rangle - b)
\end{aligned} \tag{4.3}$$

where L is the Lagrangian and $\eta_i, \eta_i^*, \alpha_i, \alpha_i^*$ are the Lagrangian multipliers. The dual variables in (4.3) have to satisfy positivity criteria, thus $\alpha_i, \alpha_i^*, \eta_i, \eta_i^* \geq 0$. At the optimal solution, the partial derivatives of L with respect to the primal variables $(\omega, b, \xi_i, \xi_i^*)$ must be zero and hence

$$\frac{\partial L}{\partial b} = \sum_{i=1}^n (\alpha_i^* - \alpha_i) = 0 \tag{4.4}$$

$$\frac{\partial L}{\partial \omega} = \omega - \sum_{i=1}^n (\alpha_i - \alpha_i^*) x_i = 0 \tag{4.5}$$

$$\frac{\partial L}{\partial \xi_i} = C - \alpha_i - \eta_i = 0 \tag{4.6}$$

$$\frac{\partial L}{\partial \xi_i^*} = C - \alpha_i^* - \eta_i^* = 0 \tag{4.7}$$

Substituting equations (4.4), (4.5), (4.6) and (4.7) into equation (4.3) will lead to the optimization problem

$$\begin{aligned}
& \max_{\alpha_i, \alpha_i^*} -\frac{1}{2} \sum_{i,j=1}^n (\alpha_i - \alpha_i^*) (\alpha_j - \alpha_j^*) \langle x_i, x_j \rangle - \varepsilon \sum_{i,j=1}^n (\alpha_i + \alpha_i^*) + \sum_{i=1}^n y_i (\alpha_i - \alpha_i^*) \\
& \text{subject to} \quad \begin{cases} \sum_{i=1}^n (\alpha_i - \alpha_i^*) = 0 \\ \alpha_i, \alpha_i^* \in [0, C] \end{cases}
\end{aligned} \tag{4.8}$$

Once α_i and α_i^* are determined, the weighting factor (ω) and b are determined from the Karush-Kuhn-Tucker (KKT) conditions which means arriving at the global optimum when the dot product between the dual variable and constraints vanishes. The final approximate function can therefore be written as

$$\omega = \sum_{i=1}^n (\alpha_i - \alpha_i^*) x_i \text{ and thus } f(x) = \sum_{i=1}^n (\alpha_i - \alpha_i^*) \langle x_i, x \rangle + b \quad (4.9)$$

The Structural Risk Minimization (SRM) approach, the basis of SVR designed to minimize errors of the fitting function is more efficient than the traditional, Empirical Risk Minimization (ERM) approach used by machine learning algorithms such as ANN. This is particularly advantageous when the available training data is limited (Vapnik, 1995; Dibike et.al, 2001), as demonstrated by studies which showed that SVM and SVR models have better generalization than ANNs when the available training data is limited (Liong and Sivapragasam, 2002; Dibike et.al, 2006; Yoon et.al 2011). In addition, unlike neural networks which, when applied to nonlinear regression problems, are susceptible to finding local than global optimal solutions, SVR are better because their optimization approach generally leads to a global optimal solution (Chitrlekha and Shah, 2010). However, albeit their comparatively better performance, SVMs are not without drawbacks when used to solve hydrologic problems. Dibike et.al (2001) and Bray and Han (2004) pointed out that the heuristic nature of determining model parameters, the demand for large computational resources and unexpected results due to the semi-black-box nature of SVMs can be some of their potential pitfalls. Some of these drawbacks have now been largely overcome with the advent of increasingly faster computers and more specifically with the Least Square-Support Vector Machines (LS-SVM), which solves a set of linear problems instead of some computationally demanding, complex quadratic programming problems the standard SVM has to solve (Suykens and Vandewalle, 1999). LS-SVM has recently been applied to predict streamflow in which it demonstrated computational efficiency, excellent generalization ability and better performance than ANN and auto-regressive integrated moving average (ARIMA) models (Maity et.al, 2010 and Bhagwat and Maity, 2012). However, the semi-black box nature of SVM means that we should be cautious using the model, or we could end up with

unrealistic outputs. Further detailed descriptions of the SVR algorithm, its advantage and potential drawbacks can be found in Vapnik (1995), Smola and Scholkopf (1998), Dibike et.al (2001), Liong and Sivapragasam (2002), Bray and Han (2004), Yu et.al (2006) and Chitralkha and Shah (2010).

4.3 Data and Methodology

Two study sites, located in different climatic regions of Canada were chosen to analyze the performance of the SVR-RFFA models. The first group of river basins is located west of the Rockies of southeastern BC. Almost all of the annual maximum streamflow within this region occurs during May to July when the stream flow in these areas is mainly dominated by the melting of snowpack from the Rockies and occasionally by summer thunderstorms. The second group of river basins is located along the Great Lakes area of southern ON. Unlike the mountainous southeastern BC, this area is relatively flat with humid continental climate where most of the annual maximum streamflow occur during February to April. In addition, river basins in the southern ON region generally have relatively smaller drainage area and streamflow discharge compared to those in southeastern BC. To investigate the versatility and the general performance of SVR-RFFA models, this study compares their performance on these two regions of Canada with significant differences in physiographic and climatic characteristics.

First, only stations with hydrometric data of a record length exceeding 15 years were selected from the Hydrometric Database (HYDAT) of Environment Canada (EC). Next, these stations were further screened according to Bulletin 17B of USGS guidelines, which recommend only using streamflow record of river basins under natural condition or with minimal regulation for

determining flood frequency. Most of the stations selected have no missing data. For those stations which have one or two missing annual maximum flow values, the missing data was gap filled with available maximum monthly streamflow data. The data from the streamflow stations was then tested for the existence of trend using the non-parametric Mann-Kendall trend test. Those streamflow stations that exhibit trend at 5% significant level were not included for the RFFA. Streamflow stations in a given region were then grouped into clusters using the Hosking and Wallace (1997) test of homogeneity (H). In this test, a group of river basins are classified to be hydrologically homogeneous if the at-site frequency distributions of annual maximum flow series of river basins within the group pass a statistical significance test on the similarity of the at-site, L-moment CV (Coefficient of Variation) statistic based on the heterogeneity measure H. Conversely, a region is regarded as “acceptably homogeneous” if $H < 1$ (Hosking and Wallace, 1997), otherwise the group of river basins are regarded as heterogeneous and not suitable for RFFA. Based on this test, a group of 26 streamflow stations, located in southeastern BC, which satisfy a homogeneity criterion of $H \approx 0.8$ and another group of 23 streamflow stations located in southern ON with homogeneity criterion of $H \approx 0.9$ were selected for this study (see Figure 4.1). The drainage area of the stations in the BC region ranges from 204 km² to 19,600 km² with a median of 1,745 km² and an average annual maximum flow record length of 49 years whereas those in the ON region have smaller drainage areas, ranging from 94 km² to 1452 km² with a median of 294 km², and an average record length of 51 years.

The flood quantiles for the stations shown in Figure 4.1 were calculated for 10, 25, 50 and 100 year return period (collectively referred to as the T year return period) using the Log-Pearson III (LP3) distribution recommended for at site flood flow frequency studies (Bulletin 17B; 1982).

Climatic variables to be used as predictors, such as precipitation, were derived from the ANUSPLIN (Australian National University Spline) dataset of Natural Resources Canada which has data available from 1950 to the present. ANUSPLIN is a 10-km resolution, daily gridded precipitation data derived from precipitation gauges operated by Environment Canada (Hopkinson et al., 2011; Hutchinson et al., 2009). Physiographic data to be used as predictors, such as the mainstream channel length and channel slope, were derived from 3 arc second DEM data from Geospatial Data Extraction website (<http://geogratis.gc.ca/site/eng/extraction>) of Environment Canada using ArcGIS software.

To estimate the flood quantile (Q) of T year return period (predictand) using a RFFA, most commonly used predictors are drainage area and mean annual rainfall, while predictors that have also been used in a RFFA analysis include design rainfall intensity, time of concentration, mainstream slope, mainstream channel length, etc. (Griffis and Stedinger 2007; Shu and Ouarda, 2007; Haddad and Rahman 2011; Aziz et.al., 2013). Predictors to be selected in a RFFA to simulate regional flood quantiles of a given geographic region realistically are selected by a trial and error approach. In this study, predictors selected are drainage area, mean annual rainfall, time of concentration, design rainfall of a T year return period, mainstream slope and mainstream channel length.

To assess the performance of the SVR-RFFA model, a jackknife resampling procedure is used. First, a station is randomly removed from the group of 26 (BC) or 23 (ON) hydrometric stations and is assumed to be ungauged. Next the SVR algorithm is trained using the remaining 25 (BC) or 22 (ON) stations and the performance of the trained SVR model in predicting flood quantiles

of the “ungauged” basin is assessed. For each “ungauged” site there are 10 separate training episodes and the trained SVR with the least relative error (usually $\leq 10\%$) is selected. The same SVR training process is repeated for 26*20 (BC) or 23*20 (ON) times, and in each case, one of the 26 (20) stations is randomly removed and assumed as “ungauged” from the group of hydrometric stations in the BC and ON study areas, respectively. The LS-SVMlab toolbox of MATLAB (Brabanter et.al, 2011) based on LS-SVM, which has been reported to have short computational training time and improved generalization ability (Dibike et.al 2001; Maity et.al 2010), was used to estimate flood quantiles in the SVR-RFFA. The Radial Basis Function kernel of LS-SVMlab was chosen for training the SVR-RFFA model after a thorough comparison with other kernel functions (Linear, Polynomial and Multilayer Perception kernels). The performance of the RFFA model was assessed using goodness-of-fit statistics such as the Nash Sutcliffe coefficient (E_f) (Nash and Sutcliffe, 1970), coefficient of determination (R^2) (Krause et.al, 2005), root mean squared error (RMSE) and mean bias (BIAS), (Ouarda et.al 2007). Given the drainage area of river basins of both study regions varies widely, statistics such as the RMSE and BIAS could be unduly dominated by errors of flood quantiles estimated for large river basins over flood quantiles estimated for relatively small river basins. To avoid getting non-representative statistics dominated by a few large river basins, beside RMSE and BIAS, relative root mean squared error (RMSE_r) and relative mean bias (BIAS_r) were also used in this study (Ouarda et.al 2007).

4.4 Discussions of Results

4.4.1 Predictor variables

A number of physiographic and climatic variables had been chosen as possible predictors for the SVR-RFFA model. As mentioned earlier, all past RFFA studies have adopted drainage area (A) as a predictor. Therefore, A is always one of the predictors considered in this study. Other physiographic variables considered are the mainstream slope in m/m (S), mainstream channel length in km (L) and time of concentration in hours (t_c) estimated using $t_c = 0.191L^{0.76}S^{-0.19}$ as suggested by the US Army Corps of Engineers (Almeida et.al., 2014). In addition, climatic predictors used in this study are standardized design rainfall intensity of T year return period in mm/d (I) and standardized mean annual precipitation in mm/yr (M). Given that cross-correlations between these predictor variables are generally low, it means that each predictor can potentially contribute some relevant information to the RFFA model (Table 4.1). However, Table 4.1 shows that L and t_c are highly correlated with each other mainly because L is directly used in estimating t_c . Therefore, in this study only t_c , instead of both t_c and L are considered in various combinations of predictors tested.

Using the list of predictors in Table 4.1, different combinations of predictors have been tested to estimate the T year flood quantile (Q10, Q25, Q50 and Q100, respectively) of a given station that is assumed as ungauged in each of the study areas (Table 4.2). All combinations contain A as a predictor. In addition, at least one climatic predictor from Table 4.1 is also considered (Table 4.2). In addition, we have also tested a relatively new predictor combination which includes the sum of standardized design rainfall and mean annual precipitation (predictor #9) as a single climatic predictor. The sum of standardized design rainfall intensity and mean annual

precipitation respectively represent the climatic conditions that directly influence the volume of flood quantile and the antecedent soil moisture conditions leading up to the flood event (regions with high mean annual precipitation are more likely to have wet antecedent soil moisture conditions during the flood event).

4.4.2 Performance based on goodness-of-fit statistics

Using thirteen combinations of predictors shown in Table 4.2, the SVR-RFFA model was used to predict the flood quantiles, Q10, Q25, Q50 and Q100, for the 26 and 23 selected river basins in southeastern BC and southern ON, respectively. The accuracy of RFFA model in predicting the flood quantile for any station considered as ungauged was estimated by the goodness-of-fit statistics of Section 4.3 and the results for each flood quantile and each set of predictors are presented in Figure 4.2 with Table 4.3 showing the mean goodness-of-fit statistics of all flood quantiles for all predictor combinations. The performance of the RFFA model for the thirteen sets of predictors is ranked primarily in terms of *RMSE* and *RMSEr* for all of the flood quantiles considered.

For both study areas the *Ef* and R^2 of the RFFA model was about 0.7 for almost all of the thirteen sets of predictors tested, which implies that the performance of the RFFA model is satisfactory. For the BC study site, the average *RMSE* and *BIAS* of the RFFA model were 270 m³/s and 0.1 m³/s, respectively. Similarly, for the ON study site, the average *RMSE* and *BIAS* were 46.2 m³/s and 0.54 m³/s respectively. Most of the *RMSEr* statistics (*RMSE* normalized by the observed flood quantile) are greater than 30%, which was mainly caused by the RFFA model's poor performance for stations of very small or very large catchment areas within each of the study

sites, which is similar to the findings of Ouarda et.al (2007). It seems that the SVR-RFFA model tend to predict reasonably accurate flood quantiles for average sized catchments in the two study sites but poorly for a few catchments that are either relatively small or large. Given the performance of machine learning algorithms such as SVRs mainly depend on the training data available, we expect a drop in the performance of such algorithms for limited amount of training data available for odd size (very small or very large) catchments.

Among thirteen sets of predictors tested, the combined predictor derived from combining the standardized T year return period precipitation with the standardized mean annual precipitation into a single climatic predictor($A(I+M)tcS$ or #9) resulted in the best overall flood quantiles estimated by the SVR RFFA model for both of the BC and ON study sites. Scatterplots of Figure 4.3 and Figure 4.4 show good agreements between local and regional flood quantiles of various return periods best predicted by the SVR model for two study sites in southeastern BC and southern ON, respectively. The results demonstrate that the SVR model based on the SRM approach, which restricts the class of fitting functions a learning machine can implement according to the amount of available training data, can predict accurate flood quantiles when there is limited training data (Vapnik, 1995; Dibiye et.al, 2001). There are also past studies that show SVR trained with limited amount of data achieving better results and more superior generalization ability than other models (e.g. Liong and Sivapragasam, 2002). In addition, by using the convex optimization approach, SVR should asymptotically arrive at the global optimal solution (Chitrlekha and Shah, 2010), which means that regional flood quantiles estimated by SVR are more likely to agree well with local flood quantiles. On a whole, these results show that

the proposed SVR-RFFA model estimated the T year flood quantile credibly for the two clusters of catchments in southeastern BC and southern ON.

4.4.3 Comparing SVR based with ANN based RFFA models

The performance of the SVR-RFFA model was also compared with an ANN based RFFA model which has been extensively applied in various RFFA studies (e.g., Shu and Burn, 2004; Shu and Ouarda, 2007; Aziz et.al, 2013). A 2-layer and 10-node per layer neural networks with Bayesian Regularization backpropagation module based on the neural network tool box of MATLAB was used to estimate flood quantiles of the ANN based RFFA model for this study. The same procedure that was used to train the SVR-RFFA model and the 13 sets of predictors (Table 4.2) were used by the ANN based RFFA model to simulate flood quantiles of T -year return period. On the basis of the mean goodness-of-fit statistics obtained for the 13 sets of predictors tested for both study sites (Table 4.4), the SVR-RFFA model performed relatively better than the ANN based RFFA model.

The main difference between the ANN and SVR-RFFA models however came from the coefficient of variation (CV) of the flood quantiles derived from each model. The CV of flood quantiles estimated by the ANN and SVR-RFFA models using the 13 sets of predictors for the two study sites is shown in Figure 4.5 and Figure 4.6. For the southeastern BC study area, the median CV of the SVR-RFFA model is about 0.006 which is significantly lower than the median CV of 0.15 for the ANN based RFFA model. Similarly, the median CV of the SVR-RFFA model for the ON study area is 0.004 whereas the median CV of the ANN based RFFA model is 0.12. Among the 13 sets of predictors tested for the two study sites, the median CV of the predictor set

that resulted in the best overall flood quantiles estimated by the SVR-RFFA model is 0.0055 and 0.0036 for southeastern BC and southern ON study areas, respectively. This was again significantly lower than the median *CV* of 0.138 (BC) and 0.097 (ON) from the best performing predictor set of the ANN based RFFA model (represented by dashed and dotted lines in Figure 4.5 and Figure 4.6, respectively). On the basis of the above median *CV* of flood quantiles estimated by both RFFA models, it seems that SVR can predict the regional flood quantiles in the study sites more consistently than ANN. This could be partly because of different approaches that ANNs and SVRs take in finding the optimal solution. In ANNs, a backpropagation algorithm based on a gradient descent or other similar optimization approaches is generally used to find an optimal solution. This is achieved by iteratively searching for optimal weights assigned to the network to minimize differences between simulations of the neural network and the observed values (Priddy and Keller, 2005). A possible pitfall of the gradient descent approach has been getting trapped in some local optima before it reaches the global optimal solution, and the possibility of this pitfall increases as a problem becomes more complex because the number of local optima tends to increase with the complexity of a problem (Minsky and Papert, 1988; Smola & Scholkopf, 1998). Because of this drawback, the accuracy of flood quantiles simulated by ANNs can vary over a relatively wide range, partly depending on the initial model parameters chosen and search directions of successive simulations of the optimization approach. However, since SVR is set up to solve a convex optimization problem, it is generally guaranteed to find the global optimal solution (Smola & Scholkopf, 1998; Chitrlekha and Shah, 2010). These results show that although the median flood quantiles predicted by the SVR and ANN based RFFA models are comparable to each other, SVR is more consistent than ANN in predicting regional flood quantiles of ungauged sites with selected

predictors, if an adequate amount of training data is available to develop such RFFA models based on machine learning algorithms. In other words, it seems the former RFFA model can estimate more reliable regional flood quantiles than the latter. In addition, the SVR-RFFA model was computationally faster taking only about half of the computational time required by the ANN-RFFA to generate flood quantile estimates of T-year return period for each river basin considered as ungauged in the two study areas. However, more extensive tests are recommended to confirm this preliminary conclusion.

4.4.4 Projected changes in future flood quantiles derived from SVR RFFA models

Trenberth (1998; 1999) and Trenberth et.al (2003) argued that the increased water holding capacity of the atmosphere at about 7% per K° rise in temperature (Clausius-Clapeyron equation) favors stronger rainfall and snowfall events, thus increasing the risk of flooding. Global warming, the human induced changes to the Earth's climate as a result of increased concentrations of greenhouse gases lead to increasing likelihood in the occurrence or strength of extreme weather and climate events (IPCC, WGI report chapter 1, Cubasch et.al 2013). The projected increase in temperature by various CMIP5 (Coupled Model Intercomparison Project phase 5) GCMs (Global Climate Models) over Canada could result in a significant change in the nature and distribution of two climate predictors (mean annual rainfall and *T* year return period rainfall) over the 21st century.

To analyze the projected changes in flood quantiles over southeastern BC and southern ON, the statistically downscaled data from RCP8.5 and RCP4.5 climate projections of five GCMs of CMIP5 were extracted from the Pacific Climate Impacts Consortium (PCIC) database. PCIC

statistically downscaled the RCPs climate scenarios using the BCCAQ (Bias Correction/Constructed Analogues with Quantile mapping reordering) (Gudmundsson et al. 2012) and BCSD (Bias-Correction Spatial Disaggregation) methods (Bürger et al., 2013). ANUSPLIN data was used as a basis to statistically downscale the GCM's climate projections using the BCSD or BCCAQ approaches. Therefore, the CMIP5 climate projections from PCIC have the same spatial resolution as ANUSPLIN data which was used to train the SVR RFFA model for historical climate thus making them suitable for future flood quantile estimations. In estimating future flood quantiles we assume that only climatic variables such as precipitation show significant change during the 21st century while changes in land use that could possibly affect physiographic variables such t_c are neglected.

Based on the RCP8.5 and RCP4.5 climate projections of five GCMs, the T year return period precipitation is projected to increase by about 22.6% and 6.2% over southeastern BC and southern ON regions, respectively, during the second half of the 21st century. Some GCMs such as CanESM2 and CCSM4 project a smaller T -year precipitation in the 2080s (2071-2100) than that of the 2050s (2041-2070) whereas the other four GCMs project a consistent increase in the T -year return period precipitation from the 2050s to the 2080s (Figure 4.7). Almost all GCMs also project a relatively wetter climate for southeastern BC and southern ON with the mean annual precipitation of the former projected to increase by about 9.4% and the latter by 7.8% in the mid- and late 21st century (Figure 4.8). The projected increase in the mean annual rainfall over the study areas increases the likelihood of wet antecedent soil moisture conditions in days leading up to occurrences of flood causing precipitation events. Such wet antecedent soil

moisture conditions combined with an increased T -year return period rainfall will result in greater runoff from a given river basin, thus increasing the T -year return period flood quantile.

To analyze projected changes in flood quantiles due to projected increase in the mean annual precipitation and T year return period rainfall, the SVR RFFA model with the set of predictors that performed the best for the historical climate of both study sites was used. For estimating future flood quantiles, the RFFA model was first trained based on the chosen set of predictors and flood quantiles of all river basins derived from the data of a given GCM for its base period (1971-2000). Using this trained RFFA model the future flood quantiles for the river basins were then estimated using the GCM's projected climate predictors for the 2050s and 2080s. As shown in Figure 4.9, the projected climate over the study areas has resulted in an increase in flood quantiles of all return periods ($T=10, 25, 50$ and 100) for almost all GCM projections. For the southeastern BC area, the median projected increase in flood quantiles derived from all GCMs is about 7.5% and 7.1% for RCP4.5 and 7.2% and 8.5% for RCP8.5 during the 2050s and 2080s, respectively. The median projected increase in flood quantiles of all GCMs for the southern ON study site was found to be around 25.8% and 18.7% for RCP4.5 and 33.4% and 36.9% for RCP8.5 during the 2050s and 2080s, respectively. The smaller drainage area of the river basins in the southern ON study sites means that extreme precipitation events could more likely occur more uniformly over the entire basin, resulting in more severe peak runoff reaching the river basin outlet. This could partly explain why considerably higher projected changes in flood quantiles for the southern ON study site are found when compared to those located in southeastern BC even though the projected increase in T year return period precipitation and mean annual precipitation of the former is relatively lower than the latter. Overall, the above

results suggest that under a climate which is projected to be wetter and more extreme during the mid and late 21st century, the southeastern BC and southern ON regions are expected to experience higher runoffs that could significantly increase the risk of flooding over both regions. However, it should be noted that the projected rise in temperature during the mid and late 21st century will increase the rate of evapotranspiration over this region. This could partly offset the contribution of an increase in mean annual rainfall to the increase in flood quantiles by reducing the likelihood of wet antecedent soil moisture conditions in the days leading up to the flood causing extreme precipitation event.

4.5 Summary and Conclusions

The performance of a RFFA model based on Support Vector Regression (SVR) in estimating regional flood quantiles was proposed and applied to a group of 26 and 23 catchments located in southeastern British Columbia (BC) and southern Ontario (ON), Canada, respectively. The SVR-RFFA model estimated flood quantiles for any given station assumed to be ungauged within each study area using 13 sets of physiographic and climatic predictors. For both study areas goodness-of-fit statistics, Ef and R^2 , of the RFFA model exceeded 0.5 for almost all of the thirteen sets of predictors tested, which implies that the performance of the RFFA model is satisfactory. The relative root mean squared error ($RMSEr$) was found to be greater than 30% for most predictor sets, which mainly indicate poor performance of the RFFA model for stations of very small or very large catchment areas within each of the two study sites. The performance of the SVR-RFFA model was also compared with an artificial neural network (ANN) based RFFA model which has been used in many previous RFFA studies. The results show that the SVR-RFFA model has consistently performed better than the ANN based RFFA model in all the 13 sets of

physiographic and climatic predictors for the two study sites. Major differences were, however found in the coefficient of variation (CV) of flood quantiles estimated by both RFFA models. The considerably smaller CV of the SVR-RFFA model suggests that this model can predict regional flood quantiles more consistently than the ANN based RFFA model. The comparison between SVR and ANN presented in this study further shows that SVR has a better generalization ability than ANN for study areas with limited amount of data to train an RFFA model, which is 26 streamflow stations in the BC and 23 stations in the ON study sites. A common problem encountered in most RFFA studies is the challenge to find a sufficiently large number of hydrologically homogeneous river basins with natural streamflow data to train the regional models. However, with ample training data, ANN-RFFA models are generally expected to perform well, as suggested by Aziz et.al (2013) who showed that ANN-RFFA models perform better with relatively large training data sets.

The SVR-RFFA model was also used to predict future flood quantiles for the two study sites based on statistically downscaled, RCP4.5 and RCP8.5 climate projections of five GCMs of CMIP5. The increase in T -year return period precipitation by 22.6% (BC) and 6.2% (ON) and the mean annual precipitation by 9.2% (BC) and 7.8% (ON) imply that the flood quantiles over the two study sites are projected to increase during the mid and late 21st century. Overall, based on the two RCP climate projections of the five GCMs, the SVR-RFFA model projected an average increase in flood quantiles of about 7% (BC) and 30% (ON) for the 2050s (2041-2070) and 8% (BC) and 28% (ON) for the 2080s (2071-2100) of T -year return period. However, we believe that such a level of projected increase in future flood quantiles by the SVR-RFFA model are conservative because the predictors considered in this study do not include climatic variables

such as temperature which GCMs unanimously project to increase. On the other hand, higher evapotranspiration loss under a warmer climate could indirectly offset some of the contribution of higher mean annual precipitation that tends to increase flood quantiles. In addition, although there is a general consensus that a warmer climate favors more extreme precipitation events (Trenberth, 1998; 1999; Trenberth et.al, 2003; IPCC, WGI report chapter 1, Cubasch et.al, 2013), there is still a great deal of improvement required with the climate change projections of contemporary GCMs of IPCC (2013) which may not agree with observations when such data becomes available. Therefore, while it is likely that we will witness more extreme flood events occurring in the mid and late 21st century, as we have observed in recent decades in different parts of the world, the projected changes in this study should not be taken as accurate projections of future flood quantiles of the study sites.

In summary, this study shows that SVR-RFFA models can credibly estimate regional flood quantiles (Q10, Q25, Q50 and Q100) for two regional study sites with “homogeneous” river basins representing different climatic regions of Canada. In addition, SVR-RFFA models could be used to project future flood quantiles under the potential impact of climate change. However, in assessing climate change impact to regional flood quantiles, other than precipitation, climate variables such as temperature could be included to provide realistic projections of future flood quantiles over the two study sites subjected to climate change impact.

Acknowledgements

Observed annual maximum stream flow data were extracted from the Hydrometric Database of Environment Canada. Statistically downscaled CMIP5 climate projections were downloaded from the Pacific Climate Impacts Consortium database. The authors appreciate the kind support of Daniel McKenny and Pia Papadopol from Natural Resources Canada for providing ANUSPLIN daily gridded precipitation data and supporting materials which was used to

compute the climatic predictor variables used in this study. The first author was supported by the University of Alberta and a NSERC strategic network grant.

4.6 References

- Almeida, I.K., Almeida, A.K., Anache, J.A.A, Steffen, J.L, Alves Sobrinho, T. 2014. Estimation of time of concentration in overland flow in watersheds: a review. São Paulo, UNESP, Geociências, 33, n. 4: 661-671, 2014 662
- Aziz, K., Rahman, A., Fang, G., Shrestha, S. 2013. Application of artificial neural networks in regional flood frequency analysis: a case study for Australia. Stoch Environ Res Risk Assess, 28: 541-554. doi 10.1007/s00477-013-0771-5
- Bhagwat, P.P. and Maity, R. 2012. Multistep-Ahead River Flow Prediction using LS-SVR at Daily Scale. Scientific Research, J of Water Resource and Protection, 4: 528-539.
- Brabanter, K.De., Karsmakers, P., Ojeda, F., Alzate, C., Brabanter, J.De, Pelckmans, B. De M., Vandewalle, J., Suykens, J.A.K. 2011. LS-SVMlab Toolbox User's Guide version 1.8. Department of Electrical Engineering, Katholieke Universiteit Leuven. <http://www.esat.kuleuven.be/sista/lssvmlab/> Last accessed July-8-2015
- Bray, M. and Han, D. 2004. Identification of support vector machines for runoff modelling. J of Hydroinformatics,06.4: 265-280.
- Bulletin 17B of the Hydrology Subcommittee, 1982. Guidelines for determining Flood Flow Frequency. US Department of the Interior, Geological Survey.
- Bürger, G., Sobie, S.R., Cannon, A.J., Werner, A.T., and Murdock, T.Q. 2013. Downscaling extremes - an intercomparison of multiple methods for future climate. Journal of Climate, 26: 3429-3449. doi: 10.1175/JCLI-D-12-00249.1
- Burnash, R.J.C., Ferral, R.L., McGuire, R.A., 1973. A generalized streamflow simulation system-conceptual modeling for digital computers. U.S. Department of Commerce, National Weather Service and State of California, Department of Water Resources.

- Chitralkha, S.B and Shah, S.L. 2010. Support vector regression for soft sensor design of nonlinear processes. 18th Mediterranean Conference on Control & Automation Congress Palace Hotel, Marrakech, Morocco, June 23-25, 2010.
- Chow, V.T. Maidment, D.R. and Mays, L.W. 1988. Applied Hydrology, McGraw-Hill, New York, NY.
- Cubasch, U., D. Wuebbles, D. Chen, M.C. Facchini, D. Frame, N. Mahowald, and J.-G. Winther, 2013: Introduction. In: Climate Change 2013: The Physical Science Basis. Contribution of Working Group I to the Fifth Assessment Report of the Intergovernmental Panel on Climate Change [Stocker, T.F., D. Qin, G.-K. Plattner, M. Tignor, S.K. Allen, J. Boschung, A. Nauels, Y. Xia, V. Bex and P.M. Midgley (eds.)]. Cambridge University Press, Cambridge, United Kingdom and New York, NY, USA.
- Dibike, Y.B., Velickov, S., Solomatine, D., & Abbott, M.B. 2001. Model Induction with Support Vector Machines: Introduction and Applications. *J of Computing in Civil Engineering*, 15(3): 208-216.
- Drucker, H., Burges, C., Kaufman, L., Smola, A., & Vapnik, V. 1997. Support Vector Regression Machines. In *Advances in Neural Information Processing Systems- Proceedings of the 1996 Conference*, volume 9, pp. 155–161. MIT Press, Cambridge, MA.
- Griffis, V.W and Stedinger, J.R. 2007. The use of GLS in regional hydrologic analysis. *J of Hydrology*, 344: 82-95. doi:10.1016/j.jhydrol.2007.06.023.
- Gudmundsson, L., Bremnes, J.B., Haugen, J.E., and Engen-Skaugen, T. 2012. Technical Note: Downscaling RCM precipitation to the station scale using statistical transformations - a comparison of methods. *Hydrology and Earth System Sciences*, 16: 3383–3390. doi:10.5194/hess-16-3383-2012.

- Haddad, K. and Rahman, A. 2011. Regional Flood Estimation in New South Wales Australia Using Generalized Least Squares Quantile Regression. Technical note, J. Hydrologic Engineering, ASCE. 16: 920-925. doi: 10.1061/(ASCE)HE.1943-5584.0000395
- Hopkinson, R.F., McKenny D.W., Milewska E.J., Hutchinson, M.F., Papadopol P., Vincent, L.A., 2011. Impact of Aligning Climatological Day on Gridding Daily Maximum–Minimum Temperature and Precipitation over Canada. J Applied Meteorology and Climatology, AMS, 50: 1654-1665. doi: 10.1175/2011JAMC2684.1
- Hosking, J.R.M and Wallis, J.R. 1997. Regional Frequency Analysis. An Approach Based on L-Moments. Cambridge University Press, UK. ISBN 0-521-43045-3
- Hutchinson, M.F., McKenny D.W., Lawrence, K., Pedlar, J.H., Hopkinson, R.F., Milewska E., Papadopol P., 2009 Development and Testing of Canada-Wide Interpolated Spatial Models of Daily Minimum–Maximum Temperature and Precipitation for 1961–2003. J Applied Meteorology and Climatology, AMS, vol 48, pp 725-741. doi: 10.1175/2008JAMC1979.1
- Kerkhoven, E., and Gan, T. Y., 2006, A Modified ISBA Surface Scheme for Modeling the Hydrology of Athabasca River Basin with GCM-scale Data, Adv. in Water Resou., 29(6), 808-826.
- Krause, P., Boyle, D.P., and Bäse, F. 2005. Comparison of different efficiency criteria for hydrological assessment. Advances in Geosciences, 5: 89-97
- Liong, S.Y., and Sivapragasam, C. 2002. Flood Stage Forecasting with Support Vector Machines. J of the American Water Resources Association, 38(1): 173-186.
- Maity, R., Bhagwat, P.P., and Bhatnagar, A. 2010. Potential of support vector regression for prediction of monthly streamflow using endogenous property. J of Hydrological Processes, 24: 917-923. doi: 10.1002/hyp.7535

- Minsky, M.L. and Papert, S. 1988. Perceptions: an introduction to computational geometry. Cambridge Mass.: MIT Press, 1988, c1969.
- Nash, J.E. and Sutcliffe, J.V. 1970. River flow forecasting through conceptual models Part I – A discussion of principles. *J of Hydrology*, 10: 282-290.
- Nor, N. I. A., Harun, S., Kassim, A. H. M. 2007. Radial basis function modeling of hourly streamflow hydrograph. *J of Hydrologic Engineering*, 12: 113-123. doi:10.1061/(ASCE)1084-0699(2007)12:1(113)
- Ouarda, T.B.M.J, Ba, K.M., Diaz-Delgado, C. A. Cârsteanu, A. Chokmani, K., Gingras, H., Quentin, E., Trujillo, E., B. Bobe'e, B. 2007. Intercomparison of regional flood frequency estimation methods at ungauged sites for a Mexican case study. *J of Hydrology*, 348: 40-58. doi:10.1016/j.jhydrol.2007.09.031
- Priddy, K.L. and Keller, P.E. 2005. Artificial Neural Networks, An Introduction. SPIE press, Bellingham, Washington USA.
- Rao, A.R, Hamed, K.H. 2000. Flood Frequency Analysis. CRC Press, New York.
- Samui, P. 2011. Application of Least Square Support Vector Machine (LSSVM) for determination of evaporation loss from reservoirs. *Scientific Research, Engineering*, 3: 431-434. doi:10.4236/eng.2011.34049
- Shu, C. and Ouarda, T.B.M.J. 2007. Flood frequency analysis at ungauged sites using artificial neural networks in canonical correlation analysis physiographic space. *Water Resources Research*, 43, doi:10.1029/2006WR005142.
- Smola, A.J. and Schölkopf, B. 1998. A tutorial on support vector regression. NeuroCOLT2 Technical Report Series, NC2-TR-1998-030.

- Stedinger, J.R. and Tasker, G.D. 1985. Regional Hydrologic Analysis 1- Ordinary, Weighted, and Generalized Least Squares Compared, *Water Resources Research*, 21, No 9: 1421-1432.
- Suykens, J.A.K and Vandewalle, J. 1999. Least Squares Support Vector Machines Classifiers. *Neural Processing Letters*, 9: 293-300.
- Thomas, D.M. and Benson M.A. 1975. Generalization of streamflow characteristics from drainage-basin characteristics. A study of relations for estimating streamflow characteristics from drainage-basin characteristics in four hydrologically different regions of the conterminous United States. United States Geological Survey Water-Supply paper.
- Trenberth, K.E. 1998. Atmospheric moisture residence time and cycling: Implication for rainfall rates and climate change. *J of Climatic Change*, 39: 668-694
- Trenberth, K.E. 1999. Conceptual framework for changes of extremes of the hydrological cycle with climate change. *Climatic Change*, 42: 327-339
- Trenberth, K.E, Dai, A., Rasmussen, R.M. and Parsons, D.B. 2003. The Changing Character of Precipitation, *BAMS, AMS*. doi: 10.1175/BAMS-84-9-1205.
- V. Vapnik and A. Chervonenkis. 1964. A note on one class of perceptrons. *Automation and Remote Control*, vol 25.
- Vapnik, V. (1995): *The Nature of Statistical Learning Theory*. Springer, NY.
- Wu, C-L., Chau, K-W. and Li, Y-S. 2008. River stage prediction based on a distributed support vector regression. *J of Hydrology*, 358: 96-111. doi:10.1016/j.jhydrol.2008.05.028
- Yoon, H., Jun, S-C., Hyun, Y., Bae, G-O., and Lee, K-K. 2011. A comparative study of artificial neural networks and support vector machines for predicting groundwater levels in coastal aquifer. *J of Hydrology*, 396: 128-138. doi:10.1016/j.jhydrol.2010.11.002

Yu, P-S., Chen, S-T., and Chang, I-F. 2006. Support vector regression for real-time flood stage forecasting. *J of Hydrology*, 328: 704-716. doi:10.1016/j.jhydrol.2006.01.021

Zakaria, Z.A. and Shabri, A. 2012. Streamflow forecasting at ungauged sites using Support Vector Machines. *J of Applied Mathematical Sciences*, 6, no. 60: 3003-3014.

Table 4.1 List of predictors used in this study and their cross-correlations

BC						
Predictors	<i>A</i> (<i>km</i> ²)	<i>I</i> (<i>mm/d</i>)	<i>M</i> (<i>mm/yr</i>)	<i>S</i> (<i>m/m</i>)	<i>L</i> (<i>km</i>)	<i>tc</i> (<i>hr</i>)
<i>A</i> (<i>km</i> ²)	1					
<i>I</i> (<i>mm/d</i>)	-0.242	1				
<i>M</i> (<i>mm/yr</i>)	-0.531	0.661	1			
<i>S</i> (<i>m/m</i>)	-0.612	0.086	0.482	1		
<i>L</i> (<i>km</i>)	0.890	-0.195	-0.598	-0.718	1	
<i>tc</i> (<i>hr</i>)	0.886	-0.195	-0.615	-0.748	0.998	1
ON						
Predictors	<i>A</i> (<i>km</i> ²)	<i>I</i> (<i>mm/d</i>)	<i>M</i> (<i>mm/yr</i>)	<i>S</i> (<i>m/m</i>)	<i>L</i> (<i>km</i>)	<i>tc</i> (<i>hr</i>)
<i>A</i> (<i>km</i> ²)	1					
<i>I</i> (<i>mm/d</i>)	-0.247	1				
<i>M</i> (<i>mm/yr</i>)	0.112	0.526	1			
<i>S</i> (<i>m/m</i>)	-0.285	-0.334	-0.451	1		
<i>L</i> (<i>km</i>)	0.749	-0.035	0.223	-0.383	1	
<i>tc</i> (<i>hr</i>)	0.772	-0.048	0.246	-0.519	0.950	1

Table 4.2 Thirteen combinations of predictors used in SVR-RFFA model

	AI	AIM	AI _{tc}	AI _S	AIM _{tc}	AIM _S	AI _{tcS}	AIM _{tcS}	A(I+M) _{tcS}	AM	AM _{tc}	AM _S	AM _{tcS}
ID	1	2	3	4	5	6	7	8	9	10	11	12	13

Table 4.3 Mean goodness-of-fit statistics of flood quantiles (Q10 to Q100) estimated by the SVR-RFFA model for the 13 sets of predictors considered for a group of 26 and 23 river basins in southeastern BC and southern ON, respectively.

	Predictor Combination (BC)												
	9	7	13	3	11	6	5	8	2	4	12	1	10
<i>RMSE</i>	236	241	255	253	257	257	270	272	294	310	373	382	393
<i>RMSEr</i>	36	55	35	49	39	65	50	52	68	67	89	62	78
<i>BIAS</i>	4.5	-4.0	-5.1	1.1	-5.5	-3.4	-19.2	-10.6	1.0	17.7	20.8	1.6	0.05
<i>BIASr</i>	3.6	-1.5	9.5	5.6	10.1	15.8	9.7	12.0	17.3	17.9	27.6	16.1	18.7
<i>Ef</i>	0.882	0.876	0.862	0.864	0.859	0.855	0.844	0.843	0.813	0.792	0.701	0.677	0.670
<i>R</i> ²	0.874	0.876	0.862	0.865	0.860	0.856	0.845	0.844	0.814	0.795	0.709	0.691	0.688
	Predictor Combination (ON)												
	9	8	10	5	2	3	7	4	1	6	12	13	11
<i>RMSE</i>	39	38	38	41	41	46	46	48	49	49	50	50	56
<i>RMSEr</i>	26	36	34	25	32	35	45	47	37	68	66	55	38
<i>BIAS</i>	6.9	0.5	1.8	-1.3	-2.0	0.6	0.5	4.9	-2.1	3.8	7.1	-0.6	-4.28
<i>BIASr</i>	5.2	6.5	9.7	2.6	5.0	4.0	2.2	15.3	6.8	15.4	20.1	9.9	6.8
<i>Ef</i>	0.736	0.771	0.771	0.714	0.741	0.653	0.667	0.632	0.614	0.627	0.604	0.619	0.497
<i>R</i> ²	0.848	0.777	0.773	0.740	0.749	0.674	0.694	0.650	0.623	0.649	0.631	0.637	0.543

Table 4.4 Comparing the mean goodness-of-fit statistics of flood quantiles estimated by ANN and SVR-RFFA models for thirteen sets of predictors considered for a group of 26 and 23 river basins in south eastern BC and southern ON, respectively.

	BC study site						ON study site					
	RMSE	RMSEr	Bias	Biasr	Ef	R ²	RMSE	RMSEr	Bias	Biasr	Ef	R ²
Q10												
ANN	324.6	72.4	7.1	16.6	0.697	0.727	42.0	41.8	0.8	8.0	0.523	0.619
SVR	267.0	54.2	-5.0	9.4	0.794	0.799	38.0	39.4	1.0	8.2	0.628	0.672
Q25												
ANN	348.2	63.3	15.2	15.4	0.720	0.744	51.3	41.4	0.4	8.0	0.515	0.608
SVR	281.7	54.0	1.7	11.7	0.815	0.818	42.5	40.7	0.8	7.7	0.681	0.703
Q50												
ANN	383.9	67.9	29.0	17.7	0.698	0.734	52.6	39.8	-1.7	6.7	0.605	0.650
SVR	299.1	59.1	2.7	14.2	0.817	0.820	47.9	43.5	1.4	8.8	0.676	0.696
Q100												
ANN	379.0	64.0	20.6	17.0	0.741	0.757	59.2	41.8	-0.4	7.3	0.584	0.654
SVR	319.0	60.3	0.4	14.7	0.816	0.817	53.1	43.4	1.6	8.9	0.675	0.695

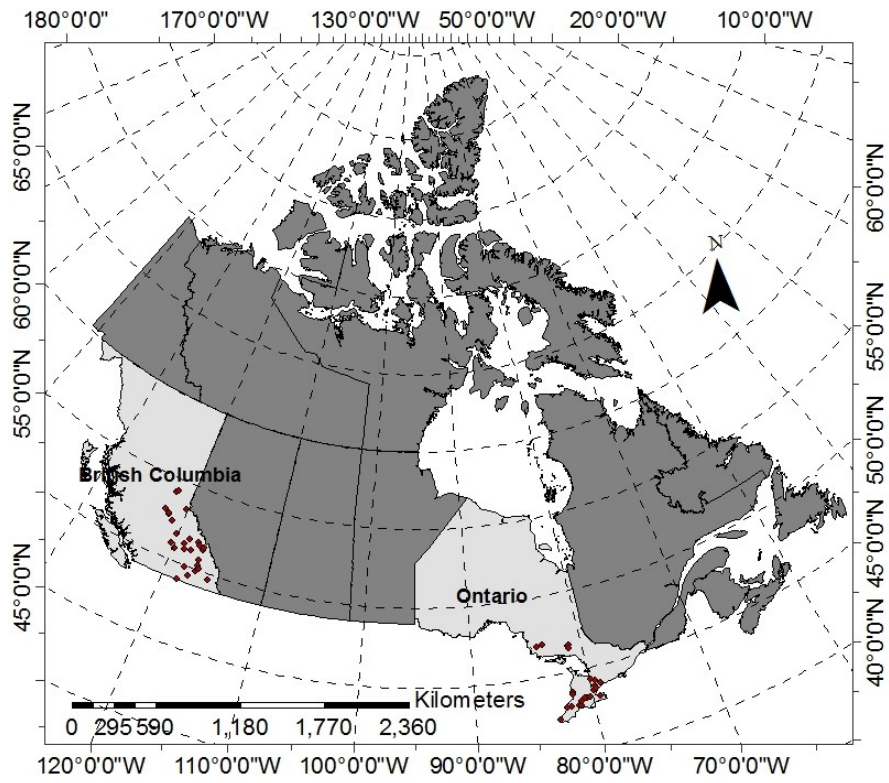


Figure 4.1 A group of 26 and 23 streamflow stations located in southeastern BC and southern ON, Canada, respectively selected for this study.

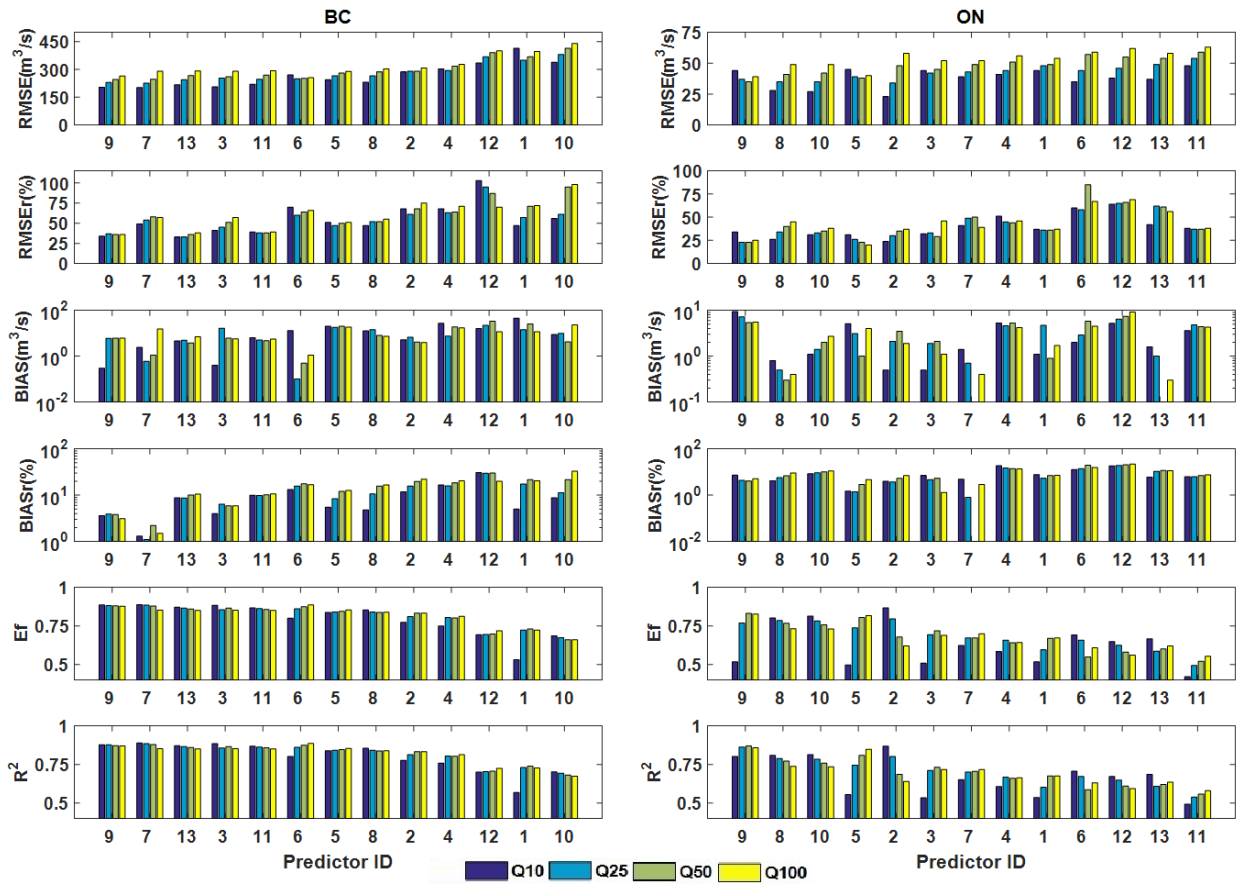


Figure 4.2 Predictor combinations used in the SVR-RFFA model arranged in descending order of their overall performance with respect to goodness-of-fit statistics of estimated flood quantiles (Q10 to Q100) for a group of 26 and 23 river basins in southeastern BC and southern ON, respectively. Note: for ease of visual presentation the absolute values of BIAS and BIASr(%) are given in log scales.

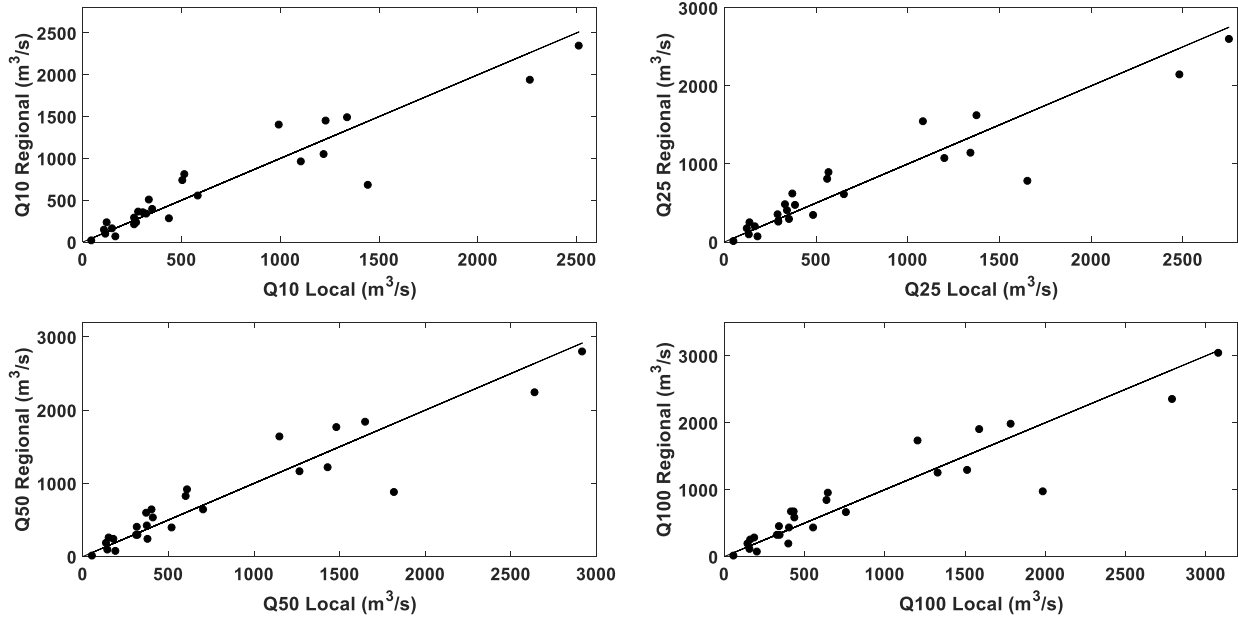


Figure 4.3 Scatterplots of local versus regional estimates of flood quantiles of various return periods that were best predicted by the SVR model based on predictors of set #9 for a group of 26 catchments selected in southeastern BC.

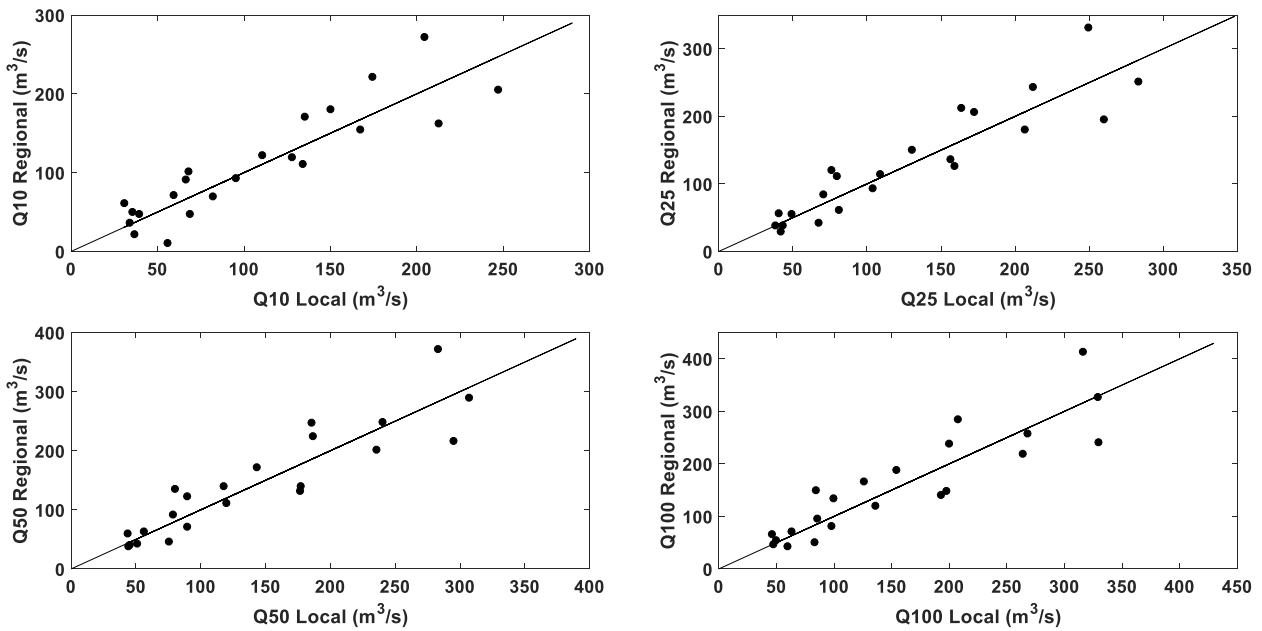


Figure 4.4 Scatterplots of local versus regional estimates of flood quantiles of various return periods that were best predicted by the SVR model based on predictors of set #9 for a group of 23 catchments selected in southern ON.

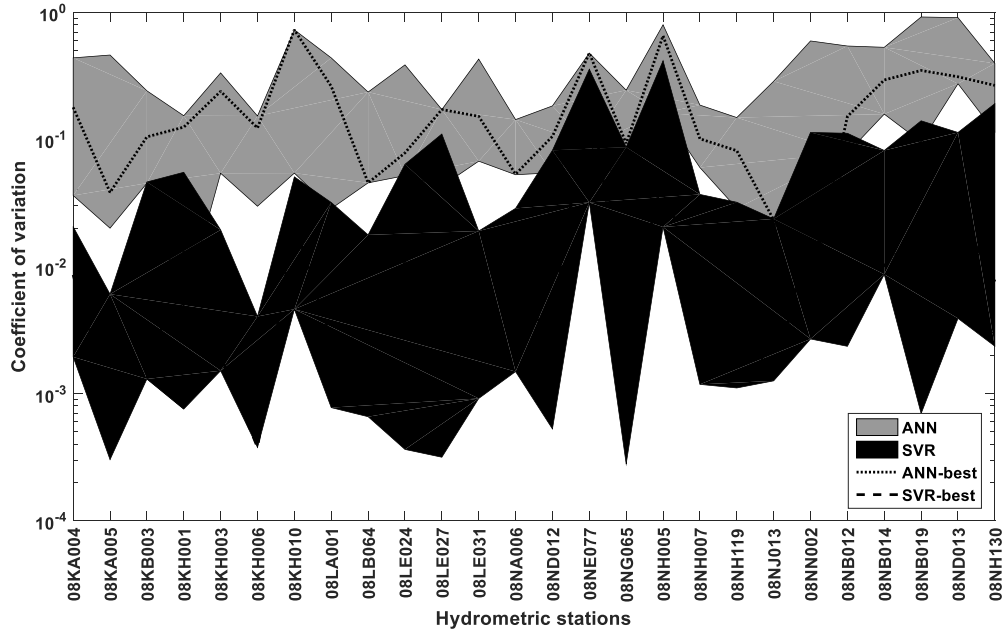


Figure 4.5 Range of *CV* of flood quantiles, Q10, Q25, Q50 and Q100 predicted by the ANN and SVR-RFFA models using 13 sets of predictors for 26 selected stations of southeastern BC. The *CV* of the set of predictors (#9) that led to the best overall flood quantile estimates is shown in dotted and dashed lines for ANN and SVR-RFFA models, respectively.

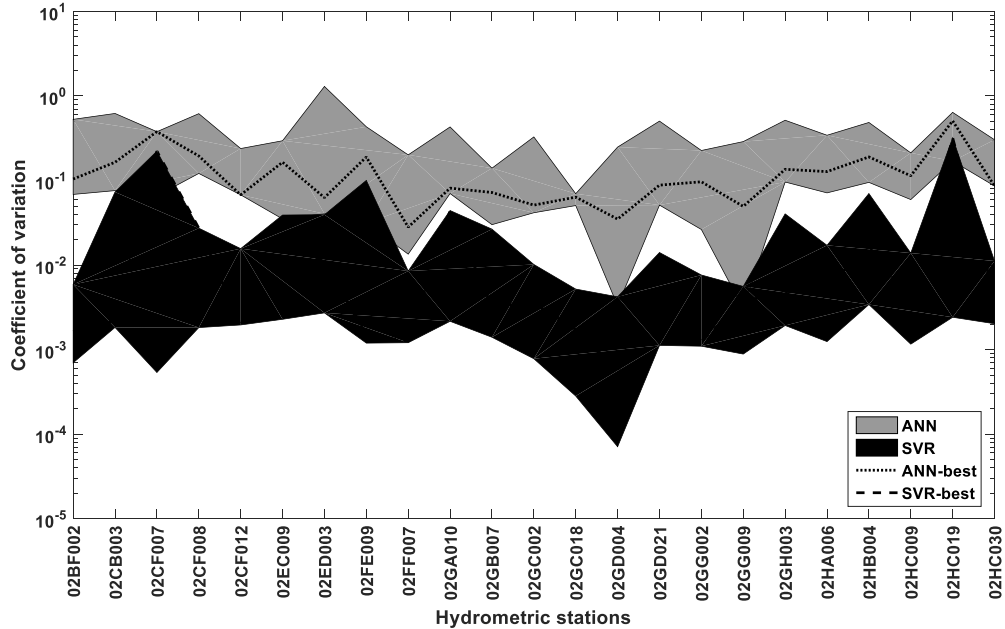


Figure 4.6 Range of *CV* of flood quantiles, Q10, Q25, Q50 and Q100 predicted by the ANN and SVR-RFFA models using 13 sets of predictors for 23 selected stations of southern ON. The *CV* of the set of predictors (#9) that lead to the best overall flood quantile estimates is shown in dotted and dashed lines for ANN and SVR-RFFA models, respectively.

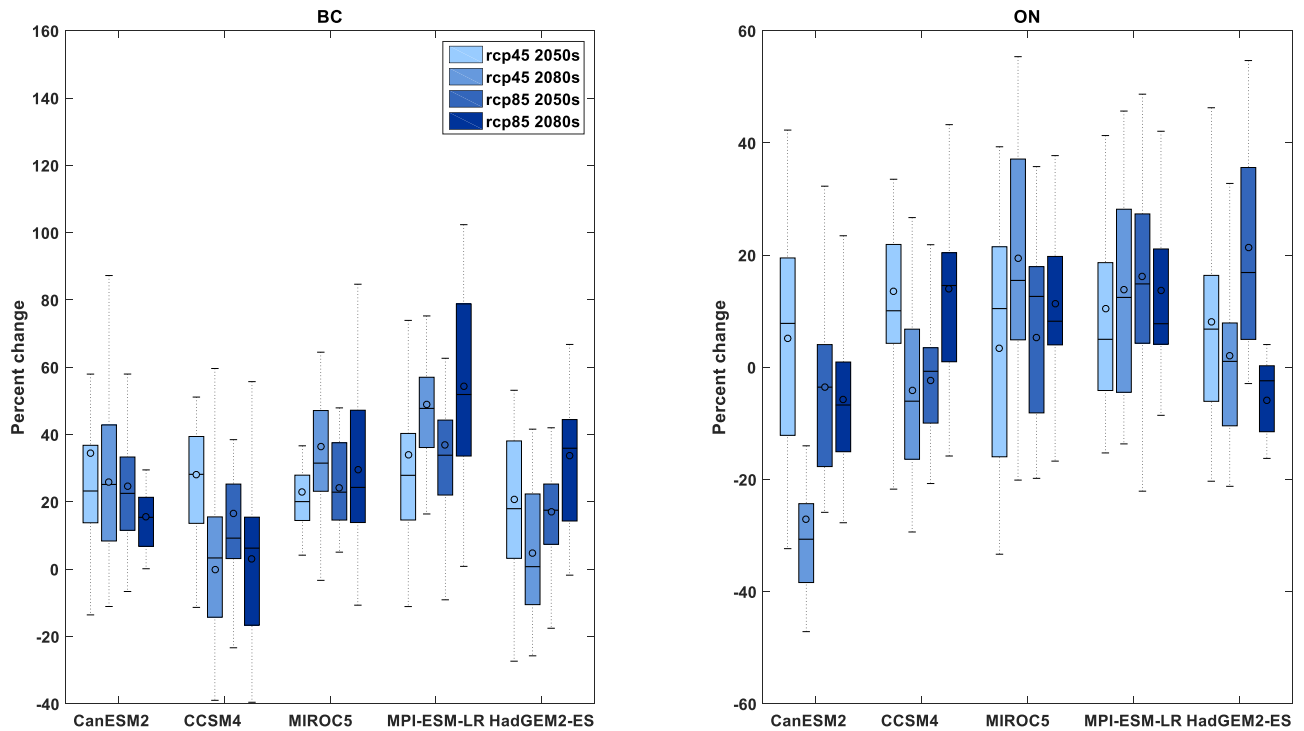


Figure 4.7 Boxplots of percent changes in T year return period precipitation between the base period (1971-2000) and 2050s and 2080s derived from RCP4.5 and RCP8.5 climate projections of five CMIP5 GCMs for the southeastern BC and southern ON study sites. The line and the circle in boxplots represent the median and the mean percent change, respectively.

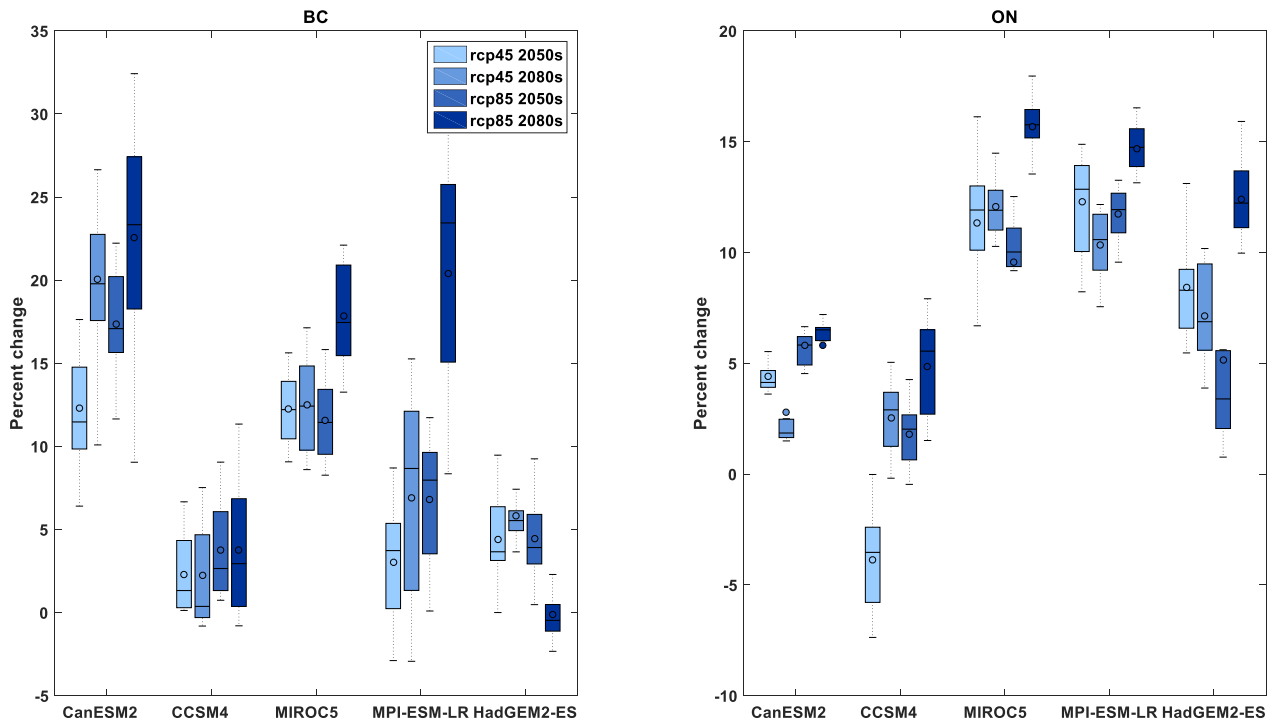


Figure 4.8 Boxplots of percent changes in the mean annual precipitation between the base period and 2050s and 2080s derived from RCP4.5 and RCP8.5 climate projections of five CMIP5 GCMs for the southeastern BC and southern ON study sites. The line and circle in boxplots represent the median and the mean percent change, respectively.

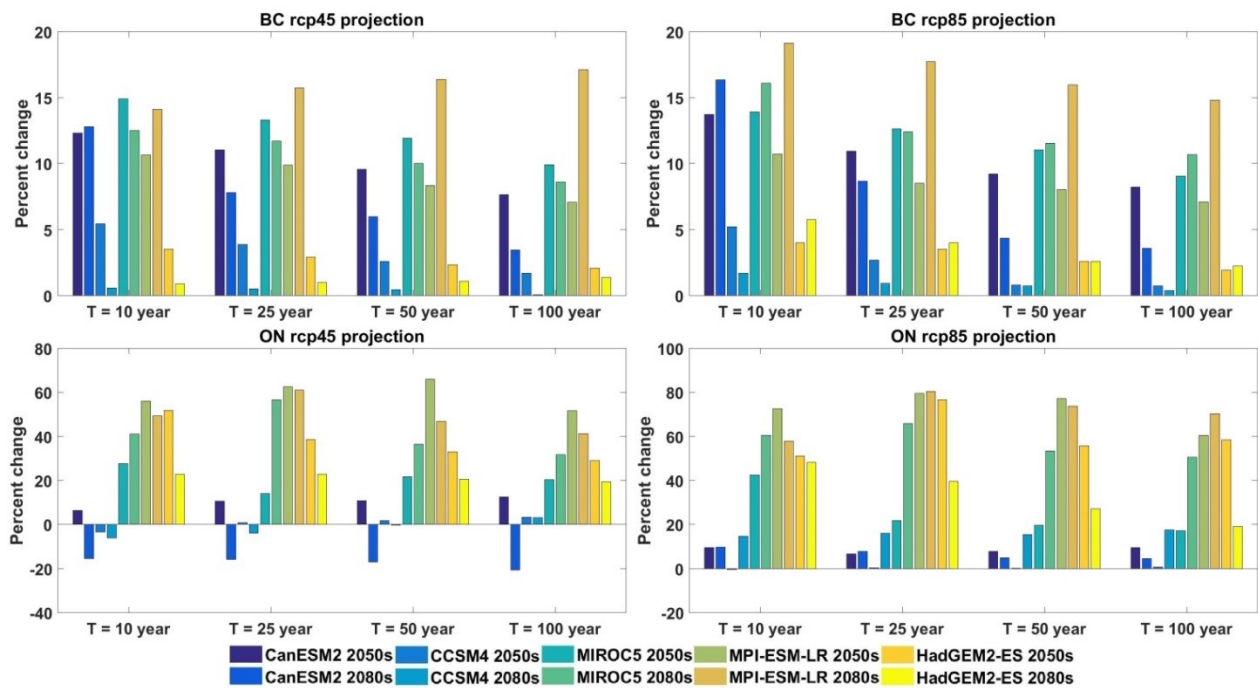


Figure 4.9 Changes in Q10, Q25, Q50 and Q100 between the base period and 2050s and 2080s derived from five CMIP5 GCMs and RCP45 and RCP85 climate projections for the southeastern BC and south ON study sites.

Chapter 5 Impact of Climate Change and El Niño Episodes on Droughts in sub-Saharan Africa

5.1 Introduction

In Africa, a dry and water scarce continent, about 300 million people suffer from water shortages (Kapangaziwiri et al., 2012) where about 80% of the land is of desert, arid and semi-arid climate (Koochafkan and Stewart, 2008), the majority of its population rely on limited water resources and rain fed agriculture (World Water Assessment Program, 2009) and about half Africans live in extreme poverty (UNDP, 2013). To make matters worse, in recent decades, hydrologic extremes have been occurring more frequently and in greater severity globally which many scientists attribute to the climate change impact. A warmer atmosphere will increase the occurrences of severe climate (Trenberth et al, 2003), reducing the reliability of global water resources, including Africa. In the midst of dwindling water resources, increasing hydrologic extremes and demand from growing population, drought prone regions of Africa are facing worsening water crisis which will affect its food security and environment, e.g., Dai (2011) detected generally decreasing precipitation and runoff trends in African rivers. Drought prone regions of Africa such as Sahel of northern Africa, Greater Horn of Africa (GHA), West Africa (WA) and southern Africa (SA) have been affected by severe droughts in recent decades (Lamb, 1982; African Watch, 1991; Vogel, 1994; Lyon, 2014).

WA, among the most vulnerable regions to drought impact worldwide, has experienced a marked decline in rainfall and streamflow since the early 1970s. Severe droughts that hit WA in the 1970s and 1980s (Lamb, 1982) lead to diminished vegetation and enhanced evaporation, which, via a positive feedback, further prolonged the droughts (Charney, 1975; Giannini et al., 2008).

GHA has a livelihood system highly sensitive and vulnerable to climate variability, and food insecurity is a regular occurrence, with $\frac{3}{4}$ of the population found in Ethiopia, Kenya, Sudan and Tanzania. Albeit various droughts of GHA in recent decades caused severe water shortage, knowledge of climate variability and observations in GHA is still lacking (Sivakumar et al., 2005).

Other than its climate, prolonged land exploitation in many parts of Africa, in particular sub-Saharan Africa (SSAF), has caused serious degradation and loss of biodiversity in the continent where the population had also increased several folds in the last 50 years, and conflicts from competing for dwindling water supply result in growing political instability. In other words, SSAF that relies on rain fed and irrigated farming agriculture is facing a worsening water crisis. Moreover, SSAF droughts are linked to desertification which means serious land degradation in dry, semi-arid and arid lands resulted from climate change and variability and human activities such as unsustainable farming, overgrazing and forest clear-cutting.

The increased frequency and severity of droughts because of climate change could further exacerbate desertification which leads to vegetation loss, reducing carbon sinks, and the release of more greenhouse gases, a positive feedback. Citing examples of desiccation, land degradation and droughts that hit Sahara, Kalahari and Sahel deserts of Africa in the early, mid- and late 20th century, respectively, Nicholson et al. (1998) even suggested it is impossible to separate drought from desertification. To make matters worse, according to the assessment reports of the Intergovernmental Panel on Climate Change (IPCC, 2007), from multi-model mean changes from 1980s to 2080s for the SRES (Special Report on Emission Scenarios) climate change

scenarios, it seems both northern and southern Africa will continue to experience decreasing precipitation, runoff and soil moisture in the 21st Century. Similarly, the latest IPCC report of 2013 also suggested that dry regions of southern Africa will likely experience increased drought events at the end of this century (Stocker et.al, 2013).

In addition to the temporal variability of annual precipitation, large scale climate anomalies due to anomalous sea surface temperature, such as El Niño Southern Oscillation (ENSO), have been attributed to increased or decreased precipitation in different parts of the world. Earlier studies have shown that the precipitation in sub-Saharan West Africa is correlated with anomalous sea surface temperature in the Atlantic Ocean and with both Pacific El Niño/La Niña sea surface temperatures (Lamb et al 1986; Otto-Bliesner, 1999). Other studies also suggest that, El Niño episodes are usually associated with below normal precipitation for SSAF, particularly for parts of GHA and SA (Lindesay and Vogel, 1990; Mason and Goddard, 2001; Lyon and Mason, 2007 and Ratnam et.al 2014). In GHA and especially for the Ethiopian highlands, El Niño episodes during the 1957-1994 period were associated with below normal precipitation from June to November where most farmers sow their seeds (Mason and Goddard, 2001). The 1983-85 severe drought event of Ethiopia can be partly attributed to the extreme El Niño event of 1982-83 and the current (2015/2016) severe drought events in parts of north eastern Ethiopia is said to be the effect of the current El Niño event of 2015/2016.

Contemporary GCMs (Global Climate Models) still lack in their ability to simulate historical ENSO events accurately, and among GCMs, there is little consensus on the projected change in the frequency of ENSO episodes for the 21st century. However, recent studies that analysed

climate projections from GCMs that simulated historical ENSO episodes with relatively good accuracy suggested that El Niño and La Niña episodes will increase in frequency under a warmer climate in the 21st century (Cai et.al 2014a; Cai et.al 2014b; Kim et.al 2014; Power et.al 2013; Santoso et.al 2013). The projected increase in frequency of El Niño events more associated with below normal precipitation in SSAF possibly indicates that droughts in 21st century could be more severe and with serious socio-economic consequences. On the other hand, increased La Niña events associated with above normal precipitation (Mason and Goddard, 2001) could give rise to devastating storms and floods, resulting in lower crop yields.

To more precisely identify drought prone regions of SSAF and the impact of climate change on possible drought events in the mid and late 21st century a spatial drought susceptibility analysis based on GCM's climate projections was conducted. The objective is to analyse changes in future droughts of SSAF with an emphasis on changes in the frequency, persistency and average drought durations projected by five GCMs of CMIP5 (Coupled Model Intercomparison Project phase 5) for the RCP4.5 and RCP8.5 (Representative Concentration Pathways) climate scenarios. The results of this study will contribute to the planning of adaptation strategies to promote drought preparedness and the implementation of warning systems so that reliable warnings can be issued quickly to mitigate potential impacts of future droughts in SSAF. With this introduction, description of the study area, data and methodology is given in Section 5.2, results and discussions in Section 5.3, and summary, conclusions and recommendations in Section 5.4.

5.2 Study area, data and methods

5.2.1 Study area

The climate of the SSAF ranges from humid in the wet equatorial region to arid in southern and northern Africa. Most parts of SSAF within the 10°N-10°S parallels, in particular countries in Central Africa (CA) and the Ethiopian highlands of GHA, receive an annual precipitation in excess of 1500 mm whereas the rest of sub-Saharan Africa receives less than 500 mm of rainfall annually. The temperature in this region is also highly variable but it is primarily governed by elevations. Most areas on either side of the Great Rift Valley of eastern Africa and some parts of the southern tip of SA have relatively higher elevation and therefore have a lower mean annual temperature of about 15 °C. The humid equatorial region of CA has a mean annual temperature of about 25 °C, whereas areas close to the Sahara desert in the northern edge of the SSAF have a mean annual temperature of up to 30 °C (Figure 5.1). Overall, most of the SSAF has a relatively dry climate which could be exacerbated under the potential impact of climate change.

5.2.2 Data

The analysis of droughts for historical and future climates was done over three 30-year periods. Historical and future drought characteristics for the SSAF during the mid and late 21st century are represented by analysis performed for the 1971-2000 base period, the 2041-2070 (2050s) and 2071-2100 (2080s) periods, respectively. Climate data such as precipitation and temperature are derived from a combination of gridded observed precipitation data, reanalysis data and selected GCMs' projections. Monthly precipitation data for the base period was derived from the Global Precipitation Climatology Centre's (GPCC) monthly gridded precipitation data of 0.5° by 0.5° resolution (Beck et.al, 2004). This product was assimilated from observed monthly precipitation

data of the Global Historical Climatology Network (GHCN) and also data taken from national meteorological and hydrological services. The maximum and minimum monthly temperature and wind data partly needed for estimating the Penman Monteith evapotranspiration was derived from 6 hourly temperature and wind values of ERA40 reanalysis data available from the European Centre for Medium-Range Weather Forecast (ECMWF) website at 0.5° by 0.5° resolution, interpolated from ERA40's original 1.125° by 1.125° resolution using bi-linear interpolation technique, which has been suggested as an adequate interpolation technique for smoothly varying variables such as temperature (NCAR, Climate Data Guide). The GPCP gridded precipitation data was chosen instead of the ERA40 reanalysis data because ERA40's monthly precipitation data suffer from under-estimation when compared to gauged data in regions such as GHA.

As an effort to address uncertainties associated with long-term climate projections, projected RCP4.5 and RCP8.5 climate scenarios of five CMIP5 GCMs of IPCC (2013) (Table 5.1) have been used to analyse the impact of climate changes on future droughts in SSAF in the 2050s and 2080s. By analysing an ensemble of 10 possible future climate projections, we will partly address some of the inherent uncertainties associated with climate projections for the 2050s and 2080s. Furthermore, the five GCMs come from major climate modelling groups of three different continents and have been key contributors to several IPCC's assessment reports.

5.2.3 Research Methodology

To analyse the possible impact of climate change to the occurrence, frequency and persistence of future drought events in SSAF, the Palmer Drought Severity index (PDSI) was chosen over other

drought indices because it is one of several popularly used drought indices. For a given time scale, a PDSI value can be discretized into predefined categories that indicate not only the severity of a drought event but also periods of excess moisture availability (Table 5.2). Since its inception by Palmer in 1965, variants of PDSI have been developed and tested in various countries, such as in tropical India by Bhalme and Mooley (1979); in Canadian Prairies by Akinremi et.al (1996); and in East Africa by Ntale and Gan (2003). Wells et.al (2004) even proposed a self-calibrating PDSI algorithm (scPDSI) designed to automatically calibrate the PDSI parameters from historical climate data at the location of interest, and so it is applicable for any region in the world. The scPDSI has been shown to provide more comparable PDSI values between regions of different climates (van der Schrier et.al 2006; Dai, 2011a; Gobena and Gan, 2013) and is therefore selected to compute the PDSI over SSAF. In this study the scPDSI parameters are calibrated using the complete period which was suggested by Wells et al (2004). This approach has also been suggested by van der Schrier et al. (2013) in order to keep the probability distribution of scPDSI between -4 and +4, as originally defined by Palmer (1965), because it guarantees that the most severe droughts and extreme wet periods are included within the calibration period. A brief description of the original PDSI (Palmer, 1965) and the modifications that led to the self-calibrating PDSI (Wells et al, 2004) are given as an Appendix B.

While calculating the moisture departure within the scPDSI algorithm, the potential evapotranspiration (PE) estimated either by the Thornthwaite (PE_{th}) or Penman Monteith (PE_{pm}) method has been shown to give marginally different PDSI values in the 20th century (van der Schrier et al, 2011; Dai 2011a). However, for the 21st century climate, Dai (2011) has

shown that using PE_{th} could over-estimate the impact of global warming, resulting in much higher PDSI than using PE_{pm}, which was therefore chosen to estimate PDSI for projected climate in the 2050s and 2080s in this study. To compute PE_{pm}, this study follows the procedures outlined by the Food and Agriculture Organization (FAO) (Allen et al., 1998). When compiling projected climate data for this study, atmospheric variables such as relative humidity (or dew point temperature) and sun shine hours which are partly used to calculate PE_{pm} were not available from the CMIP5 database. Therefore, approximate equations, as suggested in Allen et al. (1998) were used to estimate the actual vapor pressure and incoming solar radiation for PE_{pm}.

We mainly focus on the frequency and persistence of future drought events of the SSAF under the possible impact of climate change and combined impact with climate anomalies because such drought characteristics could result in significant impact to these African regions. We only limit our focus on SSAF because it is pointless to conduct drought analysis on hot deserts like the Sahara Desert (Palmer, 1965; van der Schrier et al., 2013). Even though the durations of droughts could range from a few months to several years or even longer, we have grouped historical and projected drought events under short duration and long duration droughts. The short (long) duration drought can last between six months and a year (over a year) in which the PDSI value consistently falls within the mild to extreme drought category. From changes computed for the median PDSI values, the frequency and the duration of droughts, the vulnerability of SSAF to future moisture stress or surplus in the 2050s and 2080s under the possible impact of climate change and climate anomalies will be assessed.

Rather than directly using raw RCP climate projection data of GCMs to compute drought indices, we adjusted the GPCC and the ERA40 reanalysis data of the base period for the projected climate of each GCM. This approach incorporates projected changes in precipitation and temperature data of the five selected GCMs into the GPCC and ERA40 reanalysis data so that the general spatial distribution of precipitation and temperature of these two historical datasets will more or less be maintained after the adjustments. In addition, as will be explained later, this approach is also suitable to analyze the combined impact of ENSO and climate change on future droughts of SSAF. These two datasets are adjusted for the impact of climate change using a quantile-quantile mapping approach based on empirical cumulative distribution functions (cdf) of both the datasets and GCMs' projections. The approach is similar to the BCSD (Bias Correction and Spatial Disaggregation) method of Wood et.al (2004) by aggregating the two datasets from a $0.5^\circ \times 0.5^\circ$ resolution to the resolution of the GCMs.

As mentioned before, even though recent studies (Cai et.al 2014a; Cai et.al 2014b; Kim et.al 2014; Power et.al 2013; Santoso et.al 2013) suggest an increased frequency of ENSO events under a warmer 21st century climate, contemporary GCMs still lack the ability to simulate ENSO events accurately for the historical period. Further, there is still a lack of agreement between GCMs on whether the frequency of ENSO will increase or decrease over the 21st century. Therefore, instead of using the raw GCM data directly, a bootstrap resampling approach was used to generate a 30-year period data out of observed data of the 1971-2000 base period in which ENSO was active, and then adjust this 30-year period data for the impact of climate change in the mid- and the late 21st century using the quantile-quantile mapping method. For this study, we used the extended Multi Variate Index data (MEI.ext) of Wolter and Timlin (2011)

from 1871 to 2005 expressed over four 4-month periods per year with one-month of overlap between each period. A given year will be classified as either an El Niño (La Niña) year if at least three out of the four 4-month periods represent either strong or weak El Niño (La Niña) episodes. From analysing the MEI data of Wolter and Timlin (2011) in this manner, we have identified 12 El Niño years (1977, 1979, 1980, 1982, 1983, 1987, 1991, 1992, 1993, 1994, 1995 and 1997) and 5 La Niña years (1971, 1974, 1975, 1989 and 1999) over the 1971-2000 period.

We only analyzed the impact of El Niño on drought events of the SSAF because El Niño is predominantly associated with below normal precipitation in different parts of Africa. A standard bootstrap resampling technique was used to generate 10 sets of 30-year data by re-sampling data of the 1971-2000 period when El Niño was active, followed by a quantile-quantile mapping approach to adjust each set of the resampled data to the RCP4.5 and RCP8.5 climate projections of the five selected CMIP5 GCMs for 2050s and 2080s. The median of projected changes in the future drought severity (based on PDSI values) of the SSAF subjected to the influence of El Niño are then estimated.

5.3 Results and discussions

Projected changes in the drought characteristics of SSAF in terms of PDSI computed for the base period, 2050s and 2080s under the RCP4.5 and RCP8.5 climate projections of five CMIP5 GCMs are herein discussed Table 5.1 and Figure 5.1). The results are mostly presented over four sub-regions of SSAF (Figure 5.1(a)).

5.3.1 Changes in median PDSI values and drought prone regions

Median PDSI values computed for the base period, 2050s and 2080s are shown in Figure 5.2. For the base period, almost all parts of CA and most of WA were under the near normal PDSI range (Table 5.2); parts of SA, especially the south western parts of this region, and a large portion of GHA particularly eastern Ethiopia and parts of Somalia were within the mild to moderate drought category. Compared to the base period, areas falling under the near normal PDSI category are projected to decrease by 4% (RCP4.5) and 7% (RCP8.5) by the mid and late 21st century over the sub-Saharan region, respectively. Similarly, the percentage of area within the incipient wet to slightly wet PDSI category could decrease by about 11% under RCP4.5 and by up to 22% under RCP8.5 climate projections in the mid and late 21st century. In contrast, areas under the incipient to moderate drought category could increase by about 12% and 21% over the SSAF in the 2050s and 2080s for RCP4.5 and RCP8.5 climate projections, respectively. This implies that the SSAF as a whole is projected to become drier with more frequent drought spells occurring by 2050s and 2080s.

Among different parts of SSAF, parts of WA, particularly the far western African countries such as Senegal, Ivory Coast, Guinea and Mali, are projected to shift from the near normal PDSI category during the base period to the incipient and moderate drought category under both the RCP4.5 and RCP8.5 climate projections by the 2050s, and more areas falling under these two drought categories by the 2080s. Similarly, most parts of SA, especially Namibia, the Western Cape region of the Republic of South Africa and parts of Botswana are projected to fall under the mild to moderate drought categories for RCP4.5 and RCP8.5 climate projections by 2050s and 2080s. In contrast, compared to the base period, parts of GHA are projected to become relatively

wetter, with arid parts of eastern Ethiopia, Somalia and parts of Kenya switching from moderate to mild drought PDSI category by 2050s and 2080s. However, recent studies have shown that the climate in these parts of the GHA is projected to be wetter due to the limitations of GCMs in simulating seasonal precipitation and suggest an increased drying in the GHA during the course of the 21st century (Williams and Funk, 2011; Tierney et al., 2015). On the other hand, under these two climate projections of five GCMs, some parts of CA are projected to shift from near normal to incipient dry spell category by the 2050s and 2080s (Figure 5.2).

Mild to moderate drought categories dominate the far western and eastern parts of SSAF for the base period, 2050s and 2080s as shown from the variability of the median PDSI in the meridional and zonal directions (Figure 5.3). In contrast, the CA region has experienced a normal state during the base period and is projected to remain like that under most RCP4.5 and RCP8.5 climate projections in the mid- and late 21st century. Similarly, far northern and southern parts of the SSAF are more prone to droughts than the equatorial region such as the Democratic Republic of Congo. According to most RCP4.5 and RCP8.5 climate change projections, future severe droughts could occur more frequently at all four corners of the SSAF.

5.3.2 Changes in frequency and length of persistent droughts

The frequency and average length of short drought events that persist between six months and a year and also long drought periods that extend for a year and beyond were derived from computed PDSI values of the five CMIP5 GCMs during the base period, the 2050s and 2080s. As shown in Figure 5.4a, with the exception of some projections for WA, on an average the frequency of short droughts over CA, GHA and SA is projected to increase by about 4% to 7%

in the 2050s and 2080s. Similarly, with the exception of GHA, there is also a projected increase of about 2% to 10% in the frequency of long drought events (Figure 5.4b). These results imply that parts of SSAF could experience more frequent short duration droughts (GHA) or long duration droughts (WA) or both (CA and SA). However, unlike the frequency of short drought events that are generally projected to increase, the duration of such drought events in most SSAF are projected to experience minimal change, with the exception of GHA (Figure 5.4c). Surprisingly, compared to the base period, the durations of long drought events in most parts of SSAF are projected to decrease by about 1% to 6% in the 2050s and 2080s (Figure 5.4d).

To investigate why the average duration of long drought events in SSAF is projected to decrease in 2050s and 2080s, projected changes in the characteristics of monthly precipitation in the 2050s and 2080s were analyzed. According to the WGI report of IPCC (Cubasch et.al 2013), changes to the Earth's climate induced by anthropogenic activities could lead to more frequent and extreme hydrologic events in the future. According to the Clausius-Clapeyron equation, the water holding capacity of the atmosphere increases at about 7% per K° rise in temperature, which will result in stronger heavy rainfall events and so the risk of flooding will increase (Trenberth, 1998; 1999 and Trenberth et.al, 2003). Further, with an increased water holding capacity of the atmosphere, the spatial variability of precipitation could also increase, leading to more frequent extreme precipitation occurring in some regions while other regions experience drier climate. Taking the 95th percentile monthly precipitation of the base period (P95b) as the threshold, the cumulative precipitation volume of all monthly precipitation values exceeding P95b in the 30-year periods of 2050s and 2080s are computed. Based on RCP4.5 and RCP8.5 climate projections of the five selected CMIP5 GCMs, the cumulative precipitation volume that exceeds

P95b in WA, CA and GHA are projected to increase by about 40% in 2050s and 2080s, while SA is only projected to increase by about 13% (Figure 5.5a-d). In contrast, the cumulative monthly precipitation volume below the P95b threshold is projected to decrease by about 5%, 8% and 10% for CA, WA and SA in the 2050s and 2080s, respectively. However, minimal change in the corresponding cumulative precipitation volume below the P95b was projected for GHA. Projected changes in the frequency and intensity of daily precipitation events of 5, 10 and 25 years return periods between the base period and 2050s and 2080s under RCP4.5 and RCP8.5 climate projections of the five CMIP5 GCMs are also analysed. Compared to the base period, the intensity of 5-year return period rainfall based on a Generalized Extreme Value (GEV) distribution is projected to increase by about 15% in the 2050s and 2080s (Figure 5.6). Similar results (not shown) are also found for the intensity of daily rainfall events of 10 and 25 year return periods.

These results indicate a twofold impact of climate change on the SSAF. While the warming due to rising concentrations of anthropogenic greenhouse gases enhances the evaporation loss which consequently increases the frequency of mild to severe drought events in this region, the likely positive change in the frequency and intensity of extreme precipitation events due to a warmer atmosphere could offset the impact of enhanced evaporation loss on drought durations in the mid and late 21st century. Because climate change impact could increase the frequency of future extreme precipitation events, the chances for long duration droughts to be interrupted by extreme rainfall events increases in the future, which means that the average length of long duration droughts of the mid and late 21st century could decrease. Furthermore, these results suggest that in addition to increasing the frequency of short and long persistent drought periods over most of

SSAF, climate change could also lead to more frequent occurrences of extreme precipitation events, which increase the risk of flooding. Consequently, climate change could enhance the occurrences of both types of hydrologic extremes, which is expected to exacerbate the undesirable socio-economic consequences of droughts and flooding of SSAF.

5.3.3 Impact of El Niño and combined impact of El Niño and climate change on SSAF droughts

As mentioned in the Introduction, El Niño climate anomaly has been primarily associated with below normal precipitation in different parts of SSAF (Mason and Goddard, 2001; Lyon and Mason, 2007). For the March-April-May (MAM), June-July-August (JJA), September-October-November (SON) and December-January-February (DJF) seasons of 1951-2000, precipitation composites were computed as the ratio of mean seasonal precipitation in anomalous (El Niño) years relative to the long term mean seasonal precipitation. To emphasize the effect of El Niño on seasonal precipitation, years with strong El Niño activity (1958, 1982, 1983, 1987, 1992 and 1997) were only considered in the composite analysis. Composites in Figure 5.7b show those years with strong El Niño episodes have been primarily associated with about a 10% reduction in the annual precipitation for the four regions of SSAF. Despite an overall reduction in the precipitation of all four seasons when El Niño is active, its impact on the precipitation of major rainy seasons will be of greater interest to different parts of SSAF. For instance, JJA and DJF account for more than half of the annual precipitation over northern parts of SSAF and areas bordering the CA and SA regions, respectively. Similarly, other areas, e.g., western parts of the CA and SA regions, have two major rainy seasons (Figure 5.7a). Therefore, even though the rainy season vary from region to region in SSAF, the predominantly reduction effect of El Niño

on the rainy seasons of different regions of SSAF would have more pronounced impact on the agricultural productivity and water availability, than a similar reduction in the precipitation of other seasons, of those regions.

Historical records of ENSO show varying degree of activity of this climate anomaly originated from the tropical Pacific since 1871. The MEI.ext index from 1871-2005 shows an increased ENSO activity in pre-1920s, a relative respite from 1920s to 1960s, followed by an increase in the ENSO activity in post-1960s (Wolter and Timlin, 2011) (Figure 5.8). The pre-1920 periods were mainly dominated by La Niña events while El Niño episodes were more prevalent in post-1960s, for which more than half of the El Niño events over the 1871-2005 period had occurred (Wolter and Timlin, 2011). According to successive IPCC assessment reports, the last few decades of the 20th century and the 2000's have been the warmest since instrumental records began in the 1850s (Stocker et.al 2013). Because of this, some scientists argue that the increase in El Niño activity since the late 20th century, particularly the unusual 1990-1995 El Niño episode, cannot be solely attributed to natural variability, but rather because a warmer atmosphere favors the occurrence of El Niño events (Trenberth and Hoar, 1997). Since early 2000s, we have experienced frequent El Niño events, with the latest 2015/2016 El Niño episode resulting in severe droughts and water shortages in many parts of Africa and South America. Therefore, based on recent observations and studies related to future ENSO projections (Cai et.al 2014a; Kim et.al 2014; Power et.al 2013; Santoso et.al 2013), the prospect of El Niño episodes occurring more frequently in a warmer 21st century is relatively high.

The average spatial extent and severity of drought events in SSAF when El Niño was active in the base period, or will be active in the 2050s and 2080s under the combined impact of climate

change represented by RCP4.5 and RCP8.5 climate scenarios of IPCC (2013) are herein discussed. On the other hand, drought events of the SSAF represented by PDSI values devoid of the influence of active El Niño and La Niña have also been analysed. Both sets of results were obtained from 10 sets of 30-year data generated using the bootstrap resampling technique from data with active El Niño episodes, and without ENSO episodes, respectively, during the historical climate. The historical resampled data are then adjusted for the RCP 4.5 and RCP 8.5 climate scenarios of 2050s and 2080s using the quantile-quantile mapping approach to estimate the combined impact of El Niño and climate change. By comparing the above two sets of results, we can approximately isolate the impact of El Niño on the climate of SSAF.

By assuming the climate of the SSAF was or will be without any influence of El Niño and La Niña events, we found that the areal extent of SSAF falling under the incipient to moderate drought categories (Figure 5.9c-d) is very similar to that of Figure 5.2 which shows the median PDSI values of the SSAF subjected to the influence of historical El Niño and La Niña episodes for the base period (1971-2000), and the RCP4.5 and RCP8.5 climate scenarios of the 2050s and 2080s. In addition, between the base periods and the 2050s and 2080s, the area falling under incipient to moderate drought categories remained virtually the same for this hypothetical climate, particularly for the CA and SA region (Figure 5.10 e-h).

For a hypothetical climate under the combined impact of El Niño and climate change, the corresponding area falling under the incipient to moderate drought categories is projected to increase in SA and more significantly in GHA (Figure 5.9a-b). Under this hypothetical combination of active El Niño events and climate change impact, the area falling within the

aforementioned drought categories is projected to expand in GHA, to areas that were otherwise less drought prone, such as in south-western Ethiopia, north-western parts of Ethiopian highlands and parts of Sudan and South Sudan (compare between Figure 5.2 and Figure 5.9a-b). However, in the 2050s and 2080s, even though the projected increase in the precipitation of south-eastern Ethiopia and Somalia is expected to partly offset the decrease in precipitation caused by active El Niño, the percentage of area under the incipient dry spell in the 2050s and 2080s is still projected to expand when compared to the base period (Figure 5.10 b).

The effect of active El Niño episodes on future droughts of SA is also evident in that areas that fall under the aforementioned drought categories is projected to expand significantly when compared to the hypothetical case where the climate is totally not affected by ENSO. In addition, for SA, the area affected by climate change under RCP4.5 and RCP8.5 climate scenarios combined with active El Niño is projected to expand significantly (Figure 5.9a-b and Figure 5.10). However, for both hypothetical climate (active El Niño and no ENSO, respectively), CA is still projected to remain in a near-normal state which suggests that the effect of El Niño and the combined effect of El Niño and climate change are minimal on future droughts of CA (Figure 5.9a-d). However, for WA, more area is projected to be relatively drier for a hypothetical climate not influenced by ENSO when compared to a climate influenced by active El Niño events (Figure 5.10d and h). Also, for both hypothetical climates, the area of WA that is under the incipient to moderate drought categories is marginally higher than that shown in Figure 5.2.

In conclusion, even though it is unlikely to have a 30-year period consecutively dominated by active El Niño events, extended periods of El Niño episodes such as the 1991-1995 period could

likely occur more frequently or of longer durations because of climate change impact (Bush 2006; Cai et.al 2014a; Kim et.al 2014; Power et.al 2013; Santoso et.al 2013). Consequently, areas of GHA with relatively dry climate could expand under RCP4.5 and RCP8.5 climate projections in 2050s and 2080s than the historical period, assuming similar frequency of El Niño events as the 1971-2000 base period. On the other hand, if El Niño events will occur more frequently in 2050s and 2080s, areas with dry climate are projected to expand in WA and SA although such an expansion is not projected to be as extensive as that of GHA. Virtually no change in the spatial extent and severity of drought events is projected to occur in CA even with a projected increase in the frequency and durations of active El Niño events (Figure 5.9a-b vs Figure 5.2).

5.4 Summary, Conclusions and Recommendations

The impact of climate change on the frequency, severity and spatial distribution of drought events in sub-Saharan Africa (SSAF) was analysed using a dataset with different climate variables taken from either ERA40 reanalysis and GPCP gridded observational data that has been adjusted for the impact of RCP4.5 and RCP8.5 climate scenarios of five CMIP5 GCMs for the 2050s (2041-2070) and 2080s (2071-2100). Furthermore, the possible combined impact of El Niño and climate change in the SSAF was also analysed using dataset resampled from years within the base period (1971-2000) that had been affected by strong to weak historical El Niño episodes, and adjusted with RCP4.5 and RCP8.5 climate projections of five CMIP5 GCMs for the 2050s and 2080s, respectively. The drought analysis was based on the self-calibrated PDSI with the moisture departure estimated using the Penman-Monteith evapotranspiration method.

For the base period, most parts of Central Africa (CA) and West Africa (WA) fell within the near-normal PDSI categories whereas parts of South Africa (SA), especially the south western parts of this region, and a large portion of the Greater Horn of Africa (GHA) particularly eastern Ethiopia and parts of Somalia fell within the mild to moderate drought categories of PDSI. Compared to the base period, the percentage of area that was under the near normal PDSI category is projected to decrease by 4% (RCP4.5) and 7% (RCP8.5) over the whole SSAF in the mid to late 21st century. Similarly, the percentage of area within the incipient to slightly wet PDSI categories is projected to decrease by about 11% (RCP4.5) and 22% (RCP8.5) over the same period. However, areas of SSAF that fall under the incipient dry spell to moderate drought categories of PDSI are projected to increase by about 12% (RCP4.5) and 21% (RCP8.5) in the mid to late 21st century, which suggests that SSAF and particularly its four corners are projected to experience drier climate in the future.

In general the frequency of short droughts and long droughts is projected to marginally increase by about 4-7 % and 2-10 % under the RCP4.5 and RCP8.5 climate projections in the mid to late 21st century, respectively. However, in terms of drought durations, minimal change is projected for the average duration of short droughts while long droughts in most parts of the SSAF are projected to be shorter by 1- 6% in the mid to late 21st century compared to the base period. The marginal decrease in the duration of long droughts could be attributed to the projected increase in the magnitude and frequency of future extreme precipitation events. These results suggest that a warmer climate could increase the frequency of mild to extreme drought events, but it could also increase the intensity and frequency of extreme precipitation events, which could shorten the duration of future long droughts of the SSAF.

Areas of GHA falling under the incipient dry spell to moderate drought categories of PDSI are projected to increase significantly in 2050s and 2080s, if the frequency of future El Niño events is projected to increase than if the frequency of El Niño events is assumed to remain more or less unchanged. Similarly, a projected increase in the frequency of future El Niño events is also expected to expand the drought prone regions in SA and WA but it is projected to have limited impact on the future droughts in CA. These results show that an increase in the frequency of climate anomalies such as El Niño could further exacerbate the impact of climate change on future drought events of the SSAF, particularly for the GHA region.

5.4.1 Adaptive Measures to Mitigate Impacts of Future Droughts

Even though long-term climate projections inevitably involve large uncertainties, it is only prudent that SSAF countries promote and implement adaptive measures, capacity building, and drought preparedness at national and regional levels in a timely manner to mitigate possible impact of future droughts. For many drought-prone, developing countries in SSAF, where livestock or integrated crop-livestock farming is a vital part of the economy, practical measures for preparedness and capacity building against drought hazards include building infrastructure, improve production technologies, implement stable crop and livestock pricing policies, promote interactions between government organizations and farmers, livestock health, and contingency plans. Diversification of dry-land commodities, access to market opportunities and insurance policies based on climate and forage indicators are viable strategies in poorly developed regions of Africa. Partners from various local authorities of Africa can conduct local scale experiments

to investigate sustainable, agricultural land management to mitigate future drought risk (Gan et al., 2015).

Practical options to be considered are: (1) Restoring land fertility by applying natural compost; (2) zero-tillage farming for rebuilding of critical soil organic matters; (3) rehabilitation such as land resting and planting of native plants; (4) rainfall harvesting; (5) diversify crop and animal production; (6) promote drought-resistant crop varieties; (7) breed crop seeds that could use water more efficiently; (8) reforestation; (9) Assess possible improvements in irrigated agriculture water use to increase the water use efficiency through efficient irrigation systems and also through a different crop mix; (10) Maximize crop yield by adjusting applications of fertilizers and water according to VI (vegetation indices) maps based on Landsat-TM data that can digitally divide a field into zones of low, median and high productivity; and (11) Reduce desertification problems by re-vegetation, installing windbreaks and fences, chemical engineering measures such as spraying chemical cements and oil mulch (FAO, 2011).

It is also essential to develop Early Warning Systems (EWS) for SSAF based on the latest climate information and technology to combat economic loss from droughts. Such EWS can provide decision makers practical tools to implement wise decisions speedily when droughts appear to be forthcoming, to improve risk assessment and more resilient water management for communities vulnerable to famine. EWS should incorporate Regional Climate Models (RCMs) such as such as the MM5 (Dudhia et al., 2004) and the Weather Research and Forecasting model (WRF) (Warner, 2011; Skamarock et al., 2005) that could provide reliable seasonal weather forecasts. Furthermore, given the uncertainties associated with RCM-based climate predictions,

it will be useful to combine this approach with empirical/statistical, teleconnection models which have been shown to possess reasonable skill in some parts of Africa, such as East Africa (Mwale and Gan, 2005; Ntale et al., 2003), central Southern Africa (Mwale et al., 2004), Southern Africa (Mwale and Gan, 2007), and others. In addition, it is also essential to develop regional maps/models of drought episodes based on the probability of occurrence of droughts of varying frequency or severity which can be used to estimate the degree of damage or hazard that will result from the possible increase in the occurrence of future droughts in SSAF during the mid and late 21st century.

Acknowledgements

This study was partly funded by the Natural Science and Engineering Research Council (NSERC) of Canada.

5.5 References

- Africa Watch, 1991: Evil days: 30 years of war and famine in Ethiopia. Africa Watch Rep., 381 pp. <https://www.hrw.org/sites/default/files/reports/Ethiopia919.pdf>
- Akinremi, O. O., McGinn, S. M. and Barr, A. G. 1996: Evaluation of the Palmer Drought Index on the Canadian prairies. *J. Climate*, 9: 897–905.
- Allen, R. G., Pereira, L.S., Raes, D., and Smith, M. 1998: Crop evapotranspiration (guidelines for computing crop water requirements). Food and Agriculture Organization of the United Nations Irrigation and Drainage Paper 56, 328 pp.
- Beck, C., Grieser, J. and Rudolf, B. 2004. A New Monthly Precipitation Climatology for the Global Land Areas for the Period 1951 to 2000 (published in Climate Status Report 2004, pp. 181 - 190, German Weather Service, Offenbach, Germany)
- Bhalme, H. N., and D. A. Mooley, 1979: On the performance of modified Palmer index. Proc. Int. Symp. on Hydrological Aspect of Droughts, vol. I, New Delhi, India, UNESCO, 373–383.
- Bush, A. 2006. Extratropical Influences on the El Niño–Southern Oscillation through the Late Quaternary. *AMS, J of Climate*, 20, 788-800. DOI: 10.1175/JCLI4048.1
- Cai, W., Borlace, S., Lengaigne, M., Rensch, P., Collins, M., Vecchi, G., Timmermann, A., Santoso, A., McPhaden, M.J., Wu, L., England, M.H., Wang, G., Guilyardi, E., and Jin, F-F. 2014. Increasing frequency of extreme El Niño events due to greenhouse warming. *Nature climate change, Letters*, 4: 111-116. DOI: 10.1038/NCLIMATE2100
- Cai, W., Wang, G., Santoso, A., McPhaden, M. J., Wu, L., Jin, F-F., Timmermann, A., Collins, M., Vecchi, G., Lengaigne, M., England, M.H., Dommenges, D., Takahashi, K., Guilyardi,

- E. 2014. Increasing frequency of extreme La Niña events under greenhouse warming. *Nature climate change, Letters*, 5: 132-137. DOI: 10.1038/NCLIMATE2492
- Charney, J.G. 1975. Dynamics of desert and drought in the Sahel. *Quart. J. R. Met. SOC.* 101: 193-202.
- Cubasch, U., D. Wuebbles, D. Chen, M.C. Facchini, D. Frame, N. Mahowald, and J.-G. Winther, 2013: Introduction. In: *Climate Change 2013: The Physical Science Basis. Contribution of Working Group I to the Fifth Assessment Report of the Intergovernmental Panel on Climate Change* [Stocker, T.F., D. Qin, G.-K. Plattner, M. Tignor, S.K. Allen, J. Boschung, A. Nauels, Y. Xia, V. Bex and P.M. Midgley (eds.)]. Cambridge University Press, Cambridge, United Kingdom and New York, NY, USA.
- Dai, A., 2011, Drought under global warming: a review, *WIREs Clim Change*, 2: 45-65, John Wiley and Son, DOI: 10.1002/wcc.81
- Dudhia J, Gill D, Manning K, Wang W, Bruyere C., 2004. PSU/NCAR Mesoscale Modelling System Tutorial Class Notes and Users' Guide (MM5 Modelling System). NCAR, Boulder, CO.
- FAO. 2011. The state of the world's land and water resources for food and agriculture (SOLAW) – Managing systems at risk. Food and Agriculture Organization of the United Nations, Rome and Earthscan, London.
- Gan, T. Y., Ito, M., Hülsmann S., Qin, X., Lu, X.X., Liong, S.Y., Rutschman, P., Disse, M., Koivusalo, H. 2015. Possible climate change/variability and human impacts, vulnerability of drought-prone regions, water resource and capacity building for Africa. *J of Hydrological Sciences*, 61, No 7: 1209-1226. doi:10.1080/02626667.2015.1057143

- Giannini, A., Biasutti, M., Held, I.M., and Sobel, A.H. 2008. A global perspective on African climate. *J of Climate Change*, doi: 10.1007/s10584-008-9396-y
- Gobena, A. K., and Gan, T. Y., 2013, Assessment of Trends and Possible Climate Change Impacts on Summer Moisture Availability in Western Canada based on Metrics of the Palmer Drought Severity Index. *J of Climate*, 26, 4583-4595, doi: 10.1175/JCLI-D-12-00421.1
- IPCC, 2007: *Climate Change 2007: The Physical Science Basis. Contribution of Working Group I to the Fourth Assessment Report of the Intergovernmental Panel on Climate Change* [Solomon, S., D. Qin, M. Manning, Z. Chen, M. Marquis, K.B. Averyt, M. Tignor and H.L. Miller (eds.)]. Cambridge University Press, Cambridge, United Kingdom and New York, NY, USA, 996 pp
- Kapangaziwiri, E., Hughes, D. A., Wagener, T. 2012. Incorporating uncertainty in hydrological predictions for gauged and ungauged basins in southern Africa. *J of Hydrological Sciences*, 57(5): 1000-1019. doi: 10.1080/02626667.2012.690881
- Kim, S. T., Cai, W., Jin, F-F., Santoso, A., Wu, L., Guilyardi, E., An, S-I. 2014. Response of El Niño sea surface temperature variability to greenhouse warming. *Nature Climate Change, Letters*, 4: 786-790. DOI: 10.1038/NCLIMATE2326
- Koohafkan, P., and Stewart, B. A. 2008. *Water and cereals in drylands. The Food and Agricultural Organizations of the United Nations and Earthscan, London.*
- Lamb, P. 1982. Persistence of Subsaharan drought. *Nature*, 299: 46-47.
- Lamb, P., Pepler, R.A., and Hastenrath, S. 1986. Interannual variability in the tropical Atlantic. *Nature*, 322: 238-240.

- Lindesay, J. A. and Vogel, C. H. 1990. Historical evidence for southern oscillation-southern Africa rainfall relationships. *Int. J of Climatology*, 10: 679-689.
- Lyon, B. 2014. Seasonal drought in Greater Horn of Africa and its increase during the March-May long rains. *J of Climate*, 27: 7953-7975. doi: 10.1175/JCLI-D-13-00459.1
- Lyon, B. and Mason, S. 2007. The 1997-98 summer rainfall season in southern Africa. Part I: Observations. *J of Climate*, 20: 5134-5148. doi: 10.1175/JCLI4225.1
- Mason, S. J. and Goddard, L. 2001. Probabilistic precipitation anomalies associated with ENSO. *AMS, BAMS*, 82, no 4: 619-638.
- Mwale, D. and Gan, T. Y., 2005, Wavelet analysis on variability, teleconnectivity and predictability of the September-November East African Rainfall, *J. of Applied Meteorology*, AMS, 44: 256-269.
- Mwale, D., Gan, T. Y., et al., 2007, Wavelet Empirical Orthogonal Functions Of Space-Time-Frequency Regimes & Predictability of Southern Africa Summer Rainfall, *J. Hydrologic Engin.*, 12(5): 513-523.
- Mwale, D., Gan, T. Y., and Shen, S. S. P., 2004, A new analysis on variability and predictability of seasonal rainfall of Central Southern Africa, *Int. J. of Climatology*, RMS, 24, 1509-1530.
- NCAR, Climate Data Guide. <https://climatedataguide.ucar.edu/climate-data-tools-and-analysis/regridding-overview> (accessed on August/29/2016)
- Nicholson, S. E., Tucker, C. J., & Ba, M. B., 1998, Desertification, drought and surface vegetation: an example from the west African Sahel, *Bull. American Met. Soc.*, 79, 815e829.

- Ntale, H. K., and Gan, T.Y., 2003, Drought indices and their application to East Africa, *Int J. of Climatology, RMS*, 23: 1335-1357.
- Ntale, H. K., and Gan, T.Y., Mwale, D., 2003, Prediction of East African Seasonal Rainfall Using Canonical Correlation Analysis, *J. of Climate*, 16(12), 2105-2112. DOI: [http://dx.doi.org/10.1175/1520-0442\(2003\)016<2105:POEASR>2.0.CO;2](http://dx.doi.org/10.1175/1520-0442(2003)016<2105:POEASR>2.0.CO;2).
- Otto-Bliesner, B.L. 1999. El Niño/La Niña and Sahel precipitation during the Middle Holocene. *AGU, J. of Geophysical Reseaech, Letters*. 26-1: 87-90.
- Palmer, W.C. 1965, *Meteorological Drought*. Research paper No. 45, US Weather Bureau, Washington DC.
- Power, S., Delage, F., Chung, C., Kociuba, G. and Keay, K. 2013. Robust twenty-first-century projections of El Niño and related precipitation variability. *Nature, Letter*, 502: 541-545. doi:10.1038/nature12580.
- Ratnam, J. V., Behera S.K., Masumoto and Yamagata, T. 2014. Remote effects of El Niño and Modoki events on the austral summer precipitation of southern Africa. *AMS, J of Climate*, 27: 3802-3815. doi: 10.1175/JCLI-D-13-00431.1
- Santoso, A., McGregor, S., Jin, F-F., Cai, W., England, M.H., An, S-I., McPhaden M.J. and Guilyardi, E. 2013. Late-twentieth-century emergence of El Niño propagation asymmetry and future projections. *Nature, Letter*, 504: 126-129. doi:10.1038/nature12683
- Sivakumar, H. P., Das, Brunini, O., 2005, Impacts of present and future climate variability and change on agriculture and forestry in the arid and semi-arid tropics, *Climatic Change*, 70: 31–72.
- Skamarock WC, Klemp JB, Dudhia J, Gill DO, Barker DM, Wang W, Powers JG, 2005, A description of the advanced research WRF version 2. NCAR Tech Notes-468+STR.

- Stocker, T.F., et al. 2013: Technical Summary. In: Climate Change 2013: The Physical Science Basis. Contribution of Working Group I to the Fifth Assessment Report of the Intergovernmental Panel on Climate Change [Stocker, T.F., D. Qin, G.-K. Plattner, M. Tignor, S.K. Allen, J. Boschung, A. Nauels, Y. Xia, V. Bex and P.M. Midgley (eds.)]. Cambridge University Press, Cambridge, United Kingdom and New York, NY, USA.
- Tierney, J.E., Ummenhofer, C.C., and deMenocal, P.B. 2015. Past and future rainfall in Horn of Africa. *Sci. Adv.* 1. doi: 10.1126/sciadv.1500682
- Trenberth K. E. and Hoar, T. J. 1997. El Niño and climate change. *Geophysical Research Letters*, 24, No 23: 3057-3060
- Trenberth, K. E. 1998. Atmospheric moisture residence time and cycling: Implication for rainfall rates and climate change. *J of Climatic Change*, 39: 668-694
- Trenberth, K. E. 1999. Conceptual framework for changes of extremes of the hydrological cycle with climate change. *Climatic Change*, 42: 327-339
- Trenberth, K. E, Dai, A., Rasmussen, R.M. and Parsons, D. B. 2003. The Changing Character of Precipitation, *BAMS, AMS*. doi: 10.1175/BAMS-84-9-1205.
- UNDP. 2013. Fast Facts: UNDP and poverty reduction in Africa. Accessed on August/30/2016 <http://www.africa.undp.org/content/dam/rba/docs/Outreach%20Material/Poverty%20Fast%20Facts%202013.pdf>
- van der Schrier G, Briffa, K. R, Jones P. D, Osborn T. J. 2006 Summer moisture variability across Europe. *J Clim* 19:2818–2834
- van der Schrier, G., Jones, P. D., and Briffa, K. R., 2011, The sensitivity of the PDSI to the Thornthwaite and Penman-Monteith parameterizations for the potential evapotranspiration, *J. Geophys. Res.*, 116, D03106, doi: 10.1029/2010JD015001.

- van der Schrier, G., Barichivich, J., Briffa, K. R., and Jones, P. D. 2013. A scPDSI-based global data set of dry and wet spells for 1901–2009, *J. Geophys. Res. Atmos.*, 118: 4025–4048, doi:10.1002/jgrd.50355
- Vogel, C. 1994. (Mis)management of droughts in South Africa: past, present and future. *South African Journal of Science*, 90: 4-6.
- Warner, T. T., 2011, Quality assurance in atmospheric modeling, *BAMS*, DOI:10.1175/BAMS-D-11-00054.1
- Wells, N., Goddard, S., and Hayes, M. J. 2004. A self-calibrating Palmer Drought Severity Index. *J. Climate*, 17: 2335–2351.
- Williams, A.P., and Funk, C. 2011. A westward extension of the warm pool leads to a westward extension of the Walker circulation, drying east Africa. *J of Clim Dyn.* 37:2417–2435. doi: 10.1007/s00382-010-0984-y
- Wood, A. W., Leung, L. R., Sridhar, V., and Lettenmaier, D. 2004. Hydrologic implications of dynamical and statistical approaches to downscaling climate model outputs. *J. Climatic Change.* 62:189-216.
- Wolter, K. and Timlin M.S. 2011. El Niño/Southern Oscillation behaviour since 1871 as diagnosed in a extended multivariate ENSO index (MEI.ext). *Int. J. Climatol.* 31: 1074–1087, DOI: 10.1002/joc.2336
- World Water Assessment Programme. 2009. The United Nations World Water Development Report 3: Water in a Changing World. Paris: UNESCO, and London: Earthscan

Table 5.1 CMIP5 GCMs selected to investigate possible climate change impact to future drought events in SSAF.

CMIP5 models		
Model	Institution	Resolution Lon × Lat (degrees)
CanESM2	Canadian Centre for Climate Modelling and Analysis, Canada,	2.8×2.8 (≈ 310 km)
GFDL-ESM2M	Geophysical Fluid Dynamics Laboratory, USA	2.5×2.023 (≈ 250 km)
HadGEM2-ES	Met Office Hadley Centre, UK	1.875×1.25 (≈ 175 km)
MIROC5	Atmosphere and Ocean Research Institute (The University of Tokyo), National Institute for Environmental Studies, and Japan Agency for Marine-Earth Science and Technology, Japan	1.4×1.4 (≈ 155 km)
MPI-ESM-LR	Max Planck Institute for Meteorology, Germany	1.875×1.865 (≈ 210 km)

Table 5.2 PDSI category table (Palmer, 1965)

PDSI classification			
≥4	Extremely wet	-0.5 to -0.99	Incipient dry spell
3 to 3.99	Very wet	-1 to -1.99	Mild drought
2 to 2.99	Moderately wet	-2 to 2.99	Moderate drought
1 to 1.99	Slightly wet	-3 to -3.99	Severe drought
0.5 to 0.99	Incipient wet spell	≤-4	Extreme drought
-0.49 to 0.49	Near normal		

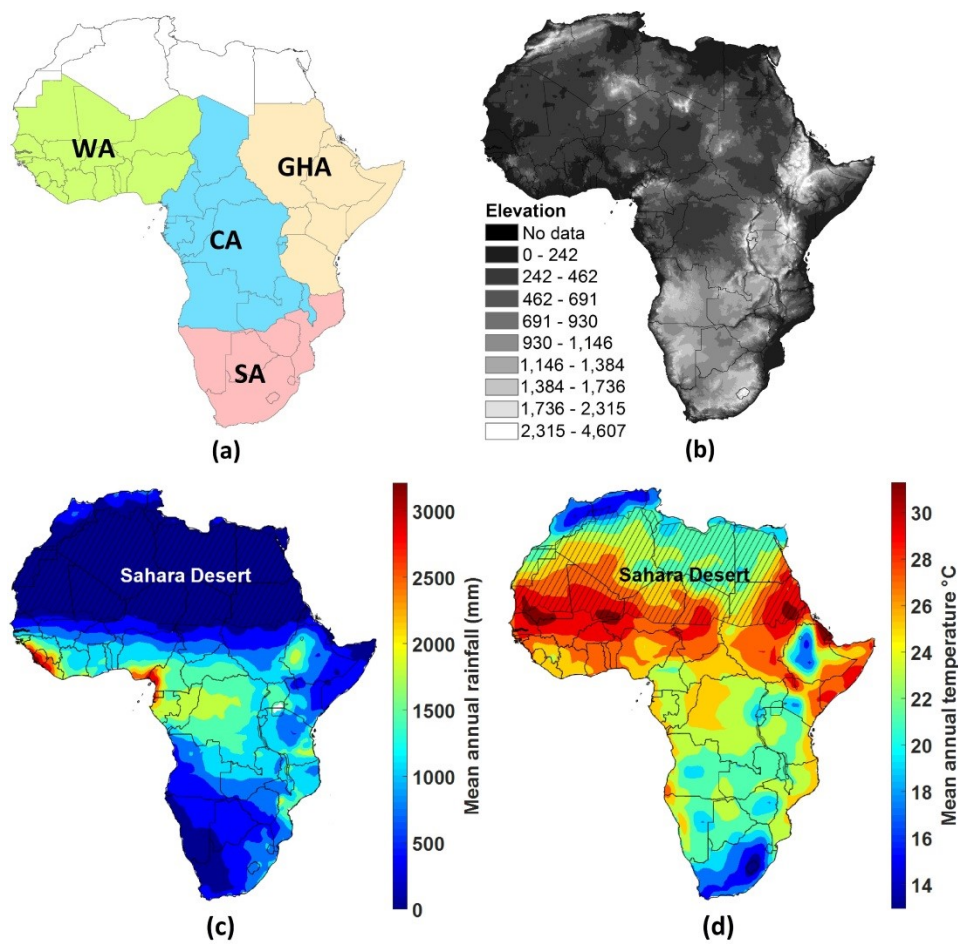


Figure 5.1 (a) Sub-regions of SSAF based on political boundaries, (b) Elevation map of Africa, (c) Mean annual precipitation for 1971-2000 derived from Global Precipitation Climatology Centre (GPCC) gridded monthly precipitation data, (d) Mean annual temperature for 1971-2000 derived from ERA40 reanalysis data.

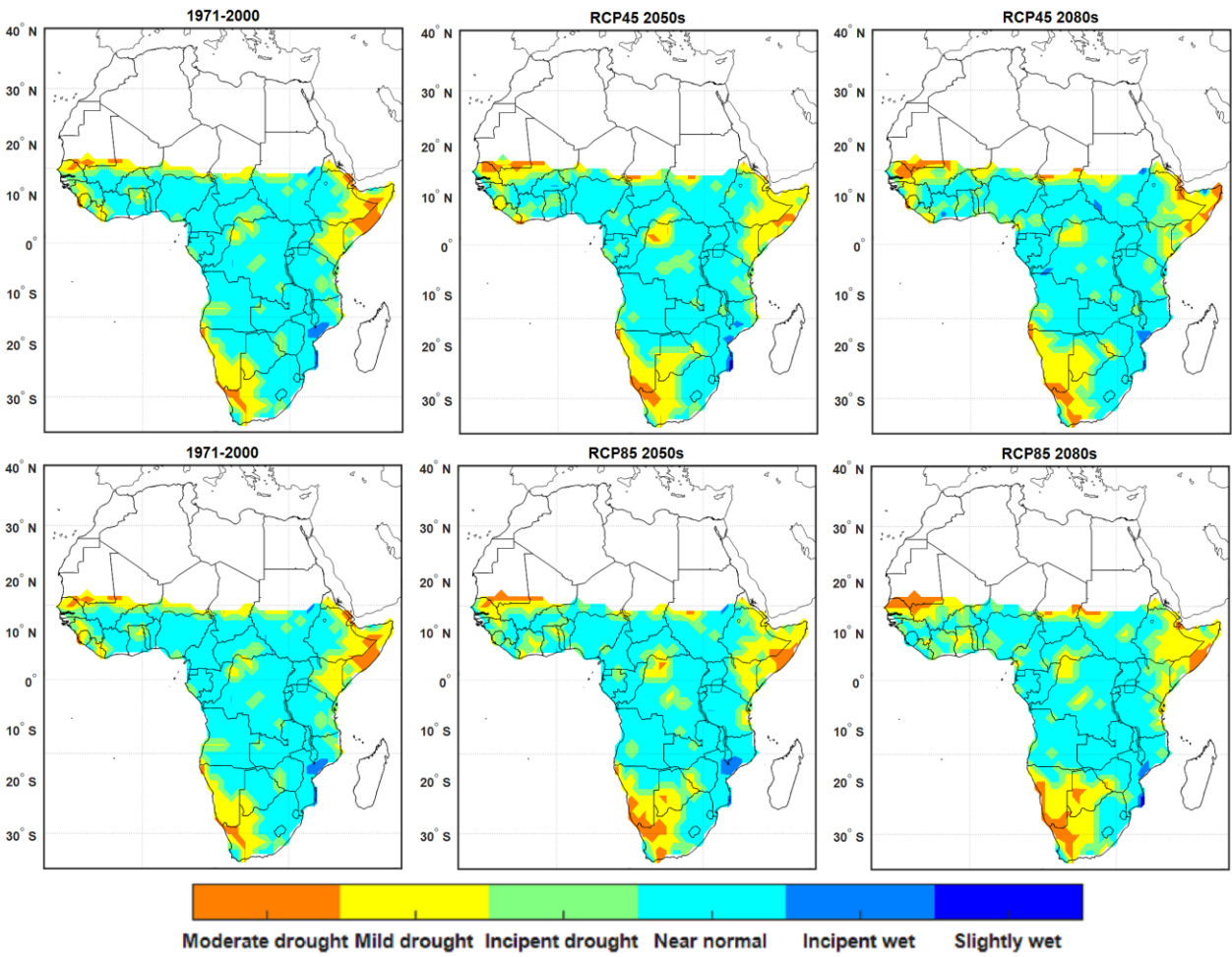


Figure 5.2 Median PDSI values of the SSAF for the base period (1971-2000), and the 2050s and 2080s under RCP4.5 and RCP8.5 climate projections of five CMIP5 GCMs.

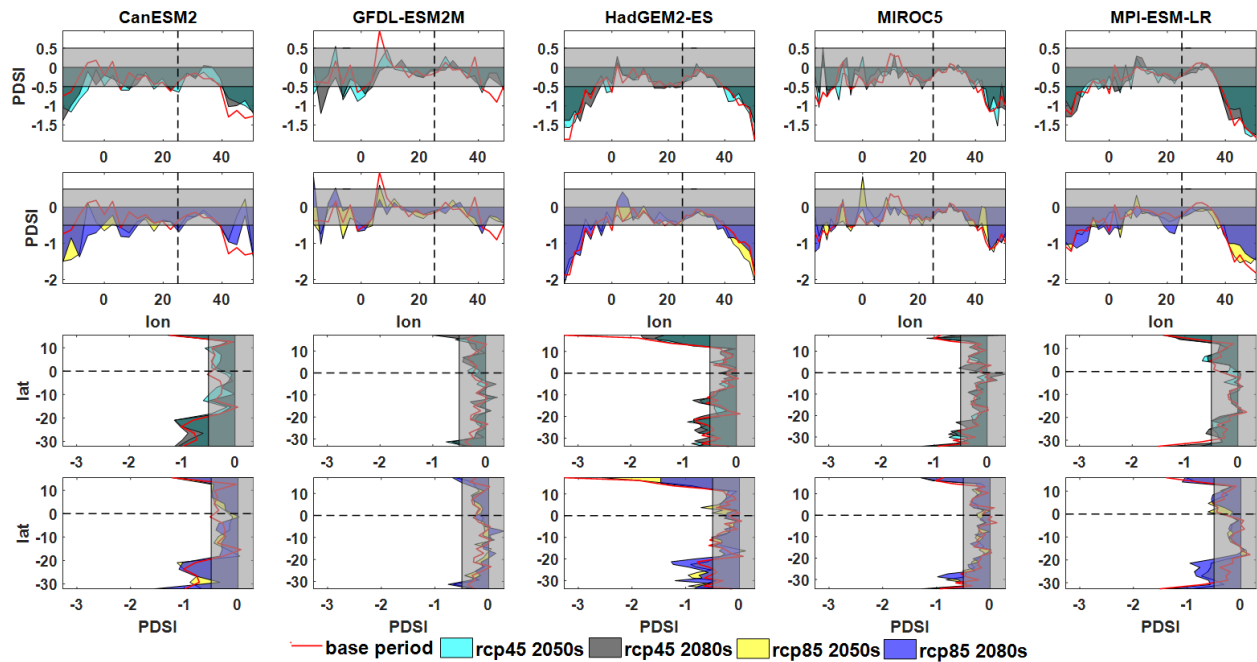


Figure 5.3 Variability of PDSI in the East-West and North-South direction of SSAF for the base period, 2050s and 2080s RCP4.5 and RCP8.5 climate projections of five CMIP5 GCMs. The light grey band in the figure shows the near normal condition whereas the dashed vertical and horizontal lines respectively represent the 25° meridian and the equator partitioning SSAF into East-West and North-South parts, respectively.

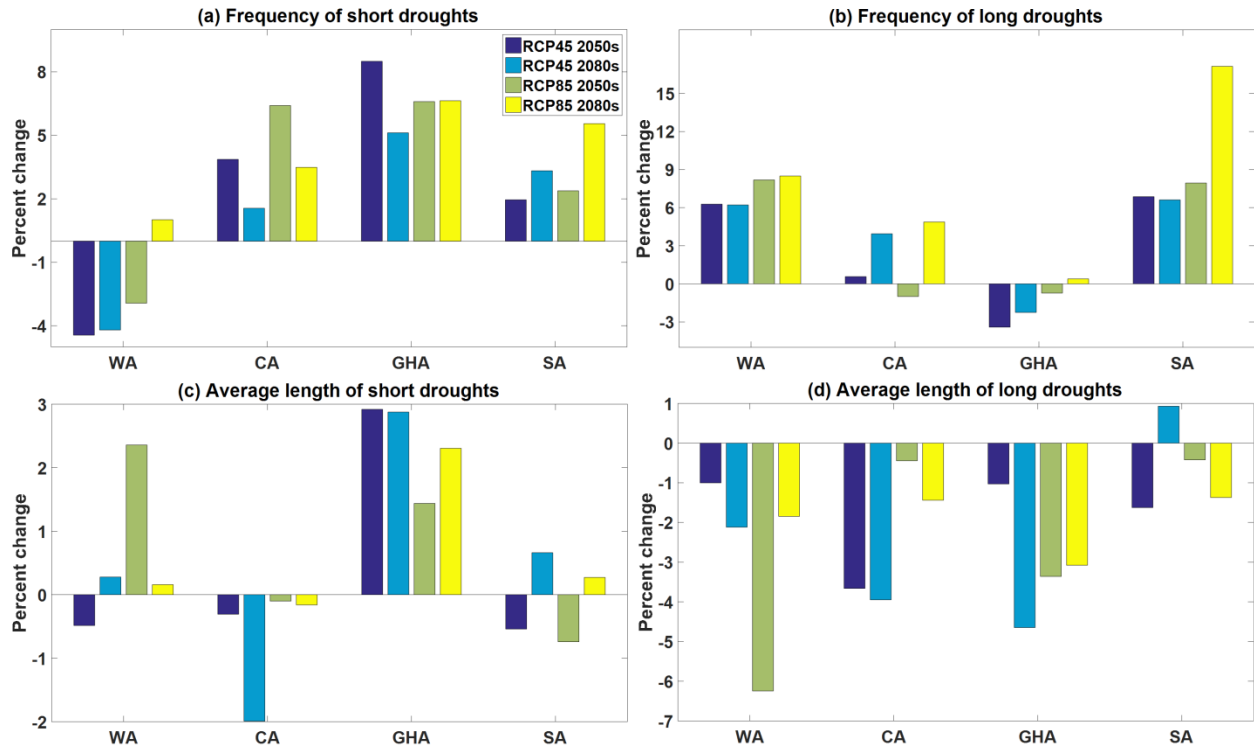


Figure 5.4 With reference to the base period, changes in the frequency (5a and 5b) and average length (5c and 5d) of short (6 to 12 months) and long (more than 12 months) duration drought events in the 2050s and 2080s based on the ensemble mean projected PDSI values of five CMIP5 GCMs.

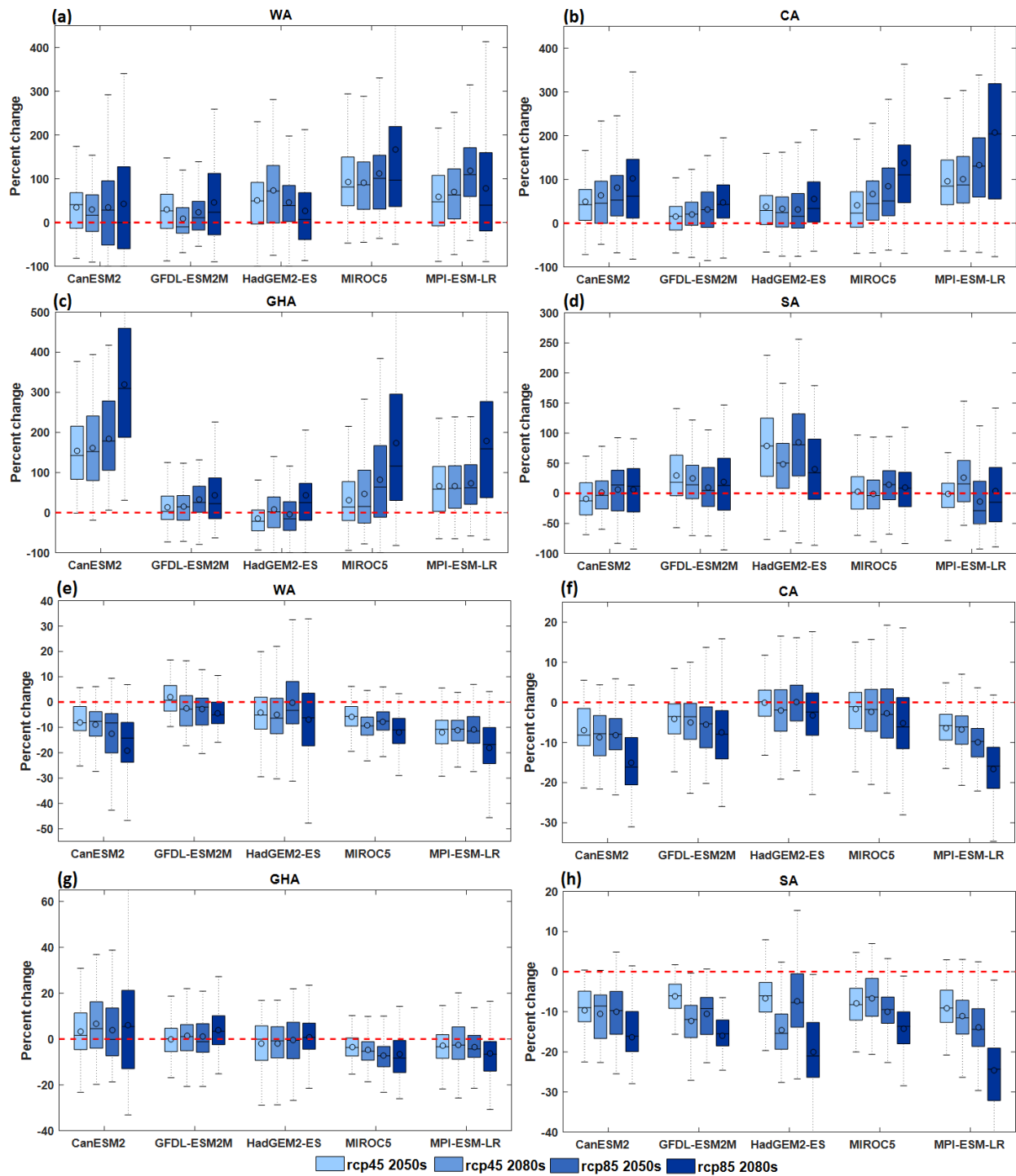


Figure 5.5 Cumulative monthly precipitation volumes in the 2050s and 2080s for WA, CA, GHA and SA that are above (a-d) or below (e-h) the P95b threshold for RCP4.5 and RCP8.5 climate projections of five CMIP5 GCMs.

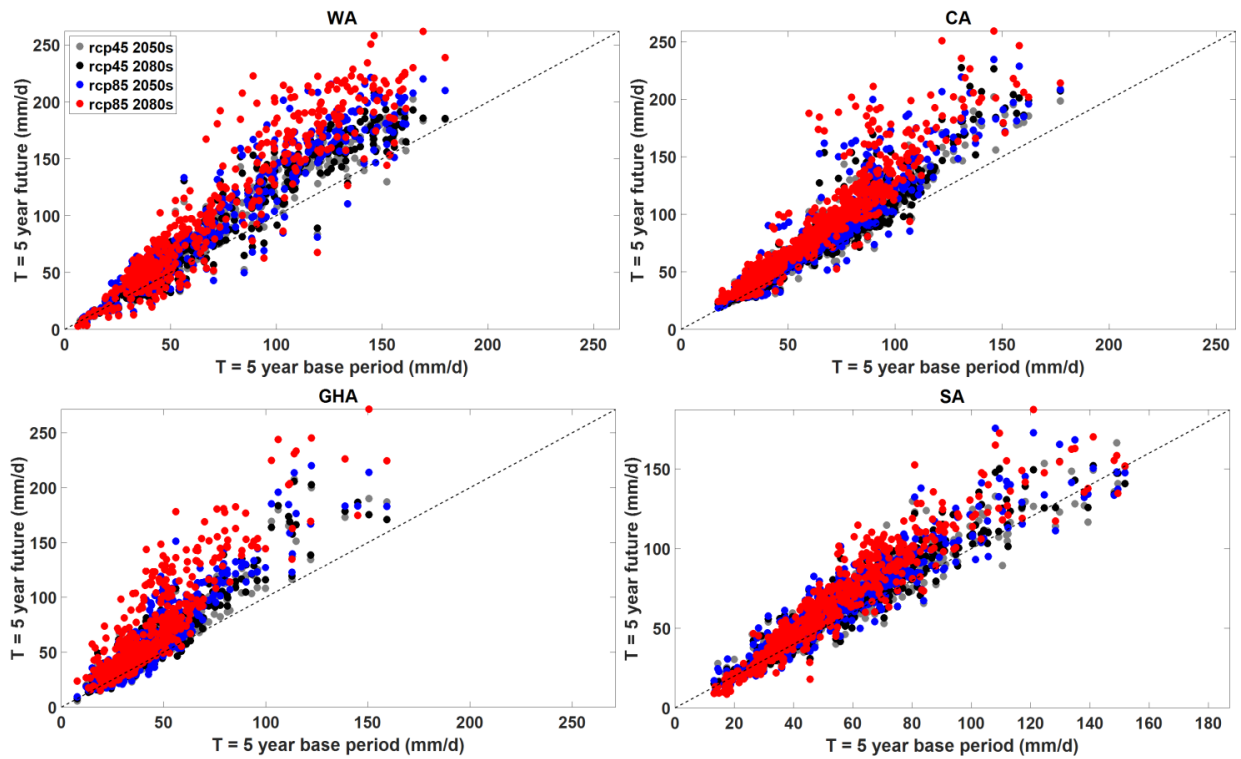


Figure 5.6 Scatterplots of 5-year return period rainfall intensity between the base period and the 2050s and 2080s under RCP4.5 and RCP8.5 climate projections of five CMIP5 GCMs.

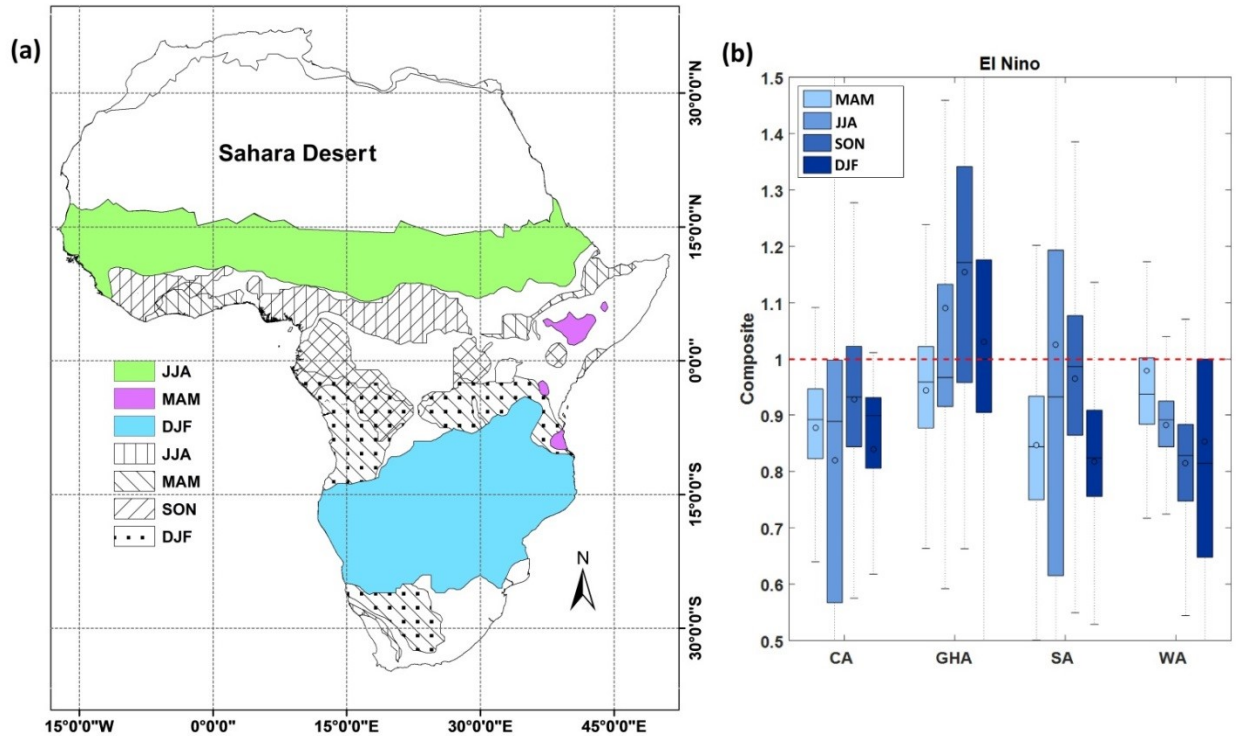


Figure 5.7 Based on GPCC data, (a) areas in SSAF that receive most of their annual rainfall in one or two rainy seasons. Coloured patches represent areas where more than half of the annual precipitation occurs in one season, while hatched and dotted patches represent areas where 30% or more of the annual precipitation occurs in two or more seasons. The seasons in the Figure refer to MAM (March to May), JJA (June to August), SON (September to November) and DJF (December to February) (b) Boxplots showing composites of MAM, JJA, SON and DJF precipitation associated with El Niño for the four regions of SSAF.

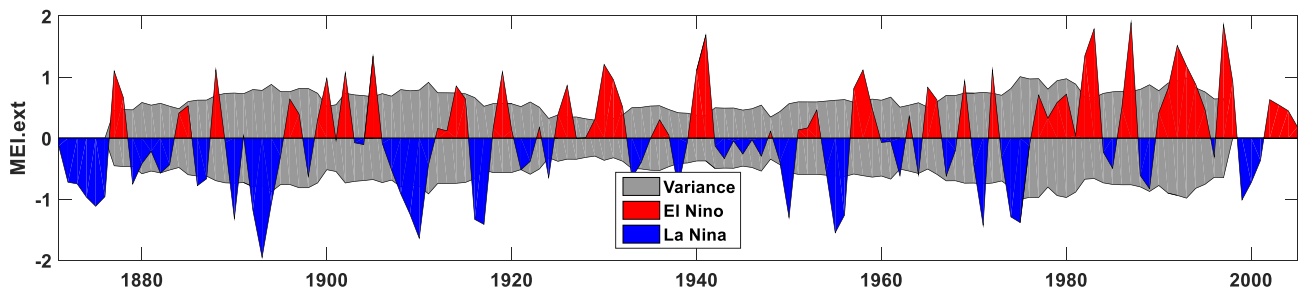


Figure 5.8 MEI.ext over the 1871-2005 periods. The grey band in the background is derived from running a 15-year variance plotted at the midpoint of the 15 year period.

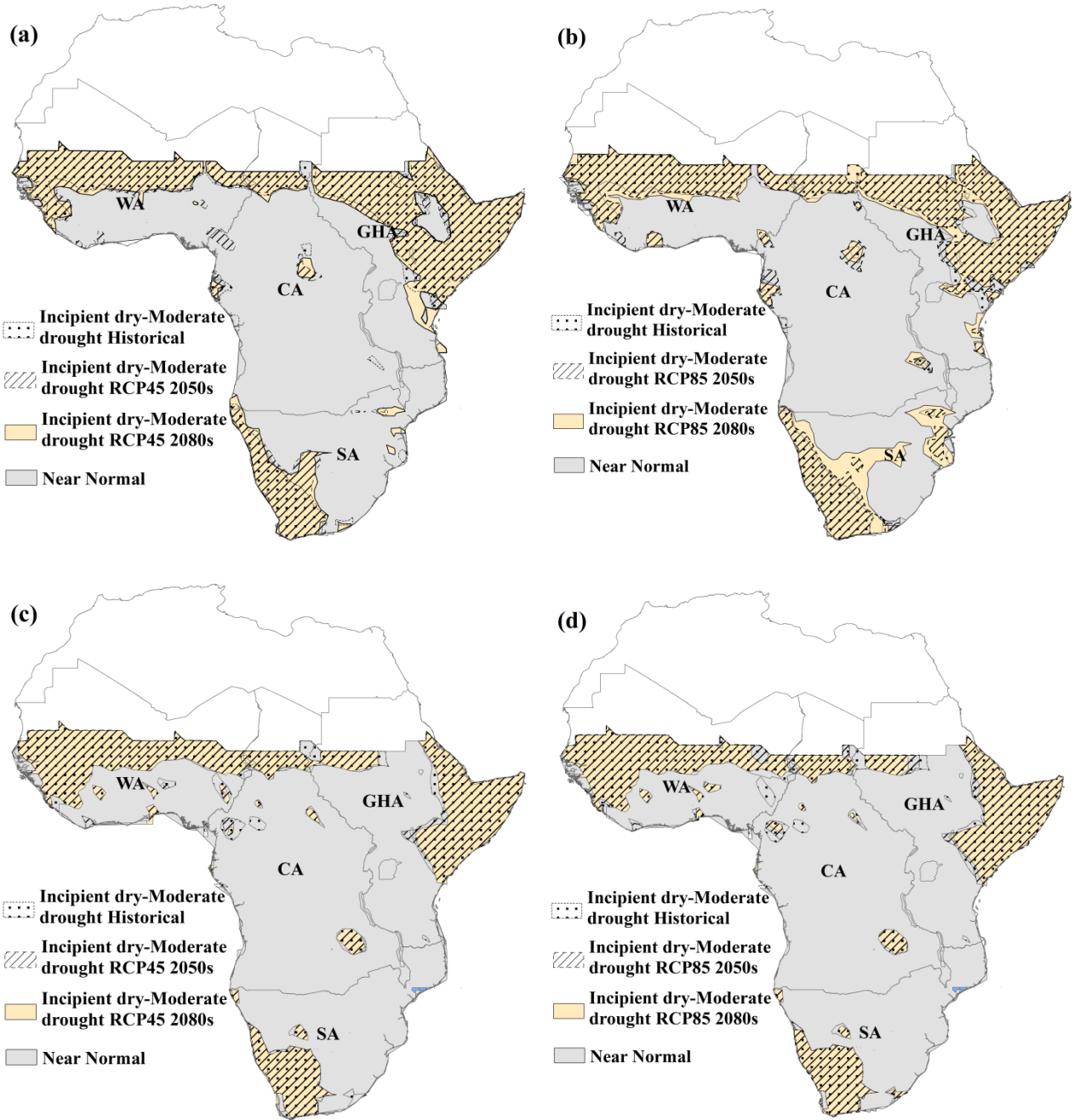


Figure 5.9 Median PDSI values derived for two hypothetical climates, one dominated by the influence of active El Niño events (a) and (b) and another that is not influenced by either El Niño or La Niña events (c) and (d) for the base period (1971-2000) and the RCP4.5 and RCP8.5 climate projections of the 2050s and 2080s.

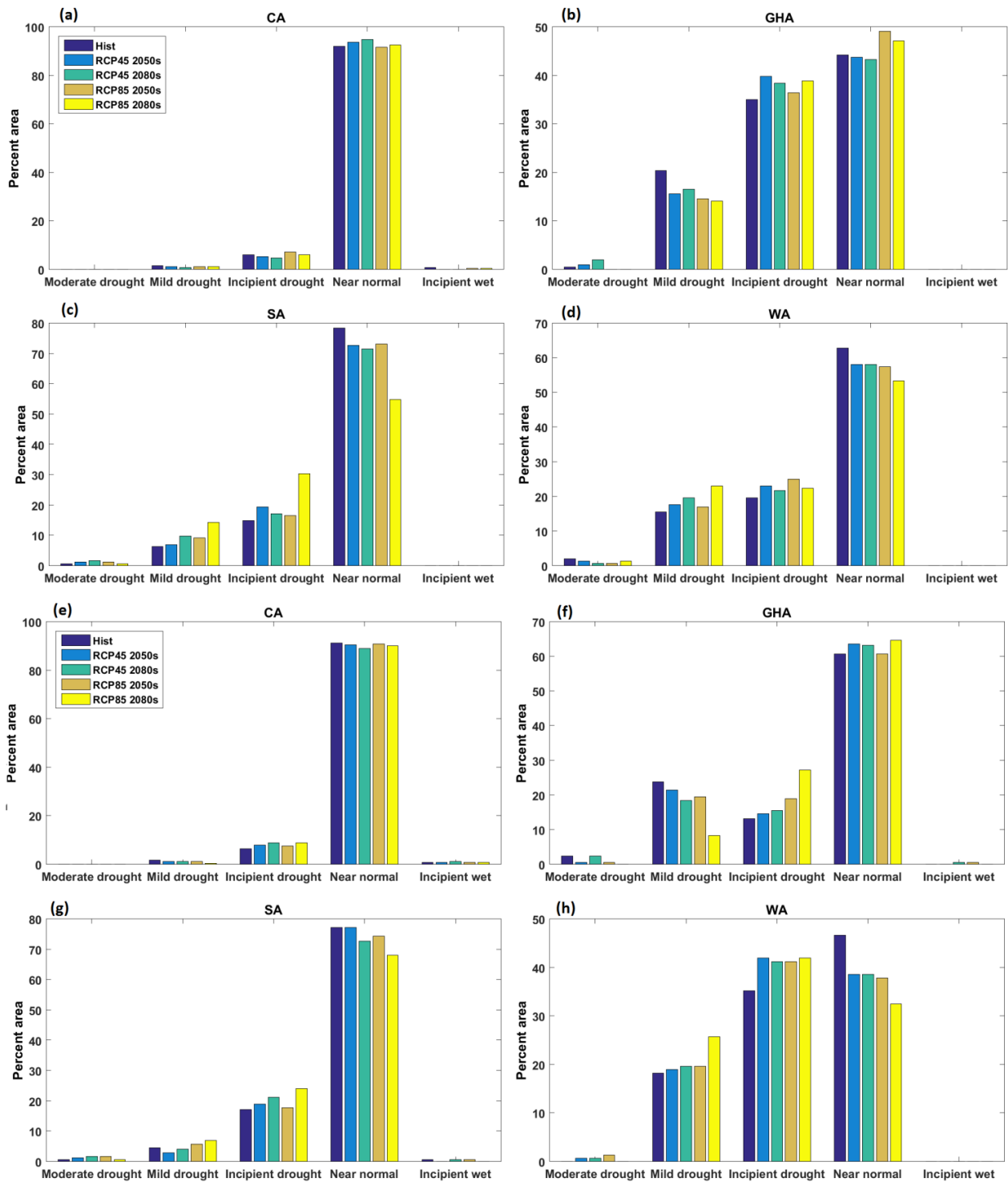


Figure 5.10 Percentage of area falling under the incipient wet to moderate drought PDSI categories for two hypothetical climates, one dominated by the influence of active El Niño events (a)-(d) and another that is totally not influenced by either El Niño or La Niña events (e) and (h) for the base period (1971-2000) and the RCP4.5 and RCP8.5 climate projections of the 2050s and 2080s.

Chapter 6 Potential Impact of climate change on streamflow of major Ethiopian rivers

6.1 Introduction

Historical temperature data since instrumental records began in the late 19th century show that the global mean surface temperature has been rising, with the recent past three decades being successively warmer than any of previous decades (IPCC, 2013). This trend of global warming could significantly alter the precipitation pattern and water availability in different parts of the world. Many regions of Africa, such as Sahel of northern Africa, Greater Horn of Africa, and western and southern Africa, have been affected by severe droughts in recent decades and in the last several millennia, and are vulnerable to negative impact of climate change (Gan et al. 2015). However, in recent decades we have also witnessed a significant increase in flood related fatalities in different parts of Africa (Di Baldassarre and Uhlenbrook, 2012; Di Baldassarre et al., 2010).

The recent warming since the 1980s have coincided with drying trends observed across Africa, including the Ethiopian region, over the 1950-2008 period (Dai, 2011). In addition, Dai et.al (2009) also found decreasing trends in the streamflow of some of the largest ocean reaching rivers of Africa for 1948-2000 period. Besides the possible drying effects due to human activities, the recent drying trends can be partly related to more frequent and intensive warm phases of El Niño Southern Oscillation (ENSO), or El Niño (Dai, 2011). Although the cause of the observed increase in El Niño activity since the late 1970s is debatable, recent studies have suggested that increased frequency of El Niño episodes are more likely due to a warmer climate

(Cai et al. 2014; Kim et al. 2014; Power et al. 2013; Santoso et al. 2013). These studies indicate that the recent observed warming might have contributed to the increased activities of the warm phase of ENSO (El Niño) which is mainly associated with below normal precipitation for different parts of Africa (Lindesay and Vogel, 1990; Mason and Goddard, 2001; Lyon and Mason, 2007 and Ratnam et al. 2014).

Ethiopia is vulnerable to impacts of climate change given the country has experienced some of the worst drought events in past several decades. Therefore many studies have been focusing on the potential impact of climate change on future streamflow volume of some Ethiopian rivers. Despite the observed drying trends and recurrent droughts in recent years, some of these studies have projected an increase in streamflow of Ethiopian rivers by the mid and late 21st century. For example, Dile et al. (2013) suggested that the streamflow of the Gilgel Abay River, which is located in the Lake Tana basin, is projected to increase for the 2070-2100. Adem et al. (2016) also simulated a consistent increase in the streamflow for the same study area over the 21st century. In contrast, based on the IPCC (Intergovernmental Panel on Climate Change) SRES (Special Report on Emission Scenarios) A2, A1B and B1 scenarios of several GCMs (Global Climate Models), Setegn et al. (2011) suggested that the streamflow of Lake Tana basin, which is the source of the Blue Nile, is mostly projected to decline for the 2080-2100. For the whole Nile basin, for which Ethiopia contributes the majority of its annual runoff, Beyene et al. (2010) simulated an increase in its streamflow for 2010-2039, followed by a consistent decrease for 2040-2069 and 2070-2099 periods. For other river basins of Ethiopia, such as the Awash basin, Hailemariam (1999) simulated a decrease in its streamflow under the impact of climate change in the 21st century.

Until now, most studies that investigated the potential impact of climate change on water resources of Ethiopia are based on SRES climate scenarios of IPCC (2007) with a primary focus on the Abay (Blue Nile) basin. Therefore the key objective of this study is to conduct a more comprehensive analysis on the possible impact of climate change on water resources of major river basins of Ethiopia by using the IPCC (2013) RCP (Representative Concentration Pathways) climate projections (RCP4.5 and RCP8.5) of 10 GCMs. The results of this study should contribute to the long term water resources planning and adaptation strategies for Ethiopian region. With this introduction, description of study area, data and methodology is given in Section 6.2, results and discussion in Section 6.3 and summary and conclusion and recommendation in Section 6.4.

6.2 Study Area, data and methodology

6.2.1 Study area

Ethiopia is a country with great topographic and climate variability. The country has among the highest and also the lowest places in Africa mainly due to its geological history associated with the formation of the great East African Rift valley which extends from south-west to the north-east corner of the country. Mountainous regions on either side of the Ethiopian rift valley could reach heights up to 4500 m above mean sea level (msl) whereas the Danakil depression in the north-eastern parts of the Ethiopian rift valley could be as low as 116 m below msl (Figure 6.1a). This large topographic variability contributes to a fairly wide range of climatic regimes found in different parts of Ethiopia. The highland areas in the north-west and south-western parts of the country are characterized by cooler temperatures (15 to 20 °C) and annual precipitation in excess

of 1500 mm whereas the lowland areas in the north-east and eastern parts of the country have arid climates with annual precipitation below 500 mm (Figure 6.1b-c).

The seasonal rainfall over Ethiopia is primarily governed by the migration of the Intertropical Convergence Zone (ITCZ). ITCZ is a zonal belt of low pressure, strong convection and heavy precipitation which encircles the Earth around the equator where the northeast and southeast trade winds meet (IPCC, 2013: AnnexIII). Over land the ITCZ tends to follow the seasonal march of the Sun, oscillating between the fringes of the Sahara Desert during the boreal summer and the northern Kalahari Desert during the austral summer (IPCC, 1997). This passage of the ITCZ over the Ethiopian region gives rise to a bimodal rainfall pattern in southern and southeastern Ethiopia with March-May (ITCZ migrating north) and September-November (ITCZ migrating south) rainfall seasons and a mono-modal rainfall pattern in northern and western Ethiopia with June-September rainfall season (Sutcliffe and Parks, 1999; Diro et al., 2011).

Based on the dominant rainfall seasons resulting from the migration of the ITCZ, Ethiopia can be roughly divided into three climatic regions (Figure 6.2) Climatic region A covers central, north-eastern and parts of eastern Ethiopia and is characterized by a dry period from October to February (locally called Bega), a short rainy season from March to May (locally called Belg) and a long rainy season from June to September (locally called Kiremt). Climatic region B covers the north-western and western parts of Ethiopia with a comparatively wetter climate where the long rainy season extends from March to November with June-September (Kiremt) period getting most of the rainfall, while October to February is the dry season. Climatic region C covers the southern and south-eastern parts of the country with two distinct rainy seasons and two dry

seasons. March to May and September to November in region C are considered as the rainy seasons whereas June to August (usually a rainy season in climatic regions A and B) and December to February period are the dry seasons (NMSA, 1996).

There are 12 major river basins in Ethiopia with an estimated total mean annual runoff of $122 \times 10^9 \text{ m}^3$. Together with Abay and Omo-Gibe river basins, the four river basins analyzed in this study, namely Awash (total area 116400 km^2), Baro (72000 km^2), Genale (82400 km^2) and Tekeze (61700 km^2) river basins, account for up to 90% of the total mean annual runoff of the entire country (Awulachew et al. 2007). The Awash River originates in the central Ethiopian highlands and flows entirely within boundaries of the Ethiopian rift valley. Tekeze and Baro Rivers are transboundary rivers respectively located in the northern and western parts of Ethiopia and eventually join the Nile River in Sudan. Genale River, located in southern Ethiopia, is also a transboundary river draining into the Indian Ocean (Figure 6.2). Based on the three climatic regions of Ethiopia the Awash and Baro river basins are entirely located in climatic regions A and B, respectively. Almost all of the Genale river basin is located in climatic region C with its upstream portions in climatic region A. The Tekeze river basin shares parts of climatic region A and B (Figure 6.2)

6.2.2 Data

6.2.2.1 Historical data

Observed daily streamflow and climate data for the four study areas were collected from the Ministry of Water Resources (MoWR) and the National Metrological Agency (NMA) of Ethiopia. From the climatic stations available, only those stations with relatively complete data

and with a record period matching the available streamflow records were selected. Missing daily precipitation or temperature data in climatic stations was filled using nearby stations with the most complete dataset in the study area based on relationships derived from long term climate records. Unlike climatic data, streamflow records of extended periods were only available after 1990 (Appendix C, Table C1). With the exception of the Awash River basin, climatic data for Baro, Genale and Tekeze river basins was only available till 2004 or 2005. Therefore the time period for which the records of streamflow and climate data overlap for each study area was chosen to calibrate a hydrologic model to simulate the streamflow of that study area. About 2/3 of the observed daily climate and streamflow data were used for the model calibration, while the remaining data was reserved for model validation. Due to the location of streamflow gauging stations or due to limited number of climatic stations with adequate data, about 33% (overall drainage area) of Baro, 12% of Genale and 73% of Tekeze located within the boundaries of Ethiopia, has been analyzed for three of the river basins (dark gray area in Figure 6.2). For Awash River basin, only about 7% of the overall drainage area, which is located upstream of Koka hydroelectric dam, was analyzed in this study because downstream from this point the streamflow hydrograph is significantly affected by the dam and large irrigated farmlands. However, based on the observed gridded data of Global Precipitation Climatology Center (GPCC) (Beck et.al, 2004), the portions of the river basins analyzed in this study receive about 20% (Awash), 50% (Baro), 22% (Genale) and 85% (Tekeze) of the mean annual precipitation falling over their respective entire river basins located within the boundaries of Ethiopia. Therefore, changes in the streamflow projected in this study should be representative of the expected changes in the total streamflow of these river basins.

6.2.2.2 GCM data

To project future streamflow of the four study areas, RCP4.5 and RCP8.5 daily climate projections of temperature, precipitation and wind were extracted from 10 CMIP5 (Coupled Model Intercomparison Project phase 5) GCMs listed in Table C2. Compared to GPCC data, all GCMs have generally simulated representative areal pattern of the 1971-2000 mean annual precipitation of Ethiopia (Appendix C, Figure C1). However, some GCMs such as MIROC5 have substantially overestimated the precipitation of central and western Ethiopia while GCMs like CMCC-CM marginally underestimated the precipitation of these regions. The areal pattern of mean annual temperature simulated by these GCMs was also similar to that of GHCN-CAMS observed gridded temperature data (Fan and Dool, 2008). However, partly because of their coarse resolutions, almost all GCMs over-simulated temperatures of the rugged Ethiopian highlands (Figure C2). Therefore, it is necessary to bias correct the precipitation and temperature data simulated by the CMIP5 GCMs selected in this study based on observed data of the four river basins (Appendix C).

6.2.3 Methodology

To analyze the impact of climate change on streamflow of major river basins in Ethiopia, long term streamflow simulations for historical and future periods were simulated using the Hydrologic Simulation Program-FORTRAN (HSPF) hydrologic model (Bicknell et.al 2001) developed by the Environment Protection Agency (EPA) of USA. HSPF is chosen for this study because it is a continuous, lumped conceptual model similar to the Stanford Watershed Model, capable of simulating streamflow, sediment load and water quality data at the catchment outlet of interest, has been tested over a wide range of watersheds (Viessman and Lewis, 2003), and

demonstrated to perform comparably with widely used physically based models such as SWAT (Saleh and Du, 2004; Singh et al., 2005; Kim et al. 2007). Climate data required for modelling basin streamflow using HSPF are precipitation and potential evapotranspiration (PET). PET was computed using Penman Monteith method following the procedures outlined by the Food and Agriculture Organization (FAO) (Allen et al., 1998). Soil characteristics, which are also essential for calibrating HSPF for the four river basins which are respectively divided into several sub-basins, are derived from the Food and Agriculture Organization (FAO) data (FAO, 1974). To account for uncertainties associated with long term climate projections, future streamflow of the four study sites was simulated by HSPF forced with RCP4.5 and RCP8.5 climate projections of 10 CMIP5 GCMs from IPCC (2013). Projected changes to streamflow of the four study sites for 2041-2070 (2050s) and 2071-2100 (2080s) with respect to the 1971-2000 control period will be useful for assessing the streamflow of these study sites of Ethiopia and is useful for long term water resources planning and adaptation strategies over the 21st century.

6.3 Results and discussion

6.3.1 Model calibration

Between the study areas, it was found that the calibrated parameters of HSPF were similar, which significantly reduced the effort of calibrating the model parameters for the four study areas. This suggests that the parameters of HSPF calibrated at certain regions of Ethiopia could be transferable to other regions of the country where the availability of observed climate and streamflow data is fairly limited.

Among the four river basins analyzed in this study, the climate of the Baro river basin was probably better represented because it has more climate stations evenly distributed over its drainage area (Figure 6.2, Table C1). As a result, HSPF was well calibrated with a Nash Sutcliffe coefficient (E_f) (Nash and Sutcliffe, 1970) of 0.881 and coefficient of determination (R^2) (Krause et al., 2005) of 0.901 (Table 6.1). Even though Awash River basin has five climate stations for rainfall, the period of observations of four of these stations do not overlap with the observation period of streamflow data at the Melka Hombole station. Therefore HSPF was calibrated for the Awash River basin using rainfall data from the Addis Ababa station adjusted for different areas of the river basin based on rainfall records of other climate stations located near or within the basin. However, the performance of the calibrated HSPF model for the Awash basin was still very good in terms of E_f (0.707) and R^2 (0.786). For the largest, Tekeze river basin, the climate stations are mostly located near the basin boundaries which made the data less representative of the basin's climate (Figure 6.2). In addition, about two out of six years of the streamflow data for August, the rainy season, was missing. For the Genale river basin, only three climate stations were available to calibrate HSPF (Figure 6.2). As a result, the calibration result of HSPF for Tekeze and Genale river basins was lower than that of Baro and Awash river basins. Overall, HSPF was well calibrated for the Awash, Baro, Genale and Tekeze river basins with the simulated streamflow hydrographs and flow duration curves compared well with the observed counterparts (Table 6.1, Figure 6.3-Figure 6.4). The calibrated HSPF model for the four river basins was validated with the remaining one-third climate and streamflow data independent of the calibration experience. Based on criteria for satisfactory model performance by Moriasi et.al (2007), the performance of HSPF was satisfactory for both the calibration and validation periods with the exception of PBIAS for some river basins during model validation

(Table 6.1). These results establish the basis for using the calibrated HSPF model to assess the potential hydrologic impact of climate change on the four study areas of Ethiopia in the mid and late 21st century.

6.3.2 Projected changes in streamflow

After bias correction, RCP climate scenarios of 10 CMIP5 GCMs selected in this study project an increase in temperature under RCP4.5 (RCP8.5) over the four study areas ranging from 1.8-2.0 °C (2.6-2.9°C) in 2050s, and 2.2-2.5 °C (3.9-4.8 °C) in 2080s when compared to the control period (Table 6.2). Projected changes in precipitation by the 10 CMIP5 GCMs for the four study areas differ significantly, with GCMs such as CanESM2 and IPSL-CM5A-MR projecting a significant increase in precipitation, particularly for RCP8.5 climate projections of the 2080s (Figure 6.5). On the other hand, GCMs such as MIROC5 and INM-CM4 generally projected a marginal decrease in precipitation for most study areas. Overall, the median of projected changes in precipitation for the four study areas under RCP4.5 (RCP8.5) ranges from 0.3-10% (4-11%) in the 2050s and 2-14% (10-23%) in the 2080s (Table 6.2 and Figure 6.5).

The median projected changes in mean annual streamflow in the 2050s and 2080s with respect to the control period simulated by the HSPF are presented in Table 6.2. The percent changes in streamflow with respect to projected increase in temperature for RCP4.5 and RCP8.5 climate scenarios for the 2050s and 2080s are shown in Figure 6.6. The changes in streamflow simulated for the four study areas vary widely due to the wide ranges of future precipitation projected by the 10 CMIP5 GCMs (Figure 6.6). In particular, a wider range of changes in streamflow was projected for RCP8.5 in the 2080s than RCP4.5 and for RCPs in the 2050s. GCMs that projected

a significant increase in precipitation (IPSL-CM5A-MR and CanESM2) result in a significant increase in the mean annual streamflow of the four study areas. GCMs that projected a marginal increase in the mean annual precipitation result in a projected decrease in the mean annual streamflow due to higher projected PET from higher temperatures. This is particularly evident for Baro and Tekeze river basins (Table 6.2 and Figure 6.6). On a whole, an increase in streamflow ranging from 2-17% was projected for Awash, Baro and Tekeze river basins located in climatic regions A and B. Under RCP4.5 climate scenarios of most GCMs, marginal decrease in streamflow ranging from -0.3 to -4% is projected for both 2050s and 2080s in Baro river basin and for the 2080s in Tekeze river basin. On the other hand, under RCP4.5 and RCP8.5 climate projections of the 2050s and 2080s, a larger increase in streamflow ranging from 16-42% was projected for the Genale river basin located mostly in climatic region C of Ethiopia.

Projected changes in streamflow are also significantly different between winter (December to February), spring (March to May), summer (June to August) and autumn (September to November). For the four river basins, a large increase in streamflow was projected in winter and spring. In particular, the winter streamflow of Awash and Genale was projected to increase over 100% in 2080s under RCP8.5 (Figure 6.7, Figure C6-C7). However, winter and spring streamflow together only account for about 7-10% of the total annual runoff for Awash, Baro and Tekeze river basins and about 25% for Genale river basin. As a result, for the former three river basins, a large projected increase in these seasonal streamflow may not contribute much to the mean annual flow. Conversely, despite the overall projected increase in the mean annual streamflow, the summer streamflow which accounts for about 44-65% of the total annual streamflow of Awash, Baro and Tekeze river basins is projected to decrease particularly for the

latter two river basins. Similarly for the 2050s, the summer streamflow of Genale river basin, which accounts to about 32% of the mean annual runoff, is also projected to decrease marginally. However, such a marginal decrease in the summer streamflow will be compensated by a 4-23% increase in the autumn streamflow which accounts for 27-45% of the total mean annual runoff in the four study areas (Figure 6.7, Figure C9). In addition, unlike Awash, Baro and Tekeze river basins, the mean annual streamflow for Genale river basin mainly occurs in spring and autumn. Therefore, a significant projected increase in these two seasonal streamflow resulted in a higher projected mean annual runoff for Genale river basin compared to Awash, Baro and Tekeze river basins.

6.3.3 Comparing projections of precipitation of Ethiopia by GCMs with observations

GCMs participating in the current CMIP5 assessment suggest that RCP climate scenarios project a notable increase in the October-March precipitation during the 21st century for Ethiopia and its surrounding countries. Little change is projected for the April-September precipitation except for the warmer RCP8.5 climate scenarios for which some increase in precipitation is projected (IPCC 2013: Annex I). This findings are also in agreement with the previous CMIP3 assessment report which also suggests a wetter climate for East Africa (Christensen et al. 2007; Shongwe et al. 2011). The projected increase in autumn, winter and spring streamflow in Section 6.3.2 is mainly attributed to an increase in the October-March precipitation projected by the 10 CMIP5 GCMs selected in this study (Figure C6-C9). Similarly, for the Ethiopian Upper Blue Nile Basin which drains into the Nile (like Baro and Tekeze rivers), Aich et al. (2014) also projected an increase in the October-May streamflow using a hydrologic model forced with RCP2.6 and RCP8.5 climate projections of five CMIP5 GCMs. Contrary to these climate

projections, recent studies suggest that the Horn of Africa will likely become more drier during the course of the 21st century. Based on a reconstructed paleoclimate data for the past 2000 years, Tierney et al. (2015) found that the recent rate of drying in the Horn of Africa (Somalia, Djibouti and eastern Ethiopia (climatic region C)) is unusual in the context of the past two millennia and is synchronous with recent global warming. Their results suggest that globally warm conditions in the past two millennia were associated with drying in eastern Horn of Africa and the present and future warm conditions will likely be followed by drying in this region. In contrast, most GCMs project an increased precipitation of the September-November “short rain” season due to a large scale weakening of the Walker circulation while the March-May “long rain” (Belg season in Ethiopia) precipitation is projected to decrease, but resulted in a net increase in 21st century mean annual rainfall in the Horn of Africa contrary to the observed drying trend in the 20th century. Tierney et al. (2015) argue that wetter climate for Horn of Africa is projected in the 21st century because of limitations of GCMs in simulating the regional climate. Williams and Funk (2011) also found that the rainfall during the Belg season has been declining particularly over the eastern flank of the Ethiopian highlands (climatic region A) and across central Kenya during the last 40 years of observed antropogenic global warming. Williams and Funk (2011) argue that the decline in precipitation during the summer (June-August) and particularly the Belg season in Ethiopia coincide with recent warming observed globally, and estimate an increased frequency in drought conditions in tropical eastern Africa due to a reduction in the Belg precipitation. This is in contrast to the relatively wetter 21st century climate projected by most GCMs over the Ethiopian region. A recent study by Rowell et al. (2015) also listed six key hypothesis to explain the paradox in observed and projected east African precipitaton during the “long rain” season. On a whole, our findings generally agree with streamflow projections for Ethiopia by other

studies based on SRES climate scenarios of IPCC (2007) (Beyene et al., 2010; Dile et al., 2013; Adem et al., 2016) or RCP climate projections of IPCC (2013) (Aich et al., 2014). However, a careful interpretation of these results is necessary given these streamflow projections do not quite reflect drying trends observed in recent years (Dai, 2013).

6.4 Summary and Conclusions

Our results show that the mean annual streamflow of the Awash, Baro and Tekeze river basins simulated by HSPF is projected to marginally increase by about 3% in 2041-2070 (2050s) and by about 6% in 2071-2100 (2080s) compared to the control period (1971-1990). On the other hand, Genale river basin located in climatic region C of Ethiopia is projected to have about 18% (2050s) and 33% (2080s) increase in its mean annual streamflow. Despite the projected increase in the mean annual streamflow, the summer streamflow which contributes a large percentage of the annual streamflow is projected to decrease particularly for Baro and Tekeze river basins. However, the projected decrease in summer streamflow will be mostly compensated by a significant projected increase in the autumn streamflow which accounts for 27-45% of the total annual streamflow of the four study areas. Overall, the projected changes in seasonal precipitation or streamflow could affect communities in different parts of Ethiopia that mainly grow specific crops in a rainy season. Therefore, more studies are recommended to develop strategies that will mitigate the potential impact of changing seasonal rainfall or streamflow in different parts of Ethiopia because of the effect of climate change (Figure C6-C9, Figure 6.7).

Acknowledgements

The first author was supported by the Natural Science and Engineering Research Council of Canada and by the University of Alberta. The authors thank Ato Suraphel Mamo from the Ministry of Water Resources of Ethiopia and Ato Zerihun Walelign from the National Meteorological Agency of Ethiopia for their cooperation in the provision of observed streamflow and climate data for this study.

6.5 References

- Adem, A.A., Tilahun, S.A., Ayana, E.K., Worklul, A.W., Assefa, T.T., Dessu, S.B., and Melesse, A.M. 2016. Climate change impact on streamflow in the Upper Gilgel Abay Catchment, Blue Nile basin, Ethiopia. In: Melesse, A.M and Abtew, W. (ed) Landscape dynamics, soils and hydrological processes in varied climate. Springer International Publishing, Switzerland, Chapter 29: 645-673. doi 10.1007/978-3-319-18787-7_29
- Aich, V., Liersch, S., Vetter, T., Huang, S., Tecklenburg, J., Hoffmann, P., Koch, H., Fournet, S., Krysanova, V., Müller, E. N., and Hattermann, F. F. 2014. Comparing impacts of climate change on streamflow in four large African river basins. *Hydrol. Earth Syst. Sci.*, 18, 1305–1321. doi:10.5194/hess-18-1305-2014.
- Awulachew, S. B., Yilma, A. D., Loulseged, M. Loiskandl, W., Ayana, M., Alamirew, T. 2007. Water Resources and Irrigation Development in Ethiopia. Colombo, Sri Lanka: International Water Management Institute. 78p. (Working Paper 123)
- Beck, C., Grieser, J. and Rudolf, B. 2004. A New Monthly Precipitation Climatology for the Global Land Areas for the Period 1951 to 2000 (published in Climate Status Report 2004, pp. 181 - 190, German Weather Service, Offenbach, Germany)
- Beyene, T., Lettenmaier, D.P., Kabat, P. 2010. Hydrologic impacts of climate change on the Nile River Basin: implications of the 2007 IPCC scenarios. *J of Climate Change*, 100: 433-461. doi 10.1007/s10584-009-9693-0
- Bicknell, B.R., J.C. Imhoff, J.L. Kittle, Jr., T.H. Jobs, and A.S. Donigian, Jr. 2001. Hydrological Simulation Program–FORTRAN (HSPF), User’s Manual for Version 12.0. USEPA, Athens, Georgia.

- Cai, W., Borlace, S., Lengaigne, M., Rensch, P., Collins, M., Vecchi, G., Timmermann, A., Santoso, A., McPhaden, M.J., Wu, L., England, M.H., Wang, G., Guilyardi, E., and Jin, F.-F. 2014. Increasing frequency of extreme El Niño events due to greenhouse warming. *Nature climate change, Letters*, 4: 111-116. DOI: 10.1038/NCLIMATE2100
- Christensen, J.H., B. Hewitson, A. Busuioc, A. Chen, X. Gao, I. Held, R. Jones, R.K. Kolli, W.-T. Kwon, R. Laprise, V. Magaña Rueda, L. Mearns, C.G. Menéndez, J. Räisänen, A. Rinke, A. Sarr and P. Whetton, 2007: Regional Climate Projections. In: *Climate Change 2007: The Physical Science Basis. Contribution of Working Group I to the Fourth Assessment Report of the Intergovernmental Panel on Climate Change* [Solomon, S., D. Qin, M. Manning, Z. Chen, M. Marquis, K.B. Averyt, M. Tignor and H.L. Miller (eds.)]. Cambridge University Press, Cambridge, United Kingdom and New York, NY, USA.
- Cubasch, U., D. Wuebbles, D. Chen, M.C. Facchini, D. Frame, N. Mahowald, and J.-G. Winther, 2013: Introduction. In: *Climate Change 2013: The Physical Science Basis. Contribution of Working Group I to the Fifth Assessment Report of the Intergovernmental Panel on Climate Change* [Stocker, T.F., D. Qin, G.-K. Plattner, M. Tignor, S.K. Allen, J. Boschung, A. Nauels, Y. Xia, V. Bex and P.M. Midgley (eds.)]. Cambridge University Press, Cambridge, United Kingdom and New York, NY, USA.
- Dai, A., Qian, T., Trenberth, K.E., and Milliman, J.D. 2009. Changes in continental freshwater discharge from 1948-2004. *AMS, J of Climate*, 22: 2773-2792. doi: 10.1175/2008JCLI2592.1
- Dai, A. 2011, Characteristics and trends in various forms of the Palmer Drought Severity Index during 1900–2008, *J. Geophys. Res.*, 116: D12115, doi:10.1029/2010JD015541.

- Dai, A. 2013. Increasing drought under global warming in observations and models. *Nature Climate Change*, 3, 52-58. doi: 10.1038/NCLIMATE1633
- Di Baldassarre, G. and Uhlenbrook, S. 2012. Is the current flood of data enough? A treatise on research needs for the improvement of flood modelling, *Hydrol. Process.*, 26, 153–158.
- Di Baldassarre, G., Montanari, A., Lins, H., Koutsoyiannis, D., Brandimarte, L., and Blöschl, G. 2010. Flood fatalities in Africa: from diagnosis to mitigation, *Geophys. Res. Lett.*, 37, L22402, doi:10.1029/2010GL045467.
- Dile, Y.T., Berndtsson, R., Setegn, S.G. 2013. Hydrological Response to Climate Change for Gilgel Abay River, in the Lake Tana Basin - Upper Blue Nile Basin of Ethiopia. *PLoS ONE* 8(10): e79296. doi:10.1371/journal.pone.0079296
- Diro, G.T., Grimes, D.I.F, and Black, E. 2011. Large scale features affecting Ethiopian rainfall. In: Williams, J.R., and Kniveton, D.R. ed. *African Climate and Climate Change, physical, social and political perspectives*. Springer, pp 13-50.
- Fan, Y. and Dool, H. 2008. A global monthly land surface air temperature analysis for 1948–present. *J. Geophys. Res.*, 113: D01103, doi:10.1029/2007JD008470.
- FAO, 1974. Soil map of the world. Volume I, Prepared by the Food and Agriculture Organization of the United Nations, Unesco-Paris
- Gan, T. Y., Ito, M., Hülsmann S., Qin, X., Lu, X.X., Liong, S.Y., Rutschman, P., Disse, M., Koivusalo, H. 2015. Possible climate change/variability and human impacts, vulnerability of drought-prone regions, water resource and capacity building for Africa. *J of Hydrological Sciences*, 61, No 7: 1209-1226. doi:10.1080/02626667.2015.1057143
- Hailemariam, K. 1999. Impact of climate change on the water resources of Awash river basin, Ethiopia. *J of Climate Research*, 12: 91-96.

- IPCC, 1997: The Regional impacts of Climate Change: An Assessment of Vulnerability
R.T.Watson, M.C. Zinyowera, R.H. Moss (Eds). Cambridge University Press, UK. pp 517.
- IPCC, 2007: Climate Change 2007: The Physical Science Basis. Contribution of Working Group I to the Fourth Assessment Report of the Intergovernmental Panel on Climate Change [Solomon, S., D. Qin, M. Manning, Z. Chen, M. Marquis, K.B. Averyt, M. Tignor and H.L. Miller (eds.)]. Cambridge University Press, Cambridge, United Kingdom and New York, NY, USA, 996 pp.
- IPCC, 2013: Summary for Policymakers. In: Climate Change 2013: The Physical Science Basis. Contribution of Working Group I to the Fifth Assessment Report of the Intergovernmental Panel on Climate Change [Stocker, T.F., D. Qin, G.-K. Plattner, M. Tignor, S.K. Allen, J. Boschung, A. Nauels, Y. Xia, V. Bex and P.M. Midgley (eds.)]. Cambridge University Press, Cambridge, United Kingdom and New York, NY, USA.
- IPCC, 2013: Annex I: Atlas of Global and Regional Climate Projections [van Oldenborgh, G.J., M. Collins, J. Arblaster, J.H. Christensen, J. Marotzke, S.B. Power, M. Rummukainen and T. Zhou (eds.)]. In: Climate Change 2013: The Physical Science Basis. Contribution of Working Group I to the Fifth Assessment Report of the Intergovernmental Panel on Climate Change [Stocker, T.F., D. Qin, G.-K. Plattner, M. Tignor, S.K. Allen, J. Boschung, A. Nauels, Y. Xia, V. Bex and P.M. Midgley (eds.)]. Cambridge University Press, Cambridge, United Kingdom and New York, NY, USA.
- IPCC, 2013: Annex III: Glossary [Planton, S. (ed.)]. In: Climate Change 2013: The Physical Science Basis. Contribution of Working Group I to the Fifth Assessment Report of the Intergovernmental Panel on Climate Change [Stocker, T.F., D. Qin, G.-K. Plattner, M.

- Tignor, S.K. Allen, J. Boschung, A. Nauels, Y. Xia, V. Bex and P.M. Midgley (eds.)].
Cambridge University Press, Cambridge, United Kingdom and New York, NY, USA
- Kim, S.M., Benham, B.L., Brannan, K.M., Zeckoski, R.W., Doherty, J. 2007. Comparison of hydrologic calibration of HSPF using automatic and manual methods. *Water Resour. Res.*, 43, W01402, doi:10.1029/2006WR004883
- Kim, S.T., Cai, W., Jin, F-F., Santoso, A., Wu, L., Guilyardi, E., An, S-I. 2014. Response of El Niño sea surface temperature variability to greenhouse warming. *Nature Climate Change, Letters*, 4: 786-790. DOI: 10.1038/NCLIMATE2326
- Kite, G.W. 1996. *Frequency and Risk Analyses in Hydrology*, Water Resources Publications, Colorado, United States of America.
- Krause, P., Boyle, D.P., Bäse, F., 2005. Comparison of different efficiency criteria for hydrological assessment. *Adv. Geosci.* 5: 89–97.
- Kuo, C.C., Gan, T.Y., Gizaw, M.S. 2015. Potential impact of climate change on intensity duration frequency curves of central Alberta. *J of Climate Change*. DOI 10.1007/s10584-015-1347-9.
- Lafon, T., Dadson, S., Buys, G., and Prudhomme, C. 2013. Bias correction of daily precipitation simulated by a regional climate model: a comparison of methods. *Royal Meteorological Society, Int. J Climatology*, 33: 1367-1381, doi: 10.1002/joc.3518.
- Lindesay, J.A. and Vogel, C.H. 1990. Historical evidence for southern oscillation-southern Africa rainfall relationships. *Int. J of Climatology*, 10: 679-689.
- Lyon, B. and Mason, S. 2007. The 1997-98 summer rainfall season in southern Africa. Part I: Observations. *J of Climate*, 20: 5134-5148. doi: 10.1175/JCLI4225.1

- Mason, S.J. and Goddard, L. 2001. Probabilistic precipitation anomalies associated with ENSO. AMS, BAMS, 82, no 4: 619-638.
- Moriasi, D.N., Arnold, J.D., Van Liew, M.W., Bingner, R.L., Harmel, R.D., and Veith, T.L. 2007. Model evaluation guidelines for systematic quantification of accuracy in watershed simulations. Transactions in ASABE.
- Nash, J.E., Sutcliffe, J.V., 1970. River flow forecasting through conceptual models PartI – a discussion of principles. J. of Hydrology. 10: 282–290.
- NMSA 1996. Climate and agro climatic resources of Ethiopia. NMSA (National Meteorological Service Agency) Meteorological Research Report Series 1.
- Power, S., Delage, F., Chung, C., Kociuba, G. and Keay, K. 2013. Robust twenty-first-century projections of El Niño and related precipitation variability. Nature, Letter, 502: 541-545. doi:10.1038/nature12580.
- Ratnam, J.V., Behera S.K., Masumoto and Yamagata, T. 2014. Remote effects of El Niño and Modoki events on the austral summer precipitation of southern Africa. AMS, J of Climate, 27: 3802-3815. doi: 10.1175/JCLI-D-13-00431.1
- Rowell, D.P, Booth, B.B.B, Nicholson, S.E, Good, P. 2015. Reconciling Past and Future Rainfall Trends over East Africa. J of Climate 28: 9768-9788. DOI: 10.1175/JCLI-D-15-0140.1
- Saleh, A. and Du, B. 2004. Evaluation of SWAT and HSPF within basins program for the upper north Bosque river watershed in central Texas. Transactions of the ASAE, 47(4):1039-1049.
- Santoso, A., McGregor, S., Jin, F-F., Cai, W., England, M.H., An, S-I., McPhaden M.J. and Guilyardi, E. 2013. Late-twentieth-century emergence of El Niño propagation asymmetry and future projections. Nature, Letter, 504: 126-129. doi:10.1038/nature12683

- Setegn, S.G., Rayner, D., Melesse, A.M., Dargahi, B., Srinivasan, R. 2011. Impact of climate change on the hydroclimatology of Lake Tana Basin, Ethiopia. *Water Resour. Res.*, 47, W04511, doi:10.1029/2010WR009248
- Shongwe, M.E., Oldenborgh, G.J., Hurk, B., Aalst, M. 2011. 2011. Projected changes in mean and extreme precipitation in Africa under global warming. PartII: East Africa. *J of Climate*, 24: 3718-3733. DOI: 10.1175/2010JCLI2883.1
- Singh, J., Knapp, H.V., Arnold, A.G., Demissie, M. 2005. Hydrological modeling of the Iroquois river watershed using HSPF and SWAT. *Journal of the American Water Resources Association (JAWRA)* 41(2): 343-360.
- Sutcliffe, J.V. and Parks, Y.P. 1999. *The hydrology of the Nile*. IAHS special publication no. 5, IAHS Press, Institute of Hydrology, Wallingford, Oxfordshire OX10 8BB, UK
- Tierney, J.E., Ummenhofer, C.C., and deMenocal, P.B. 2015. Past and future rainfall in Horn of Africa. *Sci. Adv.* 1. doi: 10.1126/sciadv.1500682
- Viessman, W., and Lewis, G. L., 2003, *Introduction to Hydrology*, 612 pages, 5th Edition, Prentice Hall.
- Williams, A.P., and Funk, C. 2011. A westward extension of the warm pool leads to a westward extension of the Walker circulation, drying east Africa. *J of Clim Dyn.* 37: 2417–2435. doi: 10.1007/s00382-010-0984-y

Table 6.1 Calibration and validation results of HSPF in terms of Nash Sutcliffe coefficient (Ef), coefficient of determination (R^2), root mean squared error (RMSE) and percent bias (PBIAS) for the Awash, Baro, Genale and Tekeze river basins of Ethiopia

River Basin	Calibration				
	Period	Ef	R^2	RMSE (m ³ /s)	PBIAS (%)
Awash at Melka Hombole	2004-2010	0.707	0.786	40.89	-2.96
Baro at Gambela	1990-1999	0.881	0.901	137.67	7.13
Genale at Chene Masa	1993-2001	0.534	0.600	69.39	3.00
Tekeze at Emba Madre	1994-1999	0.631	0.721	210.37	-13.4
Validation					
Awash at Melka Hombole	2011-2013	0.636	0.658	47.79	-33.49
Baro at Gambela	2000-2004	0.721	0.899	179.23	34.26
Genale at Chene Masa	2002-2005	0.542	0.635	114.39	9.46
Tekeze at Emba Madre	2000-2002	0.538	0.767	376.30	23.87

Table 6.2 Median changes in mean annual temperature, precipitation and streamflow in the 2050s and 2080s with respect to the control period (1971-2000) for the RCP4.5 and RCP8.5 climate scenarios of 10 CMIP5 GCMs selected for this study.

Median change with respect to 1971-2000	Awash	Baro	Genale	Tekeze
RCP4.5 2050s				
Temperature (°C)	1.9	1.8	1.8	2.0
Precipitation (%)	2.3	0.3	10.1	5.0
Streamflow (%)	3.9	-2.9	20.6	5.9
RCP4.5 2080s				
Temperature (°C)	2.3	2.2	2.2	2.5
Precipitation (%)	5.9	2.4	13.9	3.8
Streamflow (%)	6.8	-0.8	23	-4.3
RCP8.5 2050s				
Temperature (°C)	2.8	2.6	2.6	2.9
Precipitation (%)	5.0	4.4	9.4	11.5
Streamflow (%)	6.0	2.4	16.2	5.1
RCP8.5 2080s				
Temperature (°C)	4.5	4.2	3.9	4.8
Precipitation (%)	9.7	10.2	23.3	10.2
Streamflow (%)	16.9	6.4	42.2	9.1

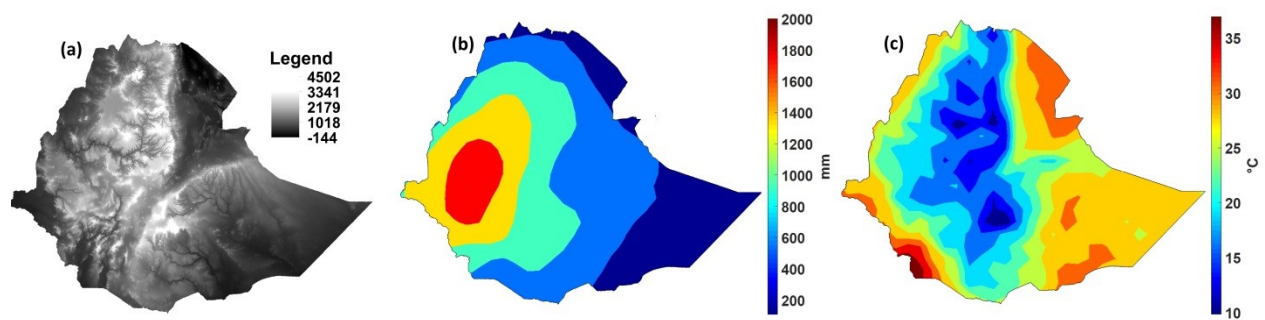


Figure 6.1 Topographic and climate variability of Ethiopia, (a) Digital Elevation Model (DEM) of Ethiopia derived from 30 arc second DEM from USGS (United States Geological Survey), (b) mean annual precipitation during 1961-1990 period derived from GPCC gridded monthly precipitation data, (c) mean annual temperature during 1961-1990 period derived from GHCN-CAMS gridded monthly average 2 m temperature data.

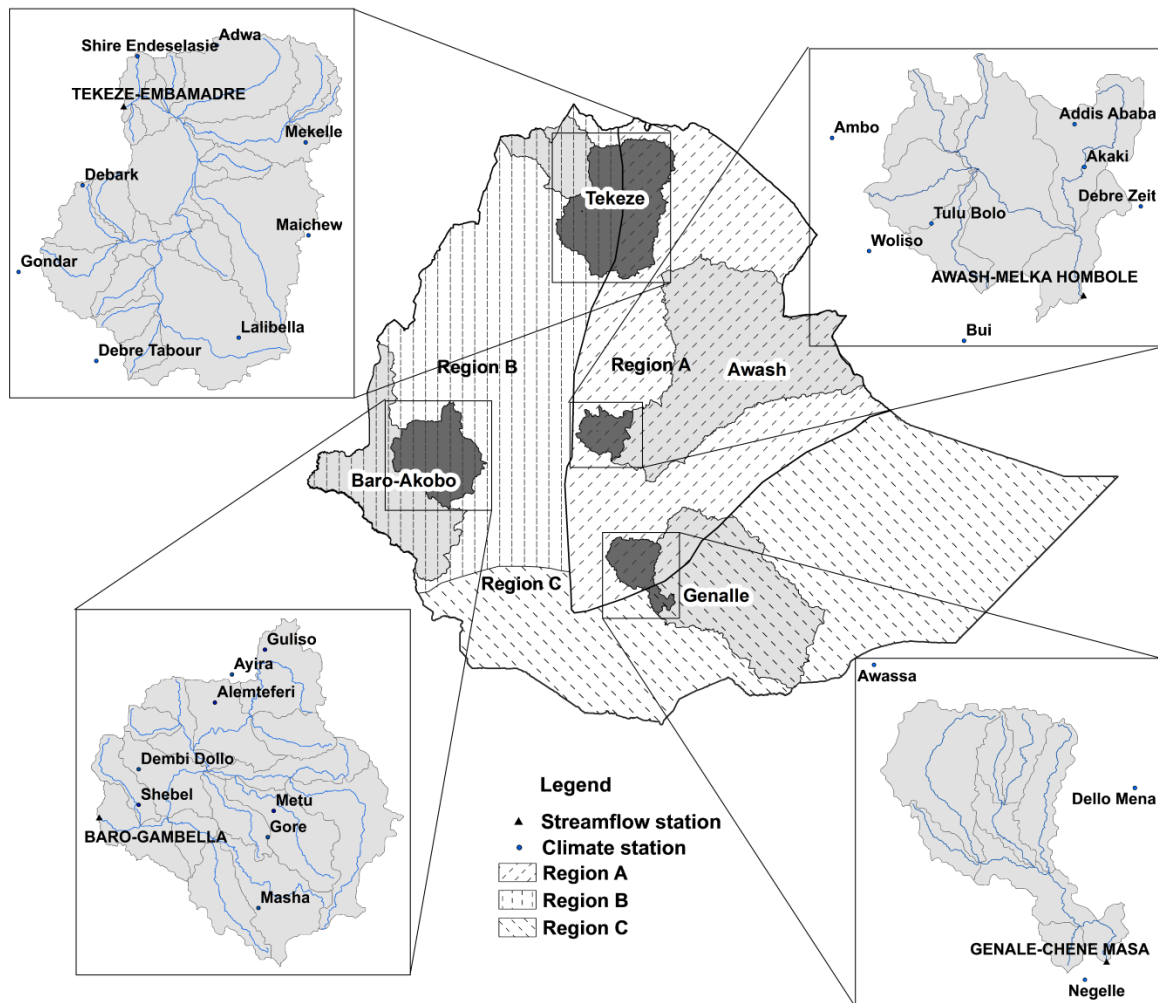


Figure 6.2 Major climatic regions (region A, B and C) in Ethiopia and the location of the four river basins analyzed in this study with respect to each climatic region. The light gray part of the river basins represents the overall drainage area within the country's political boundary while the dark gray parts represent the portion of the river basin analyzed in this study. For each of the river basin analyzed in this study, the Figure also shows the location of the streamflow and climate stations.

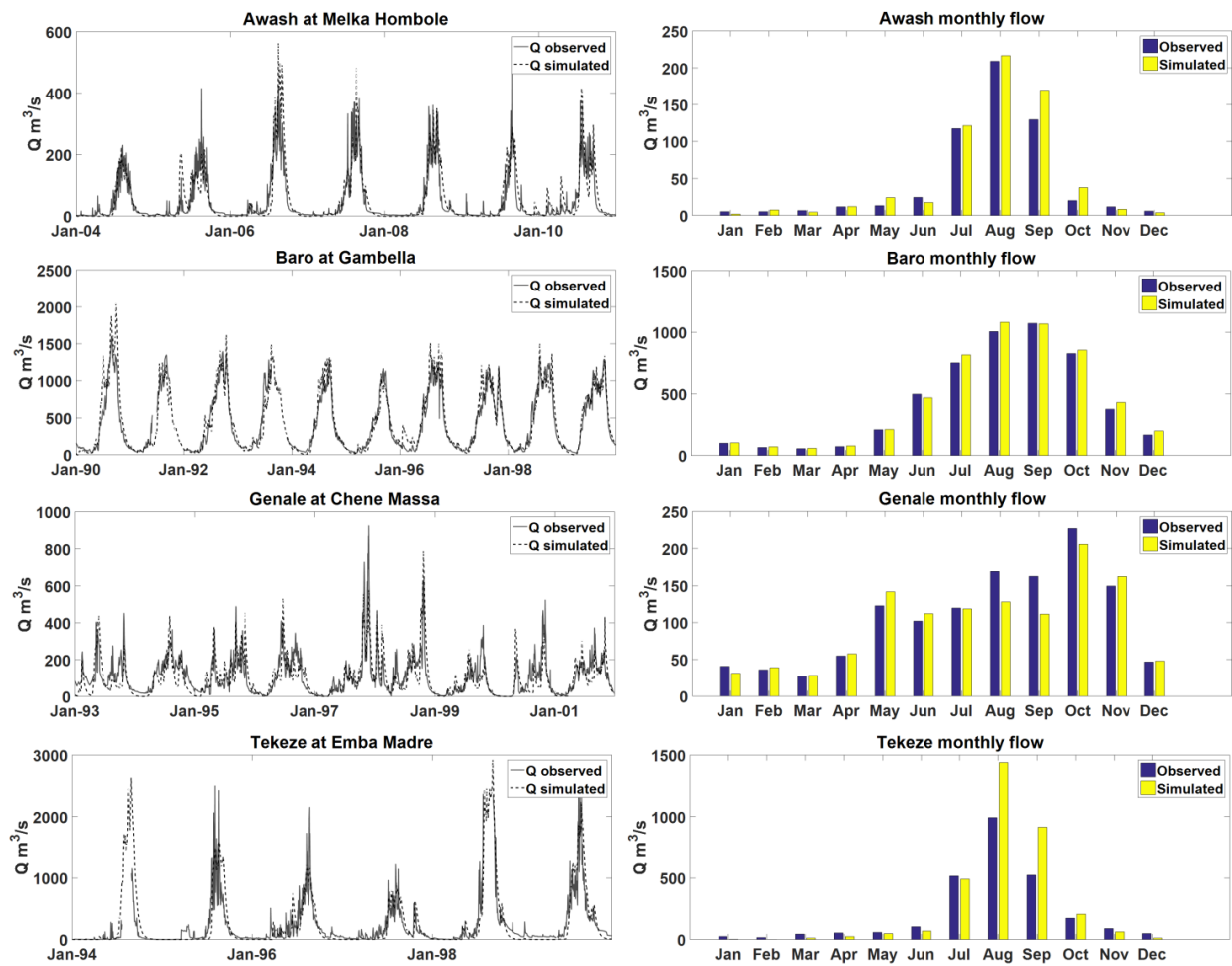


Figure 6.3 Comparison between observed and simulated daily flow for Awash, Baro, Genale and Tekeze river basins for daily flow (left) and monthly average flow (right) for calibration period.

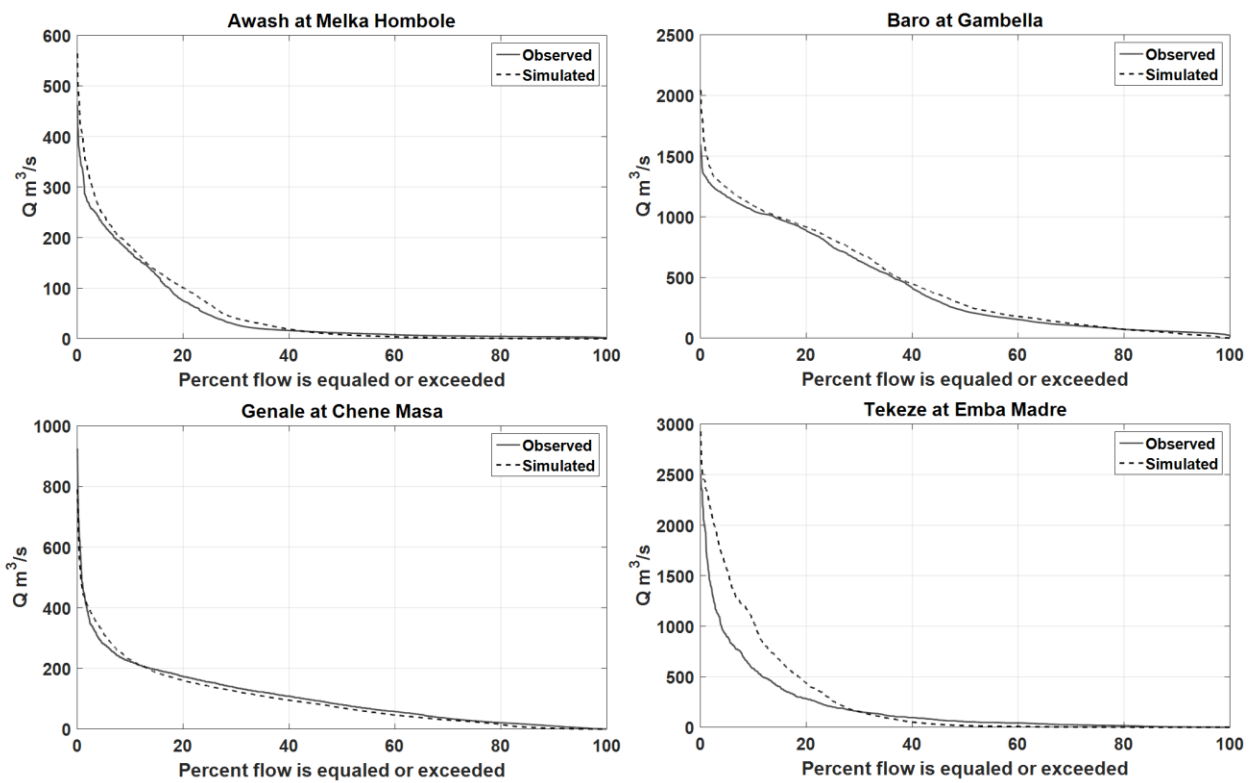


Figure 6.4 Flow duration curves of observed versus simulated streamflow of HSPF calibrated for the four selected river basins of Ethiopia for calibration period.

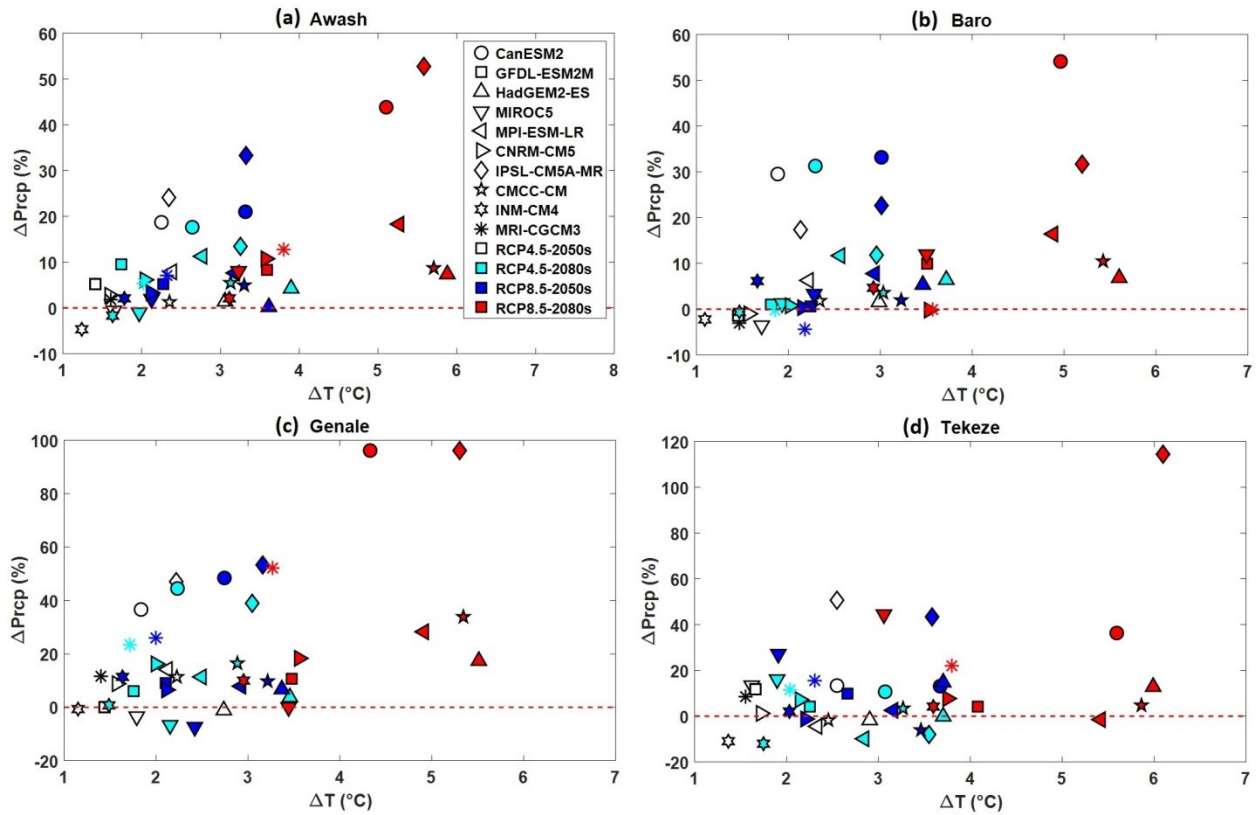


Figure 6.5 Projected changes in the mean annual air temperature versus changes in precipitation for RCP4.5 and RCP8.5 climate projections of 10 CMIP5 GCMs in the 2050s and 2080s for (a) Awash, (b) Baro, (c) Genale and (d) Tekeze River basins.

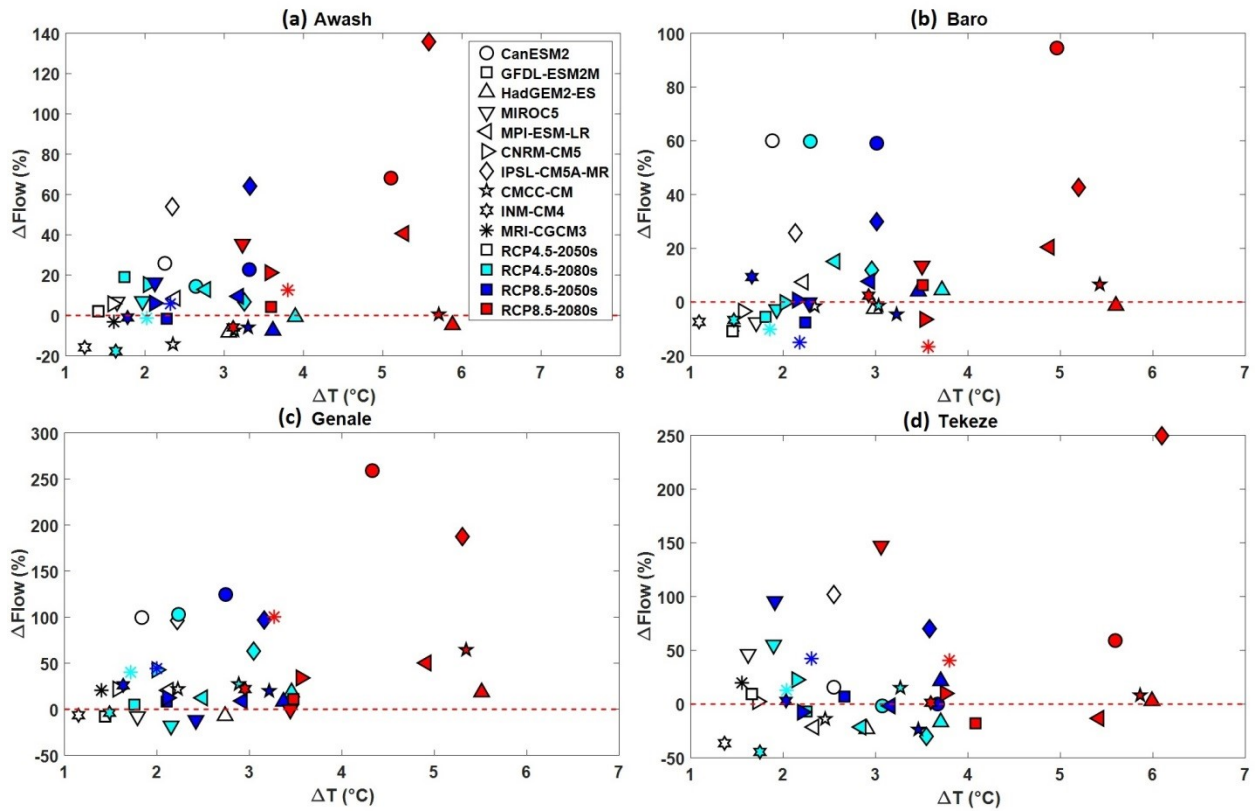


Figure 6.6 Projected changes in the mean annual air temperature versus changes in streamflow simulated (%) by HSPF forced with RCP4.5 and RCP8.5 climate projections of 10 CMIP5 GCMs in the 2050s and 2080s for (a) Awash, (b) Baro, (c) Genale and (d) Tekeze River basins.

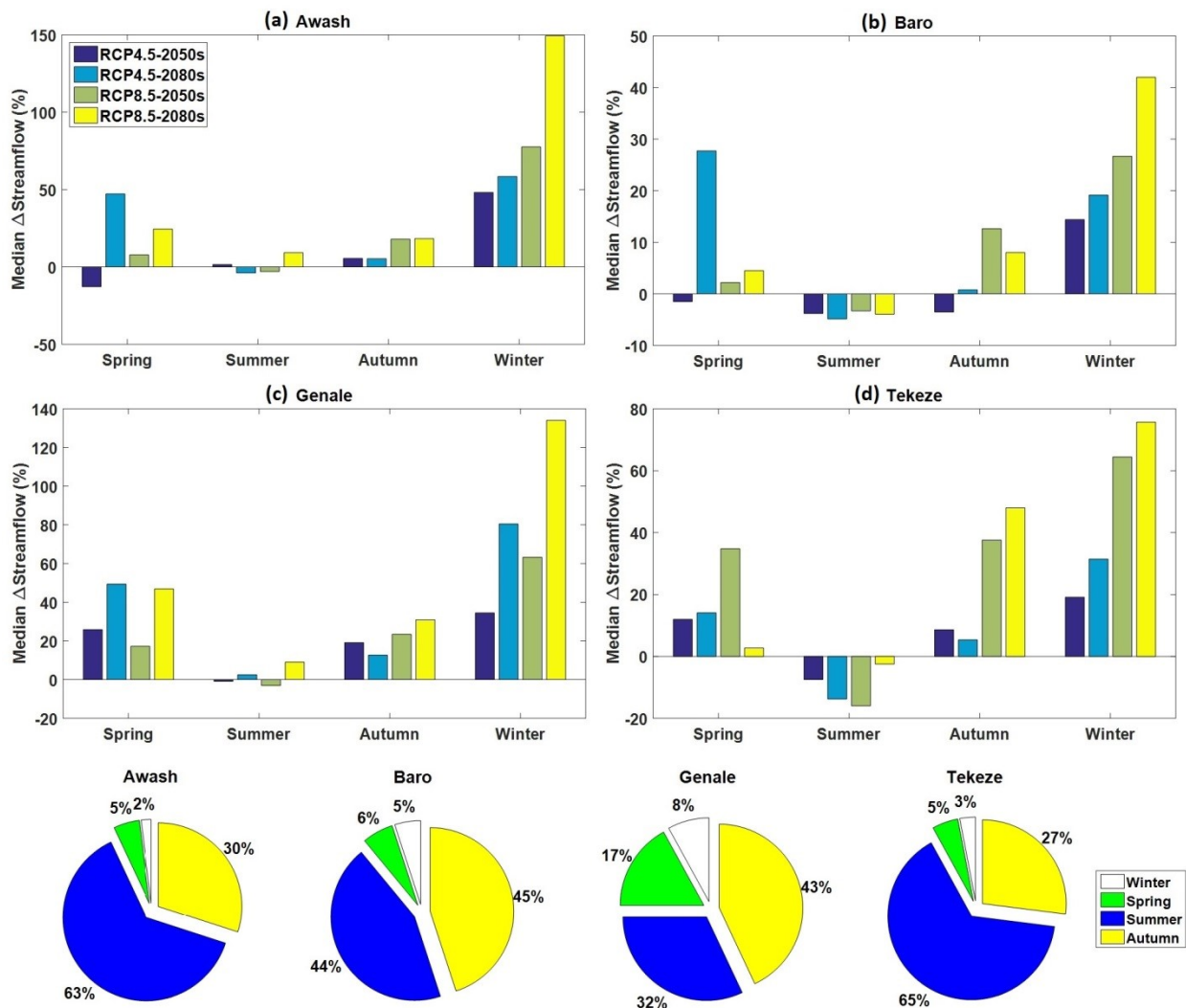


Figure 6.7 Projected changes in spring, summer, autumn and winter streamflows of (a) Awash, (b) Baro, (c) Genale and (d) Tekeze river basins, for the RCP4.5 and RCP8.5 climate projections of the mid- and late 21st century. The bottom pie charts show the seasonal streamflow contribution to mean annual runoff for the four river basins based on streamflow observations.

Chapter 7 Summary, conclusions and recommendations

7.1 Summary and Conclusions

Impacts of climate change to the global hydrologic cycle are multifaceted. For example, recent studies have shown that climate change contributed to recent increase in the frequency of occurrence of extreme hydrologic events in different parts of the world, and some regions had experienced a simultaneous increase in flood-causing extreme precipitation and severe droughts. The objective of this research project is to analyze and quantify the possible impact of climate change on hydrologic events, with emphasis on hydrologic extremes for the mid and late 21st century using climate change scenarios projected by Global Climate Models (GCMs) of IPCC (2007, 2013).

In Chapter 2, trends in Convective Available Potential Energy (CAPE), an indicator of imminent extreme precipitation events, and trends in extreme precipitation indices namely RX1day, RX5day and R20mm were analyzed for the summer (June-August) of 1979-2013 over the United States (US) and southern Canada. Monthly CAPE data were derived from the North American Land Data Assimilation System (NLDAS) while observed daily precipitation and temperature data for US and southern Canada of climate stations with minimal missing data was derived from the Global Historical Climatology Network daily data (GHCN-Daily).

Statistically significant increasing trends of large magnitude of CAPE have been detected for low laying areas near the Gulf and Atlantic coasts of US for the summer 1979-2013. In addition, marginal increasing trends of CAPE were detected for much of the northern Atlantic coast of US, the Great Lakes region, parts of southern Ontario, Québec and some parts the Canadian prairies

while much of the US Great Plains and areas west of the Rockies had experienced decreasing trends in CAPE. Increasing trends for extreme precipitation indices, up to 14 mm/decade for single storm events (RX1day) and up to 24 mm/decade for multiple storm events (RX5day), were also detected for much of eastern US and some parts of the Canadian prairies which mostly complements the increasing trends detected from the summer CAPE data. However, statistically significant trends were only detected for about 5.2% (RX1day), 6.7% (RX5day) and 2.7% (R20mm) of the GHCN stations in US and southern Canada analyzed in this study. In almost all parts of the US and southern Canada, increasing trends of up to 1.35 °C/decade were detected in the average summer temperature with about 35% of detected increasing trends for GHCN stations being statistically significant at $p < 0.05$. Similarly, increasing trends in the surface specific humidity were also detected for almost all parts of southern Canada and most parts of the Atlantic and Gulf coasts of eastern US. Given that surface temperatures influence the latent heat release which drives the upward motion of moist air in convective precipitation (Lenderink and van Meijgaard, 2008) and also the strong dependency of CAPE on surface specific humidity (Riemann-Campe et al, 2009), increasing trends in surface temperature and specific humidity could be responsible for much of the detected increase in extreme precipitation and CAPE over eastern US and parts of southern Canada dominated by convective summer precipitation. If the observed increasing trends in these climate variables will continue in the future according to climate projections of GCMs of IPCC, we will expect eastern US and parts of southern Canada such as southern Alberta to experience even more intensive extreme precipitation events over the 21st century.

In Chapter 3, the potential impact of climate change on extreme precipitation events in three sub-basins of the South Saskatchewan River Basin (SSRB) of southern Alberta, namely Oldman, Bow and Red Deer river basins (ORB, BRB and RRB), was investigated for the May-June-July-August (MJJA) rainy season using six extreme precipitation indices (R20mm, RX1day, RX5day, R95p, R99p, and P30yr). Each of these precipitation indices was derived from climate projections from four CMIP3 GCMs dynamically downscaled to 9 km resolution using the regional climate model called MM5. With reference to the 1971-2000 base period, the results show that R20mm, R95p and R99p precipitation indices are projected to increase in southern Alberta in 2050s (2041-2070) and 2080s (2071-2100) with higher projected changes in the upstream portions of ORB, BRB and RRB, but only marginal changes are projected for the downstream areas. Concurrently, RX1day and RX5day precipitation indices which represent the magnitude of single extreme precipitation events (RX1day) or the maximum cumulative precipitation over five consecutive days (RX5day) are also projected to increase in the 2050s and 2080s. As a result, the return period of daily precipitation intensity of 30-year return period (P30yr) for the base period is projected to decrease to about 15 years in the 2050s and 2080s.

Between the three southern Alberta river basins considered in this study, ORB was projected to experience the largest increase in precipitation indices representing the intensity of extremely heavy rainfall events (P30yr, RX1day and RX5day) while the projected changes in these precipitation indices for BRB and RRB was comparable. On the whole, the overall projected increase in extreme precipitation indices of ORB, BRB and RRB for the mid and the late 21st century is attributed to the monotonic increase in projected air temperature, which means a consistent increase in precipitable water is expected over the three sub-basins of SSRB, which

will potentially increase the magnitude and frequency of extreme precipitation events represented by the P30yr, RX1day and RX5day climate indices.

In Chapter 4, a Regional Flood Frequency Analysis (RFFA) model based on the Support Vector Regression (SVR) was proposed and applied to estimate regional flood quantiles for a group of 26 and 23 catchments located in southeastern British Columbia (BC) and southern Ontario (ON), Canada, respectively. The SVR-RFFA model estimated flood quantiles for any given station assumed to be ungauged within each study area using 13 sets of physiographic and climatic predictors. For both study areas, the goodness-of-fit statistics, Ef (Nash-Sutcliffe coefficient) and R^2 , of the RFFA model are about 0.7 on the average for most of the 13 sets of predictors tested, which shows satisfactory performance in the SVR-RFFA model. The SVR-RFFA model was also compared with an artificial neural network (ANN) based RFFA model which has been used in many past RFFA studies. The results show that the SVR-RFFA model has consistently performed better than an ANN-RFFA model based on the 13 sets of physiographic and climatic predictors tested for the two study sites. In addition, the coefficient of variation (CV) of flood quantiles estimated by the SVR-RFFA model was considerably lower than the CV of flood quantiles estimated by the ANN-RFFA model which suggests that SVR-RFFA model is capable of estimating the flood quantiles of a given site more consistently than the ANN-RFFA model. Furthermore, it seems that the SVR-RFFA model has better generalization ability (less prone to the pitfall of over-fitting) than the ANN-RFFA model particularly for study areas with limited amount of training data such as the two sites analyzed in this study.

After validating the performance of the SVR-RFFA model with historical data, it was used to predict future flood quantiles for the two study sites based on statistically downscaled RCP4.5 and RCP8.5 climate projections of five CMIP5 GCMs of IPCC (2013). The projected increase in precipitation of T-year return period by 22.6% (BC) and 6.2% (ON) and the mean annual precipitation by 9.2% (BC) and 7.8% (ON) respectively imply that flood quantiles over the two study sites are projected to increase in the mid and late 21st century. Overall, for the RCP4.5 and RCP8.5 climate projections, the SVR-RFFA model projected an average increase in T-year return period flood quantiles of about 7% (BC) and 30% (ON) for the 2050s and 8% (BC) and 28% (ON) for the 2080s. However, such a degree of projected increase might be conservative because predictor variables used in the SVR-RFFA model don't account for the effect of higher temperature which all GCMs unanimously project to increase in the 21st century, which can partly offset the contribution of increased annual rainfall to larger flood quantiles because of more evapotranspiration. In summary, this study showed that SVR-RFFA models can credibly estimate regional flood quantiles (Q10, Q25, Q50 and Q100) for two regional study sites with “homogeneous” river basins representing different climatic regions of Canada. In addition, SVR-RFFA models could also be used to project future flood quantiles under the potential impact of climate change.

After analyzing the impact of climate change on future extreme precipitation and flood events in Chapter 2, 3, and 4, Chapter 5 analyzes the potential impact of climate change on hydrologic droughts which represent extremes that are opposite of flood events. In this Chapter, the Palmer Drought Severity Index (PDSI) was used to analyze the impact of climate change and the combined impact of El Niño and climate change on the frequency, severity and spatial

distribution of drought events in four sub-regions of sub-Saharan Africa (SSAF), namely GHA (Greater Horn of Africa), CA (Central Africa), SA (South Africa) and WA (West Africa). The analysis was done for the base period (1971-2000), 2050s and 2080s using a combination of observational and reanalysis datasets adjusted for the impact of RCP4.5 and RCP8.5 climate projections of five CMIP5 GCMs.

By considering only the impact of climate change, the results show an increase in drying of SSAF in mid to late 21st century. Compared to the base period, the percentage of area under the slightly wet to near normal PDSI category is projected to decrease by 7% (RCP4.5) and 14% (RCP8.5) over the whole of SSAF. On the other hand, areas of SSAF that fall under the incipient dry spell to moderate drought categories of PDSI during the base period are projected to increase by about 12% (RCP4.5) and 21% (RCP8.5) in the mid to late 21st century, which suggests that SSAF and particularly its four corners are projected to experience drier climate in the future. In addition, the frequency of short (lasting between six months and a year) and long (extending over a year) droughts is projected to marginally increase by about 4-7% and 2-10% under the RCP4.5 and RCP8.5 climate projections in the mid to late 21st century, respectively. However, in terms of drought durations, minimal change is projected for the average duration of short droughts while long droughts in most parts of the SSAF are projected to be shorter by 1- 6% in the mid to late 21st century compared to the base period. The marginal decrease in the duration of long droughts could be attributed to the projected increase in the magnitude and frequency of future extreme precipitation events. These results also suggest that a warmer climate could increase the frequency of future mild to extreme drought events, but it could also increase the intensity and

frequency of extreme precipitation events, which could shorten the duration of future long droughts of the SSAF.

Similarly, parts of GHA falling under the incipient dry spell to moderate drought categories of PDSI are projected to increase significantly in 2050s and 2080s, if the frequency of future El Niño events is projected to increase than if the frequency of El Niño events is assumed to remain more or less unchanged. A projected increase in the frequency of future El Niño events is also expected to expand the drought prone regions in SA and WA but it is projected to have limited impact on the future droughts in CA. These results show that an increase in the frequency of climate anomalies such as El Niño could further exacerbate the impact of climate change on future drought events of the SSAF, particularly for the GHA region. In summary, the results from this study suggest that SSAF is projected to experience increased drying during the mid to late 21st century. The increase in the frequency of climate anomalies such as El Niño which is likely if the atmosphere gets warmer in the 2050s and 2080s could further exacerbate the occurrence of extreme drought events particularly for GHA, SA and WA.

Chapter 6 focuses on the impact of climate change on water resources of major river basins in Ethiopia, which is located in the GHA region of SSAF. In this study the streamflow of four study areas: Awash, Baro, Genale and Tekeze river basins, was simulated using the Hydrologic Simulation Program-FORTRAN (HSPF) hydrologic model. The calibrated and validated HSPF model was forced with daily climate data from 10 CMIP5 GCMs for the 1971-2000 control period and the RCP4.5 and RCP8.5 climate projections of 2050s and 2080s. The ensemble median of GCM projections suggest that the temperature in the four study areas is projected to

increase by about 2.3 °C (3.3 °C) in 2050s (2080s) whereas the mean annual precipitation is projected to increase by about 6% (9%) in 2050s (2080s). This has led to about 3% (6%) increase in the projected annual streamflow in Awash, Baro and Tekeze rivers whereas Genale river is projected to have about 18% (33%) increase in annual streamflow due to the relatively higher projected increase in precipitation in this region during the 2050s (2080s). Despite the increase in annual streamflow, the mean summer streamflow, which accounts for about 32-65% of the annual runoff, is projected to decrease for most river basins. However, such a decrease in summer streamflow was compensated with a significant increase in the autumn streamflow which accounts for 27-45% of the annual runoff. Overall, the projected changes in seasonal precipitation or streamflow of these river basins could affect communities in different parts of Ethiopia that mainly grow specific crops in a rainy season.

Overall, findings presented from Chapter 2 to Chapter 6 shed some light on the potential impact of climate change to hydrologic extremes that can potentially lead to more severe flooding or drought events. While the study shows that climate change could lead to the simultaneous increase in the frequency of intense storm events and severe droughts in some regions, the impact of one of the hydrologic extremes is usually more significant than the other in a given region. For instance this study shows that SSAF, due to its relatively dry climate and a lack of sustainable food security, is projected to be vulnerable to more frequent drought events in the mid and late 21st century, although some increase in future extreme precipitation events is also projected in this region. On the other hand, this study also shows that for countries like Canada which have well developed agricultural infrastructure, increase in the frequency of future

extreme precipitation events could result in more frequent and devastating floods leading to the loss of billions of dollars in insurance and damages to municipal infrastructures.

However, even if changes in precipitation and temperature during the mid and late 21st century will predominantly affect the hydrology of the areas analyzed in this study, significant changes in other parameters that could affect the dominant hydrologic process, e.g. vegetation cover and landuse, could also bring about changes in the hydrology of a given region, e.g., Kerkhoven and Gan (2013). Therefore, some of the results presented could change if there are significant changes in landuse and vegetation cover that were otherwise assumed as time invariant in this study.

7.2 Recommendations

To mitigate the potential impact from possible increase in future extreme precipitation events affecting different parts of Canada, current hydrologic design standards and practices have to be revised. Some of the design standards that should be revised to take into account the potential impact of climate change include:

1. Update intensity-duration-frequency (IDF) curves used by Canadian municipalities in the design of urban infrastructure and drainage systems. Since most of the current municipal IDF curves were derived from historical precipitation records collected in the 20th century, they mainly reflect the climate of the 20th century. An update of IDF curves partly based on climate projections of GCMs for the 21st century should be considered so that municipal drainage infrastructure will be adequately upgraded to cope with potential precipitation extremes of the 21st century. The city of Edmonton has already taken the initiative to update its IDF curves (Kuo et.al 2015).

2. Current flood frequency analysis is primarily based on the assumption that climate is stationary. With ever changing climate, stationarity should no longer serve as the central assumption in the design of municipal hydraulic structures (Milly et al, 2008). Therefore, new flood frequency estimation guidelines based on non-stationary frequency analysis approaches should be considered to supplement/replace classic guidelines such as the USGS's Bulletin 17B (1982).
3. To enhance the exchange of new knowledge on hydrologic extremes, collaborative platforms are necessary between different scientific centers. A good example of such platforms is Floodnet which is the latest collaborative initiative between various scientific research centers of Canadian universities and government institutes to enhance the flood forecasting and management capacity in Canada.

To mitigate the increase in the frequency of drought events in SSAF resulting from climate change, countries in SSAF should implement various structural and institutional adaptation strategies. Some of these include

1. A shift from traditional farming practice, still widespread in many parts of SSAF, to modern mechanized farming; to invest in building irrigation infrastructure and adopting new technologies that use water more efficiently.
2. Breed livestock genetically better adapted to drought prone climate, build infrastructure to improve livestock health, promote interactions between government organization and farmers.
3. Promote land fertility restoration using natural compost; zero-tillage farming for rebuilding of critical soil organic matters; rehabilitation such as land resting and planting of native plants; rainfall harvesting; drought-resistant crop varieties; reforestation etc.

4. Implement early warning technologies to detect conditions ominous of drought events with lead time extending from six months to a year. Teleconnection models relating sea surface temperature with seasonal precipitation have been shown to have reasonable skill in predicting seasonal precipitation with up to one season lead time so that immediate mitigation measures can be taken if drought is probable in the next season.
5. Increase collaboration between countries and regional institutions to enhance the development of new technologies to mitigate the impact of drought in different climatic regions of SSAF

7.3 References

- Bulletin 17B of the Hydrology Subcommittee, 1982. Guidelines for determining Flood Flow Frequency. US Department of the Interior, Geological Survey.
- IPCC, 2007: Climate Change 2007: The Physical Science Basis. Contribution of Working Group I to the Fourth Assessment Report of the Intergovernmental Panel on Climate Change (Solomon, S., D. Qin, M. Manning, Z. Chen, M. Marquis, K.B. Averyt, M. Tignor and H.L. Miller (eds.)). Cambridge University Press, Cambridge, United Kingdom and New York, NY, USA, 996 pp.
- IPCC, 2013: Summary for Policymakers. In: Climate Change 2013: The Physical Science Basis. Contribution of Working Group I to the Fifth Assessment Report of the Intergovernmental Panel on Climate Change [Stocker, T.F., D. Qin, G.-K. Plattner, M. Tignor, S.K. Allen, J. Boschung, A. Nauels, Y. Xia, V. Bex and P.M. Midgley (eds.)]. Cambridge University Press, Cambridge, United Kingdom and New York, NY, USA.
- Kerkhoven, E., and T.Y. Gan, 2013, Differences in the Potential Hydrologic Impact of Climate Change to the Athabasca and Fraser River Basins with & without Considering the Effects of Shifts in Vegetation patterns Caused by Climate Change, *Journal of Hydrometeorology*, 14(3), 963-976. DOI: 10.1175/JHM-D-12-011.1.
- Kuo, C.C., Gan, T.Y., Gizaw, M.S. 2015. Potential impact of climate change on intensity duration frequency curves of central Alberta. *J of Climate Change*. DOI 10.1007/s10584-015-1347-9.
- Lenderink, G., and van Meijgaard, E. 2008. Increase in hourly precipitation extremes beyond expectations from temperature changes. *Nature Geoscience, Letters*, 1, 511-514, doi:10.1038/ngeo262

Milly, P.C.D, Betancourt, J., Falkenmark, M., Hirsch, R.H., Kundzewicz, Z.W., Lattenmaier, D.P., and Stouffer, R.J. 2008. Stationarity is Dead: Whither Water Management? *Science*, 319: 573-574.

Riemann-Campe, K., Fraedrich, K., and Lunkeit, F. 2009. Global climatology of Convective Available Potential Energy (CAPE) and Convective Inhibition (CIN) in ERA-40 reanalysis. *Atmos. Res* 93, 534-545, doi:10.1016/j.atmosres.2008.09.037

Bibliography

- Adem, A.A., Tilahun, S.A., Ayana, E.K., Worklul, A.W., Assefa, T.T., Dessu, S.B., and Melesse, A.M. 2016. Climate change impact on streamflow in the Upper Gilgel Abay Catchment, Blue Nile basin, Ethiopia. In: Melesse, A.M and Abteu, W. (ed) Landscape dynamics, soils and hydrological processes in varied climate. Springer International Publishing, Switzerland, Chapter 29: 645-673. doi 10.1007/978-3-319-18787-7_29
- Africa Watch, 1991: Evil days: 30 years of war and famine in Ethiopia. Africa Watch Rep., 381 pp. <https://www.hrw.org/sites/default/files/reports/Ethiopia919.pdf>
- Aich, V., Liersch, S., Vetter, T., Huang, S., Tecklenburg, J., Hoffmann, P., Koch, H., Fournet, S., Krysanova, V., Müller, E. N., and Hattermann, F. F. 2014. Comparing impacts of climate change on streamflow in four large African river basins. *Hydrol. Earth Syst. Sci.*, 18, 1305–1321. doi:10.5194/hess-18-1305-2014.
- Akinremi, O. O., McGinn, S. M. and Barr, A. G. 1996: Evaluation of the Palmer Drought Index on the Canadian prairies. *J. Climate*, 9: 897–905.
- Akinremi, O.O, McGinn, M.S., Cutforth, H.W. 1998. Precipitation trends in Canadian prairies. *J Climate*, 12: 2996-3003
- Alexander, L. V. and co-authors, 2006. Global observed changes in daily climate extremes of temperature and precipitation. *J Geophys. Res.*, 111: D05109, doi:10.1029/2005JD006290.
- Allen, M.R. and Ingram, W.J. 2002. Constraints on future changes in climate and the hydrologic cycle. *Nature* vol. 419, Nature publishing group.
- Allen, R. G., Pereira, L.S., Raes, D., and Smith, M. 1998: Crop evapotranspiration (guidelines for computing crop water requirements). Food and Agriculture Organization of the United Nations Irrigation and Drainage Paper 56, 328 pp.

- Almeida, I.K., Almeida, A.K., Anache, J.A.A, Steffen, J.L, Alves Sobrinho, T. 2014. Estimation of time of concentration in overland flow in watersheds: a review. São Paulo, UNESP, *Geociências*, 33, n. 4: 661-671, 2014 662
- Alpert, P., Ben-Gai, T., Baharad, A., Benjamini Y., Yekutieli, D., Colancio, M. Diodato, L., Ramis, C., Homar, V., Romero, R., Michaelides, S., Manes, A. 2002. The paradoxical increase of Mediterranean extreme daily rainfall in spite of decrease in total values. *J Geophys. Res – Letter*, 29: 31-1 to 31-4, doi: 10.1029/2001GL013554.
- Awulachew, S. B., Yilma, A. D., Loulseged, M. Loiskandl, W., Ayana, M., Alamirew, T. 2007. *Water Resources and Irrigation Development in Ethiopia*. Colombo, Sri Lanka: International Water Management Institute. 78p. (Working Paper 123)
- Aziz, K., Rahman, A., Fang, G., Shrestha, S. 2013. Application of artificial neural networks in regional flood frequency analysis: a case study for Australia. *Stoch Environ Res Risk Assess*, 28: 541-554. doi 10.1007/s00477-013-0771-5
- Bader, D.C., C. Covey, W.J. Gutowski Jr., I.M. Held, K.E. Kunkel, R.L. Miller, R.T. Tokmakian and M.H. Zhang, 2008, *CCSP: Climate Models: An Assessment of Strengths and Limitations*. A Report by the U.S. Climate Change Science Program and the Subcommittee on Global Change Research. Department of Energy, Office of Biological and Environmental Research, Washington, D.C., USA, 124 pp.
- Beck, C., Grieser, J. and Rudolf, B. 2004. A New Monthly Precipitation Climatology for the Global Land Areas for the Period 1951 to 2000 (published in *Climate Status Report 2004*, pp. 181 - 190, German Weather Service, Offenbach, Germany)

- Berg, P., Moseley, C., and Haerter, J. O. 2013. Strong increase in convective precipitation in response to higher temperatures. *Nature Geoscience, Letters*, 6, 181-185. doi: 10.1038/NGEO1731
- Beyene, T., Lettenmaier, D.P., Kabat, P. 2010. Hydrologic impacts of climate change on the Nile River Basin: implications of the 2007 IPCC scenarios. *J of Climate Change*, 100: 433-461. doi 10.1007/s10584-009-9693-0
- Bhagwat, P.P. and Maity, R. 2012. Multistep-Ahead River Flow Prediction using LS-SVR at Daily Scale. *Scientific Research, J of Water Resource and Protection*, 4: 528-539.
- Bhalme, H. N., and D. A. Mooley, 1979: On the performance of modified Palmer index. *Proc. Int. Symp. on Hydrological Aspect of Droughts*, vol. I, New Delhi, India, UNESCO, 373–383.
- Bicknell, B.R., J.C. Imhoff, J.L. Kittle, Jr., T.H. Jobs, and A.S. Donigian, Jr. 2001. *Hydrological Simulation Program–FORTRAN (HSPF), User’s Manual for Version 12.0*. USEPA, Athens, Georgia.
- Brabanter, K.De., Karsmakers, P., Ojeda, F., Alzate, C., Brabanter, J.De, Pelckmans, B. De M., Vandewalle, J., Suykens, J.A.K. 2011. *LS-SVMlab Toolbox User’s Guide version 1.8*. Department of Electrical Engineering, Katholieke Universiteit Leuven. <http://www.esat.kuleuven.be/sista/lssvmlab/> Last accessed July-8-2015
- Bray, M. and Han, D. 2004. Identification of support vector machines for runoff modelling. *J of Hydroinformatics*, 06.4: 265-280.
- Brooks, H. E., Anderson, A. R., Riemann, K., Ebberts, I., and Flachs, H. 2007. Climatological aspects of convective parameters from the NCAR/NCEP reanalysis. *Atmos. Res.* 83, 294-305, doi:10.1016/j.atmosres.2005.08.005

- Brooks, H. E., Lee, J. W. and Craven, J. P. 2003. The spatial distribution of severe thunderstorm and tornado environments from global reanalysis data. *Atmos. Res.* 67-68, 73-94, doi:10.1016/S0169-8095(03)00045-0.
- Brooks, H.E., 2013. Severe thunderstorms and climate change. *J of Atmospheric Research*, 123: 123-138, doi:10.1016/j.atmosres.2012.04.002.
- Bulletin 17B of the Hydrology Subcommittee, 1982. Guidelines for determining Flood Flow Frequency. US Department of the Interior, Geological Survey.
- Bürger, G., Sobie, S.R., Cannon, A.J., Werner, A.T., and Murdock, T.Q. 2013. Downscaling extremes - an intercomparison of multiple methods for future climate. *Journal of Climate*, 26: 3429-3449. doi: 10.1175/JCLI-D-12-00249.1
- Burnash, R.J.C., Ferral, R.L., McGuire, R.A., 1973. A generalized streamflow simulation system-conceptual modeling for digital computers. U.S. Department of Commerce, National Weather Service and State of California, Department of Water Resources.
- Bush, A. 2006. Extratropical Influences on the El Niño–Southern Oscillation through the Late Quaternary. *AMS, J of Climate*, 20, 788-800. DOI: 10.1175/JCLI4048.1
- Cai, W., Borlace, S., Lengaigne, M., Rensch, P., Collins, M., Vecchi, G., Timmermann, A., Santoso, A., McPhaden, M.J., Wu, L., England, M.H., Wang, G., Guilyardi, E., and Jin, F-F. 2014. Increasing frequency of extreme El Niño events due to greenhouse warming. *Nature climate change, Letters*, 4: 111-116. DOI: 10.1038/NCLIMATE2100
- Cai, W., Wang, G., Santoso, A., McPhaden, M. J., Wu, L., Jin, F-F., Timmermann, A., Collins, M., Vecchi, G., Lengaigne, M., England, M.H., Dommenges, D., Takahashi, K., Guilyardi, E. 2014. Increasing frequency of extreme La Niña events under greenhouse warming. *Nature climate change, Letters*, 5: 132-137. DOI: 10.1038/NCLIMATE2492

- Charney, J.G. 1975. Dynamics of desert and drought in the Sahel. *Quart. J. R. Met. SOC.* 101: 193-202.
- Chen, C.T., Knutson, T. 2008. On the verification and comparison of extreme rainfall indices from climate models. *Notes and Correspondence, AMS*, doi: 10.1175/2007JCLI1494.1.
- Chen, J., Jönsson, P., Tamura, M., Gu, Z., Matsushita, B., Eklundh, L. 2004. A simple method for reconstructing a high-quality NDVI time-series data set based on the Savitzky–Golay filter, *Rem. Sens. Env.*, Vol. 91 (3–4), 332-344, doi.org/10.1016/j.rse.2004.03.014
- Chitralkha, S.B and Shah, S.L. 2010. Support vector regression for soft sensor design of nonlinear processes. 18th Mediterranean Conference on Control & Automation Congress Palace Hotel, Marrakech, Morocco, June 23-25, 2010.
- Chow, V.T. Maidment, D.R. and Mays, L.W. 1988. *Applied Hydrology*, McGraw-Hill, New York, NY.
- Christensen, J.H., B. Hewitson, A. Busuioc, A. Chen, X. Gao, I. Held, R. Jones, R.K. Kolli, W.-T. Kwon, R. Laprise, V. Magaña Rueda, L. Mearns, C.G. Menéndez, J. Räisänen, A. Rinke, A. Sarr and P. Whetton, 2007: Regional Climate Projections. In: *Climate Change 2007: The Physical Science Basis. Contribution of Working Group I to the Fourth Assessment Report of the Intergovernmental Panel on Climate Change* [Solomon, S., D. Qin, M. Manning, Z. Chen, M. Marquis, K.B. Averyt, M. Tignor and H.L. Miller (eds.)]. Cambridge University Press, Cambridge, United Kingdom and New York, NY, USA.
- Cloke, H.L., and Pappenberger, F., 2009. Ensemble flood forecasting: a review. *J Hydrology*, 375: 613-626, doi:10.1016/j.jhydrol.2009.06.005.
- Cubasch, U., D. Wuebbles, D. Chen, M.C. Facchini, D. Frame, N. Mahowald, and J.-G. Winther, 2013: Introduction. In: *Climate Change 2013: The Physical Science Basis. Contribution of*

Working Group I to the Fifth Assessment Report of the Intergovernmental Panel on Climate Change [Stocker, T.F., D. Qin, G.-K. Plattner, M. Tignor, S.K. Allen, J. Boschung, A. Nauels, Y. Xia, V. Bex and P.M. Midgley (eds.)]. Cambridge University Press, Cambridge, United Kingdom and New York, NY, USA.

Dai, A., Wang, J., Thorne, P., Parker, D., Haimberger, L., and Wang, X., 2011, A New Approach to Homogenize Daily Radiosonde Humidity Data, *J Climate*, 965-991, DOI: 10.1175/2010JCLI3816.1

Dai, A. 2011a, Characteristics and trends in various forms of the Palmer Drought Severity Index during 1900–2008, *J. Geophys. Res.*, 116: D12115, doi:10.1029/2010JD015541.

Dai, A., 2011b, Drought under global warming: a review, *WIREs Clim Change*, 2: 45-65, John Wiley and Son, DOI: 10.1002/wcc.81

Dai, A., Del Genio, A.D., Fung, I.Y., 1997. Clouds, precipitation and temperature range. Scientific correspondence, *Nature* 386: 665-666.

Dai, A., Qian, T., Trenberth, K.E., and Milliman, J.D. 2009. Changes in continental freshwater discharge from 1948-2004. *AMS, J of Climate*, 22: 2773-2792. doi: 10.1175/2008JCLI2592.1

Dai, A. 2013. Increasing drought under global warming in observations and models. *Nature Climate Change*, 3, 52-58. doi: 10.1038/NCLIMATE1633

Di Baldassarre, G. and Uhlenbrook, S. 2012. Is the current flood of data enough? A treatise on research needs for the improvement of flood modelling, *Hydrol. Process.*, 26, 153–158.

Di Baldassarre, G., Montanari, A., Lins, H., Koutsoyiannis, D., Brandimarte, L., and Blöschl, G. 2010. Flood fatalities in Africa: from diagnosis to mitigation, *Geophys. Res. Lett.*, 37, L22402, doi:10.1029/2010GL045467.

- Dai, A., Trenberth, K.E., 1999. Effects of Clouds, Soil Moisture, Precipitation, and Water Vapor on Diurnal Temperature Range. *J Climate*, 12: 2451-2473.
- DeMott, C. A. and Randall, D. A. 2004. Observed variations of tropical convective available potential energy. *J Geophys. Res.*, 109, D02102, doi:10.1029/2003JD003784.
- Dibike, Y.B., Velickov, S., Solomatine, D., & Abbott, M.B. 2001. Model Induction with Support Vector Machines: Introduction and Applications. *J of Computing in Civil Engineering*, 15(3): 208-216.
- Dile, Y.T., Berndtsson, R., Setegn, S.G. 2013. Hydrological Response to Climate Change for Gilgel Abay River, in the Lake Tana Basin - Upper Blue Nile Basin of Ethiopia. *PLoS ONE* 8(10): e79296. doi:10.1371/journal.pone.0079296
- Diro, G.T., Grimes, D.I.F, and Black, E. 2011. Large scale features affecting Ethiopian rainfall. In: Williams, J.R., and Kniveton, D.R. ed. *African Climate and Climate Change, physical, social and political perspectives*. Springer, pp 13-50.
- Dosio, A., Panitz, H.J., Schubert-Frisius, M., Luthi, D. 2015. Dynamical downscaling of CMIP5 global circulation models over CORDEX-Africa with COSMO-CLM: evaluation over the present climate and analysis of the added value. *J of Climate Dynamics*, 44: 2637-2661, doi 10.1007/s00382-014-2262-x
- Doswell III, C. A., and Evans, J. S. 2003. Proximity sounding analysis for derechos and supercells: and assessment of similarities and differences. *Atmos. Res* 67-68, 117-113, doi:10.1016/S0169-8095(03)00047-4

- Drucker, H., Burges, C., Kaufman, L., Smola, A., & Vapnik, V. 1997. Support Vector Regression Machines. In *Advances in Neural Information Processing Systems- Proceedings of the 1996 Conference*, volume 9, pp. 155–161. MIT Press, Cambridge, MA.
- Dudhia J, Gill D, Manning K, Wang W, Bruyere C., 2004. PSU/NCAR Mesoscale Modelling System Tutorial Class Notes and Users' Guide (MM5 Modelling System). NCAR, Boulder, CO.
- Dudhia, J., Gill, D., Manning, K., Wang, W., Bruyere, C., Kelly, S., Lackey, K. 2005. PSU/NCAR Mesoscale Modeling System, Tutorial Class Notes and User's Guide: MM5 Modeling System Version 3.
- Environment Canada. Alberta's Flood of Floods, Archived content last accessed January/25/2015:<http://www.ec.gc.ca/meteoweather/default.asp?lang=En&n=A4DD5AB1>
- Erfani A., Methot A., Goodson R., Belair S., Yeh K., Cote J., and Moffet R. 2003 Synoptic and Mesoscale Study of a Severe Convective Outbreak with the Nonhydrostatic Global Environmental Multiscale (GEM) model, *Meteorology and Atmospheric Physics*, 82: 31-53 doi: 10.1007/s00703-001-0585-8.
- Fan, Y. and Dool, H. 2008. A global monthly land surface air temperature analysis for 1948–present. *J. Geophys. Res.*, 113: D01103, doi:10.1029/2007JD008470.
- FAO, 1974. Soil map of the world. Volume I, Prepared by the Food and Agriculture Organization of the United Nations, Unesco-Paris
- FAO. 2011. The state of the world's land and water resources for food and agriculture (SOLAW) – Managing systems at risk. Food and Agriculture Organization of the United Nations, Rome and Earthscan, London.

- Gan, T. Y., Barry, R. B., Gizaw, M., Gobena, A., Balaji, R. 2013. Changes in North American snowpacks for 1979–2007 detected from the snow water equivalent data of SMMR and SSM/I passive microwave and related climatic factors. *J Geophys. Res, Atm.* 118, 7682–7697, doi:10.1002/jgrd.50507.
- Gan, T. Y., Ito, M., Hülsmann S., Qin, X., Lu, X.X., Liong, S.Y., Rutschman, P., Disse, M., Koivusalo, H. 2015. Possible climate change/variability and human impacts, vulnerability of drought-prone regions, water resource and capacity building for Africa. *J of Hydrological Sciences*, 61, No 7: 1209-1226. doi:10.1080/02626667.2015.1057143
- Giannini, A., Biasutti, M., Held, I.M., and Sobel, A.H. 2008. A global perspective on African climate. *J of Climate Change*, doi: 10.1007/s10584-008-9396-y
- Gilroy K.L., and McCuen R.H. 2012. A nonstationary flood frequency analysis method to adjust for future climate change and urbanization. *J Hydrology*, 414-415: 40-48, doi:10.1016/j.jhydrol.2011.10.009.
- Gobena, A. K., and Gan, T. Y., 2013, Assessment of Trends and Possible Climate Change Impacts on Summer Moisture Availability in Western Canada based on Metrics of the Palmer Drought Severity Index. *J of Climate*, 26, 4583-4595, doi: 10.1175/JCLI-D-12-00421.1
- Government of Alberta, 2010. Facts about water in Alberta: ISBN 978-0-7785-8970-9 last accessed January/25/2015. <http://environment.gov.ab.ca/info/library/6364.pdf>
- Griffis, V.W and Stedinger, J.R. 2007. The use of GLS in regional hydrologic analysis. *J of Hydrology*, 344: 82-95. doi:10.1016/j.jhydrol.2007.06.023.

- Groisman, P. Ya., Knight, R.W, Karl, T.R, Easterling, D.R, Sun, B. and Lawrimore, J.H. 2004. Contemporary Changes of the Hydrological Cycle over the Contiguous United States: Trends Derived from In Situ Observations. *J Hydrometeorology*, 5: 64-85.
- Gudmundsson, L., Bremnes, J.B., Haugen, J.E., and Engen-Skaugen, T. 2012. Technical Note: Downscaling RCM precipitation to the station scale using statistical transformations - a comparison of methods. *Hydrology and Earth System Sciences*, 16: 3383–3390. doi:10.5194/hess-16-3383-2012.
- Gutowski Jr W.J., Kozak K.A., Arritt R.W., Christensen J.H., Patton J.C. and Takle E.S. 2007. A Possible Constraint on Regional Precipitation Intensity Changes under Global Warming. *J Hydrometeorology*, 8: 1382-1396, doi: 10.1175/2007JHM817.1.
- Haddad, K. and Rahman, A. 2011. Regional Flood Estimation in New South Wales Australia
- Hailemariam, K. 1999. Impact of climate change on the water resources of Awash river basin, Ethiopia. *J of Climate Research*, 12: 91-96.
- Hanrahan, J., Kuo, C.C., Gan, T.Y. 2014. Configuration and validation of a mesoscale atmospheric model for simulating summertime rainfall in central Alberta. *RMS, Int J Climatology*, doi: 10.1002/joc.4011.
- Hawkins, Ed., and Sutton, R. 2009. The potential to narrow uncertainty in regional climate predictions. *American meteorological society, BAMS*, 1095-1107.
- Hirsch, R. M., Slack, J. R., and Smith, R. A. 1982. Techniques of trend analysis for monthly water quality data, *Water Resour. Res.*, 18(1), 107–121.
- Hopkinson, R.F., McKenny D.W., Milewska E.J., Hutchinson, M.F., Papadopol P., Vincent, L.A., 2011. Impact of Aligning Climatological Day on Gridding Daily Maximum–

Minimum Temperature and Precipitation over Canada. *J Applied Meteorology and Climatology*, AMS. doi: 10.1175/2011JAMC2684.1.

Hosking, J.R.M and Wallis, J.R. 1997. *Regional Frequency Analysis. An Approach Based on L-Moments*. Cambridge University Press, UK. ISBN 0-521-43045-3

Hutchinson, M.F., McKenny D.W., Lawrence, K., Pedlar, J.H., Hopkinson, R.F., Milewska E., Papadopol P. 2009. Development and Testing of Canada-Wide Interpolated Spatial Models of Daily Minimum–Maximum Temperature and Precipitation for 1961–2003. *J Applied Meteorology and Climatology*, AMS. 48: 725-741, doi: 10.1175/2008JAMC1979.1.

IPCC, 1997: *The Regional impacts of Climate Change: An Assessment of Vulnerability* R.T.Watson, M.C. Zinyowera, R.H. Moss (Eds). Cambridge University Press, UK. pp 517.

IPCC, 2007: *Climate Change 2007: The Physical Science Basis. Contribution of Working Group I to the Fourth Assessment Report of the Intergovernmental Panel on Climate Change* (Solomon, S., D. Qin, M. Manning, Z. Chen, M. Marquis, K.B. Averyt, M. Tignor and H.L. Miller (eds.)). Cambridge University Press, Cambridge, United Kingdom and New York, NY, USA, 996 pp.

IPCC, 2013: *Annex I: Atlas of Global and Regional Climate Projections* [van Oldenborgh, G.J., M. Collins, J. Arblaster, J.H. Christensen, J. Marotzke, S.B. Power, M. Rummukainen and T. Zhou (eds.)]. In: *Climate Change 2013: The Physical Science Basis. Contribution of Working Group I to the Fifth Assessment Report of the Intergovernmental Panel on Climate Change* [Stocker, T.F., D. Qin, G.-K. Plattner, M. Tignor, S.K. Allen, J. Boschung, A. Nauels, Y. Xia, V. Bex and P.M. Midgley (eds.)]. Cambridge University Press, Cambridge, United Kingdom and New York, NY, USA.

- IPCC, 2013: Annex III: Glossary [Planton, S. (ed.)]. In: Climate Change 2013: The Physical Science Basis. Contribution of Working Group I to the Fifth Assessment Report of the Intergovernmental Panel on Climate Change [Stocker, T.F., D. Qin, G.-K. Plattner, M. Tignor, S.K. Allen, J. Boschung, A. Nauels, Y. Xia, V. Bex and P.M. Midgley (eds.)]. Cambridge University Press, Cambridge, United Kingdom and New York, NY, USA
- IPCC, 2013: Chapter 2. Hartmann, D.L., A.M.G. Klein Tank, M. Rusticucci, L.V. Alexander, S. Bronnimann, Y. Charabi, F.J. Dentener, E.J. Dlugokencky, D.R. Easterling, A. Kaplan, B.J. Soden, P.W. Thorne, M. Wild and P.M. Zhai, 2013: Observations: Atmosphere and Surface. In: Climate Change 2013: The Physical Science Basis. Contribution of Working Group I to the Fifth Assessment Report of the Intergovernmental Panel on Climate Change (Stocker, T.F., D. Qin, G.-K.Plattner, M. Tignor, S.K. Allen, J. Boschung, A. Nauels, Y. Xia, V. Bex and P.M. Midgley (eds.)). Cambridge University Press, Cambridge, United Kingdom and New York, NY, USA.
- IPCC, 2013: Summary for Policymakers. In: Climate Change 2013: The Physical Science Basis. Contribution of Working Group I to the Fifth Assessment Report of the Intergovernmental Panel on Climate Change [Stocker, T.F., D. Qin, G.-K. Plattner, M. Tignor, S.K. Allen, J. Boschung, A. Nauels, Y. Xia, V. Bex and P.M. Midgley (eds.)]. Cambridge University Press, Cambridge, United Kingdom and New York, NY, USA.
- Jones, R.G. Murphy, J.M. and Noguer, M. 1995. Simulation of climate change over Europe using a nested regional climate model. I: Assessment of control climate, including sensitivity to location of lateral boundaries. Q.J.R Meteorol. Soc, 121: 1413-1449.
- Kain J.S., 2004. The Kain–Fritsch Convective Parameterization: An Update. J Applied Meteorology, 43(2004): 170-181.

- Kanamitsu, M., Ebisuzaki W., Woollen, J., Yang, S., Hnilo, J. J., Fiorino, M., and Potter, G. L. 2002. NCEP-DOE AMIP-II REANALYSIS (R-2). AMS, BAMS, 1631-1643, doi: 10.1175/BAMS-83-11-1631
- Kapangaziwiri, E., Hughes, D. A., Wagener, T. 2012. Incorporating uncertainty in hydrological predictions for gauged and ungauged basins in southern Africa. *J of Hydrological Sciences*, 57(5): 1000-1019. doi: 10.1080/02626667.2012.690881
- Kendall, M. G. (1975), *Rank Correlation Methods*, pp. 272, Charles Griffin, London.
- Kerkhoven, E., and Gan, T. Y., 2006, A Modified ISBA Surface Scheme for Modeling the Hydrology of Athabasca River Basin with GCM-scale Data, *Adv. in Water Resou.*, 29(6), 808-826.
- Kerkhoven E., and Gan T.Y. 2011. Differences and sensitivities in potential hydrologic impact of climate change to regional-scale Athabasca and Fraser River Basins of the leeward and windward sides of the Canadian Rocky Mountains respectively. *J. Clim. Change* 106: 583–607, doi:10.1007/s10584-010-9958-7.
- Kerkhoven, E., and T.Y. Gan, 2013, Differences in the Potential Hydrologic Impact of Climate Change to the Athabasca and Fraser River Basins with & without Considering the Effects of Shifts in Vegetation patterns Caused by Climate Change, *Journal of Hydrometeorology*, 14(3), 963-976. DOI: 10.1175/JHM-D-12-011.1.
- Kim, S. T., Cai, W., Jin, F-F., Santoso, A., Wu, L., Guilyardi, E., An, S-I. 2014. Response of El Niño sea surface temperature variability to greenhouse warming. *Nature Climate Change, Letters*, 4: 786-790. DOI: 10.1038/NCLIMATE2326

- Kim, S.M., Benham, B.L., Brannan, K.M., Zeckoski, R.W., Doherty, J. 2007. Comparison of hydrologic calibration of HSPF using automatic and manual methods. *Water Resour. Res.*, 43, W01402, doi:10.1029/2006WR004883
- Kite, G.W. 1996. *Frequency and Risk Analyses in Hydrology*, Water Resources Publications, Colorado, United States of America.
- Klein Tank, A.M.G, Zwiers F.W, Zhang X. 2009. Guidelines on Analysis of extremes in changing climate in support of informed decision for adaption. World Meteorological Organization, Climate Data and Monitoring, WCDMP-No. 72.
- Koohafkan, P., and Stewart, B. A. 2008. *Water and cereals in drylands*. The Food and Agricultural Organizations of the United Nations and Earthscan, London.
- Krause, P., Boyle, D.P., and Bäse, F. 2005. Comparison of different efficiency criteria for hydrological assessment. *Advances in Geosciences*, 5: 89-97
- Kuo, C.C., Gan, T.Y., Gizaw, M.S. 2015. Potential impact of climate change on intensity duration frequency curves of central Alberta. *J of Climate Change*. DOI 10.1007/s10584-015-1347-9.
- Kuo, C.C., Gan, T.Y., Hanrahan, J.L. 2014. Precipitation frequency analysis based on regional climate simulations in Central Alberta. *J Hydrology*, 510(2014): 436-446, doi: 10.1016/j.jhydrol.2013.12.051.
- Lafon, T., Dadson, S., Buys, G., and Prudhomme, C. 2013. Bias correction of daily precipitation simulated by a regional climate model: a comparison of methods. *Royal Meteorological Society, Int. J Climatology*, 33: 1367-1381, doi: 10.1002/joc.3518.
- Lamb, P. 1982. Persistence of Subsaharan drought. *Nature*, 299: 46-47.

- Lamb, P., Pepler, R.A., and Hastenrath, S. 1986. Interannual variability in the tropical Atlantic. *Nature*, 322: 238-240.
- Lemmen, D.S., Warren, F.J, Lacroix, J., and Bush, E., editors 2008: From impacts to Adaptation: Canada in a Changing Climate 2007; Government of Canada, Ottawa, ON, 448 p.
- Lenderink, G. and van Meijgaard, E. 2008. Increase in hourly precipitation extremes beyond expectations from temperature changes. *Nature Geoscience, Letters*, 1, 511-514, doi:10.1038/ngeo262
- Leung, L.R and Ghan, S.J 1999. Pacific Northwest climate sensitivity simulated by a regional climate model driven by a GCM. Part II: 2xCO₂ simulations; *AMS, J Climate*, 12, no. 7: 2031-2053.
- Lindesay, J. A. and Vogel, C. H. 1990. Historical evidence for southern oscillation-southern Africa rainfall relationships. *Int. J of Climatology*, 10: 679-689.
- Liong, S.Y., and Sivapragasam, C. 2002. Flood Stage Forecasting with Support Vector Machines. *J of the American Water Resources Association*, 38(1): 173-186.
- Lyon, B. 2014. Seasonal drought in Greater Horn of Africa and its increase during the March-May long rains. *J of Climate*, 27: 7953-7975. doi: 10.1175/JCLI-D-13-00459.1
- Lyon, B. and Mason, S. 2007. The 1997-98 summer rainfall season in southern Africa. Part I: Observations. *J of Climate*, 20: 5134-5148. doi: 10.1175/JCLI4225.1
- Maheras, P., Tolika, K., Anagnostopoulou, C., Vafiadis, M. Patrikas, I. and Flocas, H. 2004. On the relationship between circulation types and changes in rainfall variability in Greece. *Int J Climatology*, 24: 1695-1712, doi: 10.1002/joc.1088.

- Mailhot A, Beaugregard I, Talbot G, Caya D, Biner S. 2012. Future changes in intense precipitation over Canada assessed from multi-model NARCCAP ensemble simulations. *Int. J. Climatol.* 32(8): 1151–1163, doi: 10.1002/joc.2343.
- Maity, R., Bhagwat, P.P., and Bhatnagar, A. 2010. Potential of support vector regression for prediction of monthly streamflow using endogenous property. *J of Hydrological Processes*, 24: 917-923. doi: 10.1002/hyp.7535
- Mann, H. B. 1945. Nonparametric tests against trend, *Econometrica*, 13, 245–259.
- Mason, S. J. and Goddard, L. 2001. Probabilistic precipitation anomalies associated with ENSO. *AMS, BAMS*, 82, no 4: 619-638.
- Menne, M. J., Durre, I., Vose, R. S., Gleason, B. E., and Houston, T. G. 2012: An overview of the Global Historical Climatology Network-Daily Database. *Journal of Atmospheric and Oceanic Technology*, 29, 897-910, doi:10.1175/JTECH-D-11-00103.1
- Mesinger, F. et al 2006. North American Regional Reanalysis. *AMS, BAMS*, 340-360. DOI:10.1175/BAMS-87-3-343
- Meukaleuni, C., Lenouo, A., and Monkam, D. 2016. Climatology of convective available potential energy (CAPE) in ERA-Interim reanalysis over West Africa. *Atmos. Sci. Let.* 17: 65–70, DOI: 10.1002/asl.601
- Milly, P.C.D, Betancourt, J., Falkenmark, M., Hirsch, R.H., Kundzewicz, Z.W., Lattenmaier, D.P., and Stouffer, R.J. 2008. Stationarity is Dead: Whither Water Management? *Science*, 319: 573-574.
- Minsky, M.L. and Papert, S. 1988. *Perceptions: an introduction to computational geometry.* Cambridge Mass.: MIT Press, 1988, c1969.

- Mitchell, K. E., et al. 2004. The multi-institution North American Land Data Assimilation System (NLDAS): Utilizing multiple GCIP products and partners in a continental distributed hydrological modeling system, *J. Geophys. Res.*, 109, D07S90, doi:10.1029/2003JD003823.
- Mlawer E.J., Taubman S.J., Brown P.D., Iacono M.J., and Clough S.A. 1997. Radiative Transfer for Inhomogeneous Atmospheres: RRTM, a Validated Correlated-k Model for the Longwave, *Journal of Geophysical Research*, 102: 16663-16682.
- Moriasi, D.N., Arnold, J.D., Van Liew, M.W., Bingner, R.L., Harmel, R.D., and Veith, T.L. 2007. Model evaluation guidelines for systematic quantification of accuracy in watershed simulations. *Transactions in ASABE*.
- Murugavel, P., Pawar, S. D., and Gopalakrishnan V. 2012. Trends of Convective Available Potential Energy over the Indian region and its effect on rainfall. *RMS, Int. J. Climatol.* 32: 1362–1372. DOI: 10.1002/joc.2359
- Mwale, D. and Gan, T. Y., 2005, Wavelet analysis on variability, teleconnectivity and predictability of the September-November East African Rainfall, *J. of Applied Meteorology*, AMS, 44: 256-269.
- Mwale, D., Gan, T. Y., and Shen, S. S. P., 2004, A new analysis on variability and predictability of seasonal rainfall of Central Southern Africa, *Int. J. of Climatology*, RMS, 24, 1509-1530.
- Mwale, D., Gan, T. Y., et al., 2007, Wavelet Empirical Orthogonal Functions Of Space-Time-Frequency Regimes & Predictability of Southern Africa Summer Rainfall, *J. Hydrologic Engin.*, 12(5): 513-523.

- Nash, J.E. and Sutcliffe, J.V. 1970. River flow forecasting through conceptual models Part I – A discussion of principles. *J of Hydrology*, 10: 282-290.
- NCAR, Climate Data Guide. <https://climatedataguide.ucar.edu/climate-data-tools-and-analysis/regridding-overview> (accessed on August/29/2016)
- Nicholson, S. E., Tucker, C. J., & Ba, M. B., 1998, Desertification, drought and surface vegetation: an example from the west African Sahel, *Bull. American Met. Soc.*, 79, 815e829.
- NMSA 1996. Climate and agro climatic resources of Ethiopia. NMSA (National Meteorological Service Agency) Meteorological Research Report Series 1.
- Nor, N. I. A., Harun, S., Kassim, A. H. M. 2007. Radial basis function modeling of hourly streamflow hydrograph. *J of Hydrologic Engineering*, 12: 113-123. doi:10.1061/(ASCE)1084-0699(2007)12:1(113)
- Ntale, H. K., and Gan, T.Y., 2003, Drought indices and their application to East Africa, *Int J. of Climatology*, RMS, 23: 1335-1357.
- Ntale, H. K., and Gan, T.Y., Mwale, D., 2003, Prediction of East African Seasonal Rainfall Using Canonical Correlation Analysis, *J. of Climate*, 16(12), 2105-2112. DOI: [http://dx.doi.org/10.1175/1520-0442\(2003\)016<2105:POEASR>2.0.CO;2](http://dx.doi.org/10.1175/1520-0442(2003)016<2105:POEASR>2.0.CO;2).
- Otto-Bliesner, B.L. 1999. El Niño/La Niña and Sahel precipitation during the Middle Holocene. *AGU, J. of Geophysical Reseaech, Letters*. 26-1: 87-90.
- Ouarda, T.B.M.J, Ba, K.M., Diaz-Delgado, C. A. Cârsteanu, A. Chokmani, K., Gingras, H., Quentin, E., Trujillo, E., B. Bobe´e, B. 2007. Intercomparison of regional flood frequency estimation methods at ungauged sites for a Mexican case study. *J of Hydrology*, 348: 40-58. doi:10.1016/j.jhydrol.2007.09.031

- Palmer, W.C. 1965, Meteorological Drought. Research paper No. 45, US Weather Bureau, Washington DC.
- Pietroniro, A., Toth, B., and Toyra, J. 2006: Water availability in the South Saskatchewan River basin under climate change; presentation at Climate Change and Water in the Prairies Conference, Saskatoon, Saskatchewan, June 22, 2006.
- Power, S., Delage, F., Chung, C., Kociuba, G. and Keay, K. 2013. Robust twenty-first-century projections of El Niño and related precipitation variability. *Nature, Letter*, 502: 541-545. doi:10.1038/nature12580.
- Priddy, K.L. and Keller, P.E. 2005. *Artificial Neural Networks, An Introduction*. SPIE press, Bellingham, Washington USA.
- Rao, A.R, Hamed, K.H. 2000. *Flood Frequency Analysis*. CRC Press, New York.
- Rasmussen, E. N. and Blanchard, D. O. 1998. A Baseline Climatology of Sounding-Derived Supercell and Tornado Forecast Parameters. *AMS, Weather and Forecasting*, 13, 1148-1164.
- Ratnam, J. V., Behera S.K., Masumoto and Yamagata, T. 2014. Remote effects of El Niño and Modoki events on the austral summer precipitation of southern Africa. *AMS, J of Climate*, 27: 3802-3815. doi: 10.1175/JCLI-D-13-00431.1
- Reisner J., Rasmussen R.M., and Bruintjes R.T. 1998. Explicit Forecasting of Supercooled Liquid Water in Winter Storms using the MM5 Mesoscale Model, *Quarterly Journal of the Royal Meteorological Society*, 124: 1071-1107 doi: 10.1002/qj.49712454804.
- Riemann-Campe, K., Fraedrich, K., and Lunkeit, F. 2009. Global climatology of Convective Available Potential Energy (CAPE) and Convective Inhibition (CIN) in ERA-40 reanalysis. *Atmos. Res* 93, 534-545, doi:10.1016/j.atmosres.2008.09.037

- Roeckner, E., Bäuml, G. Bonaventura, L., Brokopf, R., Esch, M., Giorgetta, M., Hagemann, S., Kirchner, I., Kornbluh, L., Manzini, E., Rhodin, A., Schlese, U., Schulzweida, U., Tompkins, A. 2003. The atmospheric general circulation model ECHAM5, Part I. Model description. Max Planck Institute for Meteorology. Report No 349. Last accessed January 23, 2015. http://www.mpimet.mpg.de/fileadmin/publikationen/Reports/max_scirep_349.pdf
- Roeckner, E., Brokopf R., Esch M. Giorgetta S., Hagemann and Kornbluh L. 2006. Sensitivity of Simulated Climate to Horizontal and Vertical Resolution in the ECHAM5 Atmosphere Model. American Meteorological Society, J Climate – Special Section, vol 19 pp. 3771-3791.
- Rowell, D.P, Booth, B.B.B, Nicholson, S.E, Good, P. 2015. Reconciling Past and Future Rainfall Trends over East Africa. J of Climate 28: 9768-9788. DOI: 10.1175/JCLI-D-15-0140.1
- Saleh, A. and Du, B. 2004. Evaluation of SWAT and HSPF within basins program for the upper north Bosque river watershed in central Texas. Transactions of the ASAE, 47(4):1039-1049.
- Samui, P. 2011. Application of Least Square Support Vector Machine (LSSVM) for determination of evaporation loss from reservoirs. Scientific Research, Engineering, 3: 431-434. doi:10.4236/eng.2011.34049
- Santoso, A., McGregor, S., Jin, F-F., Cai, W., England, M.H., An, S-I., McPhaden M.J. and Guilyardi, E. 2013. Late-twentieth-century emergence of El Niño propagation asymmetry and future projections. Nature, Letter, 504: 126-129. doi:10.1038/nature12683
- Seeley, J. T., and Romps, D. M. 2015. Why does tropical convective available potential energy (CAPE) increase with warming? Geophys. Res. Lett., 42, 10,429–10,437, doi:10.1002/2015GL066199.

- Sen, P. K. 1968. Estimate of the regression coefficient based on Kendall's tau. *Journal of the American Statistical Association* 63, 1379-1389.
- Setegn, S.G., Rayner, D., Melesse, A.M., Dargahi, B., Srinivasan, R. 2011. Impact of climate change on the hydroclimatology of Lake Tana Basin, Ethiopia. *Water Resour. Res.*, 47, W04511, doi:10.1029/2010WR009248
- Shoma, T and Gan, T.Y 2012. Potential impact of climate change on the water availability of South Saskatchewan River Basin. *J Climatic Change*, 112, no 2, doi: 10.1007/s10584-011-0221-7.
- Shongwe, M.E., Oldenborgh, G.J., Hurk, B., Aalst, M. 2011. 2011. Projected changes in mean and extreme precipitation in Africa under global warming. PartII: East Africa. *J of Climate*, 24: 3718-3733. DOI: 10.1175/2010JCLI2883.1
- Shu, C. and Ouarda, T.B.M.J. 2007. Flood frequency analysis at ungauged sites using artificial neural networks in canonical correlation analysis physiographic space. *Water Resources Research*, 43, doi:10.1029/2006WR005142.
- Sillmann, J., V. V. Kharin, F. W. Zwiers, X. Zhang, and D. Bronaugh (2013b), Climate extremes indices in the CMIP5 multimodel ensemble: Part 2. Future climate projections, *J. Geophys. Res. Atmos.*, 118, doi:10.1002/jgrd.50188.
- Sillmann, J., V. V. Kharin, X. Zhang, F. W. Zwiers, and D. Bronaugh (2013a), Climate extremes indices in the CMIP5 multimodel ensemble: Part 1. Model evaluation in the present climate, *J. Geophys. Res. Atmos.*, 118, doi:10.1002/jgrd.50203.
- Singh, J., Knapp, H.V., Arnold, A.G., Demissie, M. 2005. Hydrological modeling of the Iroquois river watershed using HSPF and SWAT. *Journal of the American Water Resources Association (JAWRA)* 41(2): 343-360.

- Sivakumar, H. P., Das, Brunini, O., 2005, Impacts of present and future climate variability and change on agriculture and forestry in the arid and semi-arid tropics, *Climatic Change*, 70: 31–72.
- Skamarock WC, Klemp JB, Dudhia J, Gill DO, Barker DM, Wang W, Powers JG, 2005, A description of the advanced research WRF version 2. NCAR Tech Notes-468+STR.
- Smola, A.J. and Schölkopf, B. 1998. A tutorial on support vector regression. NeuroCOLT2 Technical Report Series, NC2-TR-1998-030.
- Solman, S.A, Nuñez, M.N., Rowntree, P.R. 2003. On the evolution of the representation of mid-latitude transient in the Southern Hemisphere by HadAM2B GCM and the impact of horizontal resolution. *Atmósfera* 257-283.
- Stedinger, J.R. and Tasker, G.D. 1985. Regional Hydrologic Analysis 1- Ordinary, Weighted, and Generalized Least Squares Compared, *Water Resources Research*, 21, No 9: 1421-1432.
- Stocker, T.F. et al. 2013: Technical Summary. In: *Climate Change 2013: The Physical Science Basis. Contribution of Working Group I to the Fifth Assessment Report of the Intergovernmental Panel on Climate Change* [Stocker, T.F., D. Qin, G.-K. Plattner, M. Tignor, S.K. Allen, J. Boschung, A. Nauels, Y. Xia, V. Bex and P.M. Midgley (eds.)]. Cambridge University Press, Cambridge, United Kingdom and New York, NY, USA.
- Sutcliffe, J.V. and Parks, Y.P. 1999. The hydrology of the Nile. IAHS special publication no. 5, IAHS Press, Institute of Hydrology, Wallingford, Oxfordshire OX10 8BB, UK
- Suykens, J.A.K and Vandewalle, J. 1999. Least Squares Support Vector Machines Classifiers. *Neural Processing Letters*, 9: 293-300.

- Tebaldi, C. and Knutti, R. 2007. The use of the multi-model ensemble in probabilistic climate projections, *Review. J Phyl. Trans.,R.Soc. A*, 365: 2053-2075, doi:10.1098/rsta.2007.2076.
- Tebaldi, C., Hayhoe, K., Arblaster, J.M., Meehl, G.A. 2006. Going to the extremes. An intercomparison of model-simulated historical and future changes in extreme events. *J of Climate Change*, 79: 185-211, doi: 10.1007/s10584-006-9051-4.
- Theil, H. 1950. A rank-invariant method of linear and polynomial regression analysis. *Indagationes Mathematicae* 12, 85-91.
- Thomas, D.M. and Benson M.A. 1975. Generalization of streamflow characteristics from drainage-basin characteristics. A study of relations for estimating streamflow characteristics from drainage-basin characteristics in four hydrologically different regions of the conterminous United States. United States Geological Survey Water-Supply paper.
- Tierney, J.E., Ummenhofer, C.C., and deMenocal, P.B. 2015. Past and future rainfall in Horn of Africa. *Sci. Adv.* 1. doi: 10.1126/sciadv.1500682
- Trenberth K. E. and Hoar, T. J. 1997. El Niño and climate change. *Geophysical Research Letters*, 24, No 23: 3057-3060
- Trenberth, K. E, Dai, A., Rasmussen, R.M. and Parsons, D. B. 2003. The Changing Character of Precipitation, *BAMS, AMS*. doi: 10.1175/BAMS-84-9-1205.
- Trenberth, K. E. 1998. Atmospheric moisture residence time and cycling: Implication for rainfall rates and climate change. *J of Climatic Change*, 39: 668-694
- Trenberth, K. E. 1999. Conceptual framework for changes of extremes of the hydrological cycle with climate change. *Climatic Change*, 42: 327-339

- Trenberth, K.E., Fasullo J., Smith, L. 2005. Trends and variability in column-integrated atmospheric water vapor. *J of Climate Dynamics* 24: 741-758, doi: 10.1007/s00382-005-0017-4.
- UNDP. 2013. Fast Facts: UNDP and poverty reduction in Africa. Accessed on August/30/2016 <http://www.africa.undp.org/content/dam/rba/docs/Outreach%20Material/Poverty%20Fast%20Facts%202013.pdf>
- Using Generalized Least Squares Quantile Regression. Technical note, *J. Hydrologic Engineering, ASCE*. 16: 920-925. doi: 10.1061/(ASCE)HE.1943-5584.0000395
- Utsumi, N., Seto, S., Kanae, S., Maeda, E. E., and Oki, T. 2011. Does higher surface temperature intensify extreme precipitation? *Geophys. Res. Lett.*, 38, L16708, doi:10.1029/2011GL048426
- V. Vapnik and A. Chervonenkis. 1964. A note on one class of perceptrons. *Automation and Remote Control*, vol 25.
- van der Schrier G, Briffa, K. R, Jones P. D, Osborn T. J. 2006 Summer moisture variability across Europe. *J Clim* 19:2818–2834
- van der Schrier, G., Barichivich, J., Briffa, K. R., and Jones, P. D. 2013. A scPDSI-based global data set of dry and wet spells for 1901–2009, *J. Geophys. Res. Atmos.*, 118: 4025–4048, doi:10.1002/jgrd.50355
- van der Schrier, G., Jones, P. D., and Briffa, K. R., 2011, The sensitivity of the PDSI to the Thornthwaite and Penman-Monteith parameterizations for the potential evapotranspiration, *J. Geophys. Res.*, 116, D03106, doi: 10.1029/2010JD015001.
- Vapnik, V. (1995): *The Nature of Statistical Learning Theory*. Springer, NY.

- Vertenstein, M., Craig, T., Henderson, T., Murphy, S., Carr, G.R.Jr and Norton, N. 2004. CCSM 3.0 User's Guide. Community Climate System Model National Center for Atmospheric Research, Boulder, CO. Last accessed January 23, 2015. <http://www.cesm.ucar.edu/models/ccsm3.0/ccsm/doc/UsersGuide/UsersGuide.pdf>
- Viessman, W., and Lewis, G. L., 2003, Introduction to Hydrology, 612 pages, 5th Edition, Prentice Hall.
- Vincent, L.A., & Éva Mekis. 2006. Changes in Daily and Extreme Temperature and Precipitation Indices for Canada over the Twentieth Century, *Atmosphere-Ocean*, 44:2, 177-193, doi: 10.3137/ao.440205.
- Vogel, C. 1994. (Mis)management of droughts in South Africa: past, present and future. *South African Journal of Science*, 90: 4-6.
- Warner, T. T., 2011, Quality assurance in atmospheric modeling, *BAMS*, DOI:10.1175/BAMS-D-11-00054.1
- Wells, N., Goddard, S., and Hayes, M. J. 2004. A self-calibrating Palmer Drought Severity Index. *J. Climate*, 17: 2335–2351.
- Wilcox, R. R. 1998a. A Note on the Theil-Sen regression estimator when the regressor is random and the error term is heteroscedastic. *Biometrical Journal* 40, 3, 261-268
- Wilcox, R. R. 1998b. Simulations on the Theil-Sen regression estimator with right-censored data. *Statistics & Probability Letters* 39, 43-47
- Williams, A.P., and Funk, C. 2011. A westward extension of the warm pool leads to a westward extension of the Walker circulation, drying east Africa. *J of Clim Dyn*. 37:2417–2435. doi: 10.1007/s00382-010-0984-y

- Wolter, K. and Timlin M.S. 2011. El Niño/Southern Oscillation behaviour since 1871 as diagnosed in an extended multivariate ENSO index (MEI.ext). *Int. J. Climatol.* 31: 1074–1087, DOI: 10.1002/joc.2336
- Wood, A. W., Leung, L. R., Sridhar, V., and Lettenmaier, D. 2004. Hydrologic implications of dynamical and statistical approaches to downscaling climate model outputs. *J. Climatic Change.* 62:189-216.
- World Water Assessment Programme. 2009. The United Nations World Water Development Report 3: Water in a Changing World. Paris: UNESCO, and London: Earthscan
- Wu, C-L., Chau, K-W. and Li, Y-S. 2008. River stage prediction based on a distributed support vector regression. *J of Hydrology*, 358: 96-111. doi:10.1016/j.jhydrol.2008.05.028
- Xia, Y., et al. 2012. Continental-scale water and energy flux analysis and validation for the North American Land Data Assimilation System project phase 2 (NLDAS-2): 1. Intercomparison and application of model products, *J. Geophys. Res.*, 117, D03109, doi:10.1029/2011JD016048.
- Ye, B., Geno, A.D., Lo, K.K. 1998. CAPE variations in the current climate and in a climate change. *J of Climate* 11: 1997-2015.
- Yoon, H., Jun, S-C., Hyun, Y., Bae, G-O., and Lee, K-K. 2011. A comparative study of artificial neural networks and support vector machines for predicting groundwater levels in coastal aquifer. *J of Hydrology*, 396: 128-138. doi:10.1016/j.jhydrol.2010.11.002
- Yu, P-S., Chen, S-T., and Chang, I-F. 2006. Support vector regression for real-time flood stage forecasting. *J of Hydrology*, 328: 704-716. doi:10.1016/j.jhydrol.2006.01.021
- Zakaria, Z.A. and Shabri, A. 2012. Streamflow forecasting at ungauged sites using Support Vector Machines. *J of Applied Mathematical Sciences*, 6, no. 60: 3003-3014.

Zhang, X., Hogg, W.D. and Mekis, E., 2001. Spatial and temporal characteristics of heavy precipitation events over Canada. American Meteorological Society, J Climate, 14: 1923-1936

APPENDIX A

This Appendix contains figures that show the spatial coverage of all extreme climate indices analyzed in this study for the 2050s and 2080s.

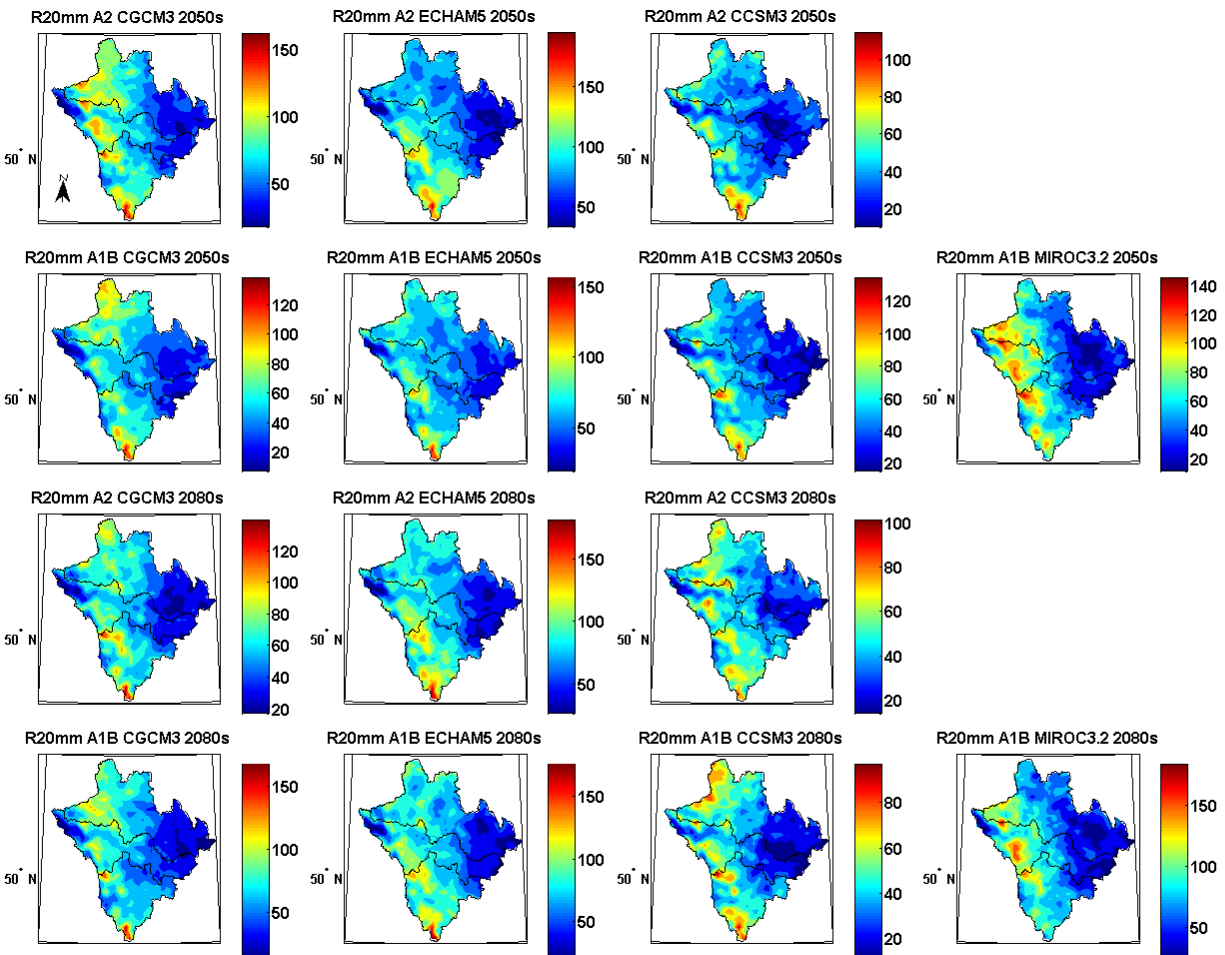


Figure A1: R20mm index over ORB, BRB and RRB for 2050s and 2080s of CGCM3, ECHAM5, CCSM3 and MIROC3.2 for A2 and A1B scenarios respectively.

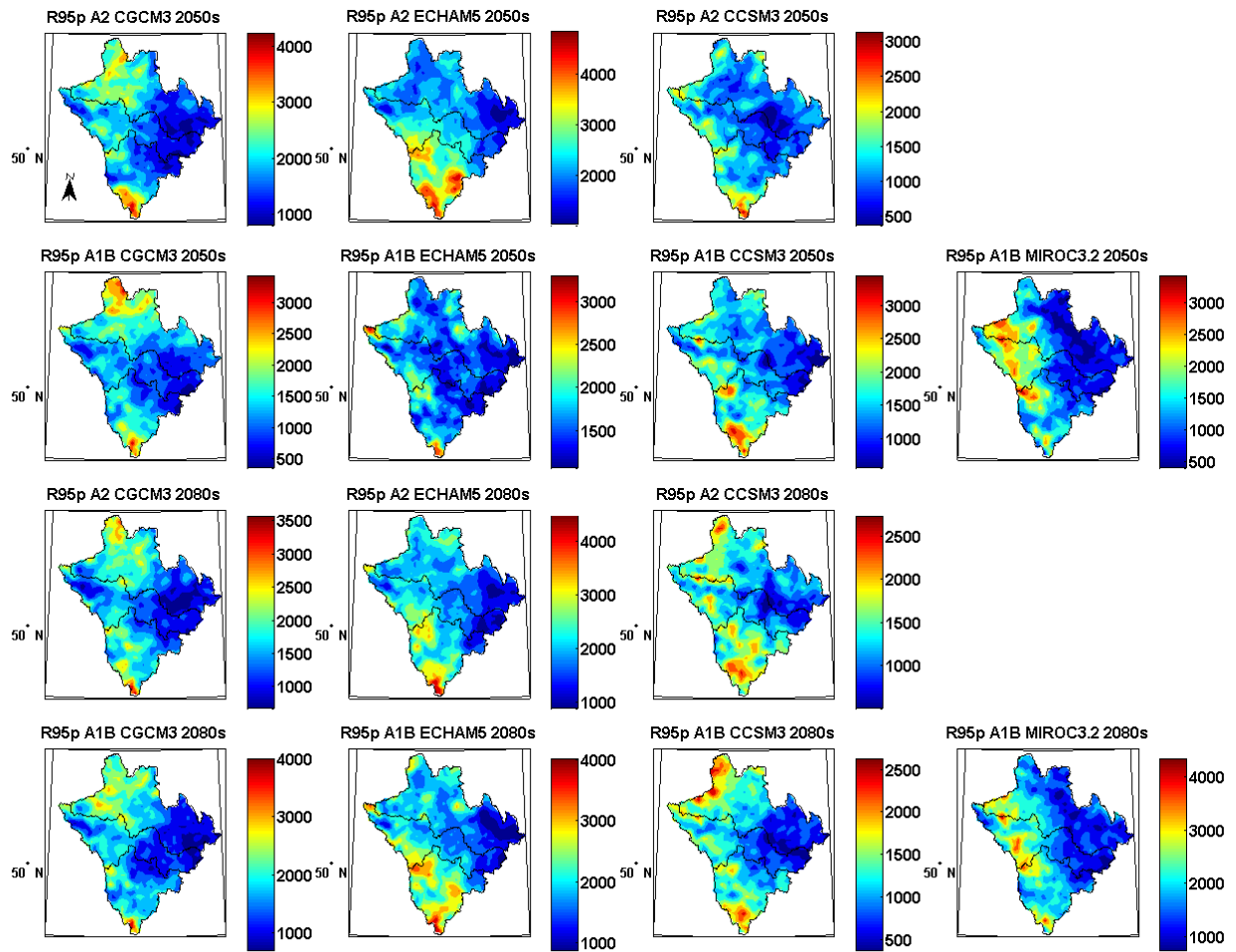


Figure A2: R95p index over ORB, BRB and RRB for 2050s and 2080s of CGCM3, ECHAM5, CCSM3 and MIROC3.2 for A2 and A1B scenarios respectively.

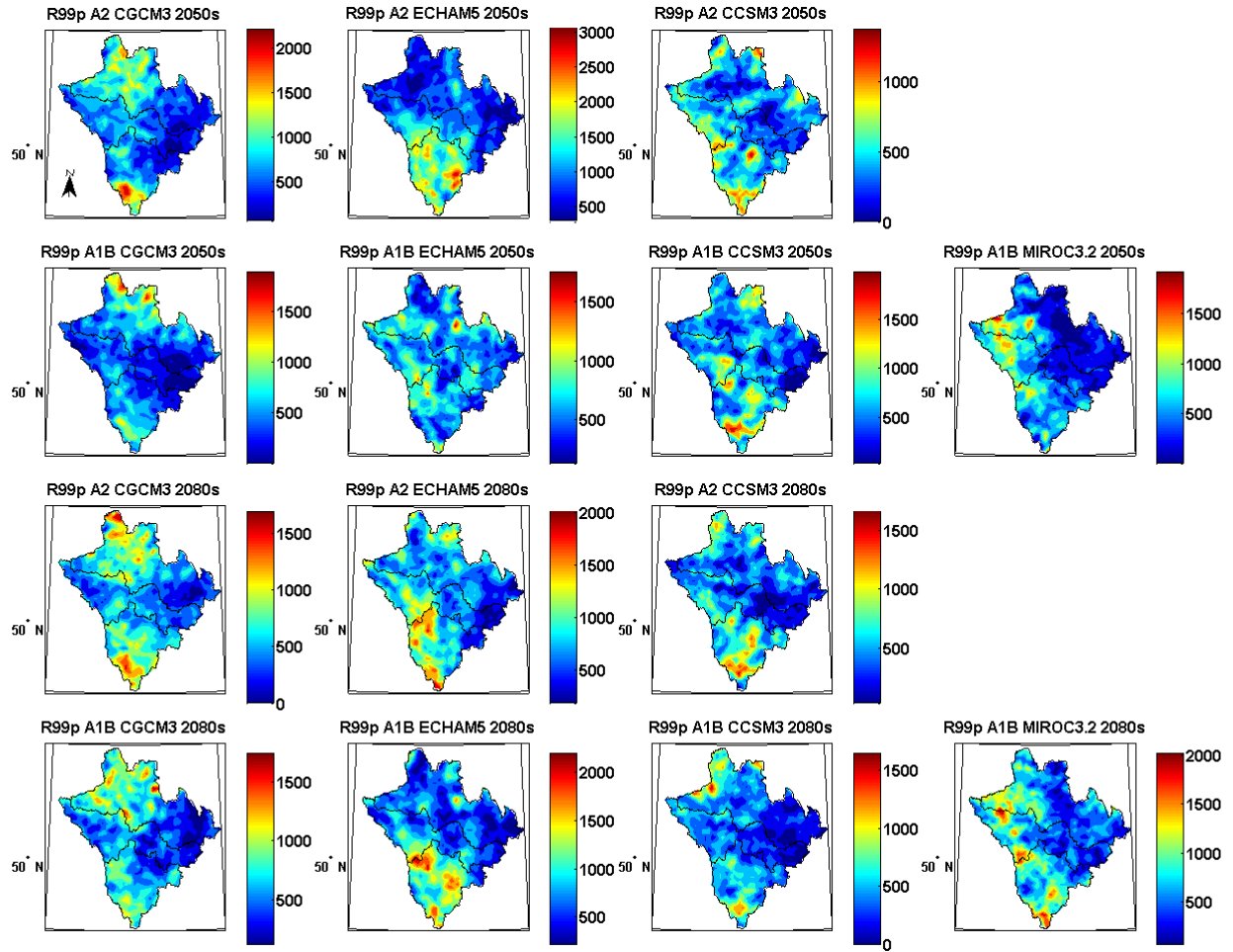


Figure A3: R99p index over ORB, BRB and RRB for 2050s and 2080s of CGCM3, ECHAM5, CCSM3 and MIROC3.2 for A2 and A1B scenarios respectively.

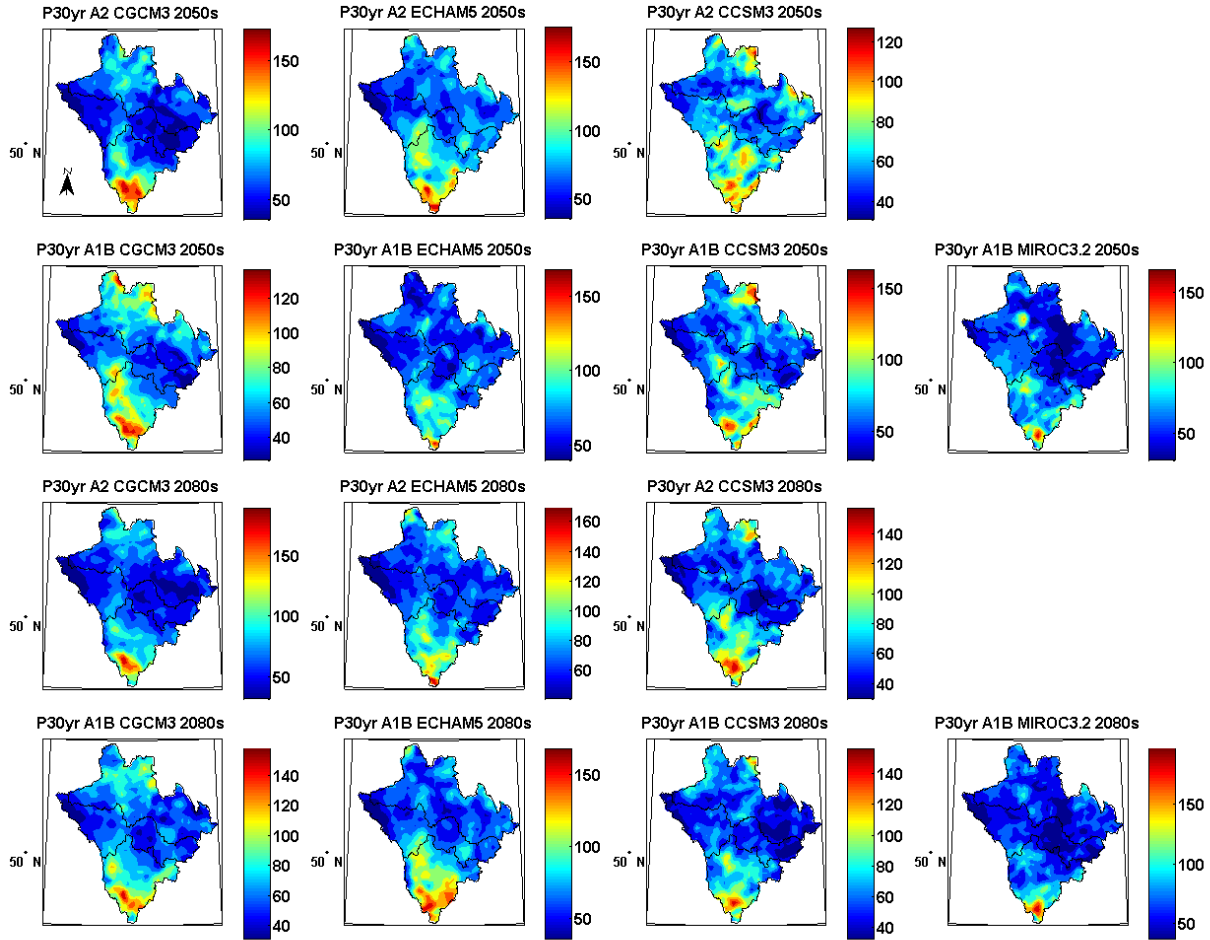


Figure A4: P30yr index over ORB, BRB and RRB for 2050s and 2080s of CGCM3, ECHAM5, CCSM3 and MIROC3.2 for A2 and A1B scenarios respectively.

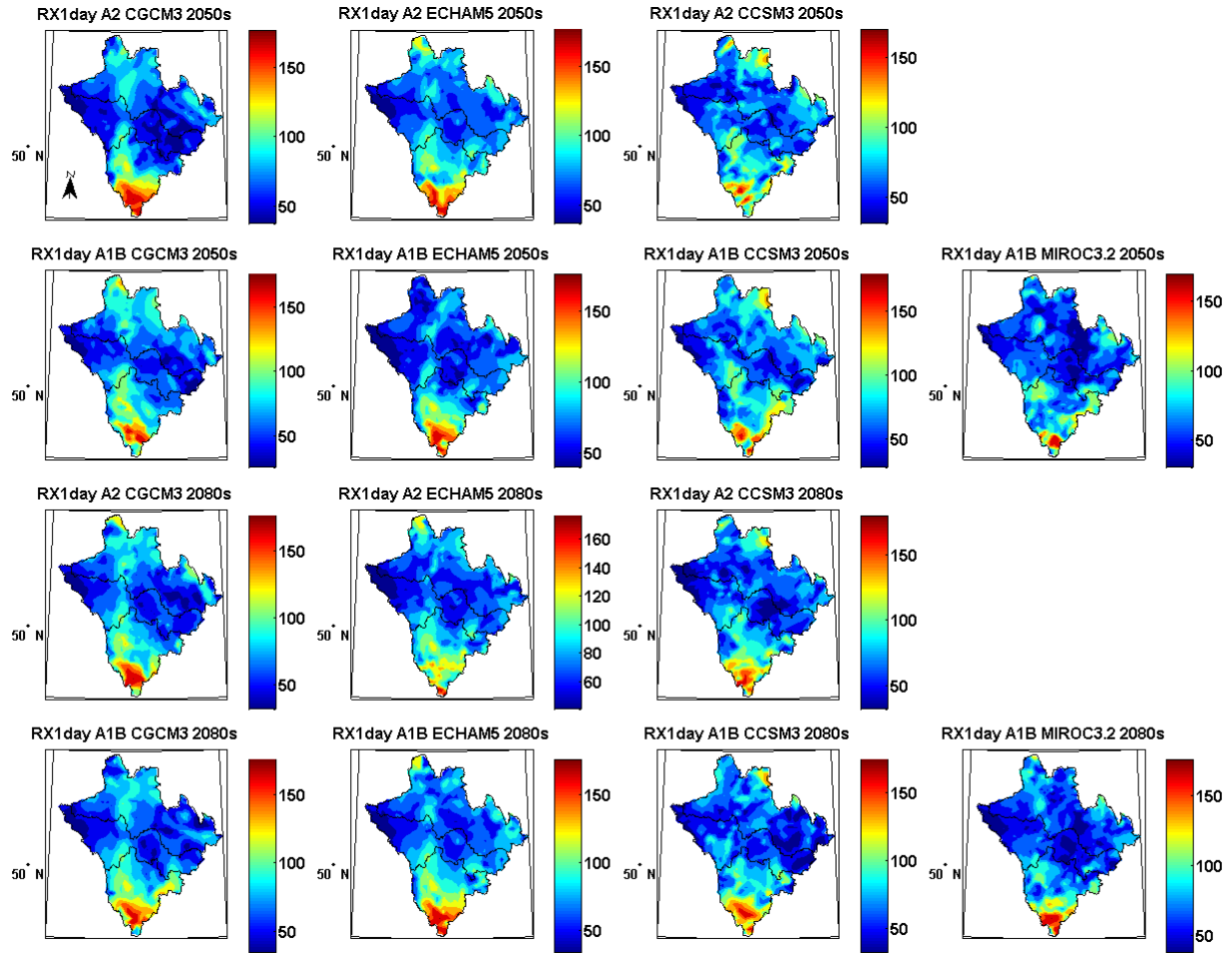


Figure A5: RX1day index over ORB, BRB and RRB for 2050s and 2080s of CGCM3, ECHAM5, CCSM3 and MIROC3.2 for A2 and A1B scenarios respectively.

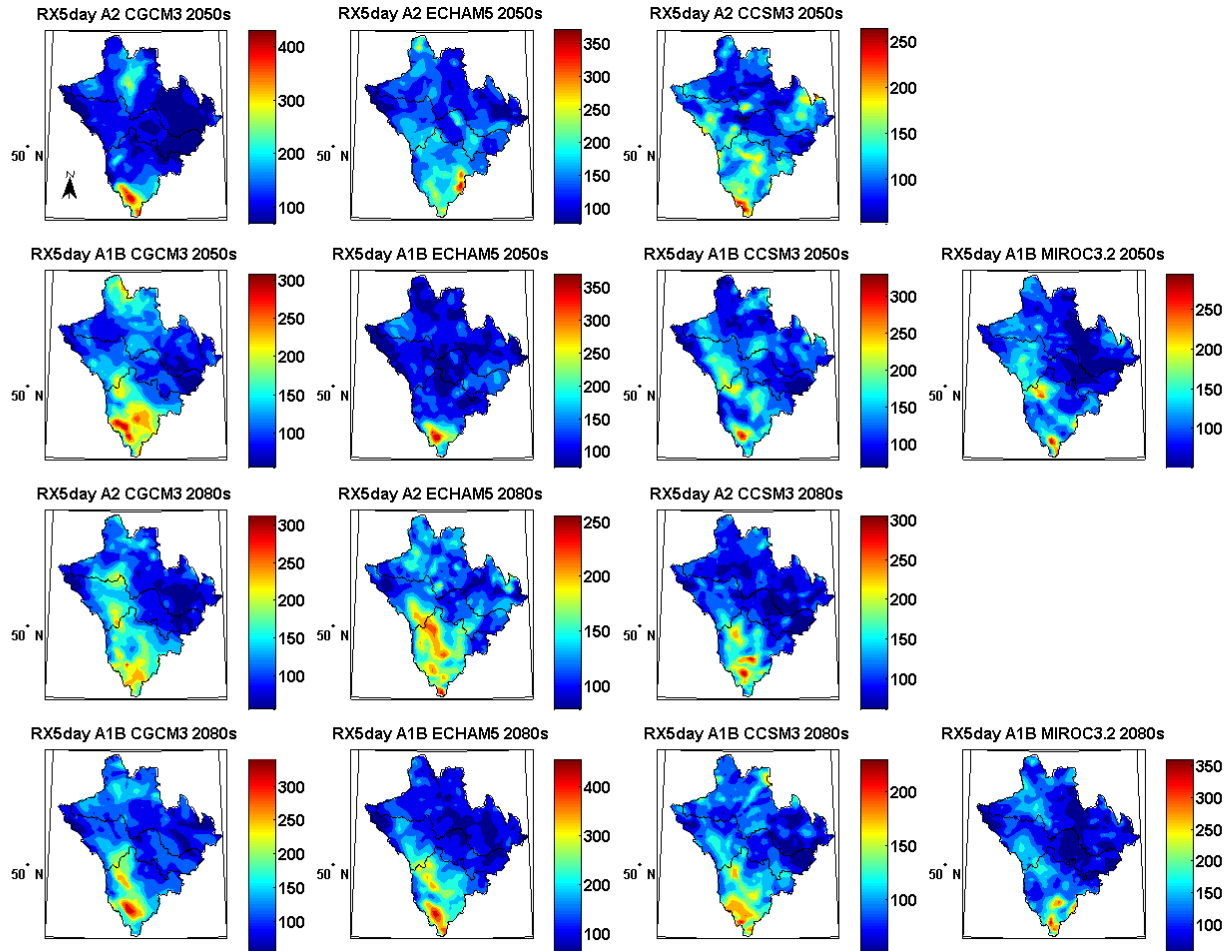


Figure A6: RX5day index over ORB, BRB and RRB for 2050s and 2080s of CGCM3, ECHAM5, CCSM3 and MIROC3.2 for A2 and A1B scenarios respectively.

APPENDIX B

The Palmer Drought Severity Index (PDSI) (Palmer, 1965) is a relative measure of drought that uses precipitation, temperature and local available water content data to assess the soil moisture. First, four variables related to soil moisture, namely evapotranspiration (ET), recharge (R), runoff (RO) and loss (L), and their complementary potential values, namely potential evapotranspiration (PET), potential recharge (PR), potential runoff (PRO) and potential loss (PL) are computed for each month. The four potential values are weighted according to the climate of the area using α , β , γ , and δ , to express them as climatically appropriate for existing conditions (CAFEC) potential values. The CAFEC potential values are combined to give the CAFEC precipitation (P') given as

$$P' = \alpha_i PE + \beta_i PR + \gamma_i PRO - \delta_i PL \quad (1)$$

$$\alpha_i = \frac{\overline{ET}_i}{\overline{PET}_i} \quad \beta_i = \frac{\overline{R}_i}{\overline{PR}_i}$$

$$\gamma_i = \frac{\overline{RO}_i}{\overline{PRO}_i} \quad \delta_i = \frac{\overline{L}_i}{\overline{PL}_i}$$

where:

$$\overline{ET}_i = \frac{\sum_{\text{all years}} ET_i}{\text{number of years}} \quad (\text{same applies for } \overline{PET}_i, \overline{R}_i, \dots)$$

i ranges over the months of the year

The difference between the actual precipitation (P) and CAFEC precipitation (P') will then give us the moisture departure (d) referred to as an excess or a deficit in precipitation. Since the same d can mean different things at different times or locations, Palmer (1965) introduced correction factors K' and K given as

$$K' = 1.5 \log_{10} \left(\frac{\frac{\overline{PE}_i + \overline{R}_i + \overline{RO}_i}{\overline{P}_i + \overline{L}_i} + 2.8}{\overline{D}_i} \right) \quad (2)$$

$$K = \frac{17.67 K'_i}{\sum_{j=1}^{12} \overline{D}_j K'_j} \quad (3)$$

where

\overline{D} is the monthly mean of the absolute value of d

Multiplying d by K will give the moisture anomaly index Z which is used to calculate the PDSI for a given month (X_i) using the general formula given as

$$Z_i = d_i K_i \quad (4)$$

$$X_i = 0.897 X_i + \frac{1}{3} (Z_i) \quad (5)$$

Palmer (1965) derived the empirical constant 17.67 in Equation 3 using data from nine different locations in seven states of the United States and the constants 0.897 and 1/3 in Equation 5 from locations in western Kansas and central Iowa of the United States. Because some of its empirical coefficients are derived from data at specific locations, the original PDSI has been criticized for giving unrealistic values when it is applied in regions other than the United States and also has been reported to have issues of comparability across different climatic regions (Guttman et al., 1991; Akinremi et al., 1996; Wells et al. 2004; van der Schrier et al. 2006)

In order to overcome these problems with the original PDSI, Wells et al (2004) developed the self-calibrating PDSI (scPDSI) where empirical coefficients in PDSI computation are directly derived based on the climate of the location where PDSI is computed. Wells et al (2004) focused on replacing the empirically derived climatic characteristic (K) in Equation 3 and the duration factors (0.897 and 1/3) in Equation 5 with values automatically calculated based on the historical

climate data of the location where the PDSI values are computed. The reader is directed to Palmer (1965) and Wells et al (2004) for detailed description of the PDSI algorithms and modifications that led to the scPDSI.

Unlike the original PDSI which results in higher frequency of extreme drought (wet) conditions when applied to regions outside of United States where it was first designed for, the scPDSI has the advantage of showing an extreme drought only when the conditions dictate extreme drought conditions relative to that area and not relative to some default locations in the United States. When tested at different locations, scPDSI follows the general pattern of the original PDSI but mostly gives values in the range of -5 to 5 so that we can compare PDSI computed from different regions (Wells et al., 2004). This advantage of scPDSI makes it applicable any part of the world, including Africa, for which the parameters in the original PDSI may not necessarily represent the climate in that region.

References

- Akinremi, O. O., McGinn, S. M. and Barr, A. G. 1996: Evaluation of the Palmer Drought Index on the Canadian prairies. *J. Climate*, 9, 897–905.
- Guttman, N. B., 1991: A sensitivity analysis of the Palmer Hydrologic Drought Index. *Water Resour. Bull.*, 27, 797–807.
- Palmer, W.C. 1965, *Meteorological Drought*. Research paper No. 45, US Weather Bureau, Washington DC.
- van der Schrier, G., Briffa, K.R., Jones, P.D., and Osborn, T. J. 2006: Summer moisture variability across Europe. *J. Climate*, 19, 2818–2834.

Wells, N., Goddard, S., and Hayes, M.J. 2004. A self-calibrating Palmer Drought Severity Index. *J. Climate*, 17, 2335–2351.

APPENDIX C

Table C1 List of streamflow and climate stations for portions of Awash, Baro, Genale and Tekeze river basins analyzed in this study. The period of record for each station represents a part from the overall record for which fairly continuous streamflow or climate data was available. Superscripts 1: only rainfall data, 2: only temperature data, 3: both.

Streamflow data			Climate data	
Station	Drainage area (km ²)	Period of fairly continuous streamflow record	Station	Period of fairly continuous climate record.
Awash at Melka Hombole	7,656	2004-2014	Addis Ababa ³	1954-2014
			Akaki ²	1997-2013
			Ambo ¹	1984-2004
			Bui ¹	1990-2005
			Debre Zeit ¹	1951-2005
			Tulu Bolo ²	1987-2013
			Woliso ¹	1983-2004
Baro at Gambella	23,461	1990-2006	Alem Teferi ²	1978-2010
			Ayira ¹	1987-2004
			Dembi Dollo ¹	1978-2005
			Gore ³	1952-2013
			Guliso ²	1978-2010
			Metu ²	1967-2013
			Masha ¹	1975-2005
Shebel ²	1983-2013			
Genale at Chene Masa	10,574	1990-2007	Awassa ³	1973-2005
			Dello Mena ³	1993-2004
			Neghele ³	1952-2014
Tekeze at Emba Madre	45,694	1994-2002	Adwa ³	1992-2005
			Debark ³	1980-2005
			Debre Tabor ³	1988-2005
			Gondar ³	1952-2005
			Lalibella ³	1978-2005
			Maichew ³	1992-2004
			Mekelle ³	1959-2005
			Shere Endeselasse ³	1992-2005

Table C2 List of GCMs that were used in this study (Model information derived from <http://cmip-pcmdi.llnl.gov/cmip5/availability.html>, and <https://verc.enes.org/data/enes-model-data/cmip5/resolution>)

GCM	Institute	Model Resolution (Latitude×Longitude)
CanESM2	Canadian Centre for Climate Modelling and Analysis (Canada)	2.7906°× 2.8125°
CMCC-CM	Centro Euro-Mediterraneo sui Cambiamenti Climatici (Italy)	0.7484°× 0.75°
CNRM-CM5	Centre National de Recherches Météorologiques, and Centre Européen de Recherche et Formation Avancées en Calcul Scientifique (CNRM-CERFACS) (France)	1.4008°× 1.40625°
GFDL-ESM2M	Geophysical Fluid Dynamics Laboratory (USA)	2.0225°× 2.5°
HadGEM2-ES	Met Office Hadley Centre, (UK)	1.25°×1.875°
INM-CM4	Institute for Numerical Mathematics (Russia)	1.5°×2°
IPSL-CM5A-MR	Institut Pierre-Simon Laplace (France)	1.2676°×2.5°
MIROC5	Atmosphere and Ocean Research Institute (The University of Tokyo), National Institute for Environmental Studies, and Japan Agency for Marine-Earth Science and Technology (Japan)	1.4008°×1.40625°
MPI-ESM-LR	Max Planck Institute for Meteorology (Germany)	1.8653°×1.875°
MRI-CGCM3	Meteorological Research Institute (Japan)	1.12148°×1.125°

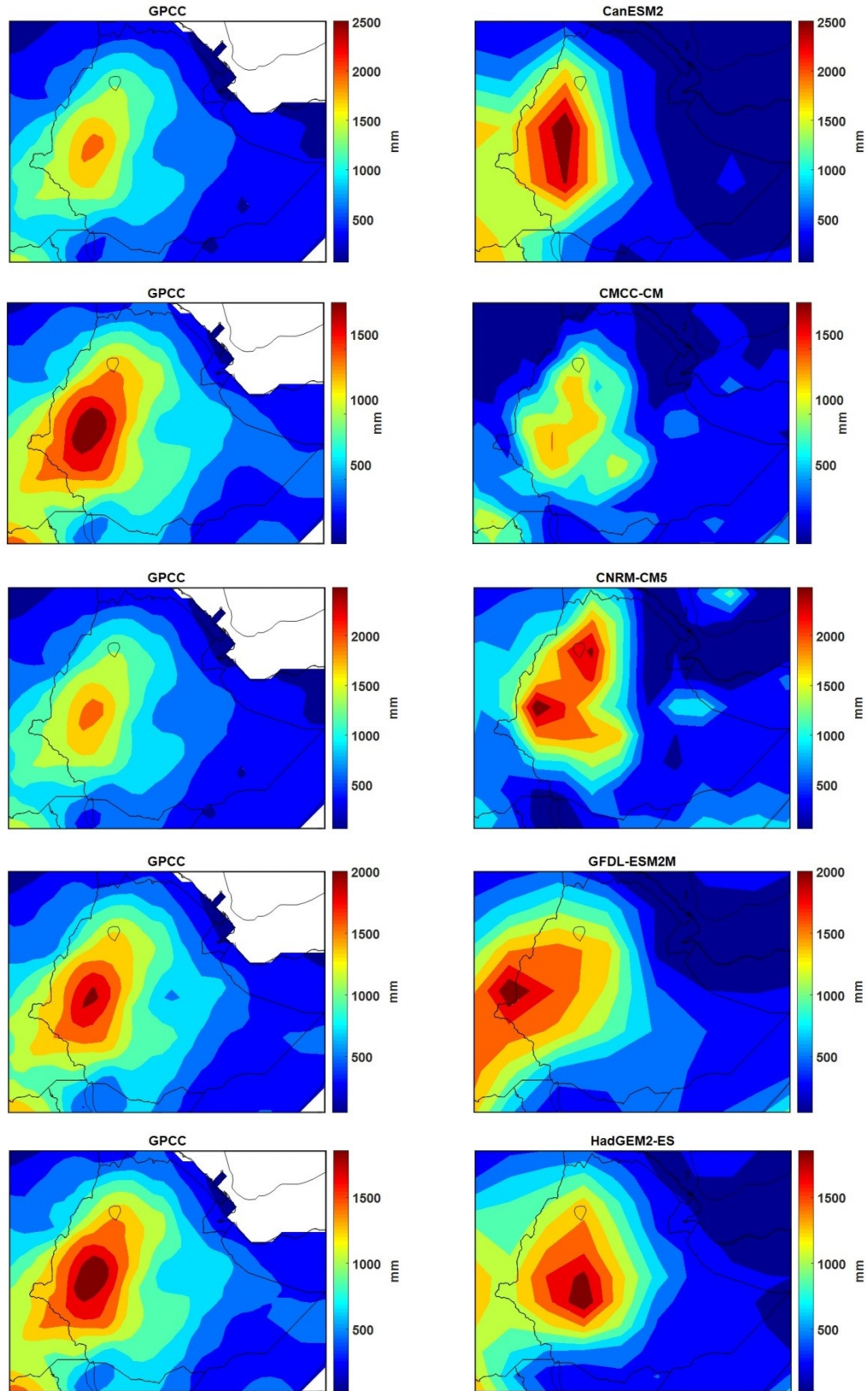


Figure C1 Comparison of mean annual precipitation over the Ethiopian region between GPCCC observed gridded data and GCM for the 1971-2000 period.

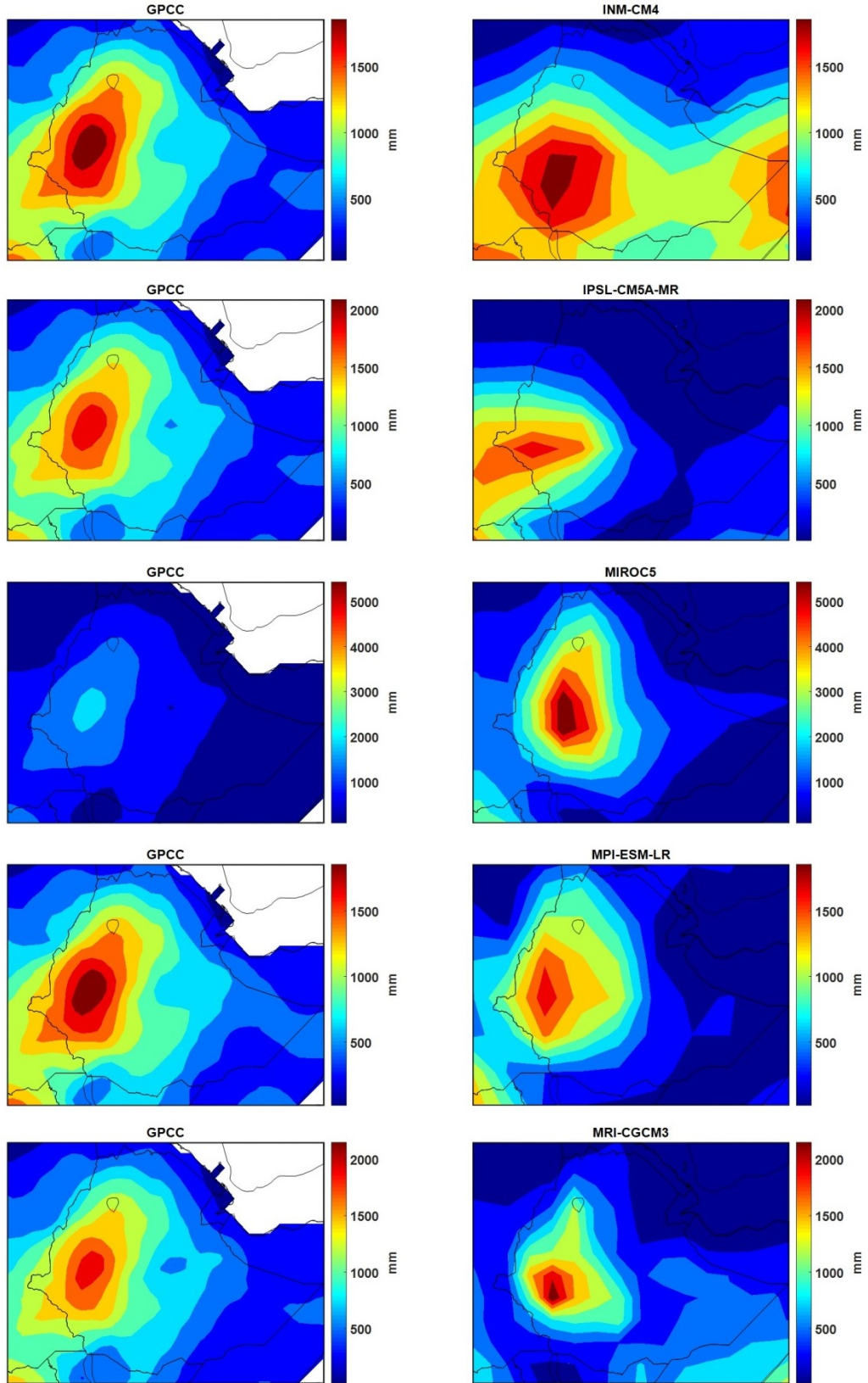


Figure C1 Continued.

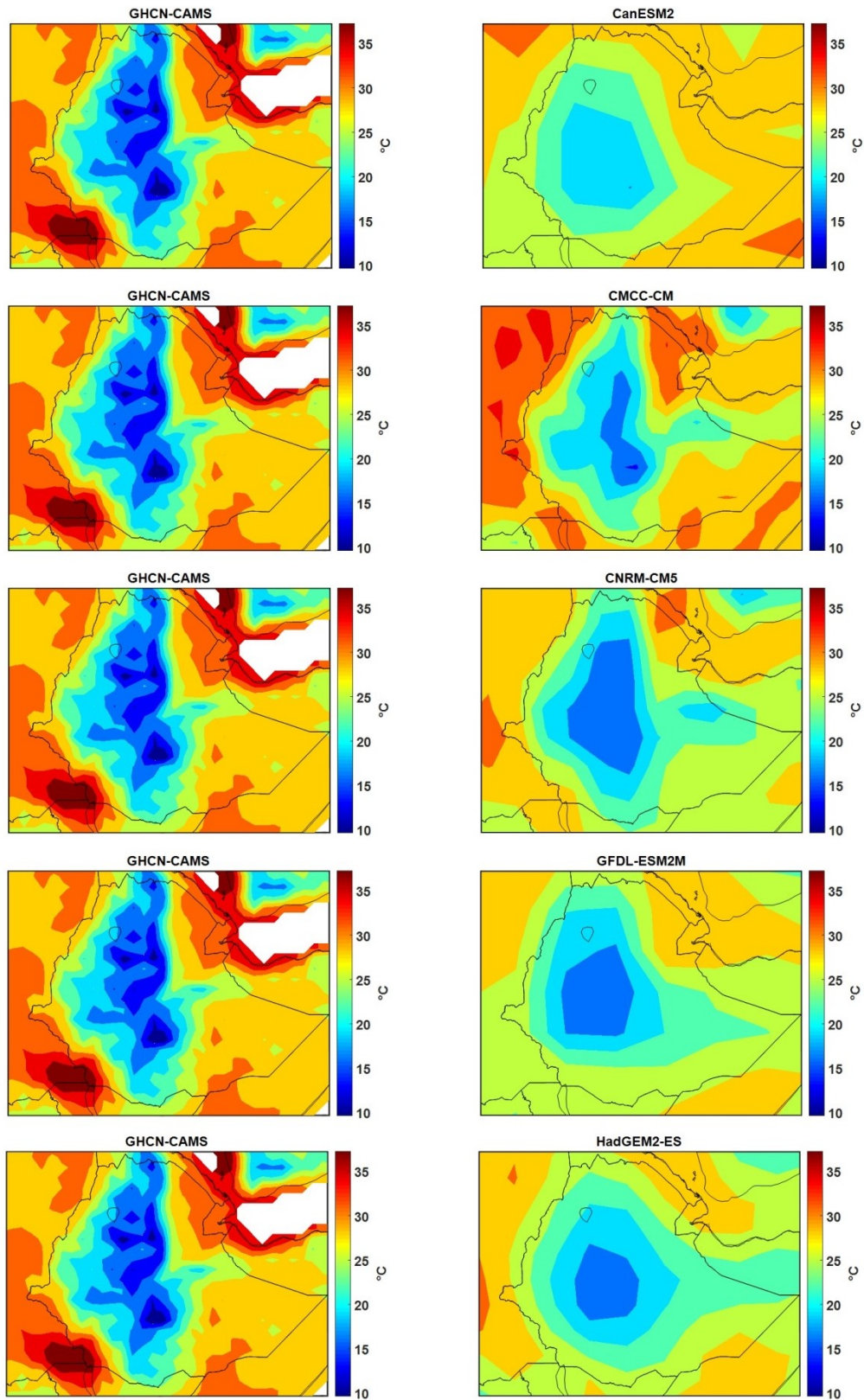


Figure C2 Comparison of mean annual temperature over the Ethiopian region between GHCN-CAMS observed gridded data and GCM for the 1971-2000 period.

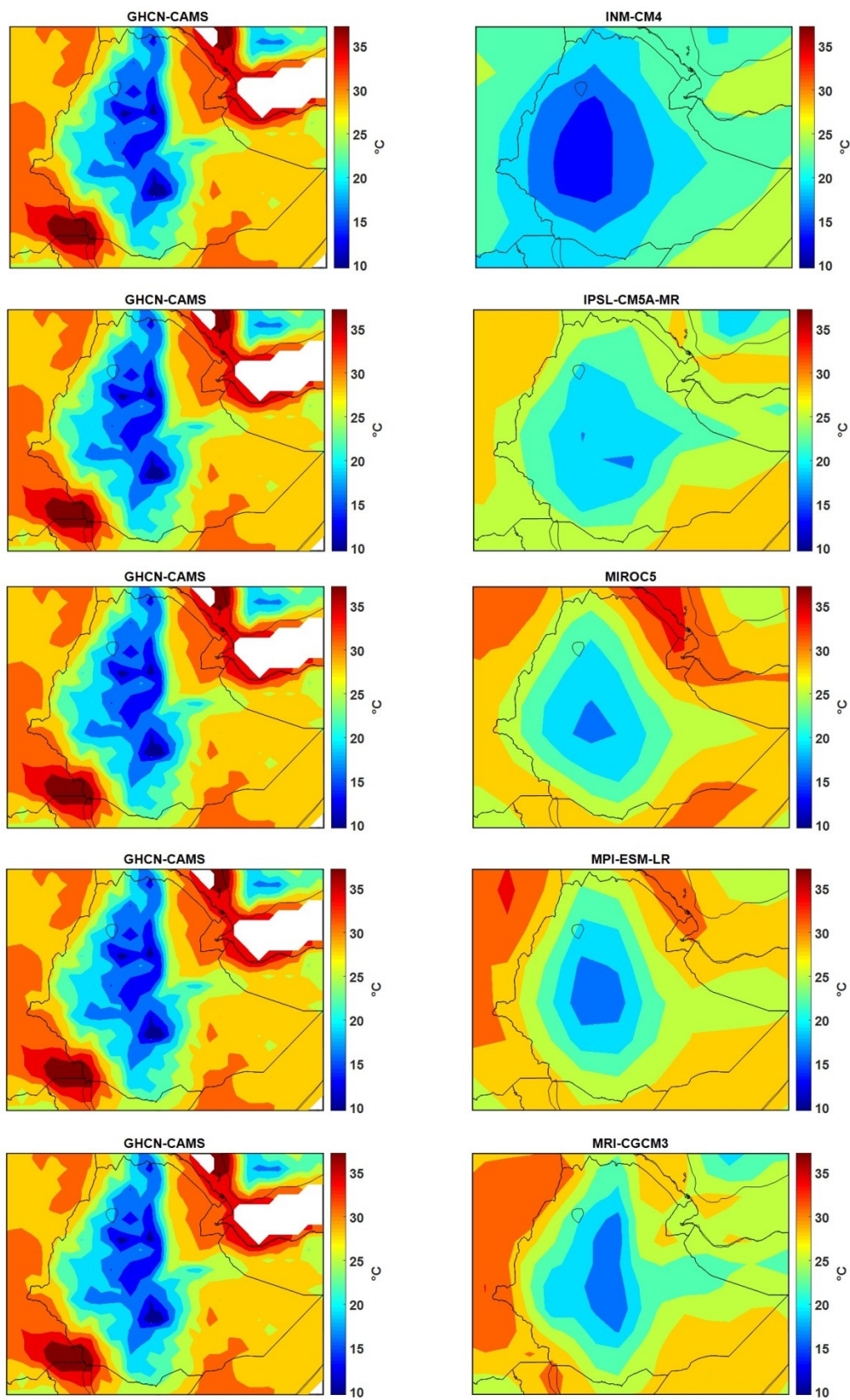


Figure C2 Continued.

Bias correction of GCM data

Climate data of the 10 CMIP5 GCMs used in this study was first re-gridded from the native resolution of each GCMs to a 0.5° resolution using the “scatteredInterpolant” toolbox of MATLAB. The precipitation and temperature data at the climate stations used to calibrate HSPF for Awash, Baro, Genale and Tekeze river basins were then extracted from the re-gridded GCM data using the aid of MATLAB. As shown in Figure C3, most GCMs generally represented the temperature and precipitation patterns in the four study areas. However, there is significant difference among GCMs in representing the seasonal magnitudes of temperature and precipitation for the four study areas.

Recent studies have shown that quantile-quantile bias correction approaches can be used to bias correct climate data for hydrologic studies (Lafon et al. 2013). Based on daily data of a given month, for a cumulative probability (F), the difference (Δx) between quantiles of observed and GCM data was first estimated for the control period. By this procedure, the difference Δx derived for a given F (Figure C4) of each month was used to adjust the daily temperature of each GCM for the control period, the 2050s and 2080s. However, because of the difference in the number of precipitation days between climate observations and GCMs, quantile-quantile bias correction was found to result in relatively higher bias corrected precipitation when compared to monthly observations. Therefore, the ratio of the monthly observed to monthly GCM precipitation of the control period was used to adjust the GCM precipitation for the control period, the 2050s and 2080s. As shown in Figure C5, the bias correction approach has effectively removed the precipitation and temperature bias from the GCM data for the four study areas, except for IPSL-CM5A-MR and MRI-CGCM3 precipitation data for Tekeze basin.

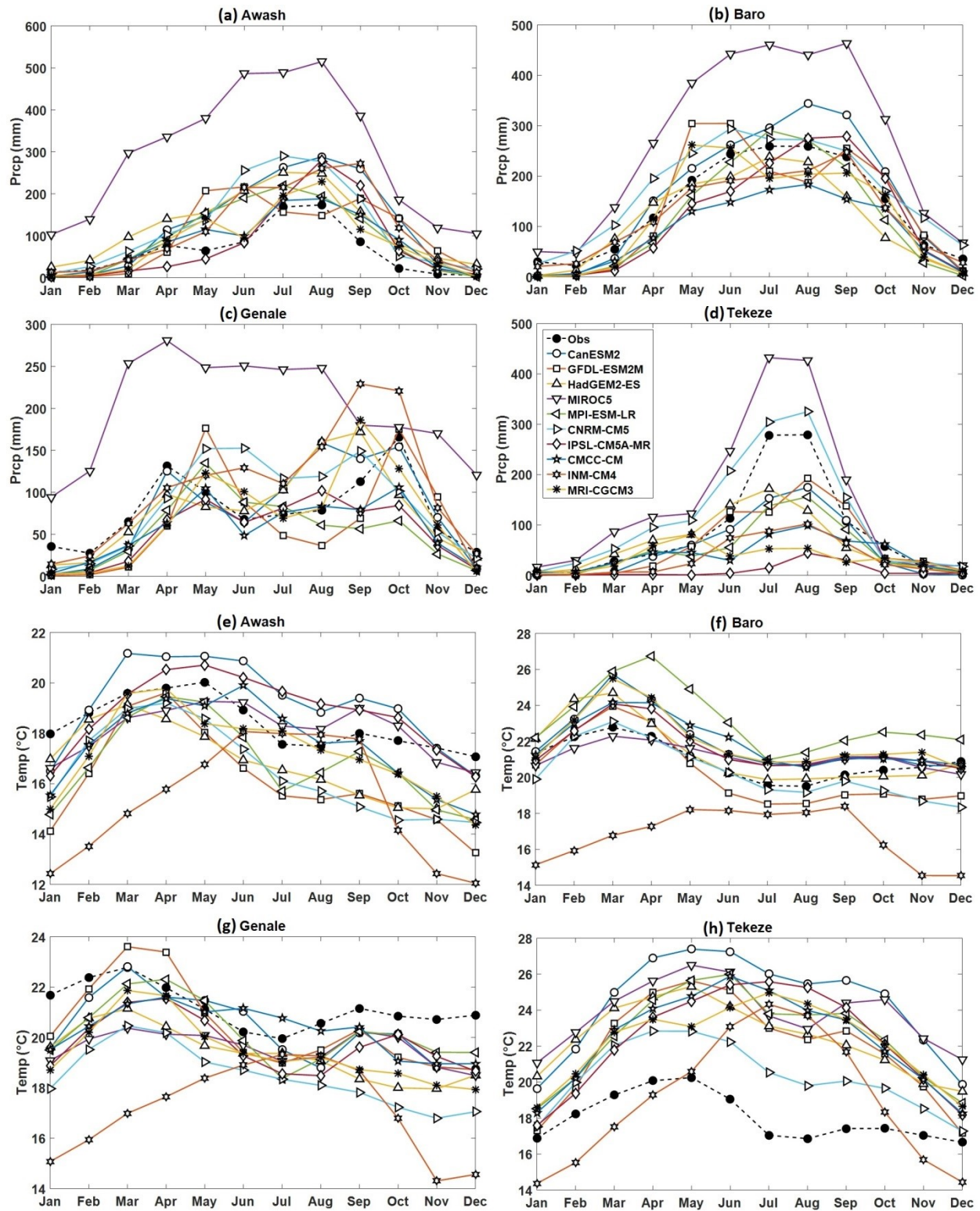


Figure C3 Comparison between the mean observed monthly precipitation (a-d) and monthly temperature (e-h) data with the climate data of 10 CMIP5 GCMs for Awash, Baro Genale and Tekeze river basins for the control period.

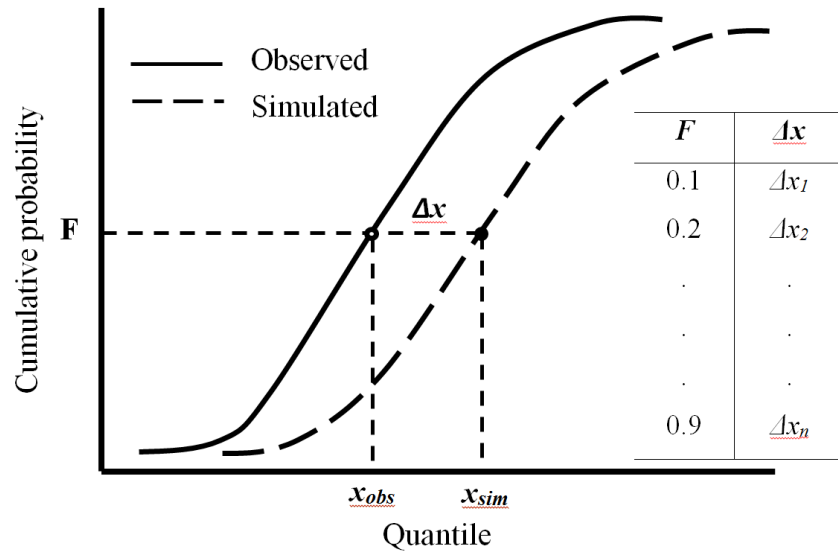


Figure C4 Quantile-quantile bias correction approach used to correct the bias in temperature data of 10 CMIP5 GCMs for Awash, Baro, Genale and Tekeze river basins.

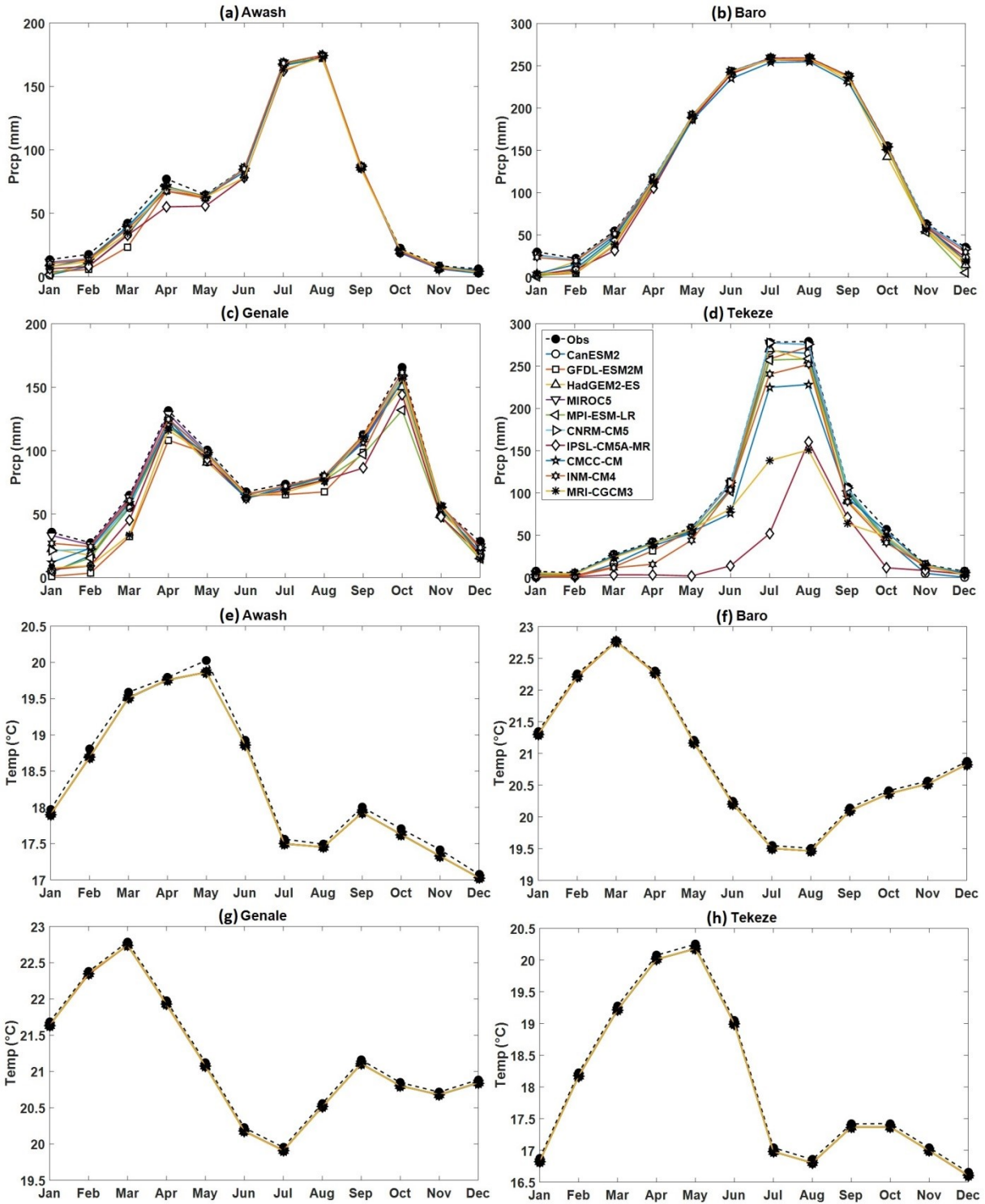


Figure C5 Comparison between observed average monthly precipitation (a-d) and observed average monthly temperature (e-h) with bias corrected climate data from 10 CMIP5 GCMs for Awash, Baro, Genale and Tekeze river basins for the control period.

Changes in seasonal precipitation and temperature

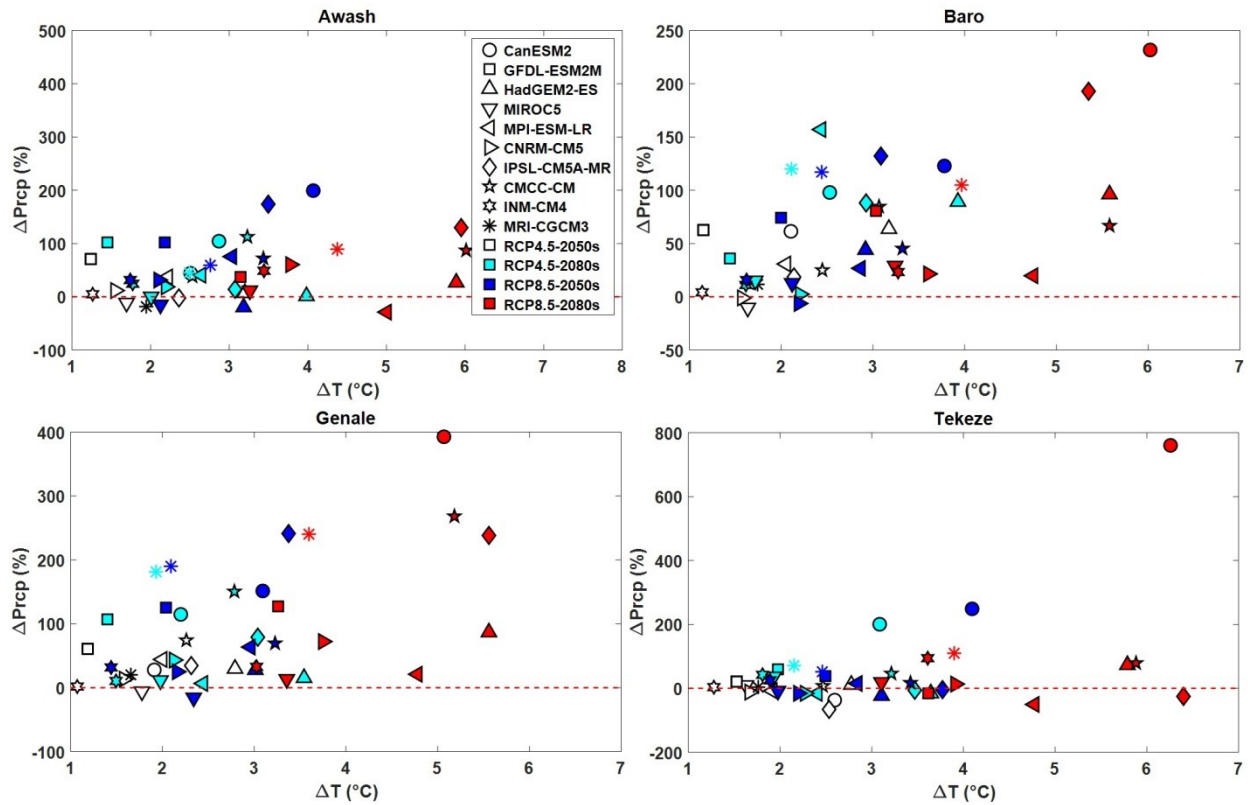


Figure C6 Projected changes in the mean winter air temperature versus changes in precipitation for RCP4.5 and RCP8.5 climate projections of 10 CMIP5 GCMs in the 2050s and 2080s for (a) Awash, (b) Baro, (c) Genale and (d) Tekeze River basins.

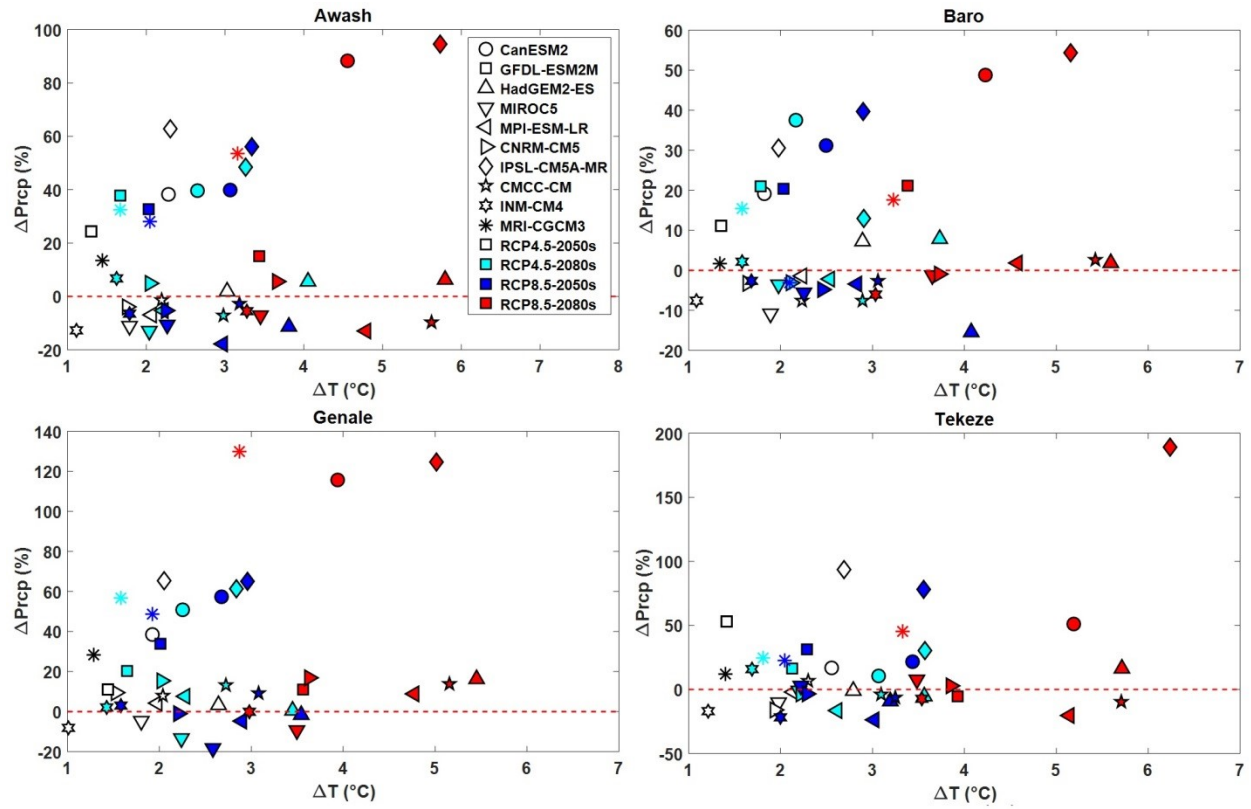


Figure C7 Projected changes in the mean spring air temperature versus changes in precipitation for RCP4.5 and RCP8.5 climate projections of 10 CMIP5 GCMs in the 2050s and 2080s for (a) Awash, (b) Baro, (c) Genale and (d) Tekeze River basins.

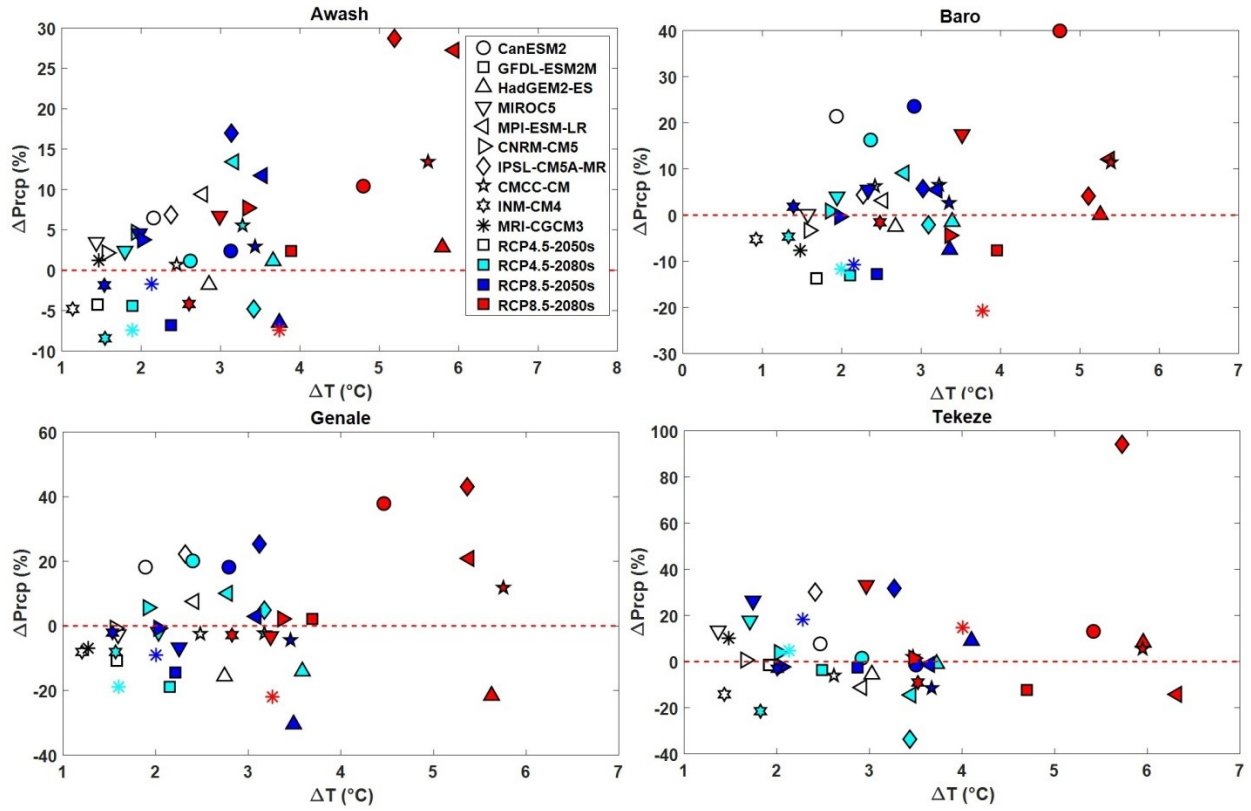


Figure C8 Projected changes in the mean summer air temperature versus changes in precipitation for RCP4.5 and RCP8.5 climate projections of 10 CMIP5 GCMs in the 2050s and 2080s for (a) Awash, (b) Baro, (c) Genale and (d) Tekeze River basins.

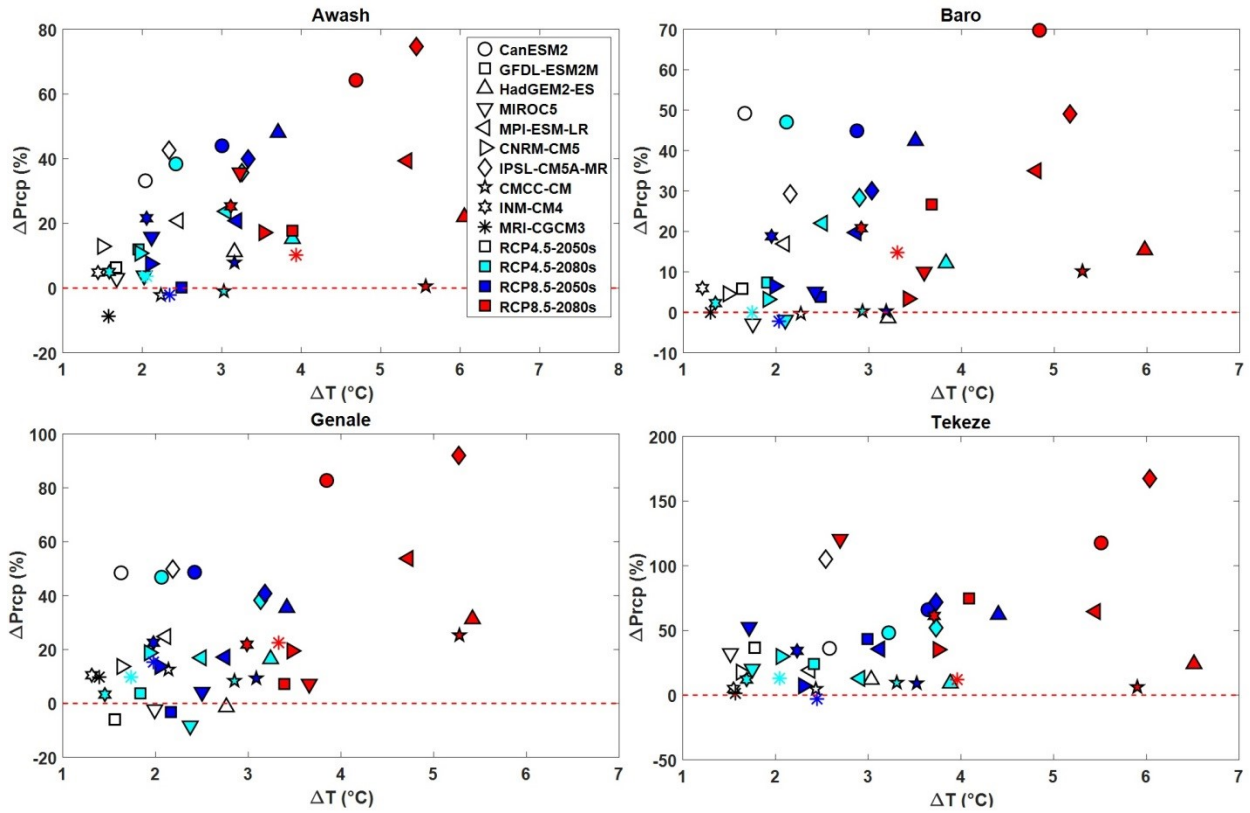


Figure C9 Projected changes in the mean autumn air temperature versus changes in precipitation for RCP4.5 and RCP8.5 climate projections of 10 CMIP5 GCMs in the 2050s and 2080s for (a) Awash, (b) Baro, (c) Genale and (d) Tekeze River basins.

References

Lafon, T., Dadson, S., Buys, G., and Prudhomme, C. 2013. Bias correction of daily precipitation simulated by a regional climate model: a comparison of methods. Royal Meteorological Society, *Int. J Climatology*, 33: 1367-1381, doi: 10.1002/joc.3518.